January 2013

Mass Spectrometry-based Methods for the Detection and Characterization of Protein-Tyrosine Nitration

Kent W. Seeley
University of South Florida, kseeley@mail.usf.edu

Mass Spectrometry-based Methods for the Detection and Characterization of Protein-Tyrosine Nitration

by

Kent William Seeley

A dissertation submitted in partial fulfillment
of the requirements for the degree of
Doctor of Philosophy
Department of Cell Biology, Microbiology & Molecular Biology
College of Arts and Sciences
University of South Florida

Major Professor: Stanley M. Stevens Jr., Ph.D.
Gary Daughdrill, Ph.D.
Richard Pollenz, Ph. D.
Kathleen Scott, Ph.D.

Date of Approval:
June 17, 2013

Key words: proteomics, mass spectrometry, selected/multiple reaction monitoring, stable isotope-labeling, nitroproteome, nitroprotein, nitropeptide, pentapeptide

Dedication

I dedicate this dissertation to my wife, Jennifer, for her immeasurable support and patience throughout this process. If not for her maintaining me in the lifestyle to which I had become accustomed, I would likely have aged even more evidently than I did over the past eight years. I would also like to dedicate this to my parents, John Seeley and Barbara Ziegler, for their genetic, intellectual, and financial contributions toward my success in this endeavor. I hope to continue to show my appreciation to all of these wonderful people as I venture into a meaningful career made possible by the education and training I have acquired with their assistance.

Acknowledgments

This work was made possible through the advice and support of Dr. Stanley M. Stevens, Jr. I would also like to acknowledge Dr. Richard Pollenz, for accepting me into the Cell & Molecular Biology graduate program as both my antecedent mentor and the Director of Graduate Studies. Finally I would like to acknowledge Dr. Gary Daughdrill and Dr. Kathleen Scott for helping preserve my focus throughout the development of this project toward a meaningful conclusion. Thank you all for your individual influences in my growth as a scientist during both my undergraduate and graduate study. I have found your continued advice to be both productive and rewarding.

Table of Contents

List of Tables

List of Figures

Abstract

Protein tyrosine nitration (PTN) is a posttranslational modification resulting from oxidative/nitrosative stress that has been implicated in a wide variety of disease states. Characterization of PTN is challenging due to several factors including its low abundance in a given proteome, preferential site modification, multiple target site proximity within unique peptide sequences, and analytical method and instrument limitations. Current analytical techniques are insufficiently sensitive to identify endogenous nitration sites without incorporation of either nitrotyrosine or target protein enrichment. However, enrichment proficiency can also be inadequate. Chemical derivatization of the nitro- moiety can be incomplete or result in undesirable byproduct formation, while immunoaffinity proficiency is contingent upon antibody specificity.

To overcome analytical method and enrichment deficiencies, we aimed to develop a comprehensive nitroproteome-specific workflow using molecular methods combined with mass spectrometry. Our approach was to systematically address all relevant factors contributing to PTN such as primary sequence, protein conformation, solvent accessibility, and nitrating agent concentration. Our ultimate goal was to increase mass spectrometric sensitivity for PTN identification. All putative nitroprotein/nitropeptide identifications were then subjected to rigorous validation by either manual spectrum analyses or peptide

synthesis. We further developed MS methods for quantitation of nitropeptides from complex mixtures with minimal sample processing. Successful application of our nitroproteome-specific mass spectrometric workflow is expected to provide powerful tools for comprehensive PTN investigation that will elucidate its role in the onset and progression of a variety of disease states as well as facilitate discovery of therapeutic targets.

Chapter One: Introduction

Protein-tyrosine nitration overview

Posttranslational modifications induced by oxidative or nitrative stress can contribute to the pathophysiological events associated with the progression of certain diseases (1-8). Protein tyrosine nitration (PTN) is such a modification characterized by covalent addition of a nitro- group ($–NO_2$) to the ortho position carbon on the phenolic ring of a protein-bound tyrosine residue (Fig. 1B). PTN alters the physicochemical properties of the modified Tyr residue as well as the protein containing it, resulting in aberrant function, turnover rate, protein: protein interaction, and cell signaling (3, 9-12).

The significance of tyrosine nitration is exemplified by the fact that over fifty disease states including Alzheimer's, Parkinson's, Amyloid Lateral Sclerosis, diabetes, and cancer have been associated with PTN (5, 13, 14). Nitration found above normal endogenous levels is considered a biomarker for tissue damage caused by oxidative and/or nitrative stress (6, 15). However, its potential role as a causative factor in human disease and the molecular mechanism by which PTN confers toxicity remain largely unknown.

PTN has been linked to modulation of enzymatic activity (1-8) as well as increased nitroprotein turnover rates (16, 17). There is also evidence that nitration can impact cellular signal transduction through various activities (3, 10,

18-20). The nitro- group (–NO_2) itself is considered a signaling molecule in an oxygen tension-dependent nitration/denitration cycle (3, 21) or as a modulator of kinase-directed tyrosine phosphorylation (3, 10, 18-20).

PTN has also been shown to increase with age—indicating a potential role in aging and age-related diseases such as cancer (22). Elevated reactive oxygen and nitrogen species (ROS and RNS, respectively) often result from inflammatory stress triggers—producing oxidative/nitrative stress conditions. A major outcome of oxidative/nitrative stress is the overproduction of both superoxide ($O_2^{\bullet -}$) and nitric oxide (NO), which can react in a diffusion-limited manner (23-25) to form the RNS, peroxynitrite anion ($ONOO^-$; Fig. 1a).

Although $ONOO^-$ is generated constitutively as a byproduct of cellular respiration, PTN resulting from normal endogenous $ONOO^-$ generation occurs at levels elusive to current detection methods. However, increased $ONOO^-$ production due to oxidative/nitrative stress initiated by activated macrophage response to lipopolysaccharide (LPS) or the presence of other foreign substances is considered to be the key contributing factor for PTN under physiological conditions (1, 2, 16, 26-28).

Since oxidative/nitrative stress-induced PTN levels are likely to be significantly higher than normal endogenous levels, induction of these conditions is expected to facilitate detection. Assuming molecular and mass spectrometric methods are sufficiently sensitive for PTN detection under these circumstances, enrichment strategies such as those required to detect normal endogenous nitration (3, 15, 29) are expected to be superfluous.

Nitrating agents for *in vitro* study

Tetranitromethane

Tetranitromethane (TNM) was a popular *in vitro* tyrosine nitrating agent in the late 1960's and early 1970's (3, 30-34). A typical experiment would have been the reaction of ≤ 10 mM TNM (33) with protein suspensions at a pH of 8. The pH was critical for tyrosyl residue nitration, because at pH ≤ 6, cysteine would be preferentially nitrated (32). Today, TNM use for *in vitro* PTN study is limited since it lacks biological relevance. Additionally, TNMs reactivity specificity is inconsistent at different concentrations (i.e. it frequently modifies other amino acid residues such as cysteine, methionine, and tryptophan). It is also prone to side reactions that may result in Tyr-nitrosylation (R—N=O) (3, 35)—perturbing qualitative and quantitative analysis.

Peroxynitrite

Peroxynitrite is an oxidized form of NO more commonly used for current *in vitro* protein-bound tyrosine nitration experiments. It is considered to be the major contributor to PTN in biological systems. Peroxynitrite is formed from the reaction between superoxide ($O_2^{\bullet-}$) and NO in a diffusion-limited manner (23-25, 36) and has a half life of less than one second (2, 3, 17, 37).

Superoxide is generated during cellular respiration via the mitochondrial electron transport chain (38) and alternate sources such as activated polymorphonuclear leukocytes (e.g. macrophages, neutrophils) may contribute to $O_2^{\bullet-}$ generation via the oxidative burst. Endogenous NO production is controlled by NO synthase (NOS) isoforms, which use molecular oxygen to catalyze the

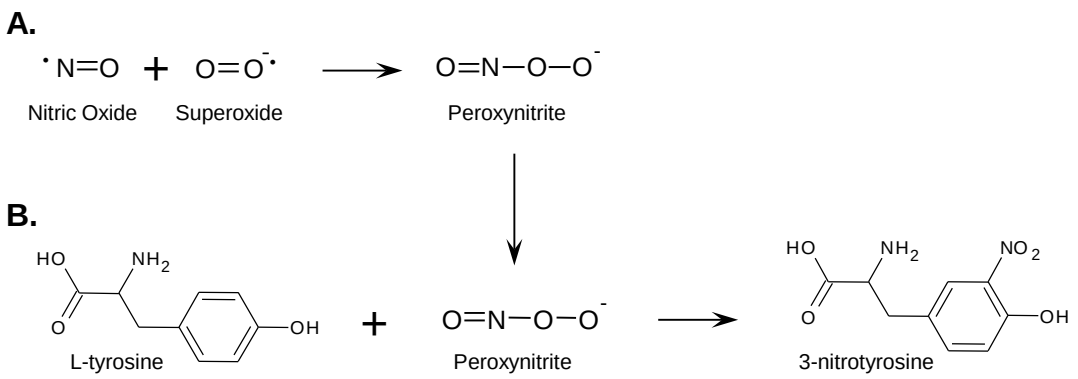

Figure 1. Peroxynitrite formation and subsequent tyrosine nitration. A) Nitric oxide and superoxide combine to form the nitrate isomer, peroxynitrite. B) L-tyrosine reacted with peroxynitrite is modified to 3-nitrotyrosine in the presence of carbon dioxide or a transition metal.

oxidation of L- arginine to citrulline (11, 39). Expression of inducible NOS (iNOS), a high-output form of NOS (40), is elevated in certain cells such as activated macrophages.

Nitric oxide is an important free radical signaling molecule involved in regulation of cell and tissue function (41-44) that has strong affinity for transition metal centers and ROS (43). It also interacts with cytochrome oxidase depending on NO and oxygen concentrations to modulate cellular respiration (11, 39, 45), ATP production (45), and oxygen free-radical production (46). Exogenous NO can also be introduced via inhaled drugs of abuse—potentially altering NO-mediated signaling and/or increasing $ONOO^-$ generation and subsequent nitration (18).

Mechanism for peroxynitrite-mediated protein-tyrosine nitration

Although several mechanisms have been proposed to describe peroxynitrite-mediated PTN occurring either under normal physiological or

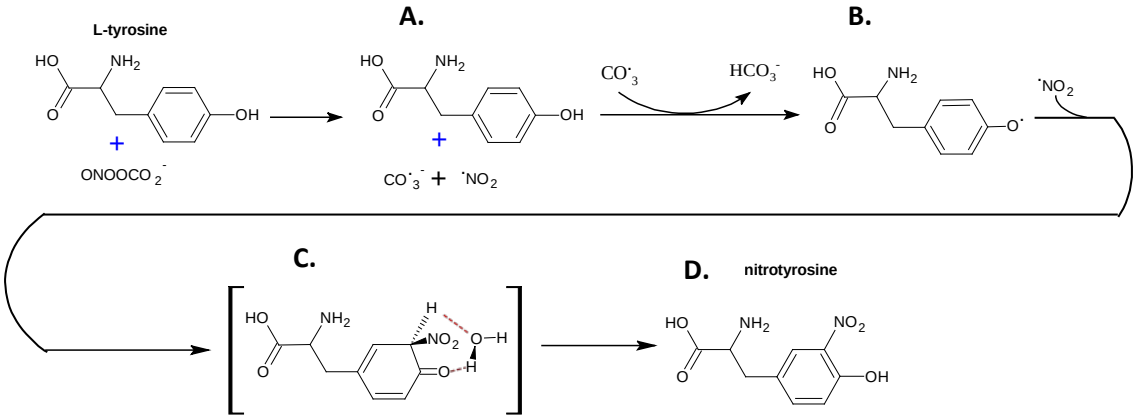

Figure 2. Radical pathway for peroxynitrite-mediated Tyr-nitration. A) L-tyrosine in the presence of nitrosoperoxycarbonate radical decomposition products results in tyrosyl radical formation (B). Nitrogen dioxide radical ($NO_2^{\bullet}$) reacts with the tyrosyl radical forming the water-stabilized transition state (C) before re-aromatization of the phenolic ring to form 3-nitrotyrosine (D). Adapted from Gunaydin & Houk, 2009.

inflammatory conditions in the cell (2, 3), it is generally accepted that nitration occurs through a radical-driven pathway (2, 3, 47-49) such as the one depicted in Figure 2. The exothermic reaction (19.1 kcal/mol) between intracellular carbon dioxide (CO_2) and peroxynitrous acid (HNO_3) results in formation of a nitrosoperoxycarbonate ($ONOOCO_2$) intermediate (16). Nitrosoperoxycarbonate decomposes to form radical products (Fig. 2A) that can ultimately react with the tyrosyl radical (Fig 2B). Water molecule assistance stabilizes the transition state depicted in Figure 2C, prior to re-aromatization of the phenolic ring—yielding 3-nitrotyrosine (3NT) (Fig. 2D). Decomposition of HNO_3 to $NO_2^{\bullet}$ and $^{\bullet}OH$ is the rate-limiting reaction (16). Free or bound transition metal ions can also augment nitration efficiency through catalysis of radical formation (26).

Physicochemical consequences of protein-tyrosine nitration

Nitration to protein-bound tyrosine shifts the pK_a of the phenolic hydroxyl group from ~ 10.1 to ~ 7.2—altering side-chain reactivity at physiological pH (50).

Nitration also confers a 35 $Å^3$ bulk addition to Tyr (3, 12) and shifts its spectrophotometric absorbance from 276 nm (Tyr) to 427 nm (3NT) at physiological pH. At acidic pH (~ pH 3), 3NT has a characteristic absorbance maximum at 356 nm and its hydrophobicity increases—two physical properties that become analytically advantageous as described in Chapter Two. The resultant physicochemical changes can impart local or remote conformational changes affecting enzymatic activities, protein: protein interactions, turnover rates, and cell signaling (3, 10, 12, 27).

Functional consequences of protein-tyrosine nitration

Accelerated degradation

Although 3NT occurs at a low steady state—affecting fewer than $10E^{-5}$ tyrosine residues (2, 3), nitro- modified proteins are degraded at accelerated rates. This phenomenon can result in functional loss and have downstream effects on related pathways. For example, mitochondrial proteins undergoing *in vitro* generated nitrative stress (incubated with L-Arginine for 30 minutes) were degraded much faster than unmodified cognate proteins (26). The half-lives for nitroproteins were measurable in hours as compared to days (Table 1) for the unmodified isoforms (26). Supporting these results, native Tyr-containing protein half-lives found in this study were in agreement with degradation rates reported by Grisolia in 1981 (51).

Antioxidant interference

Another possible functional consequence resulting from PTN is antioxidant interference. An example of this can be found in interruption of the bond on

Table 1. Nitrated mitochondrial protein half-lives.

Protein	Molecular Weight (kDa)	pI	Half-Lif of Proteins in vivo, days*	Half-Life of Proteins, days	Half-life of Nitrated Proteins, hours
Carbamoyl phosphate synthetase I	160	6.5	7.7	5.90	0.80
β-Subunit F_oF_1-ATPase	49.4	4.9	3 -4	0.59	0.50
Glutamate dehydrogenase	53.4	7.1	1	0.97	3.80

* Half-life data from Grisolia, et al. (1981)

Mitochondria incubated with L-Arg for 30 min, then washed, were analyzed by tandem 2D gels. One gel was blotted and stained for nitrotyrosine, while the second was trypsin-digested and analyzed by matrix-assisted laser desorption ionization time-of-flight (MALDI-TOF). Isoelectric point and molecular weights were also considered for protein identifications. Adapted from Beckman, 1992 (26).

Cytochrome-*c* (Cyt-c) heme iron-methionine 80 (Met^{80}) conferred by Tyr^{74} nitration (12). The bond shift was confirmed by circular dichroism (CD) and nuclear magnetic resonance (NMR) spectroscopy analyses performed at physiological pH (12). Cyt-c functions as an electron scavenger in the electron transport chain (ETC), as well as an apoptosis initiator upon release from the mitochondrion (12). The conformational change conferred by PTN can alter Cyt-c functionality possibly resulting in heightened oxidative stress or apoptosis initiation. These consequences imply a potential causative role for PTN in disease pathology.

Another aspect of PTN cytotoxicity through antioxidant impairment is its propensity to be self-perpetuating. For example, enzymes involved in the antioxidant response (phase II drug metabolizing enzymes) have been previously identified to be PTN-susceptible targets (52). This result is likely due to the fact that phase II enzyme expression increases under oxidative stress conditions.

However, nitration can diminish their ROS scavenging and disposition capacities, resulting in exacerbated cell damage.

Altered enzyme activity

Enzyme activity can also be modulated by Tyr-nitration. For example, TNM treatment to ATP synthase β-subunit (ATPase-β) induced nitration to two residues (Tyr^{345} and Tyr^{368}), resulting in a 66% activity loss (53). Although TNM conferred nitration to a total of five ATPase- β Tyr residues, an earlier study (54) reported finding *in vivo* nitration to Tyr^{345} and Tyr^{368}, indicating the physiological relevance of the two targets. To validate these findings, site-directed mutagenesis was performed severally at either location (Phe substitutions: Y368F and Y345F), which resulted in reversal of ATPase inactivation by 54% and 28%, respectively (55).

Age-related effects

Evidence has also been found indicating age-related ATPase activity loss related to, but not directly caused by, PTN (55). Nitration to rat liver mitochondrial ATPase-β (Tyr^{345} and Tyr^{368}) was found to diminish enzymatic activity by two-fold in old (80 weeks) rats as compared to young (4 weeks) (55). Since ATP binding affinity was invariant between young and old rats, a yet to be determined age-related factor appears to be acting concomitantly with PTN modification to suppress ATPase activity in aging rats.

Protein conformational changes

The three-dimensional (3D) crystal structure of ATPase-β (Protein Data Bank 1MAB) confirms Tyr^{345} and Tyr^{368} solvent accessibility—a prerequisite to

$ONOO^-$-mediated nitration susceptibility under physiological conditions (55). Also, the primary sequence surrounding the Tyr^{345} and Tyr^{368} satisfies a proposed nitration susceptibility consensus sequence (11). However, tandem mass spectrometric (MS/MS) data indicated the less activity-altering Tyr^{368} to be the predominantly-nitrated species. The increased susceptibility of Tyr^{368} appears to be due to its maintaining a lower pKa under standard conditions (7.6 v. 8.2 for Tyr^{345}). Interestingly, Tyr^{345} was found to be the predominantly-nitrated species in conditions of constitutively high NO concentrations achieved by L-Arg perfusion (55). Taken together, these results can be interpreted to link conformational changes imparted by Tyr^{345} nitration to oxidative stress-induced ATPase activity loss and diminished energy metabolism.

Altered signal transduction

PTN has also been implicated in modulation of intracellular signal transduction, especially tyrosine phosphorylation (3, 10, 18-20). Nitro-modification may not only compete with phosphorylation for specific Tyr sites, but it may also disrupt normal phosphorylation indirectly through nitration of tyrosine kinase (TK)—a previously identified potential peroxynitrite-mediated nitration target (9). Nitrated TK activity is generally associated with reduced phosphorylation (9); however, it could potentially result in constitutive TK activity and hyper-phosphorylation. An example of activity gain can be found in insulin phosphorylation, which has been demonstrated to show increased activity in the presence of low levels of peroxynitrite (3, 19). The implication is that there exists a balance of nitrating agent and nitroprotein that effectively modulate kinase-

directed signal transduction pathways (3). This also implies the nitro- group itself acts as a signaling molecule in an oxygen tension-dependent nitration/denitration cycle (21).

Impact on human health

Nitration as a potential causative factor in disease

Although PTN is generally thought of as little more than a marker for disease (6, 15), it is also suspected of being a causative factor (56). The presence of PTN in over fifty disease states (5, 13) is evidentiary of its having a causative role in at least some cases. PTN has been shown to influence essential cell processes such as energy metabolism, ROS disposition, and signaling as discussed previously in this chapter. As analytical methods improve, it is expected that a more defined account will develop of PTNs impact in certain disease pathologies. This section will review some of the recent studies connecting PTN to specific disease states.

Proliferation

Uncontrolled proliferation has been identified as one of the six major hallmarks of tumorigenesis in cancer (57). PTN has been implicated as having mitogenic activity through inhibition of prostaglandin 2 synthase (PGI_2 synthase). Increased expression of PGI_2 synthase works to switch vascular cells from proliferating states to differentiation (58). Thus, highly-proliferating cells are expected to express low-levels of PGI_2 synthase (58). PTN can alter PGI_2 synthase activity, mimicking low-level expression and resulting in uncontrolled proliferation.

Another study found bovine PGI_2 synthase from aortic microsomes to be 50% nitrated correlating with a 50% reduction in activity upon treatment with 25 μM $ONOO^-$ (59). Thermolysin in-gel digestion of PGI_2 synthase-containing SDS-PAGE bands, followed by mass-spectrometric characterization using nano-flow reversed-phase high performance liquid chromatography-Fourier transform ion cyclotron resonance (HPLC-FTICR) analysis identified a nitration site at Tyr^{430}. The site was validated through synthetic peptide analysis as well as Edman microsequencing. Because nitration was absent on all other proteins prior to treatment with 500 μM $ONOO^-$ (nitration remained specific for PGI_2 synthase up to 250 μM $ONOO^-$), it was postulated that low level endothelial generation of $ONOO^-$ was responsible for PGI_2 synthase-specific inhibition.

A subsequent study by Spisni et al (2001) determined the localization of PGI_2 synthase to be near the caveolar membrane (60). Also localized near the caveolae is eNOS, which is regulated by caveolin-1 (61). This places PGI_2 synthase in proximity to a possible $ONOO^-$ generation source. This finding supports the assertion that PGI_2 is a likely PTN target, considering PGI_2 synthase is likely to be exposed to normal levels of endogenous $ONOO^-$ generation. It also explains how PGI_2 could be a more susceptible nitration target than proteins not associated with caveolae.

It is also important to note that PGI_2 synthase is constitutively expressed (58), thus excluding variant expression as a factor in modification susceptibility. Taken together, PTN appears to serve at least a regulatory role for PGI_2 synthase activity and that excessive nitration-induced PGI_2 synthase inhibition

could potentially mimic mitogen activity, resulting in uncontrolled proliferation and tumorigenesis.

Metabolism

Since $ONOO^-$ was thought to be the product of $O_2^{\bullet -}$ leakage from the ETC and NO from a constitutively-expressed mitochondrial NOS (mNOS), the mitochondrion was the focus of many early nitration studies (7, 9, 11, 42, 55, 62-66). Thus, the mitochondrion was considered a nitration "hot spot" where peroxynitrite generated in the matrix affected proteins involved in energy metabolism (11).

To better characterize the mitochondrial global nitration profile, Elfering et al (2004) acquired whole rat liver mitochondria and sub-fractionated it to evaluate 3NT sub-mitochondrial localization. Fractions isolated were the outer membrane, inter-membrane space, inner membrane, contact sites, and the matrix (11). Whole mitochondria and subfractions were analyzed by Western blot stained for 3NT (11). Quantification was performed by calculating the ratio of the percentage of nitroprotein content compared to total protein in each fraction. The results correlated to expectations that the major sub-mitochondrial fractions containing 3NT would be the matrix (58.3%) and the inner membrane (30.5%).

Additionally, sustained NO production was induced via L-arginine supplementation to isolated mitochondria and assayed for 3NT generation. The results showed a greater than two-fold nitration increase on ATPase-β—supporting the claim of the existence of mitochondrial NOS (11) and linking PTN to energy metabolism disruption via decline of the functional ATP synthase pool.

The nitrated ATPase-β half-life had been reduced to 0.5 hours (11), in contrast to the unmodified ATPase-β half-life of 0.59 days (51).

Neurodegenerative diseases

Synucleinopathic lesions in Parkinson's disease caused by aggregation of α-synuclein have been linked to PTN (14). In this study, anti-nitro-α/β-synuclein monoclonal antibodies were raised to ensure specificity for 3NT-containing α-synuclein. The efficacy of the novel antibodies were validated by enzyme-linked immunosorbent assay (ELIZA) containing nitro-α/β-synuclein, unmodified α/β-synuclein and other 3NT-containing proteins. The antibodies raised were demonstrated to show better specificity than a commercially-available polyclonal anti-3NT antibody used in parallel—an analytical issue that will be discussed later in this chapter.

The study concluded that overproduction of reactive oxygen/nitrogen species and/or impairment of antioxidative responders contributes to the onset and progression of neurodegenerative synucleinopathies (14). Synucleinopathic lesion formation correlated with the presence of nitro-α/β-synuclein as demonstrated by immunostaining, immunofluorescence, and silver-enhanced immunoelectron microscopy (14). The results of this investigation provided further evidence of PTN as a byproduct of oxidative/nitrative stress. It also demonstrated the potential for PTN to be a causative factor in a neurodegenerative disease.

Another study investigated the effects of site-specific nitration and dityrosine bridging of tau protein in Alzheimer's disease (13). *In vitro*

peroxynitrite ($ONOO^-$) reactions with tau resulted in the formation of SDS-insoluble aggregates containing 3,3′-dityrosine (3,3′-DT). These results indicate a possible pathophysiological link between nitrative stress and Alzheimer's disease. However, at present PTN can only be confirmed as a biomarker for the disease. Nitration site-specificity will be discussed in more detail in the following section.

Protein-tyrosine nitration site-specificity

Evidence for protein-tyrosine nitration site preference

Although tyrosine comprises 3.2% of the proteome (3, 67); residue abundance does not correlate with nitration susceptibility (4, 7, 68). Random tyrosine nitration has been refuted by both *in vivo* and *in vitro* assays (3, 11, 16, 69). Fundamental requirements for Tyr nitration susceptibility are solvent accessibility and the absence of steric interference to a RNS such as $ONOO^-$. The slightly hydrophilic character imparted on Tyr imparted by the presence of a hydroxyl group on its phenolic ring is partially responsible for its localization to aqueous environments (70). In fact, 85% of Tyr residues are found in solvent-accessible environments (7, 68). Thus, PTN site-preference appears to be driven by alternative factors since most tyrosines are available for peroxynitrite-mediated nitration under normal physiological conditions (3).

Factors influencing site-specific nitration

Since nitration can alter major biological processes such as tyrosine kinase-regulated signal transduction pathways (3, 10, 18-20), identification of modification sites can help predict functional outcomes in the cell. Although high

molecular weight proteins would intuitively be more susceptible to nitration based on tyrosine abundance, experimental data show that nitration preference does not correlate with the number of available tyrosine residues on an individual protein (16). For example, β-casein (~ 2% tyrosine content), has been shown to be more susceptible to nitration than phospholipase A2, which has ~ 8% tyrosine content (16). Also preferential nitration was observed on two of 18 available sites on human serum albumin (71). Thus protein accessibility to a nitrating agent is another likely factor in nitration susceptibility.

Models for nitration susceptibility prediction

Although nitration targets specific Tyr residues, there does not appear to be a consensus sequence driving susceptibility. Rather, the microenvironment, electrostatic forces, and secondary structure appear to be the major factors influencing nitration site-preference (7, 68, 69). Souza et al. (1999) and Ischiropoulos (2003) postulated that Tyr localization near turn-inducing residues (i.e. Pro, Gly) and acidic residues (Asp, Glu) favors nitration. However, the propensity for nitration near negatively-charged and hydrophobic residues remains dubious based on recent findings (69).

Multiple consensus sequences for tyrosine nitration susceptibility have also been postulated based on experimental data from *in vitro* nitration to proteins in native conformation (3). One example is the proposed structural motif, [LMVI]X-[DE]-[LMVI]X(2,3)-[FVLI]X (3,5)**Y**, where X can be substituted for any amino acid residue (11). This model is based in part on the susceptibility of ATPase-β Tyr^{345} (3, 11) (see: *Functional Consequences*). This sequence,

simplified as L-DL---V-----Y--, is based on alignment (ClustalX) of a sparse sample set of ten proteins. Additionally, there is no indication of a consensus residue (or positive substitution) for the site adjacent to Tyr on the carboxy terminal side, and gaps of three and five amino acids are found between residues. Although this model may apply to ATPase-β and a small sample of other proteins, experimental data is too scarce to support universal applicability. Moreover, recent work has demonstrated that adjacent residues to the Tyr site can significantly influence nitration susceptibility (69).

It should also be noted that consensus sequences are primary sequences inferred from proteins reacted with nitrating agents in their native conformations. The native state allows susceptibility to be influenced by solvent accessibility and three-dimensional structure, conditions that are likely inconsistent throughout a given proteome. In other words, a short primary sequence shared by a scant number of proteins cannot reliably predict the localization of that sequence among a vast number of alternately structured proteins. Likewise, it is unintuitive to purport primary structure as the major factor driving modification susceptibility without having isolated and tested it outside the influence of three-dimensional structure. In Chapter Two, these issues were addressed as they applied to a unique case of site-selective PTN.

Using bioinformatics for nitration site prediction

Bioinformatic prediction algorithms are also limited by a native state bias. In August 2011, Liu et al (72) published GPS YNO2 (available at http://yno2.biocuckoo.org/), a program which claims 76.51% accuracy, 50.09%

sensitivity, and 80.18% specificity for nitration site preference. However, there remains limited empirical data to validate the program's efficacy since site preference is calculated based exclusively on sparse empirical data from *in vitro* nitration reactions with proteins in their native states. Again, prediction is based on primary sequence with no experimental data relevant to primary structure influences on nitration susceptibility. In Chapter Two, nitration susceptibilities of short sequences containing amino acid substitutions with dissimilar chemical properties were isolated and tested. These data were expected to complement existing prediction programs—especially in the case of preferential nitration to adjacent tyrosine residues located within a similar microenvironment.

Limitations to protein-tyrosine nitration characterization

Dityrosine formation

As stated previously, 3NT occurs at extremely low endogenous levels and shows preference for specific proteins and sites. Moreover, a study by Pfeiffer, Schmidt, & Mayer asserts that 3NT is not the predominant product of peroxynitrite radical reaction evolved from enzymatic production of $^{\bullet}NO$ and $O_2^{\bullet-}$ (73). This study demonstrated that *in vitro* mimicry of endogenous $ONOO^-$ formation using NO generated from (*Z*)-1-{*N*-[3-aminopropyl]-*N*-[4-(3-aminopropylammonio) butyl]-amino}diazen-1-ium-1,2-diolate] (SPER/NO) and $O_2^{\bullet-}$ generated from 32.5 μM hypoxanthine/xanthine oxidase was less efficient at tyrosine nitration (nitration efficiency = 0.17%) than reaction with 70 μM authentic peroxynitrite (nitration efficiency = 4.9%). Moreover, generation of low steady-state peroxynitrite was found to result in tyrosyl radical intermediates which were

more likely to self-bond forming dityrosine than proceed through to nitro-modification to tyrosine (73).

Denitration

Another important aspect to consider in the study of PTN with regard to detection and quantification is the availability of proteins conferred with the nitro-modification for analysis at a given interval. In addition to protein turnover rates, evidence has been found that *in vivo* 3NT levels continue to diminish in conditions of proteolytic inhibition (3, 21, 74, 75)—indicating reversal of the nitro-modification. While the existence of a "denitrase" remains unresolved, current data appear to be more indicative of denitration occurring through a chemical process (3, 10, 21, 74, 75). Taken together, the results of these studies indicate that some form of denitration, either through a catalytic or chemical process, is actively diminishing the pool of nitroproteins concomitantly with increased degradation rates under normal proteolytic conditions.

Misidentification

Misidentification of 3NT can adversely affect site prediction algorithms and possibly confound our understanding of metabolic pathways modulated by PTN. Many studies have relied on MS/MS search algorithms to identify and localize site-specific nitration from large-scale experiments. Often a shotgun proteomic approach is taken, where complex mixtures of tryptic peptides from a biological sample are analyzed by a single HPLC MS/MS run (76, 77). Unfortunately, lower abundance peptides can be missed due to ion suppression (78, 79) and low-stringency database search parameters typical for processing such data may

Table 2. Evaluation of published nitropeptides by *de novo* sequencing.

Reported nitropeptide sequence*	Charge State	Actual Peptide Sequence	Charge State	Theoretical Δ m/z	Approximate theoretical resolution (M/ΔM) required to resolve ESI-generated ions of reported nitropeptides from those of actual peptides
EY*RKDLEESIR	2	KVQHELDEAEER	2	0.0000	N/A [b]
ERYAAWoxMY*TY*SGLFCVTVNPYK	3	DQEGQDVLLFIDNIFR	2	- 0.3800	2,500
Y*EEEIK	1	SIHELEK	1	-0.0840	10,000
SYKY*LLLSMVK	2	NLVHITHGEEK	2	-0.0019	350,000

[a] oxM, oxidized methionine; *nitration,

[b] Not applicable

The above table is a summary of validations of putative nitropeptides (81) using the protocol proposed by Stevens et al. (2008). The first column lists the reported nitropeptide sequences, while the third column enumerates the actual sequences as determined by manual evaluation of the published spectra to determine the likely actual peptide sequences, which were subsequently synthesized and analyzed by HPLC-MS/MS. These data demonstrate the need for stringent identification criteria for the reporting of PTN using mass spectrometric data (adapted from Stevens et al, 2008).

lead to erroneous nitration site localization (80).

For example, the Δm for nitration (+45 Da) can be mimicked by chemical modifications that occur during sample preparation such as the combined Δm imparted by asparagine deamidation to iso-Asp (Δm = +1 Da) and primary amine carbamylation (Δ m = +43 Da) (http://www.ionsource.com). The net 44 Da precursor mass increase can confound database search outputs in cases where spectra originate from an analysis allowing ≥ 2 m/z isolation width since nitration confers a Δm of +45 Da. This phenomenon resulted in the misidentified sites (81) enumerated in Table 2 as evaluated in 2008 by Stevens et al (80). Although high-resolution MS/MS analyses can produce more confident nitration site identifications using spectra derived from accurate precursor masses, manual

evaluation of putative nitropeptide spectra may remain necessary for validation (80).

To strengthen manual spectral validation, LC-MS/MS analysis of high-quality synthetic nitropeptides can be performed. The synthetic cognate peptides should elute at the authentic nitropeptides' characteristic chromatographic retention times (RT) and produce identical MS/MS spectra. With the goal of ensuring reliable data reporting for PTN, appropriate guidelines for validation and publication of MS data were proposed by Stevens et al (2008) that have been adopted by many subsequent studies.

Molecular methods for protein-tyrosine nitration study

Electrophoretic separation and immunostaining

The current standard for PTN study relies on one or two-dimensional (1D or 2D) gel electrophoresis followed by either immunochemical analyses such as western blotting or mass spectrometry. Although gel electrophoresis can yield high-resolution protein separation, it is limited to relative quantitation of 3NT with little confidence in target protein specificity. Site-specificity cannot be determined by immunochemical detection. Mass spectrometry can by employed to identify potential protein targets from 1D or 2D gels; however, site identification is rare. Moreover, redundancy among nitroprotein identifications is scarce among various methods (i.e. no single technique appears to be sufficient to identify the full complement of nitroproteins from a given protein set).

Two examples of inconsistency among nitroprotein identifications can be found in PTN studies of aging rat heart (82) and brain (81). Whole heart and

heart mitochondrial lysates were analyzed by 1D gel electrophoresis (1DE) of and 2D gel electrophoresis (2DE) of 3NT immunoprecipitates (IP) (82), while brain lysates were analyzed by either 1DE, isoelectric focusing (IEF), or combined 1DE/IEF (81).

Twenty-three nitroproteins were identified from whole heart lysate, and 34 from heart mitochondria (82). Of the 57 total nitroproteins identified, 24 were unique to 2DE and 29 to IP/1DE (82). Results from the rat brain analyses were even more contrasting as the combination of all three approaches yielded 34 total identifications, with only three unique to IEF. The latter results also contained misidentified nitropeptides (81), as outlined in Table 2. Neither study was able to confirm specific nitration sites.

Immunoblotting in parallel with Coomassie-stained gels can be exploited for locating prospective 3NT-containing bands as well as for confirmation of 3NT target molecular weights. Mass spectrometric analysis can be performed on digests of cognate bands from the 1D or 2D gels to determine likely PTN targets. However, anti-3NT antibody specificity is questionable (3) and site identification remains challenging due to insufficient starting material for MS analysis or incomplete extractions that can result in limited sequence coverage and nitropeptide omissions.

Immunoaffinity capture and chemical derivatization

Although 3NT becomes more abundant under oxidative stress conditions, it typically remains below the analytical limit of detection (LOD) for current mass-spectrometric approaches. Immunological or chemical derivatization enrichment

strategies (3, 15, 29) are often employed to acquire enough material to surpass the LOD. However, enrichments can be problematic due to unreliable antibody specificity, excessive sample processing, and generation of unwanted chemical artifacts (3). Also, mass spectrometry is limited by the separation method, amount of material, complexity of sample, sample processing, trypsin efficiency, extraction efficiency (from gel matrices), solubility and protein mass (3).

Perhaps the most widely used chemical approach has been enrichment by dithionite reduction of 3NT to aminotyrosine followed by various labeling strategies for affinity capture to facilitate detection (3, 83). However, quantitation is difficult due to the potential for aminotyrosine re-oxidation to 3NT and/or inconsistent reduction of proteins, especially surface and membrane-bound due to the instability of dithionite at room temperature (3, 9, 21, 84).

Regardless of the shortcomings inherent to immunoaffinity and chemical derivatization, Petre et al, (2012) have recently concluded that enrichment of either 3NT-containing proteins or peptides is essential to acquire enough material to exceed mass spectrometric LOD (85). Immunoaffinity continues to be subject to the aforementioned issues regarding antibody specificity and reproducibility, while chemical enrichment strategies have consistently yielded undesirable side-reactions and 3NT regeneration, precluding accurate quantitation (3, 62, 86). Inspired by the limitations to conventional molecular approaches, our major aim was to develop proteomics and mass spectrometry-based methods to improve PTN detection sensitivity facilitating accurate quantitation and better characterization of PTN with limited sample manipulation.

Mass spectrometry-based methods for protein-tyrosine nitration study

Enzymatic digestion of protein suspensions

A common method for protein and PTM identification from complex mixtures incorporates the use of a proteolytic enzyme such as trypsin (which cleaves at the carboxy termini of Arg and Lys residues, except when followed by Pro) prior to analysis. After preparing the samples in an aqueous solution at acidic pH, the peptide mixture complexity is reduced by reversed-phase high-performance liquid chromatography (HPLC)—a method that separates analytes based on their characteristic hydrophobicities (87). The peptide mixture is then delivered to a mass spectrometer for MS/MS analysis to collect peptide and peptide fragmentation mass data. Since protein identifications are dependent upon peptide identifications, this is considered a “bottom-up” proteomic approach (88, 89).

Chromatographic separation

Reversed phase HPLC is achieved by use of a pump system to deliver an aqueous peptide-containing solution to a column containing a stationary-phase composed of porous silica beads bound to long alkyl (e.g. C_{18}) chains (87, 90). The long alkyl chains create a hydrophobic environment with strong affinity for peptides containing one or more hydrophobic residues (87, 90, 91). The peptides are loaded onto the column in aqueous solvent (e.g. 0.1% formic acid in water) and are eluted in order of least to greatest hydrophobicity through introduction of organic solvent such as methanol or acetonitrile in a linear gradient over time (87, 90, 91).

Electrospray peptide ionization

As peptides elute they are delivered to the mass spectrometer as positively-charged ions, due in part to their solution pH of ~3 and an applied voltage prior to their release into the atmosphere at the ion source (92-94). The solvated charged ions are forced through a ~ 10 μm orifice where the solution forms a "Taylor Cone" (95) followed by a jet stream and a spray plume emission (Fig. 3). Electrostatic repulsion and heat help eject the peptide ions into the gas phase (92-94) as they enter the vacuum of the mass spectrometer. This entire process is termed electrospray ionization or ESI (92-94, 96). Its inventor, John Fenn, was awarded the Nobel Prize in Chemistry in 2002 (http://www.nobelprize.org).

Ion movement and mass analysis

Peptide ions enter the mass spectrometer by means of a vacuum interface and a low electrical potential in a heated capillary (ion transfer tube). As they move toward the analyzer, the ions are focused by multipole optics in an oscillating electrical field (97). The vacuum increases as electrical potential continues to decrease pulling the ions forward until they reach an ion trap—a quadrupole that has alternating RF frequency and the ability to trap the ions by quickly ramping up the electrical potential at two small quadrupoles on either end—trapping the ions in an oscillating spiral pattern controlled by direct current (DC) and RF (98-100). The trapped ions are scanned out of the trap by increasing RF voltage that resonates with all ions with mass-to-charge ratios (m/z) within the mass range of the instrument (98).

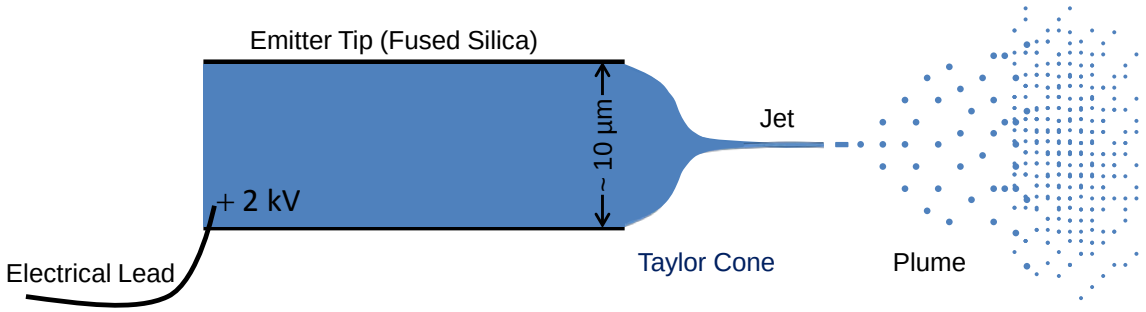

Figure 3. Electrospray ionization. Nano-flow emitters are typically constructed of 20 µm ID polyimide fused-silica tapered by pulling under flame or laser to ~ 10 µm ID. High voltage is applied to the analyte/solvent solution prior to atmospheric emission. The voltage causes a change in solvent tension that forms a solvent cone (Taylor Cone). The solvent propels forward as a jet, then atomizes into a plume of solvent spray containing analyte ions. The solvent is heat-evaporated from the analyte ions, which enter the gas phase at the interface between atmospheric pressure and the vacuum of the mass spectrometer at the heated capillary.

In full-scan mode on a linear ion trap MS, ions of all m/z are ejected sequentially to the detection system—conversion dynodes whose signals are amplified by electron multipliers (99). The calibration of the instrument is such that each ion ejected at a given frequency is of a particular m/z, while the intensity of the peak transmitted by the detector is proportional to the number of ions present. Thus, the resulting mass spectrum (MS) is a graphical representation of all the ions present and their relative intensities during a single scan.

Data-dependent tandem mass spectrometry

The ion trap also functions as a collision cell to induce fragmentation of peptide ions to produce a spectrum of daughter ions (98, 101). The trap can isolate a particular mass by scanning all other m/z out as in full-scan, while omitting the resonance frequency for the desired mass. This isolation is done

until the cell is filled with a preset number of ions (e.g. 3×10^4) of the selected m/z or for a specified time (e.g. 100 ms). Mass selection is typically within a range of $\pm$ 1 Da to account for mass error. The selected ions are then kinetically fragmented by collision with an inert gas such as helium or argon (101-103). Peptides most commonly break at their amide (peptide) bonds (101) in a process known as collision-induced dissociation (CID) (101-103). The fragment ions that retain a positive charge are ejected to the detectors as they lose stability in the trap (98) because they are no longer isobaric with the precursor m/z. The signal received by the detectors is amplified by electron multipliers where the electrical signal intensities are proportional to the abundance of the ions initially striking the conversion dynode surface. The resulting peaks represent the full spectrum of positively-charged fragment ion masses for each peptide (102, 104).

A typical tryptic peptide carries a charge of +2 imparted by protonation of the amino terminus and the terminal basic residue—either Arg or Lys. Peptide ions fragment in one location during CID, on average. One of the fragment ions typically carries the positive charge, with the fragmentation spectrum containing mainly two types of fragment ions, b-type and y-type ions (101). B-type fragment ions are those containing the amino acid residues from the amino terminus to the broken peptide bond, where y-type are those containing the residues to the C-terminus of the broken peptide bond (101). This entire process is known as tandem MS, or MS/MS (101-103) and is outlined in Figure 4.

Data-dependent scanning can be used as a “shotgun” (105) approach for identifying the majority of a proteome from a complex peptide solution based on

progressively lower full scan MS intensities. Data-dependent method parameters are set by the analyst for optimal output based on the requirements of the experiment. A typical instrument method will have a scanning cycle beginning with a full survey scan, followed by isolation of the (e.g. top ten) most intense ions from the mass spectrum (i.e. precursor ions). This process continues for the top ions from each subsequent full scan; however, previously-selected precursor masses are commonly placed on an exclusion list after one-to-several appearances in the top-10 for a set period of time related to chromatographic peak width. Thermo Scientific terms this function “Dynamic Exclusion”, which allows for lower-abundance ions to be isolated and fragmented—significantly augmenting the identification potential of the overall experiment.

Bioinformatic peptide, protein, and posttranslational modification identification

Precursor ion m/z combined with MS/MS spectra are used to identify the peptides present in a bottom-up experiment, and likewise the proteins of origin. Each spectrum can be analyzed manually to determine the peptide sequence by calculating the Δm between each pair of sequential fragment ion peaks, which is equal to the amino acid residue mass. This approach is referred to as *de novo* sequencing (106). However, data from a typical HPLC-MS/MS analysis often consists of thousands of spectra, with many containing alternate ion types (a, $c^{\bullet}$, x, $z^{\bullet}$), dehydration losses, ammonia losses and other gas phase fragmentations or rearrangements (101) that contribute to the complexity of sequence determination.

Thus, database search programs such as Mascot (107) are employed to determine peptide sequences by searching annotated databases containing comprehensive mass lists such as the UniProt knowledge base (UniProtKB, http://www.uniprot.org/). Search parameters include the expected constant modification from trypsin digestion preparation (carbamidomethyl-C) and a few possible variable modifications (e.g. Met oxidation, nitro-Tyr), as well as any of the aforementioned chemical changes that occur in gas-phase in the mass spectrometer.

Mascot identifications are often subjected to a more stringent validation process such as the Scaffold platform (108), which compares theoretical spectra including expected fragment ion intensities to the acquired spectra from the MS/MS analysis. Scaffold then scores the probabilities of all identifications using the Peptide Prophet (109) and Protein Prophet (110) algorithms based on spectrum comparison to theoretical and percentage of identified product ions for each precursor m/z. Scaffold PTM can also be a useful resource for site validation by providing a probability-based score for site-specific modifications using the Ascore (111) algorithm.

High-resolution mass spectrometry

A high-resolution hybrid linear ion trap/ FT mass analyzer (Orbitrap) can be exploited to determine precursor masses with resolving power of up to 150, 000 (112). However, resolution settings for a typical protein identification experiment range from 30,000 to 100,000 at 400 m/z to accelerate scan times. The Orbitrap analyzes mass by their specific ion frequencies as they revolve

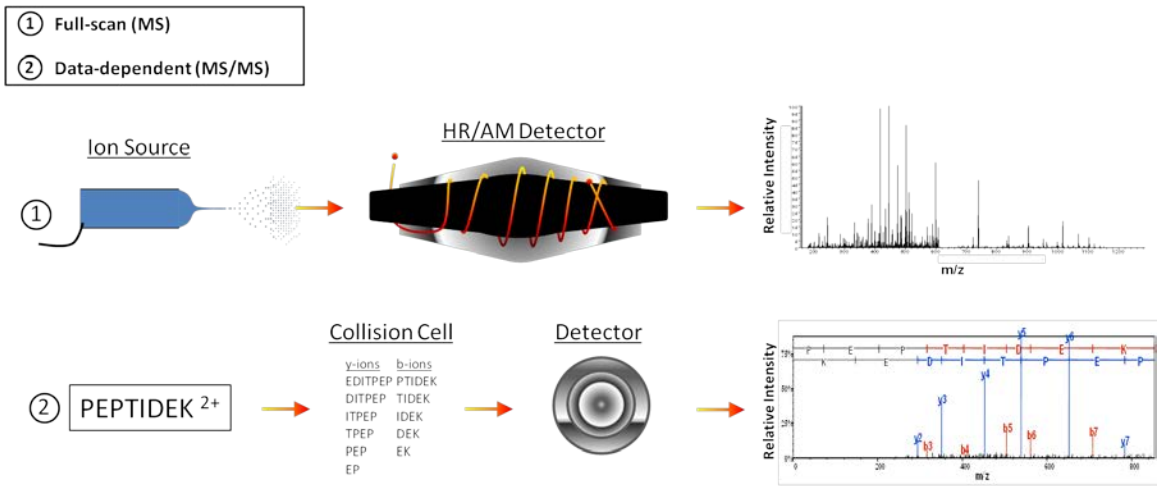

Figure 4. Data-dependent acquisition with high-resolution precursor scanning. In (1), a tryptic peptide (PEPTIDEK) is introduced to the mass spectrometer via ESI at the ion source among all ions eluting at a particular time point. Assuming it is one of the top-ten most abundant ions in the full-scan mass spectrum resulting from high resolution/accurate mass (HR/AM) analysis in the Orbitrap, PEPTIDEK (2) is isolated in the collision cell (linear ion trap mass analyzer) and fragmented by CID in helium gas. The fragment (b- and y-type) ions are scanned out of the ion trap and are amplified by dual conversion dynode electron multipliers (detector) resulting in the spectrum to the right. The spectrum shown for PEPTIDEK is an example of a typical Scaffold annotation.

around a central electrode and oscillate harmonically back and forth in the trap (112). The outer shell is an electrode-detector that records an image of all the m/z oscillation frequencies (112). The frequency (ω_z) of the axial oscillations can be used to determine all the masses present in the trap because they are dependent exclusively upon the m/z and the field curvature (k) as indicated by the relationship $\omega_z = \sqrt{\frac{k}{m/z}}$ (112). Fourier transformation (113) is then applied to determine the mass spectrum for a full scan and select the most abundant ions for MS/MS fragmentation in the linear ion trap or the high-energy collision-induced dissociation (HCD) cell, which is unique to an Orbitrap. HCD product ions are directed into an Orbitrap analyzer for high-resolution daughter ion

spectra. The high-resolution precursor masses, combined with their MS/MS spectra, furnish the analyst with high confidence peptide identifications and posttranslational modification site identification.

Orbitrap analysis can also facilitate relative quantification of low mass reporter ions such as those used in iTRAQ (Life Technologies, Grand Island, NY, USA) post-digestion chemical labeling by taking advantage of HCD fragmentation and the extended m/z range of an Orbitrap mass analyzer. An Orbitrap also allows for identification of low mass immonium ions resulting from internal peptide fragmentation, such as the characteristic 181.06 Da 3NT diagnostic ion, in cases where the precursor mass is greater than three times the product ion mass—a limitation that applies to linear ion trap detection.

Multiple Reaction Monitoring mass spectrometry

An extremely powerful tool for quantification of analytes of known m/z and chromatographic retention time (RT) is the Triple-Stage Quadrupole MS (TSQ Ultra, Thermo, USA). A major advantage of a TSQ is its ability to determine *absolute* quantitation of specific analytes from complex mixtures. Exploiting this feature, however, requires extensive knowledge of the target analyte and pure samples for calibration and internal standard incorporation.

Multiple Reaction Monitoring (MRM) MS is a method that can be developed for a specific analyte on a TSQ. In method development mode, the analyte of choice is delivered by direct infusion—facilitating optimization of ion optic parameters that are specific to the analyte. This process improves detection sensitivity as well. Often the analyte is introduced via a “T” connector

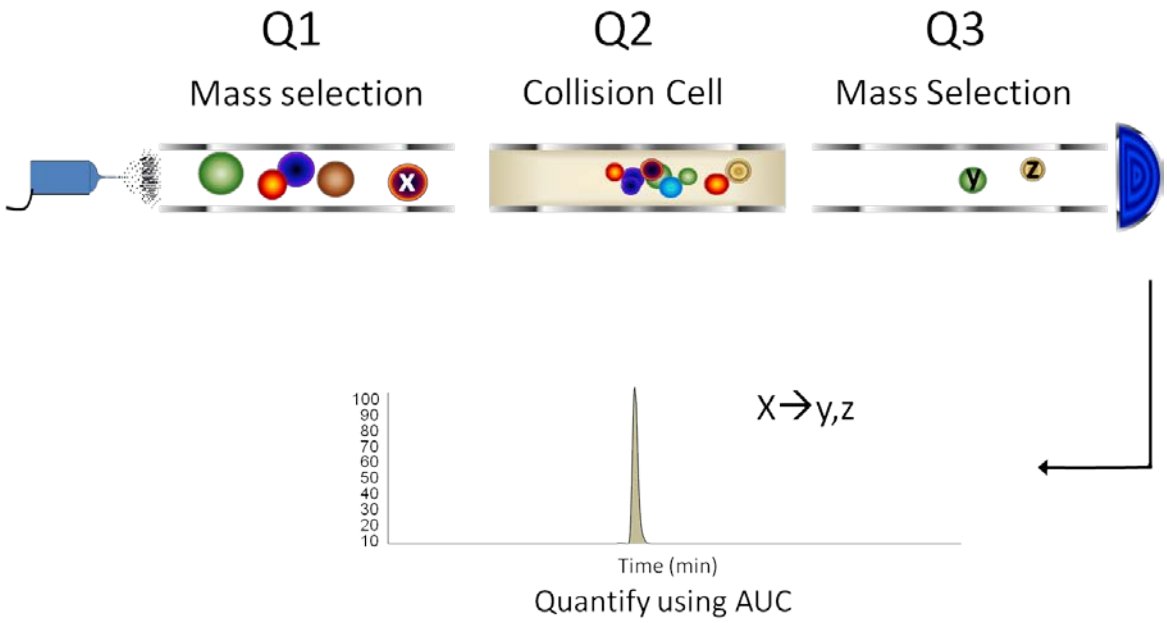

Figure 5. Multiple Reaction Monitoring mass spectrometry. A triple-stage quadrupole (Q1-Q3) mass spectrometer can be used to quantify analyte "X" from a complex mixture. In Q1, X is selected with all other m/z scanned-out. X is fragmented in the collision cell (Q2), allowing all product ions to pass to Q3. In this example, Q3 selects for the x-specific product ions, y and z, by scanning-out all other m/z. This is indicative of method optimization having been performed prior to analysis to determine X-specific product ions of most intense signal strength. The AUC for X→y, z is normalized to the AUC of an internal standard and is quantified using an external calibration curve constructed from linear regression of the resultant AUCs from serial dilution of known amounts of X.

into the HPLC solvent composition at the anticipated flow rate to optimize source parameters such as ESI voltage as well as sheath and auxiliary gas pressures.

After precursor mass optimization, a user-designated number of product (fragment, daughter) ions are detected after collision energy (CE) ramping in the collision cell. The collision cell in a Thermo TSQ Ultra is filled with argon, which imparts fragmentation proportional to CE, unlike helium (typical collision gas in a linear ion trap), which has a finite CE fragmentation limit. Product ions are

recorded hierarchically by their respective signal intensities. Once the spectrum of product ions is determined by CE ramping, CE is optimized individually for a pre-determined number of MRM transitions (product ions). These data are subsequently entered into the method for each analyte. Method optimization is performed for all relevant analytes for a given experiment including an internal standard (IS). For absolute quantitation, an IS must be present at equimolar concentration in each analytical sample. Although specifics pertinent to each experiment will dictate the appropriate processing step for IS spike-in, it is suggested that it is introduced at the earliest step possible to ensure consistency among replicates.

After MRM transition optimization is complete for all analytes of interest as well as the IS, the HPLC-MRM instrument method can be established. MRM exploits the benefits of a TSQ in the following manners for sensitive and specific analysis of the analytes of interest. First, each analyte's precursor ion is isolated as it passes through quadrupole 1 (Q1). Next each precursor is fragmented individually in the collision cell (Q2). Precursor-specific product ions (transitions) are then selected by Q3 (Fig. 5)—becoming the only ions allowed to reach the detector. The output from the detector is in the form of a peak composed of transition signal intensities throughout the elution time of each analyte. The AUC of the peak is relevant to the amount of analyte in each sample.

Another method parameter for increased sensitivity is the segment function. Data point acquisition can be improved for analyte peaks that can be resolved chromatographically. For example, if analyte A has a RT of 3.5 min,

analyte B has a RT of 5 min, and analyte C's RT is 8 min; three distinct analytical segments can be designated where only the analyte expected to elute at each time point and the IS are scanned for (i.e. A: 0-4 min, B: 4-6 min, and C: 6-10 min). Segment analysis provides for more data points across a given peak for more accurate quantitation.

Consolidated mass spectrometric method workflow

The approach of choice for nitroprotein identification and site quantitation is a consolidation of all of the aforementioned methods. First a nitration site is identified from data-dependent HPLC-MS/MS analysis on an Orbitrap. After informatics and manual spectral quality validations, it is preferred that the representative peptide prospect meet specific criteria prior to isotope-labeled synthesis of each permutation. A MRM peptide prospect must be unique to the protein of interest and be detectable in both modified and unmodified permutations. It should lack missed cleavages (unless it is consistently missed) and it should be free of variably modified residues (e.g. by oxidation) such as Cys, His, and Met.

AQUA (Thermo Scientific, USA) or similar high-quality, high-purity isotope-labeled peptides are then synthesized, representing all permutations of the variably modified peptide as well as an IS. The synthetic peptides are then analyzed by HPLC-MS/MS on the Orbitrap to validate RT and spectral characteristics. Finally, MRM optimizations are performed by the previously described method on the TSQ for each AQUA peptide. A calibration curve is generated for each target modification including the IS for normalization.

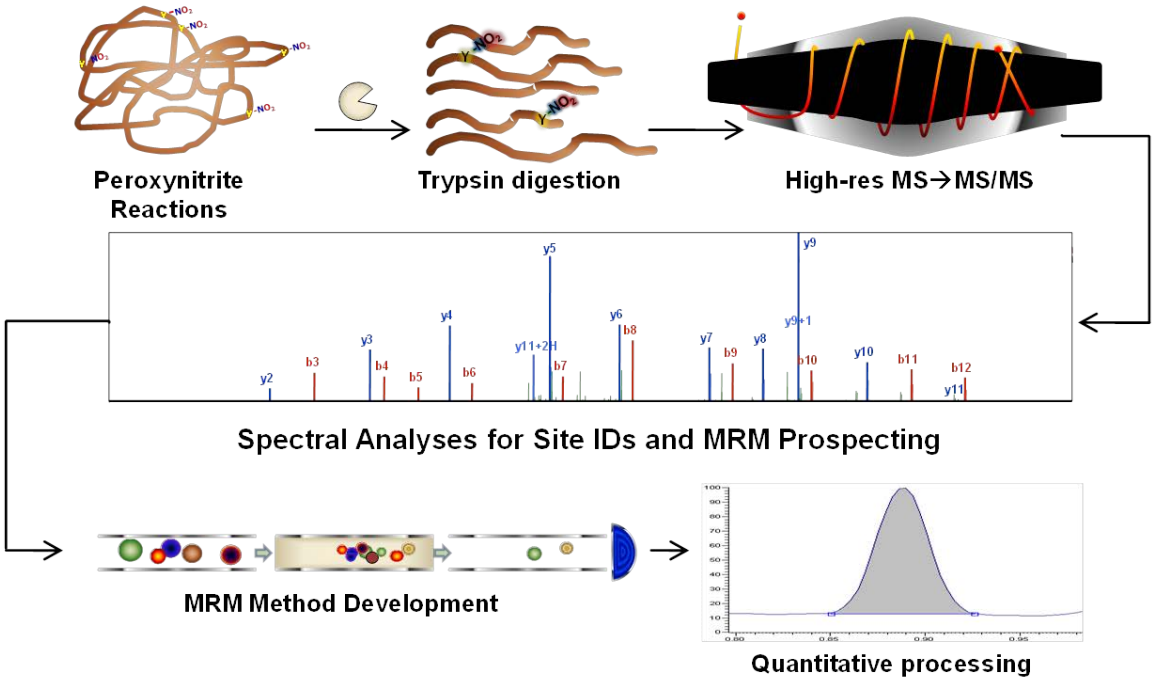

Figure 6. MS workflow for the identification and quantitation of PTN. In this example, *in vitro* peroxynitrite reactions were performed on a protein standard (BSA) to develop and test the method. Reacted protein was digested with trypsin and analyzed by HPLC-MS/MS in a LTQ Orbitrap XL. A peptide prospect meeting the MRM development criteria was identified by both Scaffold PTM and manual analysis. AQUA peptides were synthesized and MRM transition parameters were optimized. The strong signal to noise ratio depicted by the peak shown at the quantitative processing step is typical for this type of experiment as the specificity of MRM allows detection only when CID of the precursor ion results in the designated product ions within a particular time-frame. Quantitation is made by averaging the areas under the curve (AUC) for all analytical replicates of each sample, normalized to the AUCs of the IS for each replicate.

Absolute quantitative analysis can then be performed on *in vitro* treatments or biological samples.

The IS used for a calibration curve can either be diluted to a median concentration (e.g. 2.5 orders of magnitude above its LOD) for use as the solvent for serial dilution of the AQUA peptides, or it may be uniformly spiked-in to each sample prior to analysis. The IS should be introduced into the biological samples by spike-in as early as possible, typically before the desalt step to ensure

consistency among sample recoveries. Quantitation of each target analyte is performed by averaging the normalized AUCs for all analytical replicates and calculating the mass using the linear regression of the calibration standard. Figure 6 represents the entire combined workflow as it was performed using peroxynitrite-treated BSA standard in Chapter Two.

Summary of approaches and project aims

The following chapters summarize the development, optimization, and application of novel proteomic and mass-spectrometric approaches for improved PTN characterization. Chapter Two describes the development of the combined mass-spectrometric workflow described above as well its application to a PTN target identified form a peroxynitrite-treated protein standard. Chapter Two also determines the nitration susceptibility of Tyr based exclusively on primary structure influence. Chapter Three describes the application of global and targeted approaches for the identification of PTN originating from biological systems. Finally, Chapter Four describes the development of an alternative mass-spectrometric approach to improve sensitivity for PTN identification using a novel stable isotope labeling technique with low mass fragment ion screening and relative quantitation. The consolidation of these analytical methods are expected to improve the sensitivity and selectivity for PTN with the ultimate objective of providing tools that promote better characterization of PTN's role in the onset and progression of human disease. Improved PTN site prediction is also expected by taking primary structure as well as tertiary conformation into

consideration. Identification of specific protein targets and sites is expected to benefit targeted therapeutics.

References cited

1. Pfeiffer S, Leopold E, Hemmens B, Schmidt K, Werner ER, Mayer B. Interference of carboxy-PTIO with nitric oxide- and peroxynitrite-mediated reactions. Free Radical Biology and Medicine. 1997;22(5):787-94.

2. Pfeiffer S, Schmidt K, Mayer B. Dityrosine formation outcompetes tyrosine nitration at low steady-state concentrations of peroxynitrite. Journal of Biological Chemistry. 2000 March 3;275(9):6346-52.

3. Abello N, Kerstjens HAM, Postma DS, Bischoff R. Protein tyrosine nitration: Selectivity, physicochemical and biological consequences, denitration, and proteomics methods for the identification of tyrosine-nitrated proteins. Journal of Proteome Research. 2009 07/06;8(7):3222-38.

4. Ischiropoulos H. Biological tyrosine nitration: A pathophysiological function of nitric oxide and reactive oxygen species. Arch Biochem Biophys. 1998 Aug;356(1):1-11.

5. Neumann H, Hazen JL, Weinstein J, Mehl RA, Chin JW. Genetically encoding protein oxidative damage. J Am Chem Soc. 2008 03/01;130(12):4028-33.

6. Pfeiffer S, Lass A, Schmidt K, Mayer B. Protein tyrosine nitration in cytokine-activated murine macrophages. Journal of Biological Chemistry. 2001 September 07;276(36):34051-8.

7. Ischiropoulos H. Biological selectivity and functional aspects of protein tyrosine nitration. Biochem Biophys Res Commun. 2003 JUN 6;305(3):776-83.

8. Batthyany C, Souza JM, Duran R, Cassina A, Cervenansky C, Radi R. Time course and site(s) of cytochrome c tyrosine nitration by peroxynitrite. Biochemistry. 2005 06/01;44(22):8038-46.

9. Aulak KS, Koeck T, Crabb JW, Stuehr DJ. Dynamics of protein nitration in cells and mitochondria. American Journal of Physiology - Heart and Circulatory Physiology. 2004 January 01;286(1):H30-8.

10. Koeck T, Fu X, Hazen SL, Crabb JW, Stuehr DJ, Aulak KS. Rapid and selective oxygen-regulated protein tyrosine denitration and nitration in mitochondria. Journal of Biological Chemistry. 2004 June 25;279(26):27257-62.

11. Elfering SL, Haynes VL, Traaseth NJ, Ettl A, Giulivi C. Aspects, mechanism, and biological relevance of mitochondrial protein nitration sustained by mitochondrial nitric oxide synthase. American Journal of Physiology - Heart and Circulatory Physiology. 2004 January 01;286(1):H22-9.

12. Abriata LA, Cassina A, Tórtora V, Marín M, Souza JM, Castro L, et al. Nitration of solvent-exposed tyrosine 74 on cytochrome c triggers heme iron-methionine 80 bond disruption: Nuclear magnetic resonance and optical spectroscopy studies. Journal of Biological Chemistry. 2009 January 02;284(1):17-26.

13. Reynolds MR, Berry RW, Binder LI. Nitration in neurodegeneration: Deciphering the “Hows” “nYs”. Biochemistry (N Y). 2007 06/01; 2012/12;46(25):7325-36.

14. Giasson BI, Duda JE, Murray IVJ, Chen Q, Souza JM, Hurtig HI, et al. Oxidative damage linked to neurodegeneration by selective α-synuclein nitration in synucleinopathy lesions. Science. 2000 November 3, 2000;290(5493):985-9.

15. Herce-Pagliai C, Kotecha S, Shuker DEG. Analytical methods for 3-nitrotyrosine as a marker of exposure to reactive nitrogen species: A review. Nitric Oxide. 1998 10;2(5):324-36.

16. Gunaydin H, Houk KN. Mechanisms of peroxynitrite-mediated nitration of tyrosine. Chem Res Toxicol. 2009 05/18;22(5):894-8.

17. Jiao K, Mandapati S, Skipper PL, Tannenbaum SR, Wishnok JS. Site-selective nitration of tyrosine in human serum albumin by peroxynitrite. Anal Biochem. 2001 6/1;293(1):43-52.

18. Kielbasa W, Fung H. Nitrite inhalation in rats elevates tissue NOSIII expression and alters tyrosine nitration and phosphorylation. Biochem Biophys Res Commun. 2000 Aug 28;275(2):335-42.

19. Monteiro HP. Signal transduction by protein tyrosine nitration: Competition or cooperation with tyrosine phosphorylation-dependent signaling events? Free Radical Biology and Medicine. 2002 9/15;33(6):765-73.

20. Luo C, Durgin BG, Watanabe N, Lam E. Defining the functional network of epigenetic regulators in arabidopsis thaliana. Mol Plant. 2009 /7/1;2(4):661-74.

21. Kuo W, Kanadia RN, Shanbhag VP, Toro R. Denitration of peroxynitrite-treated proteins by ‘protein nitratases’ from rat brain and heart. Molecular and Cellular Biochemistry. 1999;201(1):11-6.

22. Ferrer-Sueta G, Radi R. Chemical biology of peroxynitrite: Kinetics, diffusion, and radicals. ACS Chemical Biology. 2009 03/20;4(3):161-77.

23. Muijsers RBR, Folkerts G, Henricks PAJ, Sadeghi-Hashjin G, Nijkamp FP. Peroxynitrite: A two-faced metabolite of nitric oxide. Life Sci. 1997 4/18;60(21):1833-45.

24. Beckman JS, Beckman TW, Chen J, Marshall PA, Freeman BA. Apparent hydroxyl radical production by peroxynitrite: Implications for endothelial injury from nitric oxide and superoxide. Proceedings of the National Academy of Sciences. 1990 February 01;87(4):1620-4.

25. Kirsch M, de Groot H. Formation of peroxynitrite from reaction of nitroxyl anion with molecular oxygen. J Biol Chem. 2002 April 19, 2002;277(16):13379-88.

26. Beckman JS, Ischiropoulos H, Zhu L, van der Woerd M, Smith C, Chen J, et al. Kinetics of superoxide dismutase- and iron-catalyzed nitration of phenolics by peroxynitrite. Arch Biochem Biophys. 1992 11/1;298(2):438-45.

27. Elfering SL, Haynes VL, Traaseth NJ, Ettl A, Giulivi C. Aspects, mechanism, and biological relevance of mitochondrial protein nitration sustained by mitochondrial nitric oxide synthase. American Journal of Physiology - Heart and Circulatory Physiology. 2004 January 01;286(1):H22-9.

28. Radi R. Nitric oxide, oxidants, and protein tyrosine nitration. Proc Natl Acad Sci U S A. 2004 Mar 23;101(12):4003-8.

29. Duncan MW. A review of approaches to the analysis of 3-nitrotyrosine. Amino Acids. 2003 12/01;25(3):351-61.

30. Riordan JF, Sokolovsky M, Vallee BL. Tetranitromethane. A reagent for the nitration of tyrosine and tyrosyl residues of Proteins1. J Am Chem Soc. 1966 09/01; 2013/01;88(17):4104-5.

31. Riordan JF, Sokolovsky M, Vallee BL. Environmentally sensitive tyrosyl residues. nitration with tetranitromethane*. Biochemistry (N Y). 1967 01/01; 2013/01;6(1):358-61.

32. Sokolovsky M, Riordan JF, Vallee BL. Tetranitromethane. A reagent for the nitration of tyrosyl residues in proteins*. Biochemistry (N Y). 1966 11/01; 2013/01;5(11):3582-9.

33. Sokolovsky M, Riordan JF. On the use of tetranitromethane as a nitration reagent for tyrosyl residues. FEBS Lett. 1970 /8/17/;9(4):239-41.

34. Cuatrecasas P, Fuchs S, Anfinsen CB. The tyrosyl residues at the active site of staphylococcal nuclease: Modifications by tetranitromethane. J Biol Chem. 1968 September 25, 1968;243(18):4787-98.

35. Lee SJ, Lee JR, Kim YH, Park YS, Park SI, Park HS, et al. Investigation of tyrosine nitration and nitrosylation of angiotensin II and bovine serum albumin with electrospray ionization mass spectrometry. Rapid Communications in Mass Spectrometry. 2007;21(17):2797-804.

36. Goldstein S, Merenyi G. The chemistry of peroxynitrite: Implications for biological activity. Globins and Other Nitric Oxide-Reactive Proteins, Pt a. 2008;436:49-61.

37. Beckman JS. Oxidative damage and tyrosine nitration from peroxynitrite. Chem Res Toxicol. 1996 01/01;9(5):836-44.

38. Salvemini D, Doyle TM, Cuzzocrea S. Superoxide, peroxynitrite and oxidative/nitrative stress in inflammation. Biochem Soc Trans. 2006;34:965-70.

39. Giulivi C, Poderoso JJ, Boveris A. Production of nitric oxide by mitochondria. Journal of Biological Chemistry. 1998 May 01;273(18):11038-43.

40. Xie Q, Nathan C. The high-output nitric oxide pathway: Role and regulation. J Leukoc Biol. 1994 11/01;56(5):576-82.

41. Moncada S, Palmer RM, Higgs EA. Nitric oxide: Physiology, pathophysiology, and pharmacology. Pharmacological Reviews. 1991 June 01;43(2):109-42.

42. Pacher P, Beckman JS, Liaudet L. Nitric oxide and peroxynitrite in health and disease. Physiological Reviews. January 2007 January 2007;87(1):315-424.

43. Hill BG, Dranka BP, Bailey SM, Lancaster JR, Darley-Usmar VM. What part of NO don't you understand? some answers to the cardinal questions in nitric oxide biology. Journal of Biological Chemistry. 2010 June 25;285(26):19699-704.

44. Beckman J, Koppenol W. Nitric oxide, superoxide, and peroxynitrite: The good, the bad, and the ugly. American Journal of Physiology-Cell Physiology. 1996 NOV;271(5):C1424-37.

45. Giulivi C. Functional implications of nitric oxide produced by mitochondria in mitochondrial metabolism. Biochem J. 1998 Jun 15, 1998;332(3):673-9.

46. Sarkela TM, Berthiaume J, Elfering S, Gybina AA, Giulivi C. The modulation of oxygen radical production by nitric oxide in mitochondria. Journal of Biological Chemistry. 2001 March 09;276(10):6945-9.

47. Bartesaghi S, Ferrer-Sueta G, Peluffo G, Valez V, Zhang H, Kalyanaraman B, et al. Protein tyrosine nitration in hydrophilic and hydrophobic environments. Amino Acids. 2007 05/01;32(4):501-15.

48. Schöneich C, Sharov VS. Mass spectrometry of protein modifications by reactive oxygen and nitrogen species. Free Radical Biology and Medicine. 2006 11/15;41(10):1507-20.

49. Ghesquière B, Colaert N, Helsens K, Dejager L, Vanhaute C, Verleysen K, et al. In vitro and in vivo protein-bound tyrosine nitration characterized by diagonal chromatography. Molecular & Cellular Proteomics. 2009 December 01;8(12):2642-52.

50. Guingab-Cagmat JD, Stevens SM, Ratliff MV, Zhang Z, Gold MS, Anagli J, et al. Identification of tyrosine nitration in UCH-L1 and GAPDH. Electrophoresis. 2011;32(13):1692-705.

51. Grisolia S, Timoneda J, Hernandezyago J, Soler J, Dearriaga M. Intracellular degradation of mitochondrial-enzymes. Acta Biol Med Ger. 1981;40(10-1):1407-18.

52. Talalay P. Chemoprotection against cancer by induction of phase 2 enzymes. Biofactors. 2000 10;12(1-4):5.

53. Haynes V, Traaseth NJ, Elfering S, Fujisawa Y, Giulivi C. Nitration of specific tyrosines in FoF1 ATP synthase and activity loss in aging. American Journal of Physiology - Endocrinology And Metabolism. 2010 May 01;298(5):E978-87.

54. Haynes V, Traaseth NJ, Elfering S, Fujisawa Y, Giulivi C. Nitration of specific tyrosines in FoF1 ATP synthase and activity loss in aging. American Journal of Physiology - Endocrinology And Metabolism. 2010 May 01;298(5):E978-87.

55. Fujisawa Y, Kato K, Giulivi C. Nitration of tyrosine residues 368 and 345 in the beta-subunit elicits F0F1-ATPase activity loss. Biochem J. 2009 Oct 15;423:219-31.

56. Beckman JS, Carson M, Smith CD, Koppenol WH. ALS, SOD and peroxynitrite. Nature. 1993 08/12;364(6438):584-.

57. Gold L. The role for transforming growth factor-beta (TGF-beta) in human cancer. Crit Rev Oncog. 1999;10(4):303-60.

58. Spisni E, Bartolini G, Orlandi M, Belletti B, Santi S, Tomasi V. Prostacyclin (PGI2) synthase is a constitutively expressed enzyme in human endothelial cells. Exp Cell Res. 1995 /8;219(2):507-13.

59. Schmidt P, Youhnovski N, Daiber A, Balan A, Arsic M, Bachschmid M, et al. Specific nitration at tyrosine 430 revealed by high resolution mass spectrometry as basis for redox regulation of bovine prostacyclin synthase. J Biol Chem. 2003 April 11, 2003;278(15):12813-9.

60. Spisni E, Griffoni C, Santi S, Riccio M, Marulli R, Bartolini G, et al. Colocalization prostacyclin (PGI2) Synthase–Caveolin-1 in endothelial cells and new roles for PGI2 in angiogenesis. Exp Cell Res. 2001 5/15;266(1):31-43.

61. Feng Y, Venema VJ, Venema RC, Tsai N, Caldwell RB. VEGF induces nuclear translocation of flk-1/KDR, endothelial nitric oxide synthase, and caveolin-1 in vascular endothelial cells. Biochem Biophys Res Commun. 1999 /3/5/;256(1):192-7.

62. Yeo W, Lee S, Lee J, Kim K. Nitrosative protein tyrosine modifications: Biochemistry and functional significance. BMB Reports. 2008;41(3):194-203.

63. Zhang Q, Qian W, Knyushko TV, Clauss TRW, Purvine SO, Moore RJ, et al. A method for selective enrichment and analysis of nitrotyrosine-containing peptides in complex proteome samples. Journal of Proteome Research. 2007 06/01;6(6):2257-68.

64. Heijnen HFG, van Donselaar E, Slot JW, Fries DM, Blachard-Fillion B, Hodara R, et al. Subcellular localization of tyrosine-nitrated proteins is dictated by reactive oxygen species generating enzymes and by proximity to nitric oxide synthase. Free Radical Biology and Medicine. 2006 6/1;40(11):1903-13.

65. Liu B, Tewari AK, Zhang L, Green-Church KB, Zweier JL, Chen Y, et al. Proteomic analysis of protein tyrosine nitration after ischemia reperfusion injury: Mitochondria as the major target. Biochimica et Biophysica Acta (BBA) - Proteins & Proteomics. 2009 3;1794(3):476-85.

66. Cassina P, Cassina A, Pehar M, Castellanos R, Gandelman M, de Leon A, et al. Mitochondrial dysfunction in SOD1G93A-bearing astrocytes promotes motor neuron degeneration: Prevention by mitochondrial-targeted antioxidants. J Neurosci. 2008 Apr 16;28(16):4115-22.

67. Clementi C, Carloni P, Maritan A. Protein design is a key factor for subunit–subunit association. Proceedings of the National Academy of Sciences. 1999 August 17;96(17):9616-21.

68. Souza JM, Daikhin E, Yudkoff M, Raman CS, Ischiropoulos H. Factors determining the selectivity of protein tyrosine nitration. Arch Biochem Biophys. 1999 11/15;371(2):169-78.

69. Seeley KW, Stevens Jr. SM. Investigation of local primary structure effects on peroxynitrite-mediated tyrosine nitration using targeted mass spectrometry. Journal of Proteomics. 2012 3/16;75(6):1691-700.

70. Kyte J, Doolittle RF. A simple method for displaying the hydropathic character of a protein. J Mol Biol. 1982 5/5;157(1):105-32.

71. Elfering SL, Haynes VL, Traaseth NJ, Ettl A, Giulivi C. Aspects, mechanism, and biological relevance of mitochondrial protein nitration sustained by mitochondrial nitric oxide synthase. American Journal of Physiology - Heart and Circulatory Physiology. 2004 January 01;286(1):H22-9.

72. Liu Z, Cao J, Ma Q, Gao X, Ren J. GPS-YNO2: Computational prediction of tyrosine nitration sites in proteins. Molecular bioSystems. 2011;7(4):1197-204.

73. Pfeiffer S, Schmidt K, Mayer B. Tyrosine nitration is negligible at low peroxynitrite steady-state levels. Free Radical Biology and Medicine. 1999;27(Supplement 1):S84-.

74. Smallwood HS, Lourette NM, Boschek CB, Bigelow DJ, Smith RD, PaÅ¡a-ToliÄ‡ L, et al. Identification of a denitrase activity against calmodulin in activated macrophages using high-field liquid chromatography-FTICR mass spectrometry. Biochemistry (NY). 2007 09/01; 2012/12;46(37):10498-505.

75. Kamisaki Y, Wada K, Bian K, Balabanli B, Davis K, Martin E, et al. An activity in rat tissues that modifies nitrotyrosine-containing proteins. Proc Natl Acad Sci U S A. 1998 Sep 29;95(20):11584-9.

76. Link AJ, Eng J, Schieltz DM, Carmack E, Mize GJ, Morris DR, et al. Direct analysis of protein complexes using mass spectrometry. Nat Biotech. 1999 print;17(7):676-82.

77. Washburn MP, Wolters D, Yates JR. Large-scale analysis of the yeast proteome by multidimensional protein identification technology. Nat Biotech. 2001 print;19(3):242-7.

78. Annesley TM. Ion suppression in mass spectrometry. Clin Chem. 2003 Jul;49(7):1041-4.

79. Taylor PJ. Matrix effects: The achilles heel of quantitative high-performance liquid chromatography electrospray tandem mass spectrometry. Clin Biochem. 2005 4;38(4):328-34.

80. Stevens SM, Prokai-Tatrai K, Prokai L. Factors that contribute to the misidentification of tyrosine nitration by shotgun proteomics. Molecular & Cellular Proteomics. December 2008 December 2008;7(12):2442-51.

81. Hong SJ, Gokulrangan G, Schöneich C. Proteomic analysis of age dependent nitration of rat cardiac proteins by solution isoelectric focusing coupled to nanoHPLC tandem mass spectrometry. Exp Gerontol. 2007 7;42(7):639-51.

82. Kanski J, Hong SJ, Schöneich C. Proteomic analysis of protein nitration in aging skeletal muscle and identification of nitrotyrosine-containing sequences in vivo by nanoelectrospray ionization tandem mass spectrometry. Journal of Biological Chemistry. 2005 June 24;280(25):24261-6.

83. Prokai Tatrai K, Guo J, Prokai L. Selective chemoprecipitation and subsequent release of tagged species for the analysis of nitropeptides by liquid chromatography-tandem mass spectrometry. Molecular cellular proteomics. 2011;10(8).

84. Chen C, Chen J, Rawale S, Varadharaj S, Kaumaya PPT, Zweier JL, et al. Protein tyrosine nitration of the flavin subunit is associated with oxidative modification of mitochondrial complex II in the post-ischemic myocardium. Journal of Biological Chemistry. 2008 October 10;283(41):27991-8003.

85. Petre BA, Ulrich M, Stumbaum M, Bernevic B, Moise A, Doring G, et al. When is mass spectrometry combined with affinity approaches essential? A case study of tyrosine nitration in proteins. J Am Soc Mass Spectrom. 2012 Nov;23(11):1831-40.

86. Guo J, Prokai-Tatrai K, Prokai L. Relative quantitation of protein nitration by liquid chromatography–mass spectrometry using isotope-coded dimethyl labeling and chemoprecipitation. Journal of Chromatography A. 2012 4/6;1232(0):266-75.

87. Karger BL, Gant JR, Martkopf A, Weiner PH. Hydrophobic effects in reversed-phase liquid chromatography. Journal of Chromatography A. 1976 11/17;128(1):65-78.

88. Bogdanov B, Smith RD. Proteomics by FTICR mass spectrometry: Top down and bottom up. Mass Spectrom Rev. 2005 03/01;24(2):168-200.

89. Kelleher NL, Lin HY, Valaskovic GA, Aaserud DJ, Fridriksson EK, McLafferty FW. Top down versus bottom up protein characterization by tandem high-resolution mass spectrometry. J Am Chem Soc. 1999 02/01; 2013/04;121(4):806-12.

90. Stone KL, Elliott JI, Peterson G, McMurray W, Williams KR. 21] reversed-phase high-performance liquid chromatography for fractionation of enzymatic digests and chemical cleavage products of proteins. In: James A. McCloskey, editor. Methods in Enzymology. Academic Press; 1990. p. 389-412.

91. Vailaya A, Horvath C. Retention in reversed-phase chromatography: Partition or adsorption? Journal of Chromatography A. 1998 12/31;829(1):1-27.

92. Wilm M. Principles of electrospray ionization. Molecular & Cellular Proteomics. 2011 05/19.

93. McLuckey SA, Stephenson JL. Ion/ion chemistry of high-mass multiply charged ions. Mass Spectrom Rev. 1998 01/01;17(6):369-407.

94. Ogorzalek Loo RR, Udseth HR, Smith RD. A new approach for the study of gas-phase ion-ion reactions using electrospray ionization. J Am Soc Mass Spectrom. 1992 10;3(7):695-705.

95. Taylor G. Disintegration of water drops in an electric field. Proceedings of the Royal Society of London Series A, Mathematical and Physical Sciences. 1964 07/28;280(1382):383-97.

96. Fenn JB, Mann M, Meng CK, Wong SF, Whitehouse CM. Electrospray ionization for mass spectrometry of large biomolecules. Science. 1989 10/06;246(4926):64-71.

97. Stafford Jr. GC, Kelley PE, Syka JEP, Reynolds WE, Todd JFJ. Recent improvements in and analytical applications of advanced ion trap technology. International Journal of Mass Spectrometry and Ion Processes. 1984 /9/7/;60(1):85-98.

98. Louris JN, Cooks RG, Syka JEP, Kelley PE, Stafford GC, Todd JFJ. Instrumentation, applications, and energy deposition in quadrupole ion-trap tandem mass spectrometry. Anal Chem. 1987 07/01; 2013/03;59(13):1677-85.

99. Douglas DJ, Frank AJ, Mao D. Linear ion traps in mass spectrometry. Mass Spectrom Rev. 2005 Jan-Feb;24(1):1-29.

100. March RE. Quadrupole ion trap mass spectrometry: A view at the turn of the century. International Journal of Mass Spectrometry; Volume 200: The state of the field as we move into a new millenium. 2000 12/25;200(1):285-312.

101. Tabb DL, Smith LL, Breci LA, Wysocki VH, Lin D, Yates JR. Statistical characterization of ion trap tandem mass spectra from doubly charged tryptic peptides. Anal Chem. 2003 03/01; 2013/03;75(5):1155-63.

102. Papayannopoulos IA. The interpretation of collision-induced dissociation tandem mass spectra of peptides. Mass Spectrom Rev. 1995 01/01;14(1):49-73.

103. Alexander AJ, Boyd RK. Experimental investigations of factors controlling the collision induced dissociation spectra of peptide ions in a tandem hybrid mass spectrometer. I. leucine enkephalin. International Journal of Mass Spectrometry and Ion Processes. 1989 /6/22/;90(3):211-40.

104. de Hoffmann E, Stroob V. Mass spectrometry: Principles and applications. Third ed. Somerset, NJ: Wiley & Sons; 2007.

105. Wu CC, MacCoss MJ. Shotgun proteomics: Tools for the analysis of complex biological systems. Curr Opin Mol Ther. 2002 Jun;4(3):242-50.

106. Taylor JA, Johnson RS. Sequence database searches via de novo peptide sequencing by tandem mass spectrometry. Rapid Commun Mass Spectrom. 1997 06/15;11(9):1067-75.

107. Perkins DN, Pappin DJC, Creasy DM, Cottrell JS. Probability-based protein identification by searching sequence databases using mass spectrometry data. Electrophoresis. 1999 12/01;20(18):3551-67.

108. Searle BC. Scaffold: A bioinformatic tool for validating MS/MS-based proteomic studies. Proteomics. 2010 03/01;10(6):1265-9.

109. Keller A, Nesvizhskii AI, Kolker E, Aebersold R. Empirical statistical model to estimate the accuracy of peptide identifications made by MS/MS and database search. Anal Chem. 2002 10/01;74(20):5383-92.

110. Nesvizhskii AI, Keller A, Kolker E, Aebersold R. A statistical model for identifying proteins by tandem mass spectrometry. Anal Chem. 2003 09/01;75(17):4646-58.

111. Beausoleil SA, Villen J, Gerber SA, Rush J, Gygi SP. A probability-based approach for high-throughput protein phosphorylation analysis and site localization. Nat Biotech. 2006 print;24(10):1285-92.

112. Makarov A. Electrostatic axially harmonic orbital trapping: A high-performance technique of mass analysis. Anal Chem. 2000 03/01; 2013/02;72(6):1156-62.

113. Fourier JBJ. Théorie analytique de la chaleur. Paris: Chez Firmin Didot, père et fils; 1822.

Chapter Two: Investigation of local primary structure effects on peroxynitrite-mediated tyrosine nitration using targeted mass spectrometry

Introduction

Overview

Endogenous nitration remains difficult to characterize with conventional biochemical strategies. Immunochemical methods are limited to relative quantitation, are suspect in terms of antibody specificity, and are not informative in terms of protein identification or site localization. HPLC and gas chromatography (GC)-MS approaches typically require chemical derivatization and enrichment prior to analysis (1-3), negatively affecting reproducibility due to multiple sample preparation steps. Quantitation is also compromised due to incomplete reactions and chemical byproduct formation (1, 4). Moreover, published works annotating putative nitration sites have often neglected to follow appropriate guidelines for mass spectrometric data reporting (5), diminishing confidence in site identifications and purported nitration susceptibility factors. This chapter describes an approach designed to increase PTN detection sensitivity and site-specific quantitation via a consolidated mass spectrometric workflow (Chapter One, Fig. 6). The workflow combines high resolution MS screening with multiple reaction monitoring (MRM). MRM analyses effectively

quantified PTN site-preference on a unique BSA peptide as well as nitration susceptibility influenced exclusively by local primary structure.

Nitration site preference

HPLC-MS/MS analysis on an Orbitrap identified a unique nitropeptide (DAFLGSFLYEY$^{(nitro)}$SR) resulting from peroxynitrite reactions with bovine serum albumin (BSA). Preferential nitration to Tyr^{11} was evident—a phenomenon that merited further exploration considering the proximity of Tyr^{9}. MRM prospecting was performed by manual spectral and Scaffold PTM analyses to validate the site and site-preference probability (100% based on the Ascore algorithm).

Secondary structure influence on nitration susceptibility

Since DAFLGSFLYEY$^{(nitro)}$SR met our previously-described prototype peptide selection parameters, three synthetic stable isotope-labeled (AQUA, Thermo Scientific, USA) peptides (DAFLGSFLYEYSR$^{[13C,15N]}$, DAFLGSFLYEY$^{[3\text{-}nitro]}$SR$^{[13C,15N]}$, and DAFLGSFLY$^{[3\text{-}nitro]}$EYSR$^{[13C,15N]}$) were synthesized representing three of the possible four nitration-states (doubly-nitrated could not be synthesized). Since retention times and spectral characteristics of DAFLGSFLYEYSR and DAFLGSFLYEY$^{(nitro)}$SR were consistent with previous analyses, MRM transitions were optimized for all three permutations—allowing for quantitative analysis of variant nitration.

To test the influence of secondary structure on site preference, isotope label-free DAFLGSFLYEYSR (USF Department of Chemistry) was synthesized. MRM analysis of the products of $ONOO^-$ reaction with the synthetic peptide allowed for relative quantitation of nitration site preference due to MRM outputs

and chromatographic resolution of the two permutations (Chapter Two, Fig. 3A). The results of free nitro-DAFLGSFLYEYSR analysis indicated significant Tyr^{11} site preference, albeit to a lesser degree than native state BSA. In light of these results, we hypothesized that local primary structure influences selective nitration to specific Tyr residues in cases where more than one residue occupies a similar structural location and chemical environment.

Primary structure influence on nitration susceptibility

A novel method devised in 2001 successfully eliminated secondary structure to ascertain peptide local primary structure influence on deamidation rates of glutaminyl and asparaginyl residues (6). The approach incorporated synthesis of a complete library of the 800 possible adjacent residue combinations using the 20 ordinary amino acids with glycine termini, resulting in pentapeptides devoid of secondary conformation influence on deamidation (6).

The pentapeptides were analyzed via direct loop ESI injections into a Thermoquest (San Jose, CA, USA) LCQ ion-trap mass spectrometer. Enhanced-resolution (zoom) scans of the expected precursor masses were performed for eighteen injections of each sample (representing one time-point between 4 and 102 days). The percentage of deamidated peptide was determined by comparison of the contribution of each isotopic peak as compared to the naturally-occurring isotope ratios (Note: deamidation results in a Δm of +1 Da).

In this study, a modified method using a truncated pentapeptide library based on the adjacent residues to both tyrosines in DAFLGSFLYEYSR was used

to gain direct insight into local primary structure influence on Tyr nitration susceptibility. This approach was expected to elucidate the chemical properties influencing peroxynitrite-mediated nitration site-specificity and yield powerful data to enhance site prediction algorithm accuracy.

Results

The results for Chapter Two are contained in a previously published work (7) and can be found in Appendices A-D. The article has been reproduced with express consent of the publisher (see Appendix E).

References cited

1. Abello N, Kerstjens HAM, Postma DS, Bischoff R. Protein tyrosine nitration: Selectivity, physicochemical and biological consequences, denitration, and proteomics methods for the identification of tyrosine-nitrated proteins. Journal of Proteome Research. 2009 07/06;8(7):3222-38.

2. Prokai Tatrai K, Guo J, Prokai L. Selective chemoprecipitation and subsequent release of tagged species for the analysis of nitropeptides by liquid chromatography-tandem mass spectrometry. Molecular cellular proteomics. 2011;10(8).

3. Zhang Q, Qian W, Knyushko TV, Clauss TRW, Purvine SO, Moore RJ, et al. A method for selective enrichment and analysis of nitrotyrosine-containing peptides in complex proteome samples. Journal of Proteome Research. 2007 06/01;6(6):2257-68.

4. Duncan MW. A review of approaches to the analysis of 3-nitrotyrosine. Amino Acids. 2003 12/01;25(3):351-61.

5. Stevens SM, Prokai-Tatrai K, Prokai L. Factors that contribute to the misidentification of tyrosine nitration by shotgun proteomics. Molecular & Cellular Proteomics. December 2008 December 2008;7(12):2442-51.

6. Robinson NE, Robinson AB. Molecular clocks. Proceedings of the National Academy of Sciences of the United States of America. 2001 January 30;98(3):944-9.

7. Seeley KW, Stevens Jr. SM. Investigation of local primary structure effects on peroxynitrite-mediated tyrosine nitration using targeted mass spectrometry. Journal of Proteomics. 2012 3/16;75(6):1691-700.

Chapter Three: Application of global-scale and targeted approaches for the identification of protein-tyrosine nitration in biological systems

Introduction

Overview

As discussed previously in Chapters One and Two, nitration occurs near $O_2^{\bullet-}$ generation centers such as the mitochondrial matrix (Fig. 7), peroxisomes of liver cells, and near sites of injury (1, 2). Peroxynitrite's reactivity is diffusion-limited (3, 4) defined by its short half life of less than one second (5, 6). Thus, the early focus of this study was PTN in liver mitochondria. Another area of interest was the brain, where activation of the resident immune cells, microglia, contributes to oxidative/nitrative stress. A hallmark of classical microglia activation is increased expression of iNOS—which, in conjunction with ROS produced in the oxidative burst, is thought to promote peroxynitrite generation and subsequent PTN. Both of these systems served as biological models of nitrative stress allowing us to apply the workflow developed in Chapter Two.

To characterize a potential causative role for PTN in disease, baseline nitration must be determined under normal conditions. Then, global changes to tyrosine nitration profiles can be assayed upon introduction of oxidative/nitrative stress triggers. Nitration target protein identifications can elucidate the specific pathways affected by oxidative/nitrative stress-induced PTN. Finally, to fully

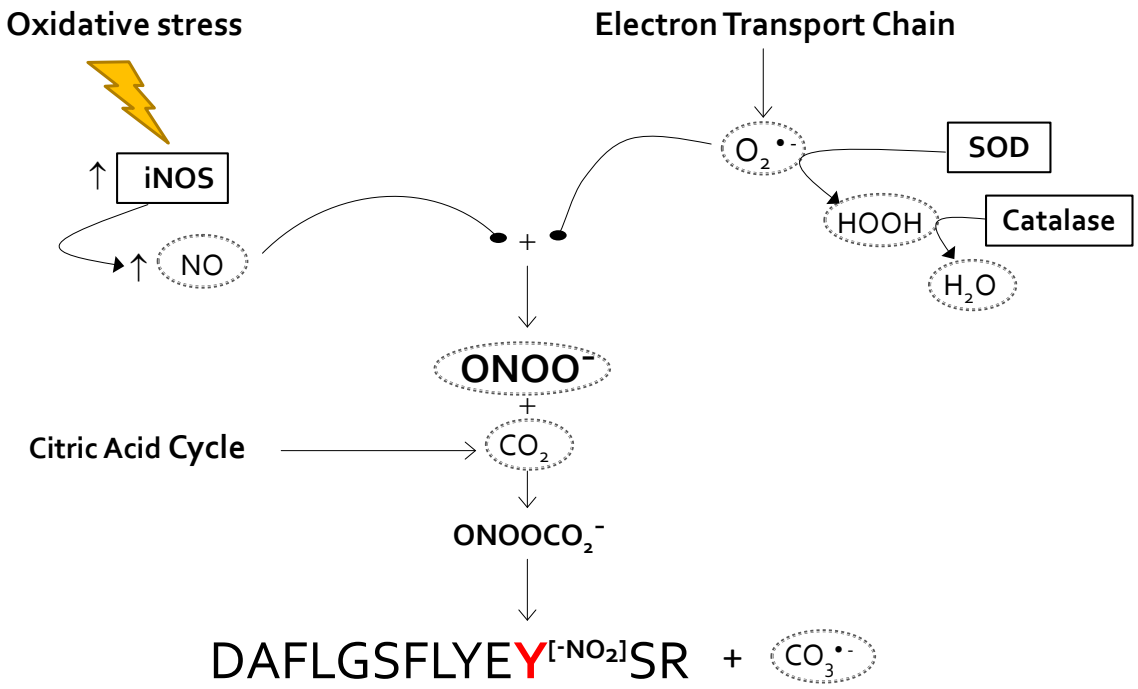

Figure 7. Tyrosine nitration in the mitochondrial matrix. Energy metabolism normally results in some electron "leakage" from the electron transport chain. Partial reduction of oxygen can lead to $O_2^{\bullet-}$ formation. Most superoxide is reduced to H_2O_2 by SOD and subsequently converted to water and molecular oxygen by catalase. However, under oxidative stress conditions, iNOS upregulation results in increased NO, which reacts with $O_2\bullet^-$ to form the highly-reactive $ONOO^-$ anion. Peroxynitrite reacts with CO_2 originating from the citric acid cycle to form nitrosoperoxycarbonate, which facilitates nitration by the radical pathway outlined in Figure 2.

ascertain the functional consequences of PTN, specific nitration sites must be both identified and quantified from biological systems in normal conditions and while undergoing oxidative/nitrative stress. Our approach was to comprehensively investigate PTN in liver mitochondria and activated microglia to elucidate the proteins and pathways involved in the onset and progression of oxidative/nitrative stress-induced disease states.

Protein-tyrosine nitration in the liver

Ethanol-induced oxidative/nitrative stress

It is well-established that oxidative stress induced by chronic alcohol (ethanol) abuse is a major contributor to liver damage (7-16). Both chronic and acute ethanol exposures increase reactive oxygen species (ROS) and reactive nitrogen species (RNS) in hepatocytes (7, 8, 11, 12, 14). Hepatotoxicity from oxygen and nitrogen radical formation can occur through either a direct pathway involving ethanol metabolism in the liver (12-15) or through an indirect pathway initiated by endotoxin-induced activation of Kupffer cells—the resident macrophages of the liver (8, 9, 16, 17).

Direct route for ethanol-induced hepatotoxicity

Direct ethanol-induced hepatotoxicity may result from impaired mitochondrial function (8, 10, 12, 14) or over-production of acetaldehyde by either alcohol dehydrogenase or cytochrome P450 2E1 (CYP2E1) (8, 11, 13, 15). ROS and RNS generated from these pathways can induce the release of tumor necrosis factor alpha (TNF-α) (8, 14, 15) or cytochrome *c* (7, 14, 18, 19) resulting in hepatocyte injury or apoptosis (Fig 8).

Indirect route for ethanol-induced hepatotoxicity

Indirect hepatotoxicity from ethanol exposure involves exorbitant release of the endotoxin, lipopolysaccharide (LPS), from resident gut flora (7-9, 14, 16). Ethanol increases the permeability of the gastrointestinal tract promoting direct passage of LPS produced by gram-negative bacteria to the liver (8, 9, 16). Kupffer cells residing in the liver are activated by LPS through CD14, a surface

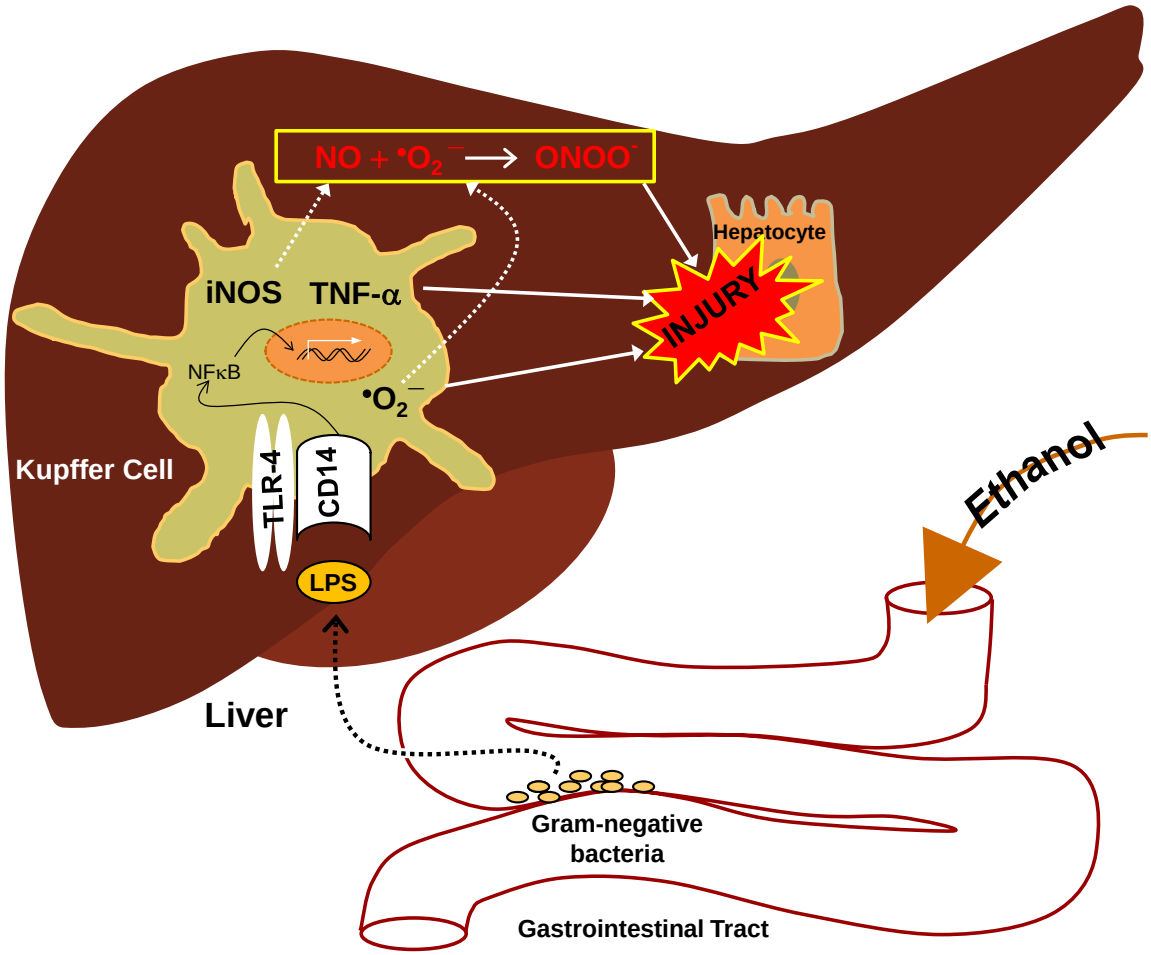

Figure 8. Indirect ethanol-induced hepatotoxicity. Ethanol perforates the GI tract resulting in LPS release into the blood stream and direct contact with the liver. Kupffer cells activated by LPS interaction with CD14 produce NFκB, which induces TNF-α, iNOS, and superoxide production. TNF-α and $O_2^{\bullet -}$ are released in response to the presence of endotoxin resulting in hepatocyte injury. Inducible NOS upregulation can promote $ONOO^-$ formation and additional injury through PTN.

receptor that has toll-like receptor 4 (TLR-4) co-receptor activity (8, 9, 20). Kupffer activation results in inflammatory cytokine (e.g. TNF-α) and $O_2^{\bullet -}$ release (7-9, 14), as well as NO via iNOS upregulation (8, 21). These factors represent ideal conditions for $ONOO^-$ formation than can result in PTN—further contributing to tissue damage.

Protein-tyrosine nitration resulting from oxidative/nitrative stress

Although PTN is seen as a biological marker for ethanol-induced oxidative stress (8, 9, 17), a causative role in ethanol-induced hepatic injury has yet to be established. We hypothesized that oxidative/nitrative stress induced by ethanol increases $ONOO^-$ levels and PTN in mitochondria, resulting in hepatotoxicity through either attenuated energy metabolism or diminished ROS scavenging by enzymes with antioxidant activity (e.g. superoxide dismutase II). However, elucidation of changes to the mitochondrial nitroproteome under oxidative/nitrative stress would first necessitate establishment of a PTN baseline occurring under normal conditions. Our approach was to develop an analytical workflow sensitive enough to detect and quantify nitration in liver mitochondria, with the long-term goal of PTN quantitation between liver mitochondria from either normal or ethanol-treated experimental groups. Alcohol's direct (8, 10, 12, 14) or indirect (7-9, 14, 17) roles in hepatotoxicity have common elements with those involved in neurotoxicity, which are outlined in more detail in the following section.

Protein-tyrosine nitration in the brain

Overview

In the brain, oxidative stress from inflammatory triggers such as alcohol and LPS promotes iNOS expression (22). Increased NO is generated concomitantly with increased ROS, including $O_2^{\bullet-}$, resulting in $ONOO^-$ formation and cytotoxicity. These properties may define the role of iNOS in host immunity (23), enabling its participation in anti-microbial and anti-tumor activities as part of

the macrophage oxidative burst. However, as in Kupffer activity, they are also damaging to the host (23). Although injury caused by acute stress is typically temporary, chronic insult by inflammatory triggers may result in protracted damage and complications. Thus, characterization of the pathways affected by oxidative/nitrative stress-induced PTN is expected to provide insight into the long-term consequences of ethanol abuse such as neuroinflammation.

Since nitration is implicated in multiple neurological disease states (24-26), our aim was to determine PTN's role in oxidative/nitrative stress pathologies in the brain. Specifically, the effects of LPS and ethanol-induced oxidative stress in neuron-like cells (B35 neuroblastoma; ATCC CRL2754) and highly aggressively proliferating immortal (HAPI) microglia (27), the resident macrophages in the brain and spinal cord (27-30) were investigated. PTN resulting from oxidative/nitrative stress was assayed after both direct and indirect microglial activation (30). Preliminary data from this study have established B35 and HAPI cell lines as a relevant *in vitro* model system to study oxidative/nitrative stress-induced nitration in the brain (30).

Microglia

Microglia are a special type of tissue-localized macrophage that comprise 10% of cells in the central nervous system (28). Microglial progenitor lineage is divergent from bone marrow-derived macrophages in that their development is independent of the transcription factor Myb (31). The disparate developmental regulation between the two cell lines is thought to result in distinct populations of functionally variant immune cells (28, 32, 33).

Microglial activation (general)

Microglia are normally inhibited by neurons through contact-dependent receptor-ligand interactions as well as through neuronal secretions such as fractalkine (28, 34). Likewise, attenuation of these signals can be activating (28). Neuronal activation of microglia can also occur through secretion of α-synuclein (35) and NFκB (36). Classical activation can also be stimulated through direct interaction with exogenous molecules such as LPS (20). Classical activation is characterized by the release of free radicals and inflammatory cytokines in response to the presence of exogenous triggers or neuronal injury (29, 37, 38).

We aimed to exploit these activation pathways to test our hypothesis that activated microglia exhibit increased PTN and that it plays a role in a previously-described non-classical microglial activation phenotype induced by alcohol (39, 40). Our approach was to induce activation directly through exogenous microglial stimulation by LPS and indirectly through secretions from neurons exposed to ethanol. The resulting microglial proteome and sub-proteome was analyzed by anti-3NT western blotting and mass spectrometric methods described in Chapters One and Two such as data-dependent and site-targeted HPLC-MS/MS, with the ultimate goal of quantifying site-specific nitration of neurotoxicologically-relevant targets.

Direct microglial activation

LPS is a TLR4 ligand that has been shown to activate the microglia-mediated inflammatory process (20, 28, 41). LPS-induced microglial activation results in upregulation of iNOS, which is thought to have ROS scavenging activity

in oxidative stress conditions (42). Inducible NOS expression occurs concomitantly with the pro-apoptotic release of caspase-3/7 (28, 41, 43) downstream of TLR4 as seen in a Parkinson's disease model (28, 44) and has recently been implicated as a component of LPS-induced inflammatory response in microglia (30).

LPS activation also stimulates increased superoxide ($O_2^{\bullet -}$) production via nicotinamide adenine dinucleotide phosphate (NADPH)-oxidase (45, 46), potentially exacerbating $ONOO^-$ formation. Evidence supporting LPS-induced $ONOO^-$ increase has been previously demonstrated in rat neuron-glia cultures (47) and primary microglial cells harvested from Fisher 344 rat pup brains (41, 45).

Indirect microglial activation

As in the case of LPS-induced inflammatory response, free radical formation upon ethanol exposure has been linked to NADPH oxidase (17). Additionally, recent experiments have shown increased iNOS expression in microglia exposed to conditioned media from neuronal cells (B35) treated with 50 mM ethanol for 24 hours (30). Taken together, these results demonstrate indirect microglial activation in response to neuronal signaling under ethanol-induced oxidative stress and the potential for $ONOO^-$-mediated PTN.

Rationale for PTN study in microglia

Since ROS combined with increased NO production constitute a microenvironment conducive to peroxynitrite formation, we hypothesized that microglia would exhibit a concomitant increase in PTN upon activation by

neuronal secreted factors induced by ethanol exposure. Our aim was to confirm a global PTN increase in HAPI microglia exposed to B35-conditioned-media, unique nitroprotein target identification, and nitration site identification and quantitation to better characterize PTN's role in microglia-mediated neurodegenerative pathologies.

Materials and Methods

All reagents were purchased from Sigma-Aldrich (St. Louis, MO, USA) unless otherwise specified.

Rat liver mitochondria isolation

Rat liver mitochondria (RLM) were isolated using the following protocol from Abcam (formerly Mitosciences, Cambridge, MA, USA) unless otherwise specified. Fresh or recently thawed rat liver stored in PBS was washed twice in mitochondrial isolation buffer, divided into ~ 0.5 g sections, and minced with a scalpel on a glass slide on ice. Cell membranes were disrupted by 20-30 strokes with pestle A in a pre-chilled Dounce glass homogenizer, followed by 20-30 strokes with pestle B. Samples were centrifuged at 1,000 $\times$ g for 10 min at 4 °C to remove whole cells and nuclei. The supernatant was collected into a clean tube and spun at 12,000 $\times$ g for 15 min at 4 °C to pelletize mitochondria. The supernatant was aspirated and the pellet resuspended and washed twice by pipette in isolation buffer containing Halt Protease and Phosphatase Inhibitor Cocktail (PI; Thermo Scientific, USA) followed by centrifugation at 12,000 $\times$ g for 15 min at 4 °C. Washed pellets were resuspended in isolation buffer with PI in 1.5 mL tubes, sonicated on ice at 20% AMPL for 18 s by six 3 s pulses with

intermittent 3 s pauses to disrupt membranes and mitochondrial deoxyribonucleic acid (mtDNA). Lysates were centrifuged at 16,000 × g for 20 min at 4 °C to clarify and supernatants transferred to clean tubes. Protein concentrations were assayed by the Pierce 660 nm 96-well plate method previously described.

Rat mitochondria nitroprotein enrichments

Mitochondria from Sprague-Dawley (SD) rat liver (Harlan Laboratories, Indianapolis, IN, USA or Bioreclamation, LLC, Jericho, NY, USA) were obtained using a Mitosciences (Eugene, OR, USA) isolation kit for tissue. Briefly, mitochondria were isolated from ~ 0.4 g of tissue by homogenization in a 2.0 mL Dounce glass homogenizer with pestles followed by differential centrifugation. The mitochondrial fractions were sonicated with 6 pulses for 3 seconds (s) with 3 s pauses between at 20% amplitude (AMPL) to disrupt membranes and nucleic acids. Lysates were clarified by centrifugation at 16,000 × g for 20 min, followed by transfer of supernatant to fresh microcentrifuge tubes.

Mitochondrial lysates were assayed for protein concentration with Pierce 660 reagent (Thermo Scientific, USA) on a Powerwave XS2 microplate reader (Biotek Instruments, Inc., Bath, UK) followed by dilution to 1 mg × mL^{-1} in 1 mL aliquots. Anti-NT immunoprecipitation (IP) was performed on the lysates by addition of 50 µg anti-nitrotyrosine immunosorbent agarose (Cayman Chemical, Ann Arbor, MI, USA) to each aliquot. Immunoprecipitation was conducted on a rocking platform set to medium speed at 4 °C for 24 h. Immunoprecipitates were then washed thrice in ice-cold PBS, with the final wash aspirated to leave a pellet of 3NT-containing proteins. Proteins were eluted at 95 °C in 50 µL of 1 ×

reducing Laemmli Buffer (62.5 mM Tris-HCl, pH 6.8, 25% glycerol, 5% β-mercaptoethanol, 2% SDS, 0.01% bromophenol blue) and loaded onto an SDS-PAGE gel for protein separation. After electrophoresis, the gel was stained with Coomassie brilliant blue to determine the relative molecular weights of precipitated proteins containing 3NT.

The IP-enriched 1D gel lane was divided into five equal fractions (Fig. 11), digested with trypsin, and analyzed by HPLC-MS/MS with data-dependent acquisition on a hybrid linear quadrupole ion trap-Fourier transform (FT) orbital ion trap mass spectrometer (LTQ Orbitrap XL, Thermo Scientific, USA) equipped with XCalibur (version 2.0.7) data acquisition software to identify enriched proteins. Raw data was searched against the UniProt rat database with the Mascot (version 2.2) search engine. Scaffold (version 3.00.08, Proteome Software Inc., Portland, OR) was used to validate MS/MS based peptide and protein identifications.

Peroxynitrite reactions with rat liver mitochondrial lysate

In vitro Tyr-nitration was performed on RLM lysate (3 mg) isolated from 4.7 g of adolescent SD rat liver. The lysate was buffer-exchanged into PBS, assayed for protein content, and aliquotted into five volumes at 1 mg $\times$ mL^{-1}. Samples were reacted with 1 mM peroxynitrite for 1 h at room temperature and quenched by addition of formic acid to five percent. IP was performed as described previously using 3NT affinity sorbent with overnight incubation at 4 °C. Nitrotyrosine-containing proteins bound to agarose beads were washed and

eluted in 1 × reducing Laemmli Buffer prior to loading on SDS-PAGE gel (Fig. 13).

The gel was stained with Coomassie brilliant blue and band regions indicated by numbers 1-4 were excised and pooled in a single tube. A standard in-gel trypsin digest was performed as described below, followed by peptide extraction and analysis by HPLC-MS/MS on a LTQ Orbitrap XL (Orbitrap) mass spectrometer. The European Bioinformatics Institute's (EBI) universal protein resource database (UniProt) rat database was searched with Mascot (version 2.2), followed by peptide and protein validation using the Scaffold platform (version 3.00.08).

In-solution trypsin digestion

In solution digests were performed by the following method on all samples unless otherwise indicated. Proteins (various concentrations) were suspended in 100 µL of 6 M urea (Acros Organics, NJ, USA) and 50 mM ammonium bicarbonate (ABC). Disulfide bonds were reduced by addition of dithiothreitol (DTT) in 50 mM ABC to a final concentration of 10 mM and incubated for 1 h at room temperature (RT). Sulfhydryl groups were blocked by alkylation reaction with iodoacetamide in 25 mM ABC at a final concentration of 40 mM at RT for 1 h in the dark. The alkylation reaction was quenched via DTT addition to 40 mM. A sufficient volume of 50 mM ABC to bring urea to less than 1 M was then added, followed by addition of L-1-tosylamido-2-phenylethyl chloromethyl ketone (TPCK)-treated trypsin (Applied Biosystems, Foster City, CA, USA) at a ratio of

1:50 trypsin: protein. Digestion proceeded overnight (16 – 20 h) at 37 °C with addition to 2.5 % formic acid to inhibit trypsin.

Desalting of peptide solutions was performed on MacroSpin 300 Å C_{18} solid-phase extraction (SPE) spin columns (The Nest Group, Inc., Southborough, MA, USA) followed by “speed-vac” centrifugal vacuum concentration at 50 °C (Labconco, Kansas City, MO, USA). Lyophilized peptides were resuspended in 0.1 % formic acid and sonicated for 10 min to ensure solubility prior to HPLC-MS/MS analyses.

In-gel trypsin digestion

In gel tryptic digests were performed as follows, unless otherwise noted. Coomassie-dyed SDS-PAGE gels were washed twice in deionized, 0.2 μM-filtered (nanopure) water for a minimum of ten minutes. Bands of interest were excised by razor blade with minimal unstained gel on their boundaries. Excised bands were carefully minced to a size that would not be drawn into a 200 μL micropipette tip allowing increased solution access to protein. SDS removal was performed by a minimum of three 10-minute cycles on a vortex in a 50:50 acetonitrile (ACN): water solution, followed by dehydration in 100% ACN for approximately 5 min. Gels were rehydrated in 100 mM ABC prior to washing in 50:50 ACN: 50 mM ABC under agitation for 15 min. After removal of wash buffer, gels were dried by speed-vac at 50 °C, then rehydrated in 45 mM DTT and incubated at 50- 55 °C for 30 min to reduce disulfide bonds. DTT buffer was removed and replaced with 100 mM iodoacetamide and alkylated in the dark for 30 min at RT. After removal of iodoacetamide-containing buffer, gels were

washed thrice in 50:50 ACN: 50 mM ABC under agitation for 15 min—ensuring no bromophenol blue remained before continuing. Gels were then completely lyophilized by speed-vac and chilled on ice before covering with the equivalent of two gel volumes with 10 ng $\times$ μL^{-1} trypsin and allowed to incubate on ice for 30-45 min (until gel was completely rehydrated). The samples were then incubated overnight (ON) at 37 °C, followed by removal of solution to a clean tube and two 200 µL washes in 50:50 ACN: water in 0.1% formic acid with wash solution transferred to tube containing original supernatant. Peptide-containing solutions were speed-vac lyophilized, then suspended in 0.1% formic acid. Digests were placed in a water bath with ultrasonics for < 10 min, centrifuged at 15K $\times$ g (to pelletize any residual polyacrylamide) and transferred to autosampler vials in preparation for HPLC-MS/MS.

Nuclear extractions from tissue culture

Nuclear extractions from tissue cultures were performed as follows, unless otherwise noted. The Thermo Scientific NE-PER Nuclear and Cytoplasmic Extraction Reagents (part #78835) were used per the manufacturer's protocol with experimental specifics as noted herein. Tissue cultures were harvested at near confluence from 75 cm^2 culture flasks with trypsin-EDTA (per ATCC recommendations for cell line). After harvest, 10 mL DMEM was added, followed by centrifugation at 500 $\times$ g (4 °C). DMEM was aspirated from the cell pellets, which were quickly resuspended in ice cold Dulbecco's phosphate-buffered saline (DPBS). Approximately 7 $\times$ 10^6 cells/flask were transferred to 1.5 mL microcentrifuge tubes and sedimented by centrifugation at 500 $\times$ g (4 °C) for 5

min. On ice, DPBS was removed and cytoplasmic extraction was performed using the appropriate ratio of CER I: CER II: NER—following the sequence of vortex-mixing and reagent addition prescribed by the manufacturer. The nuclear extraction was also performed per the manufacturer's instructions, followed by a modified version of a previously described sulfuric acid histone extraction (48), protein assay, and SDS-PAGE analysis.

Acid extraction of histones

The nuclear protein extract as described above was acid-extracted for histone isolation by a modified version of a previously published method (48). Sulfuric acid (H_2SO_4, 0.4N) was added slowly to a 5:1 H_2SO_4: nuclear protein suspension ratio on ice. The suspension was pipette-mixed and incubated for 30 min on ice with vigorous vortex-mixing every 10 min. The mixture was centrifuged at 2000 $\times$ g for 5 min at 4 °C and the supernatant was removed to a fresh microcentrifuge tube. The above was repeated once, adding the supernatant to that acquired previously. The histone solution was then concentrated to ~ 50 µL by centrifuge under vacuum at 50 °C. Protein concentrations were assayed by Pierce 660 nm on 96-well plate. Twenty µg of each was loaded onto an 18% SDS-PAGE gel and run at 150 V for 45 min, followed by 120 V for 45 min. Western transfer to a polyvinylidene fluoride (PVDF) membrane was performed at 40 V for 100 min at 4 °C. The blot was stained for 3NT-containing proteins and developed as described below. Additionally, 10 µg of each histone extraction was loaded onto a second gel (4-

20% gradient) for Coomassie detection and in-gel digestion for HPLC-MS/MS validation of histone enrichment (Fig. 26).

Western detection of nitroproteins

Western transfers followed this general protocol with electrophoresis voltages and times based on resolution requirements for proteins of varying mass ranges. SDS-PAGE gels were transferred in the BioRad (Hercules, CA) Mini Protean gel system by application of 40 V for 90 min (plus 10 min for each additional gel) with ice pack in buffer to keep it close to 4 °C for the entirety of the transfer. The resulting blot was then rinsed in tris-buffered saline with 0.1% tween-20 (TBST) for five minutes on a rocking platform. Blocking was performed by incubation of the blot for ≥ 30 min in 5% non-fat dry milk suspended in TBST (blotto) at either RT for 45 min or 4 °C for extended times. The blot was rinsed briefly in TBST, followed by addition of anti-3NT mouse monoclonal IgG clone 1A6 (EMD Millipore, Billerica, MA, USA) at a ratio of 1:1000 in blotto and incubated ON at 4 °C. The blot was washed thrice for 10 min in TBST before incubation in goat anti-mouse IgG horseradish peroxidase (HRP)—conjugate (EMD Millipore, Billerica, MA, USA) for ≥ 1.5 h at RT. The blot was then washed thrice for 10 min in TBST, followed by development with SuperSignal West Pico Chemiluminescent substrate (Thermo Scientific, USA) or equivalent for 1 min followed by x-ray film development.

Western blot stripping and re-probing

The following protocol was followed for western stripping and re-probing experiments, unless otherwise specified. Previously developed blots were

incubated in a sealed plastic container with 25 mL stripping buffer (2% SDS, 62.5 mM Tris pH 6.8, 100 mM BME) at 50 °C in a water bath with manual agitation every 10 min. After 30 min, the buffer was removed and the blot was rinsed three times for five minutes each in nanopure water. The wash was then repeated with tris-buffered saline with TBST. Blocking was performed by incubation on a rocking platform for ≥ 30 min in blotto. Typically, primary antibody staining was then performed for glyceraldehyde 3-phosphate dehydrogenase (GAPDH) with a 1:3000 dilution of mouse monoclonal anti-GAPDH clone 6C5 (EMD Millipore, Billerica, MA, USA) in blotto ON at 4 °C. Three 10 min washes in TBST were followed by secondary staining with goat anti-rabbit HRP conjugate for ≥ 1.5 hours. Three additional 10 min washes were performed prior to chemiluminescent substrate addition and x-ray film development.

Nitrotyrosine immunoprecipitation

The following protocol applies to 3NT IPs, unless otherwise specified. Tissue culture lysates were suspended in 1 mL PBS at a concentration of 1 mg × mL^{-1}. Fifty µL of 3NT affinity sorbent was added to each sample using a clipped 20 - 200 µL pipette tip (to increase inside diameter). Tubes were inverted several times and incubated on a rocking platform for 24 - 72 h at 4 °C. IPs were centrifuged at 2,000 × g for 5 min at 4 °C and the supernatant was discarded and replaced with ice-cold PBS. The agarose-bound protein mixture was mixed by pipette, and centrifuged at 2,000 × g for 5 min at 4 °C. The previous step was repeated twice. Finally, the supernatant was removed and replaced with 2×

reducing Laemmli Buffer and boiled at 100 °C for 5 minutes for immediate SDS-PAGE analysis or stored at −80 °C. For samples being prepared for direct trypsin digest via the filter-aided sample preparation (FASP) method (49), a modified 2× reducing Laemmli Buffer was prepared omitting glycerol and bromophenol blue.

In vitro peroxynitrite reactions

Peroxynitrite reactions on protein preparations were performed as described herein with exceptions noted. One milligram aliquots of RLM were buffer-exchanged to 100 µl PBS using Amicon Ultra 0.5 mL Ultracel 10K Membrane filters (EMD Millipore, Billerica, MA, USA) prior to $ONOO^-$ reaction. Peroxynitrite was quickly added at RT (in appropriate volumes for various final concentrations) to each sample and immediately mixed by rapid vortex. After reaction, the pH was tested by litmus strip to ensure neutrality. Samples above pH 7.4 were adjusted by slow addition of concentrated formic acid. Reactions were then allowed to incubate at either RT or 37 °C for 1 h. Reactions were quenched by addition of formic acid to 1-5% to achieve a pH of ~ 3.0.

HAPI cell lipopolysaccharide treatment

Lipopolysaccharide treatments adhered to the following general protocol with modifications noted. HAPI cultures were brought to ~ 80% confluence in Dulbecco's Modified Eagle's Medium (DMEM) with 5% fetal bovine serum (FBS) and PSG (10,000 units Penicillin g/mL, 10,000 microgram Streptomycin/mL, 200 mM L-Glutamine) at 37 °C in 5% $CO_{2.}$ Various amounts of LPS were pre-diluted in serum-free or 1% FBS-containing DMEM with PSG. Treatments were

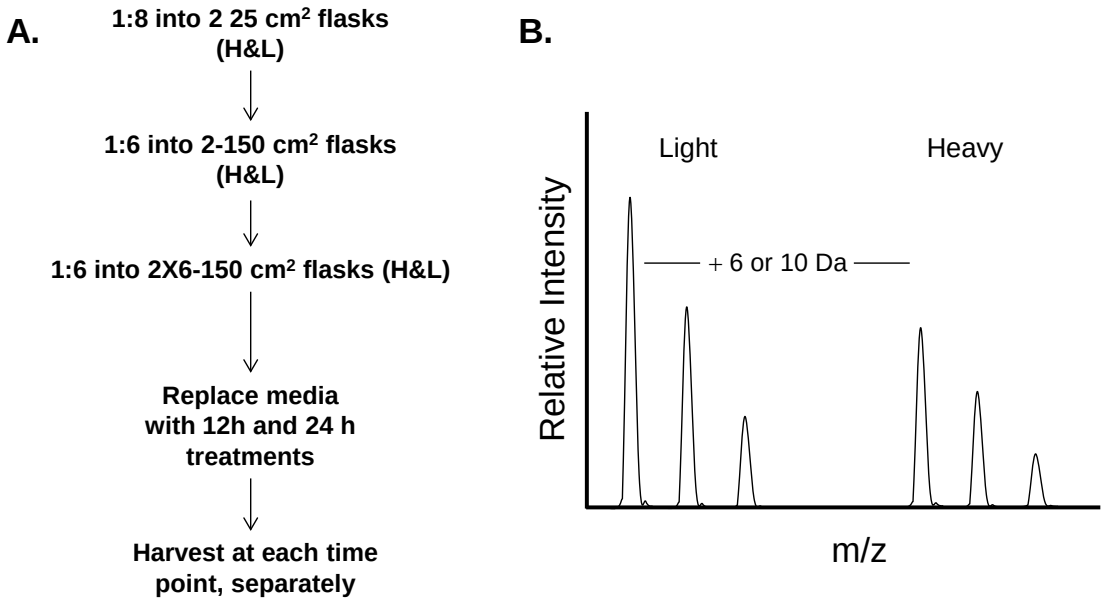

Figure 9. HAPI-LPS SILAC culture schema. A) HAPI cultures were grown in either heavy or light SILAC media to a minimum of six doublings for ≥ 97% label incorporation. B) Diagram of a theoretical doubly-charged isotope peak pair for a SILAC-labeled, Lys-terminated peptide with a 2:1 ratio of light to heavy—indicating two-fold down-regulation of the protein in the treatment group. Note: ion intensity for the majority of peak pairs is expected to be 1:1.

performed by removing media, washing thrice with pre-warmed DPBS (37 °C), and applying fresh LPS-containing or LPS-free media for controls.

HAPI cell stable isotope labeling

HAPI microglia were prepared for Stable Isotope Labeling in Cell Culture (SILAC) using a modified version of a previously-described method (29, 50). Briefly, cultures were grown to at least six doublings in dialysis-depleted medium supplemented with either "heavy" ($^{13}C_6$ and $^{15}N_4$ Arg, $^{13}C_6$ Lys) or "light" (unlabeled Arg and Lys) ensuring complete (≥ 97%) label incorporation following the scheme described in Figure 9A. Label incorporation had previously been validated for HAPI cell cultures (29).

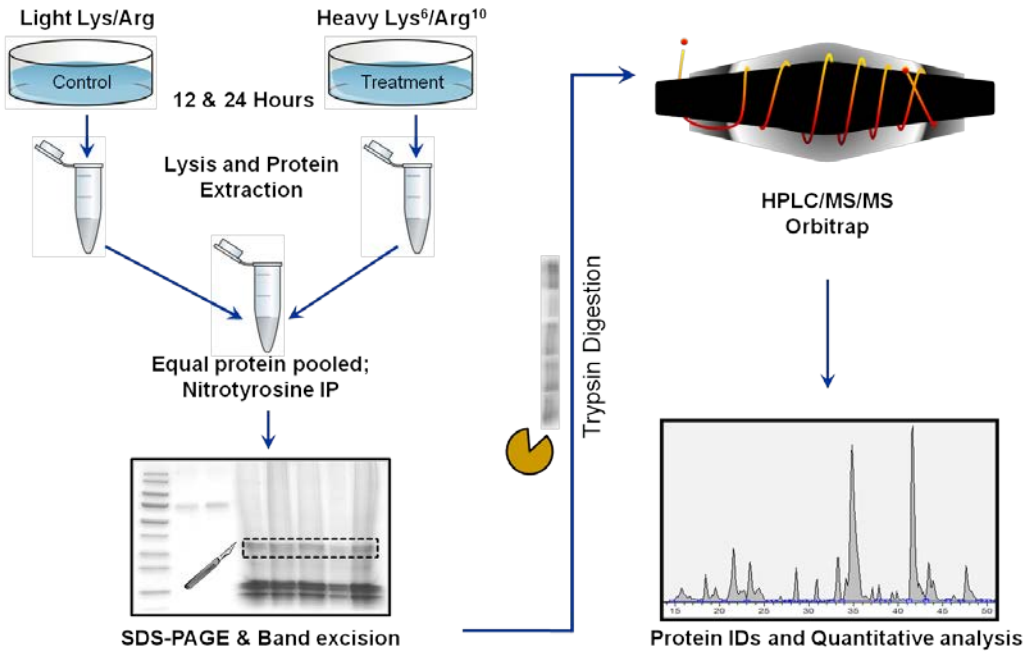

Figure 10. SILAC workflow for HAPI-LPS 3NT IP. Isotope-labeled and unlabeled cultures are harvested after 12 and 24 hours. Cells are lysed in IP-ready buffer with non-ionic detergent (nonidet 40 substitute), sonicated, and clarified by high-speed centrifugation. Equal amounts of protein from control and treatment groups are pooled prior to anti-nitrotyrosine IP. IPs are separated by SDS-PAGE and Coomassie dyed for strong nitroprotein band detection. Bands are excised, trypsin digested and analyzed by HPLC-MS/MS on LTQ-Orbitrap. The large data set is then analyzed using MaxQuant for relative quant of PTN based on IP recovery.

SILAC labeling as described above imparts a change in mass (Δm) of $^{+}10$ Da on Arg-terminated peptides and $^{+}6$ Da on Lys-terminated tryptic peptides—resulting in peak pairs separated by 10.0, 5.00, and 3.33 Da for Arg and 6.00, 3.00, and 2.00 Da for Lys, representing 1^{+}, 2^{+}, and 3^{+} ions, respectively. The majority of peak pairs will be separated by a Δm equal to $^{+}3$ and $^{+}5$ (Fig. 9B), since most tryptic peptides will carry a 2^{+} charge at acidic pH from protonation of the amino terminus and the single basic residue at the carboxy terminus.

Quantitation of SILAC is determined by the MS peak intensities acquired from peptide pairs (50). The peak intensity ratio is proportional to the relative

abundance of the representative protein from either the control or treatment groups (50). Assuming equal protein is mixed prior to HPLC-MS/MS analysis, the expected ratio for the majority of peak pairs will be 1:1, with variances expected in a subproteomic population affected by treatment. Peak pairs found to have significant intensity variation are indicative of divergent protein expression (50) or, in the case of PTN or other posttranslational modifications, variant modification. Although these data can be analyzed manually, it would be a daunting task considering the myriad data acquired from any reasonably complex mixture. Fortunately, SILAC data can be analyzed using the MaxQuant program (Max Planck Institute of Biochemistry, Martinsreid, Germany) available for free download from http://maxquant.org/downloads.htm.

Heavy-labeled Treatment mixtures (LPS—10 ng $\times$ mL^{-1}) were prepared in the heavy media containing 1% serum immediately before applying to the designated culture flasks. Control medium was prepared with the light amino acids in 1% FBS and was free of LPS. All cells were harvested after either 12 or 24 h, lysed in non-denaturing lysis buffer (20 mM Tris HCl pH 8, 137 mM NaCl, 1% Nonidet P-40 (NP-40), 2 mM EDTA) in preparation for 3NT immunoprecipitation (IP) as described above. Samples for SDS-PAGE analysis were denatured by addition of 6$\times$ LB and boiled for 3-4 minutes prior to gel loading.

Lysates were mixed at a 1:1 ratio based on protein content and loaded directly on 8 - 16% SDS-PAGE gels or were aliquotted in suspension to 1 mg $\times$ mL^{-1} prior to ON IP with 3NT affinity sorbent (Cayman). In each case, duplicate

gels were electrophoresed simultaneously allowing for western analysis in parallel with gel excision for HPLC-MS/MS analysis. The HAPI LPS treatment SILAC workflow is outlined in Figure 10.

B35 cell ethanol exposure

A modified method (30) was performed for the culture and ethanol treatment of B35 neuroblastoma cells. Briefly, B35 cells were grown to near confluence in DMEM supplemented with 10% FBS and 1% PSG at 37 °C with 5% CO_2. Cultures were rinsed thrice by gentle addition of pre-warmed serum-free DMEM followed by careful aspiration by vacuum-assisted Pasteur pipette. Ethanol-containing (50 mM) or ethanol-free 1% FBS or serum-free DMEM were added and cultures were incubated at 37 °C in 5% CO_2 for 24 h.

At the end of the treatment interval, cultures were viewed using inverted light microscopy to ensure that no detachment had occurred before proceeding. The media was transferred to 15 or 50 mL conical tubes by serological pipette without disturbing the cell monolayer. Aspirated media was centrifuged at 250 × g for 10 min at RT to pelletize any cells from suspension. The media was immediately added to prepared HAPI cultures avoiding the pellet as described below.

HAPI cell exposure to B35-conditioned media

To facilitate HAPI exposure to B35 media from ethanol treatments as described above, HAPI cultures were grown to ~ 80% confluence (as previously described) in synchronicity with the completion of the 24 h B35 ethanol treatments described above. At that time, HAPI cultures were washed thrice in

pre-warmed DPBS, prior to immersion in the B35-conditioned media. Conditioned-media treated HAPI cultures were allowed to incubate for 24 h at 37 °C and 5% CO_2 prior to aspiration of media and harvesting as described previously.

Liquid chromatographic-mass-spectrometric analyses

Rat liver mitochondria and nitrotyrosine immunoprecipitation

Peptides from RLM extracts were suspended in 0.1% formic acid. Five microliter injections were separated by reversed-phase HPLC on an Eksigent NanoLC 2D Ultra system (Dublin, CA, USA) or LC Packings Ultimate system (Thermo Fisher Scientific, USA) equipped with nano-flow outlet. Peptides were loaded onto a New Objective (Woburn, MA, USA) capillary trap 100 μm i.d. × 2 cm C_{18} column packed with 5 μm silica beads with 300 Å pore widths (ProteoPep II) for desalt prior to elution to a ProteoPep II 75 μm i.d. × 10 cm C_{18} analytical column. Mobile phase A (0.1% formic acid in water) and mobile phase B (0.1% formic acid in acetonitrile) were delivered by linear gradient of 2% - 40% B over 60 min at a flow rate of 250 or 300 nL × min^{-1}, for Eksigent or LC Packings, respectively.

Eluates were delivered by electrospray ionization (ESI) at 2 - 2.5 kV and analyzed by MS/MS on a LTQ Orbitrap XL mass analyzer equipped with XCalibur (version 2.0.7) data acquisition software. Full-scan mass resolving power was set to 60,000 (at m/z 400). Data-dependent MS/MS scans were set to acquire the top five most intense ions in the LTQ linear ion trap with dynamic exclusion durations of 180 s after one repeat.

HAPI-lipopolysaccharide stable isotope labeling

Gel extracts were suspended in 0.1% formic acid and centrifuged for 10 min at 10,000 × g to pelletize any insoluble carry-over (e.g. polyacrylamide). Samples were then carefully transferred to auto-sampler vials without disturbing the pellet. Peptides were loaded onto trap and analytical columns as described previously using a Dionex Ultimate 3000 (Thermo Fisher Scientific, USA) and delivered to the MS over a linear gradient of 2% to 40% B at a flow-rate of 300 nL × min^{-1} for 90 min.

Data-dependent MS/MS of ESI-delivered peptides was performed on an Orbitrap mass analyzer equipped with XCalibur (version 2.0.7) data acquisition software. Full-scan mass resolving power at 400 m/z was set to 60,000. Full MS was followed by data-dependent MS/MS of the top five most intense ions in the LTQ linear ion trap with dynamic exclusion set for one repeat and 180 s duration.

HAPI nitrotyrosine and histone H4 immunoprecipitation

Peptides from HAPI microglia whole cell lysates, 3NT IPs, and histone H4 IPs were analyzed by HPLC-MS/MS on a Finnigan LTQ (Thermo Scientific, USA) with delivery from a LC Packings Ultimate at 300 nL × min^{-1}. Samples were loaded onto a 150 µm i.d.×2.5 cm C_{18} capillary trap column with ProteoPep II packing material (New Objective, Woburn, MA, USA) for desalt, followed by linear gradient elution from the aforementioned 10 cm analytical column by 2% - 40% B solvent over 90 minutes.

Full MS scans were performed at normal resolution with a target of 4×10^4 ions with 2 microscans and a 50 ms maximum injection time. Tandem MS scans

selected the top-ten most intense ions with a target of 5×10^3 and dynamic exclusion for 180 s with one repeat.

Database searches and validation of peptide/protein identifications

Rat liver mitochondria and nitrotyrosine immunoprecipitations

Raw MS/MS data were searched against the UniProt rat database (74140 entries) using Mascot (version 2.2). An additional subset search was performed using X! Tandem (version 2007.01.01.1). Parent ion mass tolerance was set to 5.0 ppm and fragment ion tolerance was set to 0.50 Da. Carbamidomethylation of cysteine was specified as a fixed modification while oxidation of methionine, N-terminal acetylation, and tyrosine nitration were all specified as variable modifications. Trypsin was specified as the proteolytic enzyme. Scaffold (version 3.4.9) was used to validate MS/MS-based peptide and protein identifications. Peptides were accepted if the probability was > 95.0% as specified by the Peptide Prophet algorithm (51) and protein identifications were accepted at probabilities > 99.9% as specified by the Protein Prophet algorithm (52).

HAPI-lipopolysaccharide stable isotope labeling

Tandem mass spectra were searched against the SwissProt database (selected for Rattus, 7750 entries) using both Mascot (version Mascot) and Sequest (Thermo Fisher Scientific, San Jose, CA, USA; version SRF v. 3). Trypsin was specified as the proteolytic enzyme. Parent ion mass tolerances were 1.1 Da for Mascot and 1.2 Da for Sequest and product ion mass tolerances were 0.80 Da and 1.00 Da, respectively. Additionally, SILAC labels for Lys ($^{13}C_6$)

and Arg ($^{13}C_6$ and $^{15}N_4$), Met oxidation, nitro- oxidation of Tyr, and iodoacetamide derivative of cysteine were specified as variable modifications in both Mascot and Sequest.

Scaffold (version 3.4.9) was used to validate MS/MS-based peptide and protein identifications. Peptide identifications greater than 95.0% probability were accepted (51) and proteins that contained at least one identified peptide with probability greater than 99.0% were accepted (52). Those proteins that could not be differentiated based on MS/MS analysis due to homologous peptides were parsimoniously-grouped.

HAPI nitrotyrosine and histone H4 immunoprecipitations

Tandem mass spectra were analyzed using Mascot (version 2.2.06) and X! Tandem (version Cyclone-2010.12.01.1). Mascot and X! Tandem searches were against the Rat UniProt database including reverse and random sequences (74140 entries) assuming trypsin as the digestion enzyme. Mascot and X! Tandem were searched with parent ion mass tolerance of 2.5 Da and fragment ion mass tolerance of 0.80 Da. Cys-alkylation (iodoacetamide derivatization) was specified as a fixed modification, and Met-oxidation and nitro- modification to Tyr were specified as variable modifications in both searches.

Scaffold validation parameters were set to greater than 95% probability for peptide identifications (51) and 99% probability for protein identifications (52) with a minimum of one identified peptide. Undifferentiated proteins containing similar peptides were grouped for principle of parsimony.

Results and Discussion

Nitroprotein identifications from rat liver mitochondria

Nitroprotein immunoprecipitations

Since 3NT occurs at endogenous levels that currently fall below the LOD for mass spectrometry, enrichment is often necessary prior to HPLC-MS/MS analysis (1, 53-55). This is especially true for nitroprotein target and site identifications, which cannot be ascertained by alternate methods such as 1D and 2D gel electrophoresis. The approach taken in this study was to enrich nitroproteins in non-denaturing conditions by 3NT-specific immunoprecipitation (IP) prior to mass spectrometric analysis.

Initial experiments were conducted on mitochondrial lysates from frozen adolescent male SD rat livers fed with a normal diet. Briefly, RLM were isolated by glass homogenization and sonicated to disrupt membranes and fragment nucleic acids before clarification by centrifuge at 16,000 $\times$ g. Enrichment of 3NT-containing mitochondrial proteins in preparation for electrophoretic separation was performed by overnight IP at 4 ^{o}C using 3NT affinity sorbent agarose (Cayman). Bound proteins were pelletized and washed thrice in ice-cold PBS prior to re-suspension in 1 $\times$ reducing Laemmli Buffer.

SDS-PAGE analysis of the 3NT enriched RLM fraction revealed numerous distinct bands that were expected to contain a majority of nitroproteins. Four regions containing either one or two bands in close proximity were selected for HPLC-MS/MS analysis (Fig. 11). Coomassie-dyed bands showing a significant intensity increase as compared to their cognate control bands were of

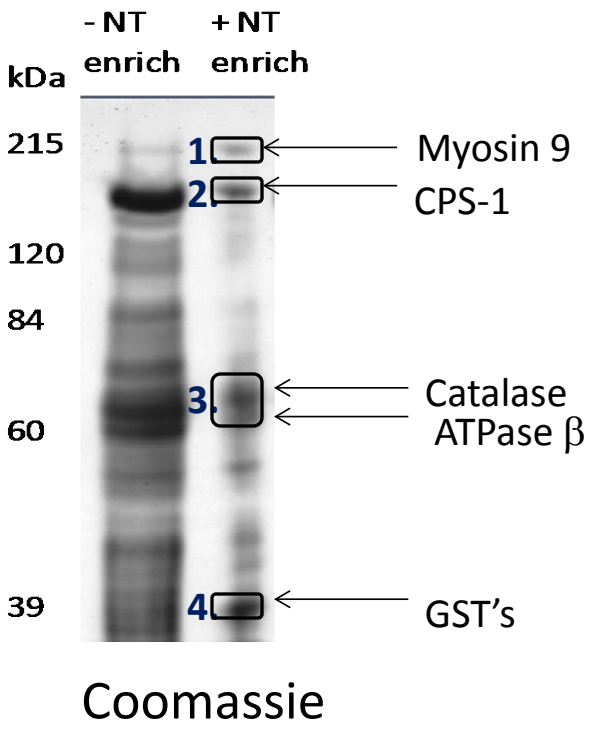

Figure 11. IP of the rat liver mitochondrial nitroproteome. Twenty μg of rat liver mitochondrial lysate (ˉNT enrich) and 3NT–containing (+NT enrich) immunoprecipitate (unknown quantity) were analyzed by SDS-PAGE to identify putative nitroprotein-containing bands. The enrichment lane was divided into four fractions that were excised and trypsin digested. Peptides were extracted and analyzed by HPLC-MS/MS to determine putative nitration targets for possible protein-targeted enrichment and/or nitration site-specific targeted mass spectrometric method development.

particular interest (i.e. bands 1 and 4, Fig. 11), since they were expected to contain nitroproteins.

Figure 11 shows putative endogenous PTN targets identified from specific gel regions. The most abundant proteins identified included: carbamoyl phosphate synthetase-1 (CPS-1), catalase, pyruvate carboxylase, aldehyde dehydrogenase; ATP synthase (ATPase) α- and β- subunits, glutamate dehydrogenase, glutathione S-transferase (GST) isoforms, Cytochrome-c oxidase, and manganese superoxide dismutase (Mn-SOD).

As expected, putative nitration targets found in mitochondria are key contributors to energy metabolism (56, 57), ethanol metabolism (58-60), ROS disposition (57, 61, 62), the urea cycle (63), gluconeogenesis (64), and lipogenesis (65). Specific targets such as ATPase-β, CPS-1, and glutamate dehydrogenase exhibited increased degradation rates in previous studies (66, 67) and nitration increase to myosin isoforms has been implicated to be a consequence of aging (68). Moreover, PTN found in mitochondria under normal conditions supports the potential for a regulatory role in metabolism discussed in Chapter One. Although the presence of PTN could not be confirmed through site identifications, the majority of proteins enriched by 3NT IP are presumed to contain nitrotyrosine. Thus, the PTN targets identified by database searches can provide insight into the metabolic pathways affected by nitration. Also, a targeted MS method can be employed to increase sensitivity for putative nitration sites on specific proteins as discussed later in this chapter.

Parallel SDS-PAGE and Western analysis of nitroproteins

A second attempt at endogenous nitration site identification was made using fresh adult male SD rat liver mitochondria. Mitochondrial isolation was followed by 3NT IP as described previously. In this attempt, two gels were run in parallel, one for in-gel digestion for HPLC-MS/MS analysis and the second designated for western blotting (Fig. 12) to select gel bands for excision based on the presence of a 3NT signal. Western blot detection correlated with the strongest Coomassie bands as indicated by the arrows shown in Figure 12A&B. MS analysis of digests from the eight bands indicated in Figure 12B resulted in

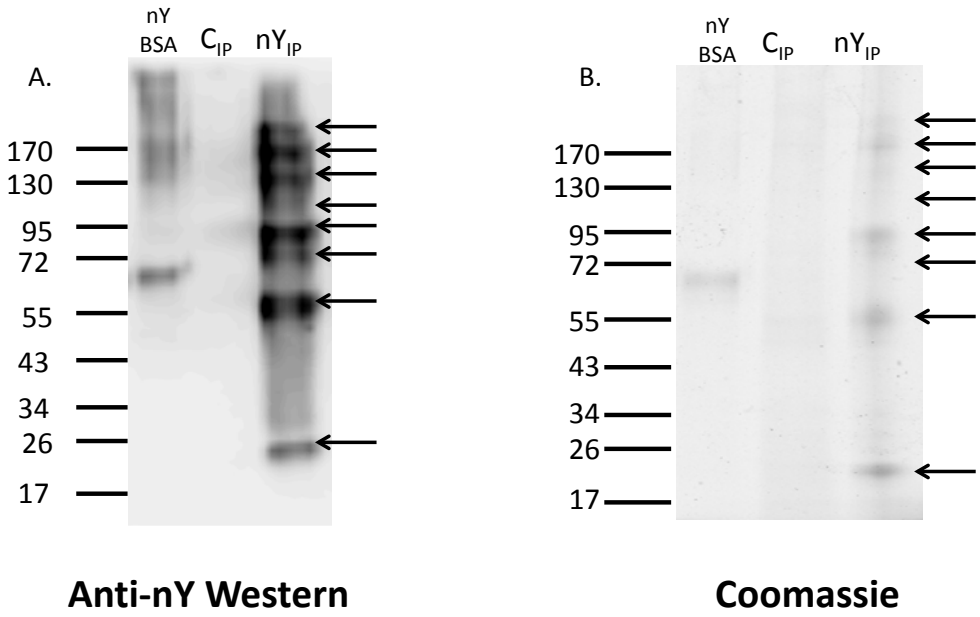

Figure 12. Western and 1D gel for ID of nitroproteins from RLM. A) Western blot of 3NT (nY) IPs from rat liver mitochondrial lysates. B). A SDS-PAGE gel run in parallel with the western analysis was coomassie dyed for detection and excision of bands at molecular masses where nitration was evident (indicated by arrows). Gels (8-16% polyacrylamide) were run at 120V for 45+ min (until dye front reached bottom of gel) to cover the entire mitochondrial proteome and maximize resolution.

similar identifications to those found previously (Fig. 11); however, PTN site identification remained elusive.

Nitropeptide target prospecting

Rationale

The absence of an identified endogenous nitration site from RLM analyses supplied motivation for alternative approaches to 3NT site identification. Since $ONOO^-$ is a physiologically-relevant nitrating agent, *in vitro* peroxynitrite reactions were performed to identify prospective nitration sites for targeted MS/MS instrument method establishment. Authentic $ONOO^-$ was reacted with

rat liver mitochondrial lysates in PBS (pH 7.4) at RT, maintaining proteins in their native states for solvent-accessible Tyr residue targeting. Our expectation was that selective nitration would occur at much higher frequency than *in vivo*—augmenting detection of the most susceptible peroxynitrite-mediated nitration target sites.

This approach also had a provision for increased starting material to exceed LOD for mass-spectrometric analysis. Multiple lanes on a gel can be pooled prior to HPLC-MS/MS analysis. Upon identification of specific nitration sites, a more sensitive targeted MS/MS method can be implemented to improve sensitivity for those sites. This is accomplished by selecting each nitropeptide precursor mass as a target for CID fragmentation during each round of MS/MS scans, a technique similar to that described in Chapter Two.

Protein tyrosine nitration target and site analysis from peroxynitrite reactions

Immunoprecipitates of *in vitro* peroxynitrite reaction products from RLM lysates from were separated by SDS-PAGE and Coomassie-stained to determine bands of highest protein concentration. Five bands from gel regions of equal mass labeled 1 – 4 (Fig. 13) were excised and pooled to increase analytical sample load. Those bands were trypsin digested and analyzed by HPLC-MS/MS to identify putative PTN sites for targeted MS method development.

Database search of the gel region number three (Fig. 13) identified a nitration site at Tyr^{8} on the peptide AIAELGIYPAVDPLSTSR, a unique ATP synthase β-subunit (ATPase-β) peptide. Manual evaluation of the nitration site was performed by evaluation of precursor mass accuracy (Δm –1.0 ppm) and

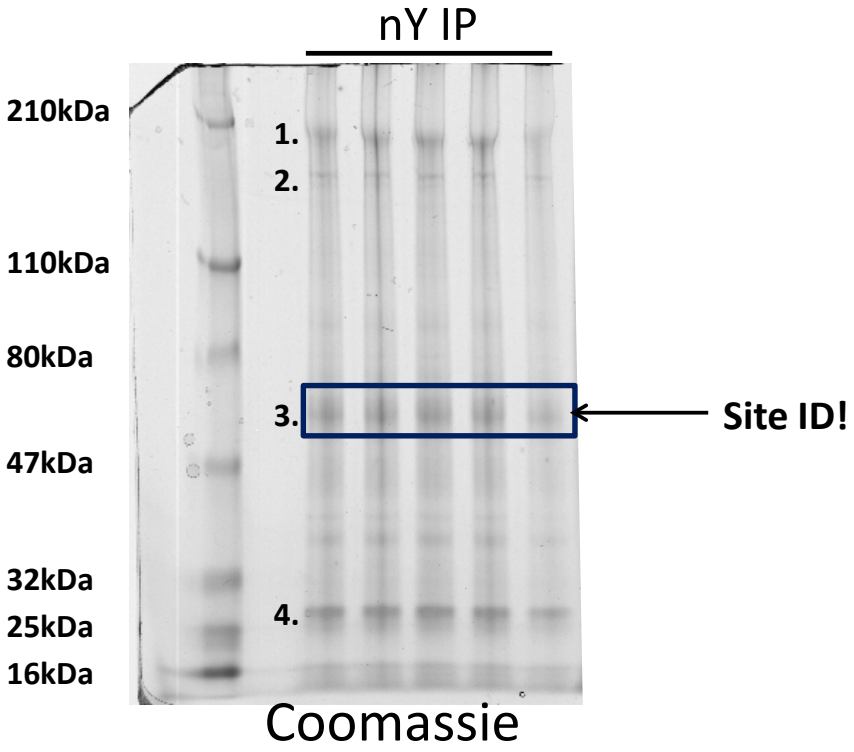

Figure 13. SDS-PAGE analysis of *in vitro* peroxynitrite reactions. Immunoprecipitates from RLM reacted with 1 mM peroxynitrite were run on an 8 – 16% SDS-PAGE gel at 150 V for 49 min. Bands at each of the four numbered rows were excised, pooled, trypsin digested, extracted and analyzed via HPLC-MS/MS. Upon database search and spectral validation, a nitration site on ATPase-β was identified from region #3 (~60 kDa). A targeted mass spectrometric method was built based on this ID to increase sensitivity for the ATPase-β nitropeptide.

comparison to the unmodified peptide spectrum for product ion intensities as seen in Figure 14A. Sequence coverage for protein identification was 41% (Fig. 14B) and AIAELGIYPAVDPLSTSR was identified in both unmodified (6 spectra) and nitro-modified (1 spectrum) permutations.

Targeted tandem mass spectrometry for improved sensitivity

The ATPase-β nitration site identification from *in vitro* $ONOO^-$ reactions furnished us with a nitropeptide target for mass spectrometric method

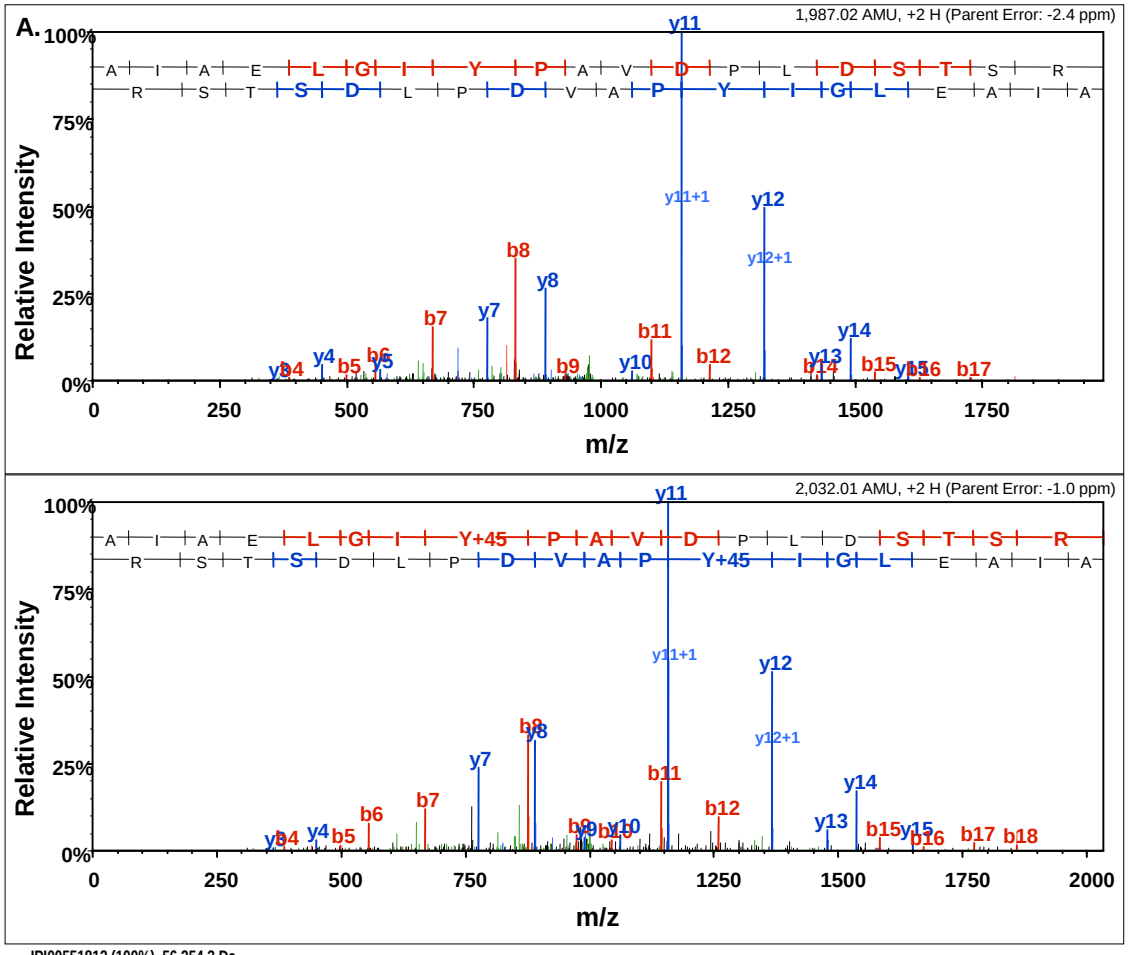

B. IPI00551812 (100%), 56,354.3 Da
ATP synthase subunit beta, mitochondrial
17 unique peptides, 21 unique spectra, 105 total spectra, 231/529 amino acids (44% coverage)

```
MLSLVGRVAS ASASGALRGL NPLAALPQAH LLLRTAPAGV HPARDYAAQS SAAPKAGTAT
GQIVAVIGAV VDVQFDEGLP PILNALEVQG RESRLVLEVA QHLGESTVRT IAMDGTEGLV
RGQKVLDSGA PIKIPVGPET LGRIMNVIGE PIDERGPIKT KQFAPIHAEA PEFIEMSVEQ
EILVTGIKVV DLLAPYAKGG KIGLFGGAGV GKTVLIMELI NNVAKAHGGY SVFAGVGERT
REGNDLYHEM IESGVINLKD ATSKVALVYG QMNEPPGARA RVALTGLTVA EYFRDQEGQD
VLLFIDNIFR FTQAGSEVSA LLGRIPSAVG YQPTLATDMG TMQERITTTK KGSITSVQAI
YVPADDLTDP APATTFAHLD ATTVLSRAIA ELGIYPAVDP LDSTSRIMDP NIVGSEHYDV
ARGVQKILQD YKSLQDIIAI LGMDELSEED KLTVSRARKI QRFLSQPFQV AEVFTGHMGK
LVPLKETIKG FQQILAGDYD HLPEQAFYMV GPIEEAVAKA DKLAEEHGS
```

Figure 14. Nitration-susceptible site identification on ATPase-β. A) Scaffold annotated MS/MS spectrum comparison between unmodified AIAELGIYPAVDPLSTSR (top) and 3NT-containing AIAELGIY$^{(nitro)}$PAVDPLSTSR shows consistent fragment ion intensities for y and b series ions. B) ATPase-β Protein sequence showing 41% coverage (yellow highlights) from tryptic digest with the nitropeptide circled in red. All fixed and/or variably modified residues appear highlighted in green.

development to increase sensitivity for the site from a biological sample. A targeted MS/MS method was built to scan for the precursor masses specific to both AIAELGIYPAVDPLSTSR (994.50) and AIAELGIY$^{(nitro)}$PAVDPLSTSR (1017.0). Targeted MS/MS increases sensitivity for a specific analyte by circumventing data-dependent MS/MS parameters. This results in isolation of the targeted m/z during each scan cycle (every four seconds on average). Targeted methods such as this can result in sensitivity increases of greater than two orders of magnitude based on results from previous analyses using a similar method (data not shown).

ATP Synthase β-subunit Tyr-345 nitration inhibits enzyme activity

The ATPase-β nitration site identified on Tyr^{345} had been previously reported to diminish ATP synthase activity as a result of *in vitro* TNM reaction (69). The study induced Tyr^{345} nitration in recombinant rat ATP synthase (69), then assayed ATP synthase activity between reacted and unreacted protein. Site-directed mutation confirmed nitro-Tyr^{345} had the most significant impact on ATPase activity.

To validate the AIAELGY$^{(nitro)}$PAVDPLDSISR spectrum (Fig. 15b), it was compared to the published spectrum resulting from TNM treatment (Fig. 15a) of validated recombinant ATPase-β (69). Confidence in both nitro-site identifications was supported by the precursor ion mass accuracies as well as fragment ion peak and spectral intensity identities. Moreover, demonstration of Tyr^{345} nitration susceptibility with peroxynitrite as the nitrating agent supports our hypothesis that it is a target of a physiologically-relevant nitrating agent.

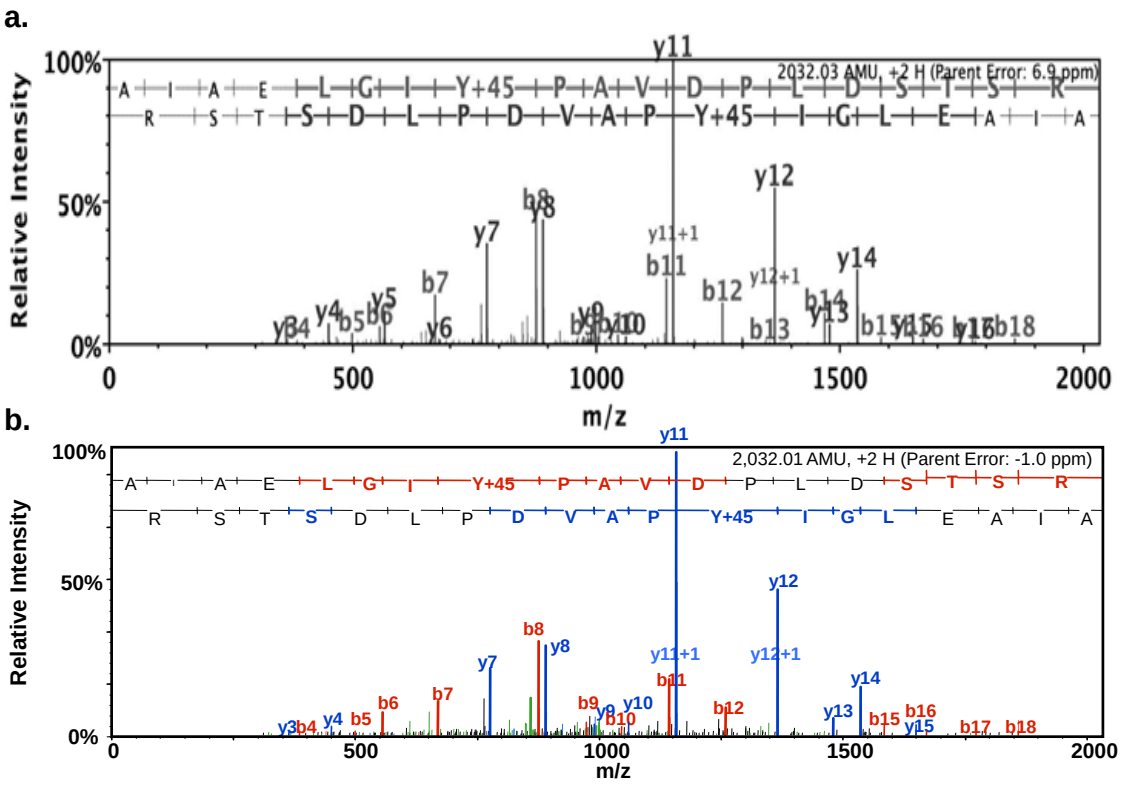

Figure 15. Tandem mass spectrum of an ATPase-β nitropeptide. a) MS/MS spectrum of the tryptic peptide AIAELGY$^{(nitro)}$PAVDPLDSISR from TNM treatment at a molar ratio of 25 TNM to ATPase-β (69). b) An unknown ATPase-β concentration to in rat liver mitochondrial lysate was reacted with 200 μM $ONOO^-$.

Three-dimensional model of ATP synthase with nitro-Tyr^{345} mutation

ATPase-β Tyr^{345} is proximal to, but not directly, in the nucleotide binding pocket of the enzyme as seen in Figure 16. Fujisawa, et al (2009) built a computational 3D model of ATPase F1 using the PyMOL Molecular Graphics System (Version 1.5.0.4 Schrödinger, LLC). The model was constructed from bovine ATPase-β (PDB reference 1BMF) because it represented all three conformational states (tight, loose, and empty). Mutation of Tyr^{345} to nitro-Tyr^{345} simulated a hypothetical conformational change conferred by 3NT to the structure of the catalytic site of ATPase-β (69). Although computational modeling

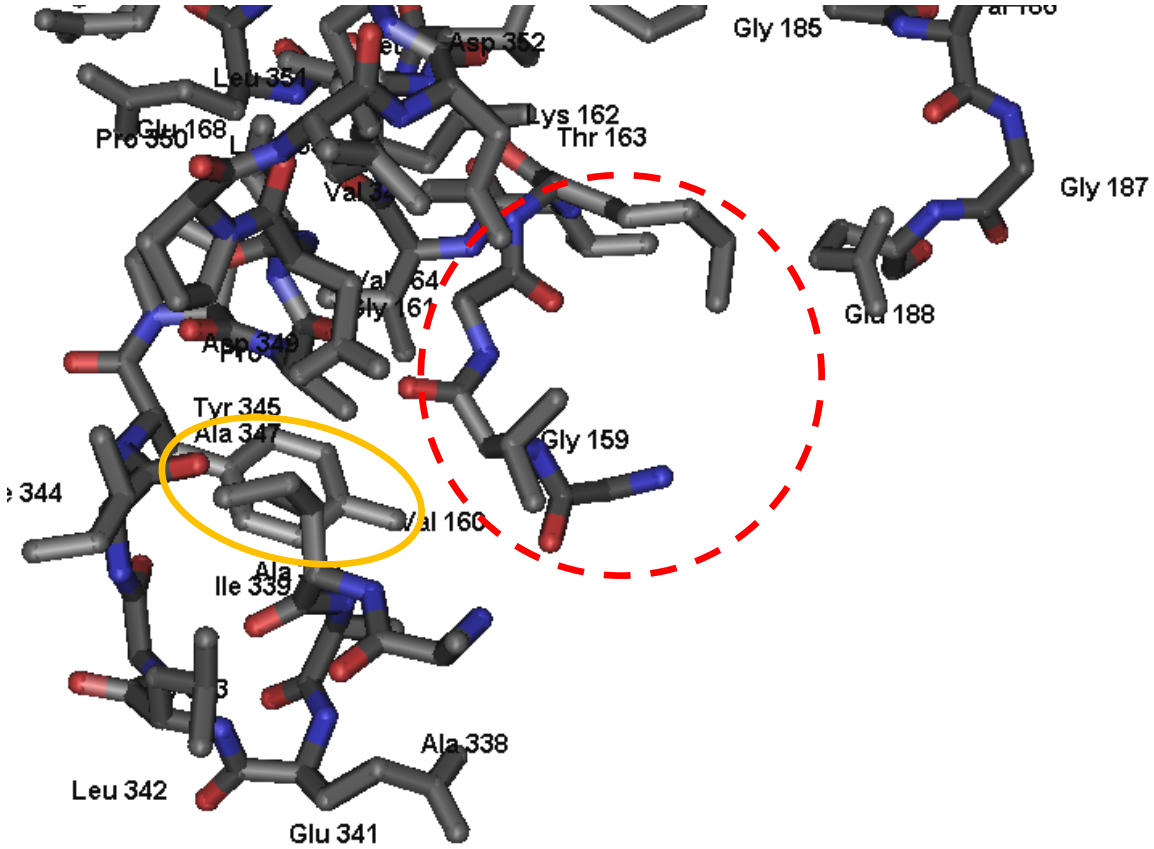

Figure 16. Three-dimensional model of the ATP binding site on ATPase-β. A Cn3D (70) model of rat liver F1 region of ATPase was constructed from the protein data bank (PDB http://www.rcsb.org/pdb) code 1mab crystal structure. All residues displayed are from ATPase-β, including AIAELGIYPAVDPLSTSR. Tyr^{345} (side chain in gold circle) is localized near the ATP binding pocket residues (shown in red dashed circle). Tyr^{345} nitration can result in a remote conformational change to the binding pocket--disrupting ATP binding (71).

can be inaccurate in predicting 3D structure under physiological conditions, the model does provide a plausible explanation for the observed ATPase activity impairment conferred by Tyr^{345} nitration (69).

Application of a targeted tandem mass spectrometric method

Because nitration site identification was absent from 3NT IP of mitochondrial fractions, *in vitro* $ONOO^-$ reactions were performed to identify

putative nitration sites that could be targeted during MS/MS acquisition. After successfully identifying a nitration site on ATPase-β from those experiments, a AIAELGY$^{(nitro)}$PAVDPLDSISR-specific targeted method was built. The targeted scans were incorporated into a data-dependent method, reducing the ten data-dependent scans to eight—preserving a functional scan time.

IP was performed in triplicate on 1 mg $\times$ mL^{-1} RLM aliquots—allowing for one analytical replicate for each SDS-PAGE gel excision. Samples were analyzed by HPLC-MS/MS acquisition on an Orbitrap using the targeted method including the m/z of both the unmodified and nitropeptide identified from ATPase-β (994.5 and 1017, respectively). Upon database search, proteins correlating to those previously found (Fig. 11 & 12), including ATPase-β, were identified. Surprisingly, the analysis did not identify either of the ATPase-β target peptides.

SDS-PAGE band pooling

Because the initial application of the targeted MS/MS method was unsuccessful in identifying the ATPase-β nitropeptide, two separate experiments designed to "bulk-up" material for increased MS sample load were performed. In the first, six bands from a standard 4 – 20% mini-gel (Precise Tris-Glycine Gels, 10 x 8cm, Thermo Scientific, USA) containing RLM 3NT-IP from 50 µl of affinity sorbent each were pooled post-digestion prior to MS/MS analysis (Fig. 17A).

The alternative method was designed to pool 3NT IP eluates prior to gel electrophoresis. Immunoaffinity sorbent from five 1 mg $\times$ mL^{-1} IPs was combined and washed using positive pressure from a 12 mL Monoject Plastic Syringe with Luer tip (BD, Franklin Lakes, NJ, USA) through a Pierce fritted 0.8 mL centrifuge

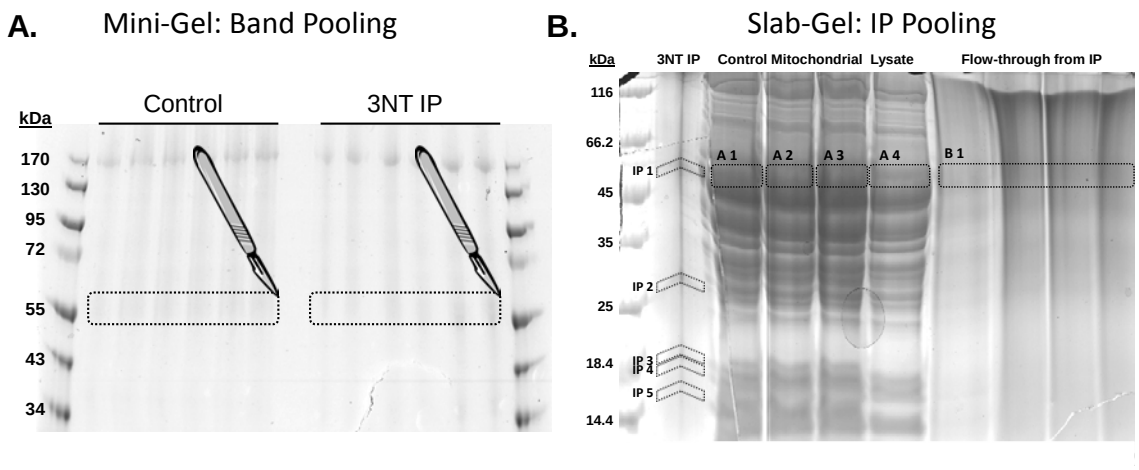

Figure 17. Pooled 3NT IP gel digests. To increase analytical sample load from 3NT immunoprecipitates, A) mini-gels were loaded and analyzed with SDS-PAGE in sextuplicate to allow for pooling of enrichment bands while B) slab-gel pooling was done at the IP step and loaded in a single lane. Bands in the range of 56 kDa were extracted, trypsin-digested, and peptides were analyzed with a combination ATPase-β peptide targeted and data-dependent MS/MS method.

column into 50 mL conical tubes. Elution was performed by syringe flushing with 250 μL of 1 × Laemmli Buffer. A 1 mm, 10% polyacrylamide slab gel was poured and fitted with a comb for high-capacity well formation. A single lane was loaded with the eluate described above, four lanes were loaded with control lysate (unreacted RLM) and an additional four lanes were loaded with the flow-through from anti-3NT IP. Nitrotyrosine-IP, control lysate, and IP flow-through bands were excised at the approximate region containing 50-60 kDa proteins (Fig 17B). The control and flow-through bands were pooled as a single sample for analysis. Gel bands were trypsin digested and analyzed using the combined targeted/data-dependent method described above.

MS analysis of both the minigel and slab gel excisions identified ATPase-β as the top hit. One spectrum representing the targeted nitropeptide was

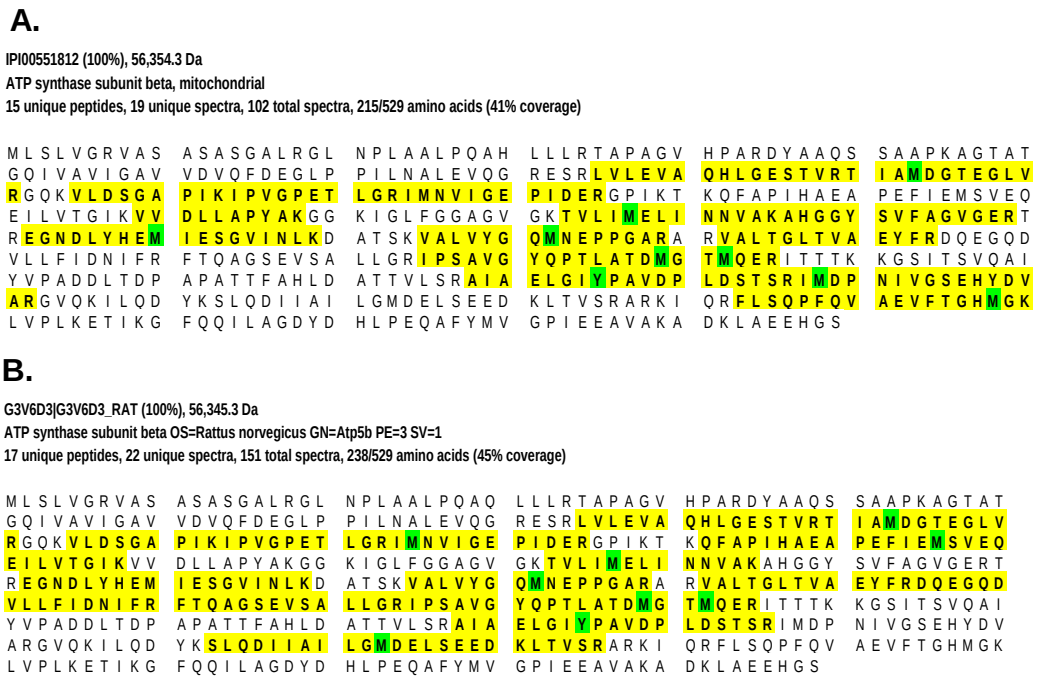

Figure 18. ATPase-β nitropeptide identification minigel v. slab gel. A) ATPase-β sequence coverage was 41% (yellow highlighting) from a mini gel containing pooled IP from ~ 0.5 mg rat liver mitochondrial lysate using 50 µL of 3NT affinity sorbent (Cayman). The analysis yielded identifications of five unmodified and one nitro- modified spectrum for AIAELGIYPAVDPLDSTSR using the MS/MS targeted method. B) Sequence coverage was 45% for the slab gel containing 3NT IP from ~ 2.5 mg rat liver mitochondrial lysate using 300 µL of 3NT affinity sorbent. Analysis identified eleven unmodified and four nitro-modified AIAELGIYPAVDPLDSTSR spectra from targeted scans on an Orbitrap. Green highlighting indicates Met oxidation and Tyr oxidation to nitro-Tyr.

identified from the pooled mini-gel digests and four spectra were identified from the pre-electrophoresis pooled single lane of the slab gel.

To summarize, the pre-pooling of IP yielded a 4-fold increase in nitropeptide AIAELGIY$^{(nitro)}$PAVDPLDSTSR identification from 17 % less starting material and an equal amount of 3NT affinity immunosorbent. Sequence coverage (Fig. 18) was also improved by 8.8 %, demonstrating the use of a slab

gel for increased sample loading in a single lane as a viable technique to incorporate into a method for enhanced PTN sensitivity.

It remains unclear whether or not the targeted MS/MS method influenced improved nitropeptide identification as an exclusively data-dependent analysis was not performed during this experiment. Typically, acquisition using multiple methods yields complementary data, thus the combination of targeted and data-dependent was the approach selected for this particular analysis. Application of a combined targeted/data-dependent MS method increases sensitivity for specific targets, while providing for discovery of unknown low-level targets.

Ethanol-induced nitration in human primary hepatocytes

Because PTN site investigation using mitochondria isolations was unsuccessful in identification of an endogenous site, assay of nitration in whole liver cell lysate was selected to improve site identification probability. Our pilot experiment was performed using metabolism-qualified primary human hepatocytes (Life Technologies, Grand Island, NY, USA) to evaluate 3NT formation as a result of acute ethanol exposure.

A significant increase in PTN was apparent in human primary hepatocytes (Fig. 19A) after twenty-four hour exposure to 50 mM ethanol (blood alcohol level equivalent of 250 mg $\times$ dL^{-1}). The increased 3NT Western blot signal was detected at molecular weights below 26 kDa, which was thought to possibly indicate histone nitration. The overall basicity of histones increase their likelihood to become PTN targets as demonstrated by the increased nitration seen in pentapeptides with high positive charge in Chapter Two.

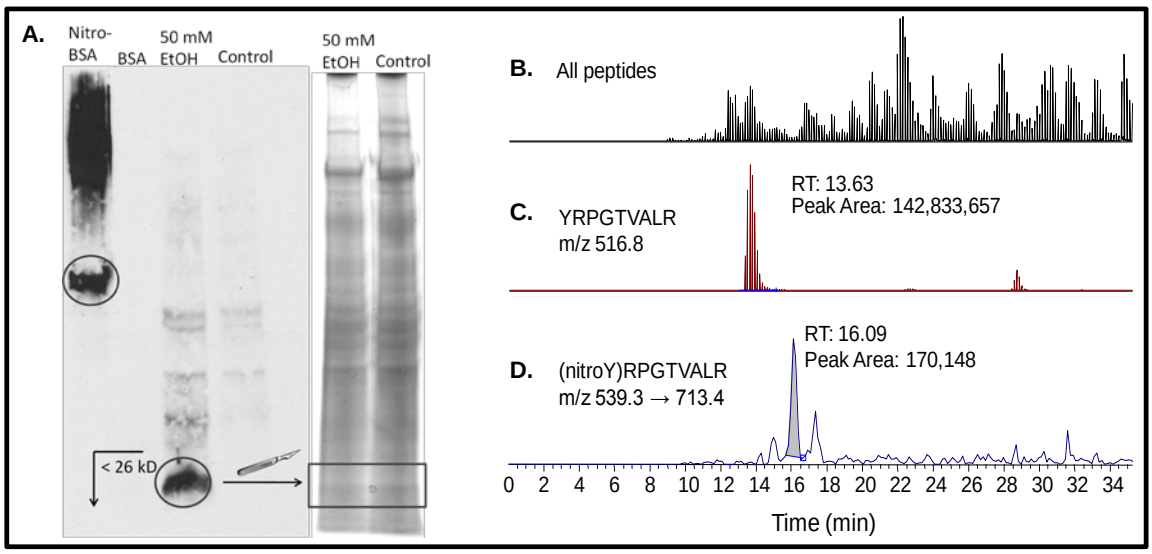

Figure 19. Ethanol-induced human hepatocyte nitration. A) Anti-3NT Western blot showing increased nitration with a strong signal in the range below 26 kDa. B) Full mass spectrum of in-gel digestion of the < 26 kDa excised band (circled in A). C) Accurate mass profile for the Tyr^{41}-containing histone H3 peptide. D) Reconstruction of a putative nitropeptide containing nitro-Tyr^{41}.

The region below 26 kDa was excised, trypsin-digested, and analyzed via HPLC-MS/MS to identify protein contents and PTN sites. A histone H3 peptide, YRPGTVALR, was identified by Mascot search of the UniProt human database. Using the accurate mass of the peptide, a profile was found at RT 13.63 min with a peak area of 142×10^6 (Fig. 19C). A putative nitropeptide chromatographic peak was reconstructed for $Y^{(nitro)}$RPGTVALR using its accurate mass and one transition. The peak appeared at RT 16.09 min with an area of 170×10^3 (Fig. 19D). Preliminary data from this experiment provided the foundation for the investigation of ethanol-induced PTN in microglia discussed in the following section.

Nitration induced by activated microglia

Rationale

As mentioned earlier in this chapter, microglial activation can be induced directly through interaction with an exogenous CD-14 substrate (20) or indirectly through neuronal signaling (28). Because NO and $O_2^{\bullet-}$ overproduction are characteristic of microglial activation, we aimed to identify peroxynitrite-mediated nitration targets to characterize PTN resulting from microglial activation by both direct and indirect induction.

Direct microglial activation induced by endotoxin

HAPI microglia exposure to 30 ng $\times$ mL^{-1} LPS for 12 h had previously been shown to significantly increase iNOS expression (30). Considering iNOS is a high output NO generator (22) and microglia are macrophages capable of oxidative burst and chemokine production (29, 37), formation of the reactive nitrogen species (RNS), peroxynitrite is likely to occur upon activation. Thus, HAPI culture was considered to represent a good model to evaluate nitrative stress in the brain.

To determine the global affect of endotoxin exposure on the nitroproteome, HAPI cultures were grown to 80% confluence and treated with 50 ng $\times$ mL^{-1} LPS for 12 h. Soluble protein fractions from cell lysates were prepared for Western analysis. The resulting blot of whole-cell lysate (Fig. 20) was stained to compare untreated and LPS-induced global nitration profiles. Although the overall pattern of nitroproteins detected did not show apparent variation, a general trend of increased nitration appeared in the treatment group (Fig. 20).

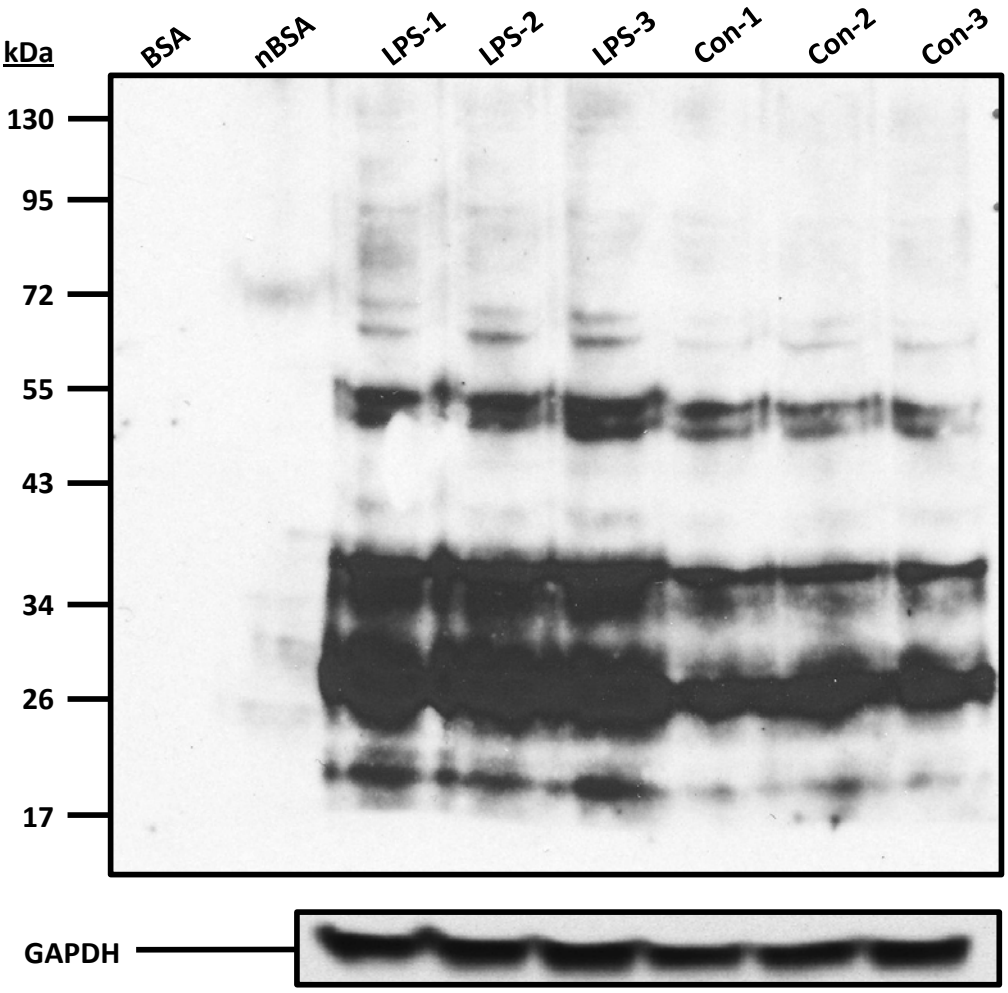

Figure 20. LPS-treated HAPI lysate anti-3NT Western blot. Lysates from HAPI cultures treated with 50 ng × mL^{-1} LPS for 12 h were run on a 4 - 20% SDS-PAGE, transferred to a PVDF membrane and stained with mouse monoclonal 1A6 anti-3NT (Millipore). Rabbit anti-mouse HRP conjugate (Millipore) was used to detect bands containing nitroproteins. Overall nitration patterns appear similar; however, a global increase in nitration was clearly evident after LPS-induced activation. GAPDH loading-control western was performed after stripping and re-probing the blot shown.

These data were convincing in support of our hypothesis that increased nitration occurs concomitantly with iNOS upregulation upon direct stimulus for microglial activation.

SILAC analysis of HAPI cell direct activation

Since a distinct nitration increase was observed in the LPS treatment group of an abundant nitroproteome seen in Figure 20, a SILAC experiment was performed as described in methods in this chapter to identify PTN targets and quantify variant nitration between normal and LPS activation nitroproteomes. LPS treatments (10 ng $\times$ mL^{-1}) were performed in triplicate for 12 or 24 hours. The 12 hour exposure was intended to replicate the conditions described for Figure 20 (with the exception of a lower dose of LPS); while the 24 hour exposure was intended to elucidate the nitration profile resulting from protracted exposure to inflammatory stimulus.

Cells were immunoprecipitated in 3NT affinity sorbent prior to anti-3NT western blotting (Fig. 21). Excised bands containing immunoprecipitates from equal light and heavy protein starting content were in-gel trypsin digested using the protocol described in methods, followed by high-resolution HPLC-MS/MS analysis on a LTQ-Orbitrap at the H. Lee Moffitt Cancer Center & Research Institute Proteomics Core Facility.

Data from Orbitrap analysis was submitted to the MaxQuant program to identify PTN targets and quantify over- and under-represented protein groups. A Mascot search with Scaffold validation was also conducted to confirm protein identifications. Scaffold label-free spectrum counting could not be used for PTN quantitation since equal amounts of protein were combined prior to 3NT IP.

MaxQuant analysis was inconclusive due to low spectral data yields from the in-gel digests. However, Scaffold analysis of the gel band labeled “F”

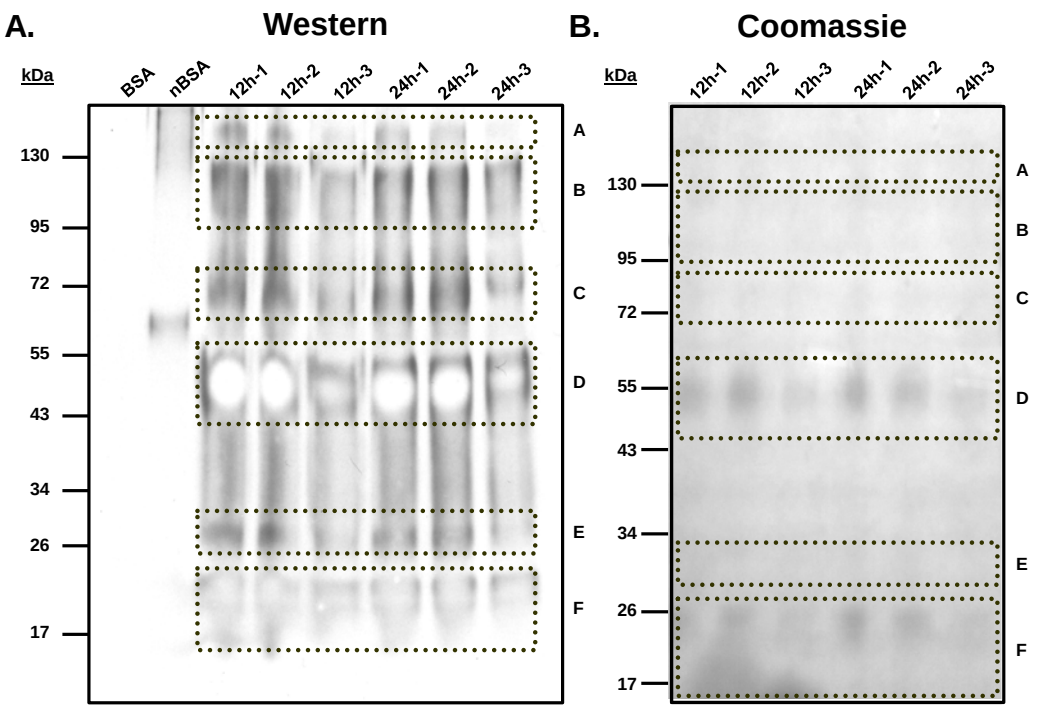

Figure 21. Parallel SDS-PAGE/ Coomassie and Western development of 12 and 24 h HAPI LPS SILAC treatments. A) Band regions A – F were identified by western detection to contain 3NT. B) Cognate bands A – F were excised from SDS-PAGE for in-gel digest followed by high-resolution HPLC-MS/MS on a LTQ-Orbitrap at the Moffitt Cancer Center Proteomics Core Facility.

resulted in identification of histone isoforms (Fig. 21B). The band labeled "F" originated from the MW region below 26 kDa and had been selected based on western detection of 3NT (Fig. 21A). Coomassie detection also showed significant protein content in the mass range below 26 kDa, which is indicative of abundant PTN considering the low MW of proteins migrating to that region.

Previous Western analysis of LPS treated HAPI total lysate had also detected PTN in the region below 26 kDa, with a clear nitration increase seen in the treatment group (Fig. 20)—indicating histones may not only be potential nitration targets, but also targets of increased nitration upon microglial activation.

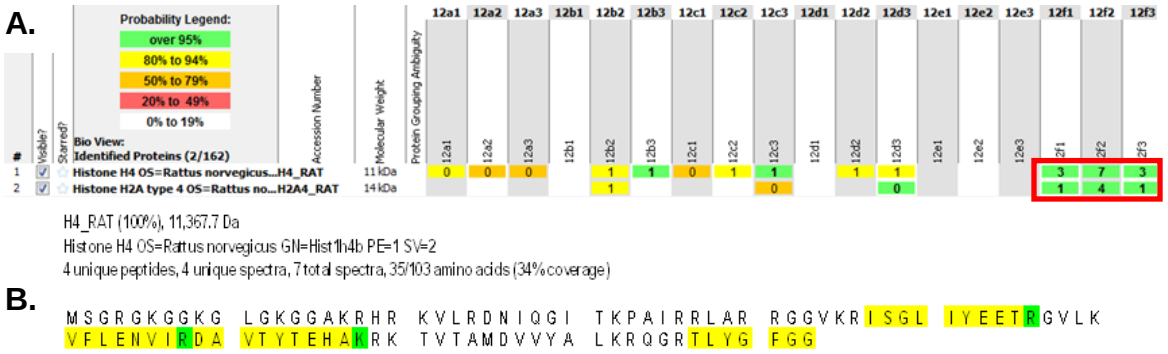

Figure 22. Scaffold histone IDs from 3NT IP of HAPI LPS SILAC gel digests. A) Spectral counts for histone peptides from 3NT-IP enrichment are shown circled in blue. Identifications were filtered using 95% peptide confidence and 99% protein confidences (51, 52). B) Sequence coverage for histone H4 highlighting isotope-labeled Arg and Lys (green). Since no filter was applied, data shown is all-inclusive for heavy and light-labeled peptides.

Scaffold analysis of gel region F identified peptides representing histones H2A and H4 (Fig. 22B). This is interesting considering histone H2A is ~15 kDa and histone H4 is ~11 kDa and gel region F was excised in the range of 26 kDa. Also, histone H4 was detected at the highest abundance with thirteen unique peptides. Five unique histone H2A peptides were identified. Histone H4 sequence coverage was 34% using the stringent Scaffold criteria described in methods (Fig. 22B).

Confidence in histone H4 identification was supported by spectral probabilities above 95% using the Peptide Prophet algorithm (51), and 99% protein probability from Protein Prophet (52) validation. Considering the limited number of protein identifications from the gel extraction (162 total IDs with keratin isoforms comprising 10%), histone H4 was considered a strong potential PTN

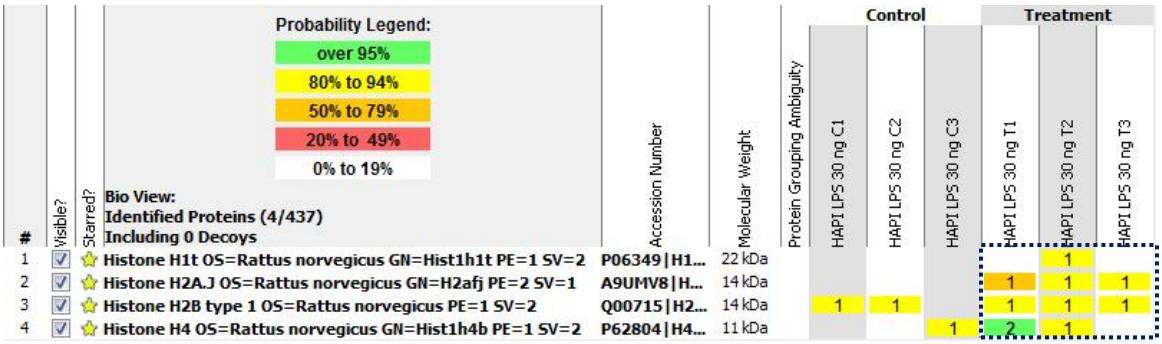

Figure 23. Shotgun analysis of LPS treated HAPI microglia 3NT IP. Histone peptides identified with probabilities ≥ 80% from HAPI cultures treated with 30 ng × mL^{-1} LPS for 24 h were 9:3 in favor of the treatment samples (T1-T3, blue box). These data combined with similar enrichment for histones H2A and H4 from SILAC analysis of HAPI treated with 10 ng × mL^{-1} LPS provided the rationale for histone-focused experiments to evaluate global and site-specific nitration to histone proteins as a potential modulator of gene expression under oxidative/nitrative stress conditions.

target warranting further investigation. Additionally, histone modifications can result in aberrant transcription through altered chromatin remodeling. An example of this was found in a study of murine Mutatect (ATCC CRL-2800) tumors where two nitration sites on histone H4 (Tyr^{72} and Tyr^{95}) were identified (72).

Histones in general represent strong PTN candidates based on the electrostatic influence on nitration susceptibility described in Chapter Two. The abundance of basic residues on histones (see Table 3) can create a predominantly positively-charged microenvironment that possibly attracts $ONOO^-$ and/or stabilizes a peroxynitrite-mediated nitration reaction intermediate. Experimental focus on histone nitration is discussed later in this chapter and Chapter Five based on these results.

HAPI lipopolysaccharide whole cell lysate immunoprecipitates

Since gel digests are limited by the amount of protein loaded per well as well as incomplete digestion and extraction, digests of 3NT IP eluates from whole cell lysates were selected for analysis by HPLC-MS/MS. This approach was expected to increase analytical sample load and provide at least complementary data to those acquired during the SILAC experiment. A potential pitfall to this one-dimensional "shotgun" (73-75) approach is the possibility of ion suppression—a phenomenon that occurs in complex mixtures where co-eluting analytes and contaminants can result in poor ion transmission from the source to the vacuum interface of a mass spectrometer (76). The omission of electrophoretic separation also negates the ability to support identifications based on known relative molecular masses of the fractions being analyzed.

HAPI microglia were grown to 80% confluence and treated with 30 ng $\times$ mL^{-1} LPS for 24 h. IP was performed on the lysate from triplicate controls and treatments in 3NT affinity sorbent and eluted in a modified Laemmli Buffer (sans glycerol and bromophenol blue). The eluates were trypsin digested using the filter aided sample preparation (FASP) method (49), a recent advance in size-exclusion based buffer exchange that is detergent compatible and facilitates proteolytic digestion in a single apparatus. FASP significantly improves peptide recovery compared to solid phase detergent removal systems. Desalted samples were analyzed in the Finnigan LTQ (Thermo Scientific, USA) for relative quantitation using the spectral counting method (75).

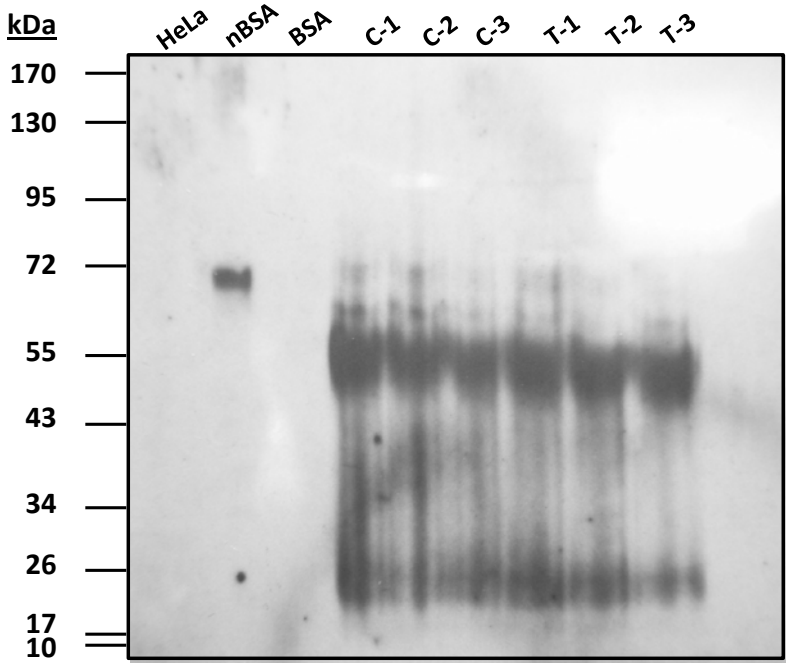

Figure 24. Anti-3NT Western of histone H4 IP from LPS-treated HAPI lysates. Apparent nitrotyrosine was detected in the histone H4 IP lanes (C1-3, T1-3). HPLC-MS/MS analyses of bands near 55 kDa and 20 kDa excised from a SDS-PAGE gel run in parallel did not identify histone H4. HeLa lysate (lane 1) was included as a positive control for histone H4 and negative control for 3NT. HeLa lysate was also negative for histone H4 detection after stripping and re-probing the blot with anti-histone H4. Nitrotyrosine-containing BSA (nBSA) was used as the positive control for 3NT.

Although spectral counts were below thresholds for significance, histone spectral counts indicated 3NT enrichment similar to that of the SILAC experiment (Fig. 22a). Additionally, histone identifications originated predominantly from the LPS treatment group—indicative of endotoxin-induced upregulation of iNOS linked to concomitant increase in Tyr nitration.

Two unique peptides representing histone H4 showed > 95% spectrum identification probability as well as 99% protein group confidence. Histone identifications from this experiment, those from SILAC analysis of LPS-treated HAPI, and a previously reported histone H4 nitration site-identification (72)

provided the foundation for histone-focused experiments. Our aim was to evaluate global and site-specific histone nitration considering PTN to be a potential modulator of gene expression under oxidative/nitrative stress conditions.

Histone H4 targeted enrichment

To validate the SILAC gel extract and direct eluate data from 3NT IP analyses, which indicated increased histone nitration upon LPS-induced inflammatory stimulus, anti-histone H4 antibody was used for protein-specific IP to enhance recovery of a putative PTN target. However, results from several attempts at histone H4 enrichment with subsequent anti-3NT Western analyses were inconclusive. Nitrotyrosine Western detections were dubious as clear protein bands could not be resolved and thus were not quantifiable. Also, the 3NT-containing bands that were detected appeared closer to 20 kDa and 50 kDa as seen in Figure 24—too high to be histone H4.

Moreover, histone H4 was not identified from HPLC-MS/MS analyses of tryptic gel digests of cognate bands excised from Coomassie-stained gels run in parallel with the 3NT westerns (data not shown). After stripping, histone H4 re-probing of the blots resulted in almost identical results to 3NT staining as seen in Figure 24, further confounding analyses.

Indirect microglial activation by ethanol-induced neuronal signaling

As mentioned in the introduction to this chapter, factors secreted by neurons inhibit microglia under normal conditions (28, 34). To determine the effect of alcohol on neuronal regulation of microglial activation, HAPI cultures

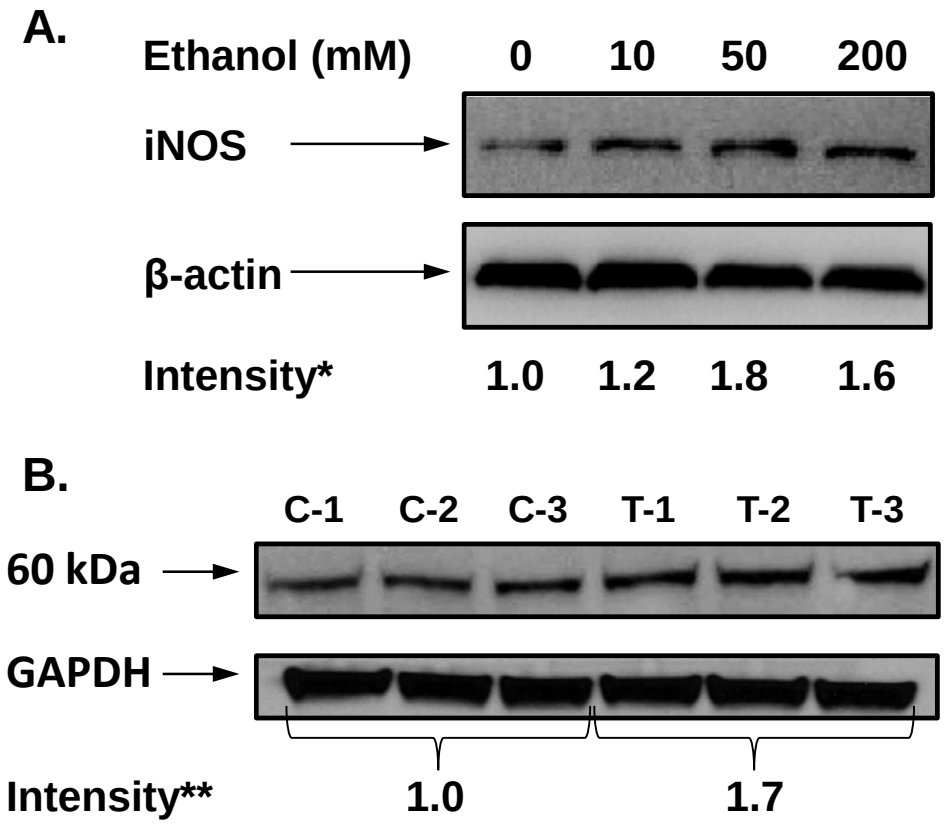

Figure 25. Ethanol-induced neuronal secretions increase nitration in microglia. A) Anti-iNOS Western analysis of HAPI microglia lysates treated with B35 neuron-conditioned media from 24 h exposure to four ethanol concentrations. B) Anti-3NT western blot of the ~ 60 kDa band from HAPI lysate treated with B35-conditioned media from 24 h exposure to 50 mM ethanol. *Normalized intensity is the mean of two experimental results; **Normalized intensity is the mean of triplicate results ($p < 0.025$, paired t-test).

were exposed to media conditioned by B35 neurons treated with 10, 50, and 200 mM ethanol for 24 h (30). Anti-iNOS western blot analysis of the HAPI lysates detected a single band located close to the expected iNOS migration (~ 131 kDa). Densitometry analysis (ImageJ) calculated the greatest iNOS expression increase to be 80% (Fig. 25A) in the 50 mM treatment group (30). These data supported our hypothesis that ethanol exposure alters neuronal secretions, resulting in classical activation of microglia (39, 40).

Thus, a concomitant nitration increase in microglia activated by ethanol-induced neuronal secretion was expected to be seen. To test this, the above experiment using 50 mM ethanol exposure was repeated and analyzed the resulting lysates by 3NT western blot (Fig. 25B). Interestingly, a single band near ~ 60 kDa was detected—a clear departure from the LPS- induced nitration profile seen in Figure 20. ImageJ densitometry analysis revealed a 70% increase in nitration on the 60 kDa band (Fig 25b) correlating to the 80% iNOS increase found previously (30) and supporting our assertion that ethanol-induced neuronal secretion induces nitration increase in indirectly-activated microglia.

HAPI cell indirect activation

LPS-induced microglial activation resulted in increased nitration to core histones, specifically histone H4. To increase sensitivity for histone nitration detection after indirect activation, the histone fraction from HAPI culture exposed to conditioned media from ethanol-treated B35 cells were enriched. Additionally, a histone nitropeptide-targeted method was developed to increase mass spectrometric sensitivity.

Tryptic peptides containing Tyr from the four core histones were ascertained by manual sequence analysis. Arg, Lys and Pro residues were highlighted to indicate potential cleavage sites. Plus two-charged nitropeptide ion precursor masses were determined by adding 45 Da for nitro- addition and 1 Da for H^+ to their calculated molecular masses from the Expasy pI/Mw computer (77, 78), then dividing by two. Precursors with m/z between 300 and 1800 were included in the targeted method. Since eleven targets were required for this

Table 3. Rat histone sequences for nitropeptide targeted method development.

Rat Histone sequences for nitropeptide targeted method development
>gi|66730355|**R**ef|NP_001019453.1| **histone H2a** [Rattus norvegicus] MSG**R**G**K**QGG**K**A**R**A**K**A**K**T**R**SS**R**AGLQFPVG**R**V**HR**LLY**K**GNYSE**R**VGASAPVY LAAVLEYLTAEILELAGNAA**R**DN**KK**T**R**IIP**RH**LQLAI**R**NDEELN**K**LLG**R**VTIAQGG VLPNIQAVLLP**KK**TES**HHK**S**K**G**K** Theoretical pI/Mw: 10.74 / 14188.51
>gi|204603|gb|AAA74755.1| **histone H2B** [Rattus norvegicus] MPEVSA**K**GTTIS**KK**GF**KK**AVT**K**TQ**KK**EG**RKRKR**C**R**EESYSIYIY**K**VL**K**QV**H**PD TGISS**K**AMSIMNSFVTDIFE**R**IAGEAS**R**LA**H**YN**K**R**R**STITS**R**EIQTAV**R**LLLPGELA **KH**AVSEGT**K**AVT**K**YTSS**K** Theoretical pI/Mw: 10.19 / 14225.51
>gi|313319|emb|CAA52035.1| **histone H3** [Rattus norvegicus] MA**R**T**K**QTA**RK**STGG**K**AP**RK**QLAT**K**AA**RK**SAPSTGGV**KK**P**HR**Y**R**PGTVAL**R**EI **RR**YQ**K**STELLI**RK**LPFQ**R**LV**R**EIAQDF**K**TDL**R**FQSAAIGALQEASEAYLVGLFED TNLCAI**H**A**K**RVTIMP**K**DIQLA**RR**I**R**GE**R**A Theoretical pI/Mw: 11.27 / 15327.91
>gi|204601|gb|AAA60735.1| **histone H4** [Rattus norvegicus] MSG**R**G**K**GG**K**GLG**K**GGA**KRHRK**VL**R**DNIQGIT**K**PAI**RR**LA**RR**GGV**KR**ISGLIYE ET**R**GVL**K**VFLENVI**R**DAVTYTE**H**A**K**R**K**TVTAMDVVYAL**K**RQG**R**TLYGFGG Theoretical pI/Mw: 11.36 / 11367.34

Manual analysis of trypsin cleavages among the core histone sequences was performed to determine nitropeptide precursor masses for targeted method development. Tyr-containing tryptic peptides representing possible nitropeptide MS/MS targets are highlighted in green (or blue to distinguish adjacent peptides). Basic residues are shown in bold for each of the four core histones. Below each sequence are the theoretical isoelectric points and molecular weights for each—calculated using the Expasy pI/MW computer (77, 78).

analysis, data-dependent scans were limited to the top-3 most intense ions to preserve a functional scan interval.

Because nitroprotein targets were determined manually, it was possible that the analytical ions would differ (e.g. missed cleavage). Thus, a second analysis of each isolate using top-ten data-dependent acquisition was performed for complementarity. The four core histone amino acid sequences are shown in Table 3 with basic residues shown in bold.

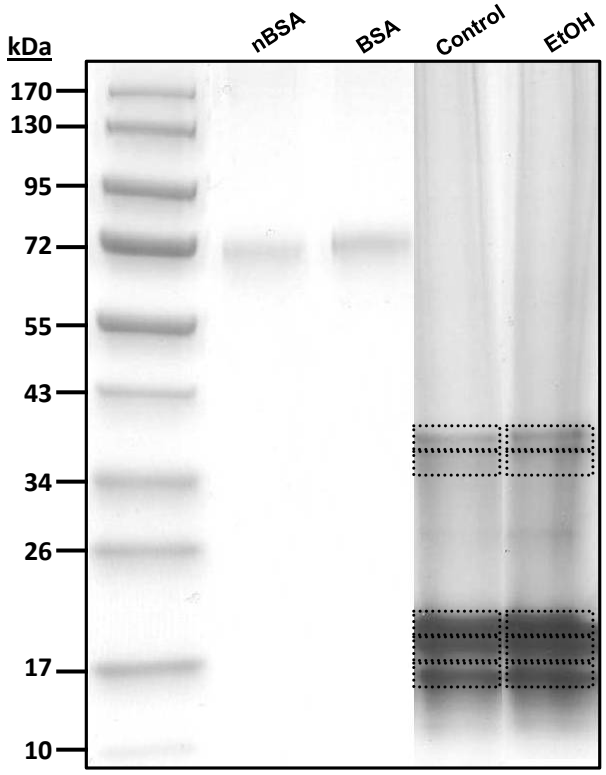

Figure 26. Histone extract analysis using SDS-PAGE & targeted HPLC-MS/MS. A 4-20% gradient SDS-PAGE gel was run for 50 min at 120V to resolve the four histone isoforms. Five bands each were excised from control and treatment lanes at locations near our target MWs (H3-15 kDa, H2B-14 kDa, H2A-14 kDa, and H4- 11 kDa as well as possible core histone complexes-34 kDa). Gel bands were trypsin digested and analyzed by data-dependent MS/MS to include all possible modification states and targeted MS/MS for 3NT-containing peptides. Doubly-charged nitropeptide precursor masses were calculated manually using the pI/MW calculator at http://web.expasy.org/compute_pi/ with addition of +45 Da for nitro- addition and +1 Da for protonation. HPLC-MS/MS analyses were used to identify band contents and determine variable modification between control and ethanol-treated B35 media-condition HAPI after 24 h exposure. The band seen near 26 kDa, expected to contain the linker histone, H1, was not analyzed.

Since a modified method for histone extraction based on Siuti and Kelleher (48) had been previously performed successfully in our laboratory using AML12 (ATCC CRL-2254) lysates (mouse hepatocytes expressing human TGF-α), it was applied to histone extractions from HAPI microglia. The method

exploits the chemistry of histones, which are readily precipitated from nuclear fractions due to their inherent basicity (see Table 3).

Nuclear isolates were acquired by centrifugation in isolation buffer followed by acid extraction of histones on ice. Because acid extraction requires addition of sulfuric acid to five times the nuclear suspension volume, our expectation was that the histone concentrations would be too low for analysis. To correct this, the extracts (900 µL) were speed-vac concentrated to ~ 50 µL. The resulting protein concentrations of the histone concentrates were ~ 0.7 mg $\times$ mL^{-1}, sufficient for SDS-PAGE and Western analysis.

Histone extracts were analyzed by SDS-PAGE on a 4-20% gradient gel. To verify histone enrichment, the gel was Coomassie stained. Three distinct bands were detected in the MW region below 20 kDa, likely representing histone isoforms. Five bands circled in Figure 26, including histone isoforms and possibly the core complex were excised and in-gel digested.

The gel digests were analyzed by both a histone nitropeptide-targeted/ top-3 and a top-10 data-dependent HPLC-MS/MS acquisition on a LTQ. Mascot search of the UniProt mouse database with Scaffold validation confirmed successful histone enrichment (Fig. 27) and a possible nitration site on a histone H3 peptide ($KPHRY^{(nitro)}RPGTVALR$) was identified (Fig 28) in both the control and treatment (one spectrum for each). Although the nitropeptide identified had one missed cleavage at the Arg adjacent to the nitration site, comparison of the nitropeptide and unmodified spectra where the sequences were identical showed identity for product ion masses and peak intensities. Histone H3 Tyr^{41} had also

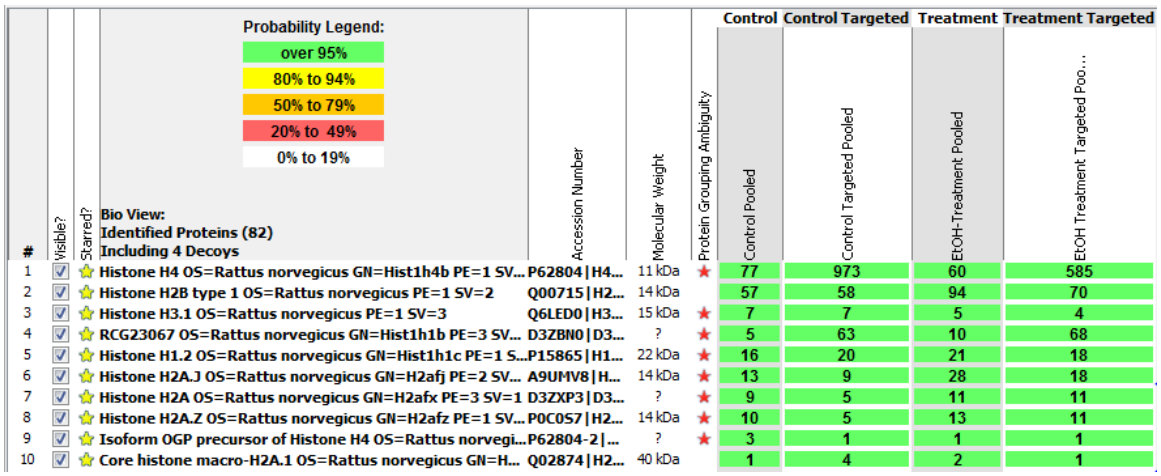

#	Visible?	Starred?	Bio View: Identified Proteins (82) Including 4 Decoys	Accession Number	Molecular Weight	Protein Grouping Ambiguity	Control Pooled	Control Targeted Pooled	EtOH-Treatment Pooled	EtOH Treatment Targeted Poo…
			Probability Legend: over 95% / 80% to 94% / 50% to 79% / 20% to 49% / 0% to 19%				Control	Control Targeted	Treatment	Treatment Targeted
1	☑	☆	Histone H4 OS=Rattus norvegicus GN=Hist1h4b PE=1 SV...	P62804|H4...	11 kDa	★	77	973	60	585
2	☑	☆	Histone H2B type 1 OS=Rattus norvegicus PE=1 SV=2	Q00715|H2...	14 kDa		57	58	94	70
3	☑	☆	Histone H3.1 OS=Rattus norvegicus PE=1 SV=3	Q6LED0|H3...	15 kDa	★	7	7	5	4
4	☑	☆	RCG23067 OS=Rattus norvegicus GN=Hist1h1b PE=3 SV...	D3ZBN0|D3...	?	★	5	63	10	68
5	☑	☆	Histone H1.2 OS=Rattus norvegicus GN=Hist1h1c PE=1 S...	P15865|H1...	22 kDa	★	16	20	21	18
6	☑	☆	Histone H2A.J OS=Rattus norvegicus GN=H2afj PE=2 SV...	A9UMV8|H...	14 kDa	★	13	9	28	18
7	☑	☆	Histone H2A OS=Rattus norvegicus GN=H2afx PE=3 SV=1	D3ZXP3|D3...	?	★	9	5	11	11
8	☑	☆	Histone H2A.Z OS=Rattus norvegicus GN=H2afz PE=1 SV...	P0C057|H2...	14 kDa	★	10	5	13	11
9	☑	☆	Isoform OGP precursor of Histone H4 OS=Rattus norvegi...	P62804-2|...	?	★	3	1	1	1
10	☑	☆	Core histone macro-H2A.1 OS=Rattus norvegicus GN=H...	Q02874|H2...	40 kDa		1	4	2	1

Figure 27. Histone enrichment validation. Scaffold analysis results validated histone enrichment from HAPI microglia incubated for 24 h in B35 neuron-conditioned media from 50 mM ethanol exposure for 24 h. Nuclear proteins were isolated using the NE-PER Nuclear and Cytoplasmic Extraction Reagents (Thermo Scientific, USA). Histones were acid extracted using a modified version of the method described by Siuti and Kelleher (2010). Histone proteins represented 12% of protein IDs with a 1.3 % peptide false discovery rate (FDR) and a 1.5 % protein FDR. Targeted analysis increased total spectral count for Histone H4 by > 10-fold due to an unmodified peptide that is isobaric with one of the nitropeptide targets.

been identified in a preliminary experiment using human primary hepatocytes (Fig. 19) and is a known phosphorylation site involved in chromatin remodeling (79). Synthetic KPHRY$^{(nitro)}$RPGTVALR can be synthesized and analyzed to validate the identification as described in Chapter Two.

Nitrotyrosine localizes to the nucleus

To validate our hypothesis that histones are subject to PTN in the nucleus the HAPI LPS treatments were repeated, since LPS induces a stronger nitrative stress response as demonstrated by Figure 20. The cells were grown to ~ 70% confluence and fixed with 4% paraformaldehyde. DNA was stained with 4',6-diamidino-2-phenylindole (DAPI), followed by immunostaining with anti- 3NT

A.

Q6LED0|H31_RAT (100%), 15,404.7 Da
Histone H3.1 OS=Rattus norvegicus PE=1 SV=3
1 unique peptides, 1 unique spectra, 1 total spectra, 13/136 amino acids (10% coverage)

M A R T K Q T A R K S T G G K A P R K Q L A T K A A R K S A P A T G G V K **K P H** **R Y R P G T V A L R** E I R R Y Q K S T E
L L I R K L P F Q R L V R E I A Q D F K T D L R F Q S S A V M A L Q E A C E A Y L V G L F E D T N L C A I H A K R V T I
M P K D I Q L A R R I R G E R A

B.

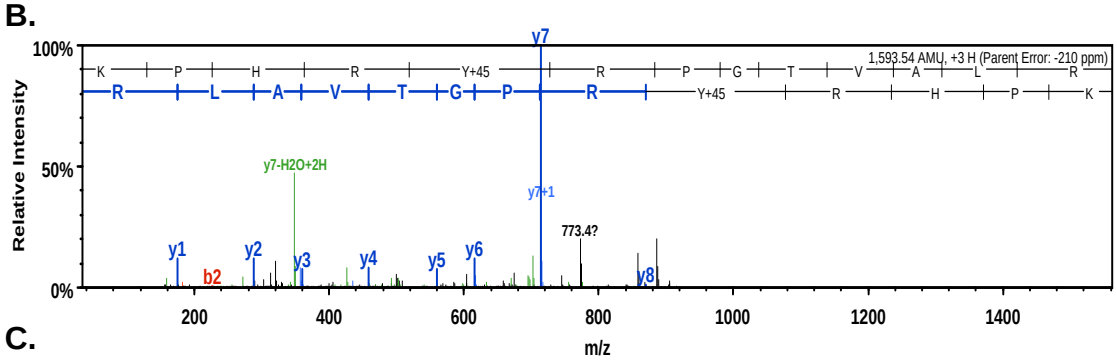

C.

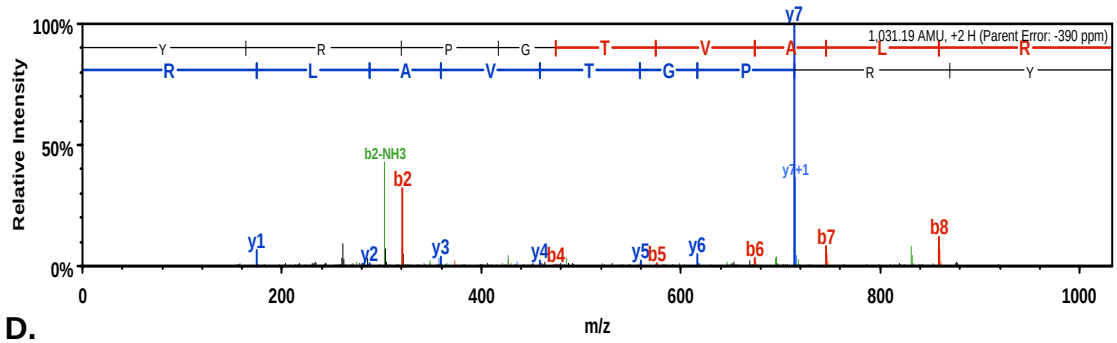

D.

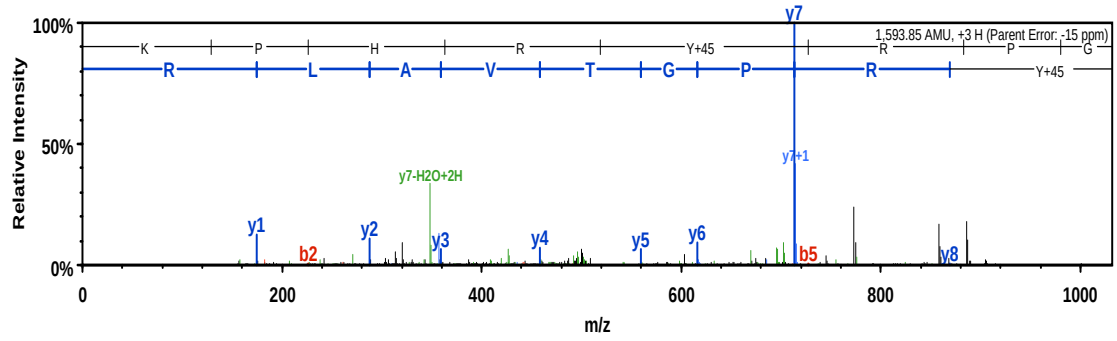

Figure 28. Histone H3 nitration site identification. A putative nitration site on histone H3 Tyr[41] was identified by targeted MS as seen highlighted in (A). Total sequence coverage for histone H3 improved from 26% for non-targeted treatment to 37% for the targeted method. The nitropeptide spectra (B & D) originated from a triply-charged precursor with one missed cleavage. The Scaffold peptide probability was 65% with a Mascot score of 30.4. The unmodified spectrum (C) originated from a doubly-charged precursor with no missed cleavages. The Scaffold peptide probability was 95% and the Mascot score was 36.2.

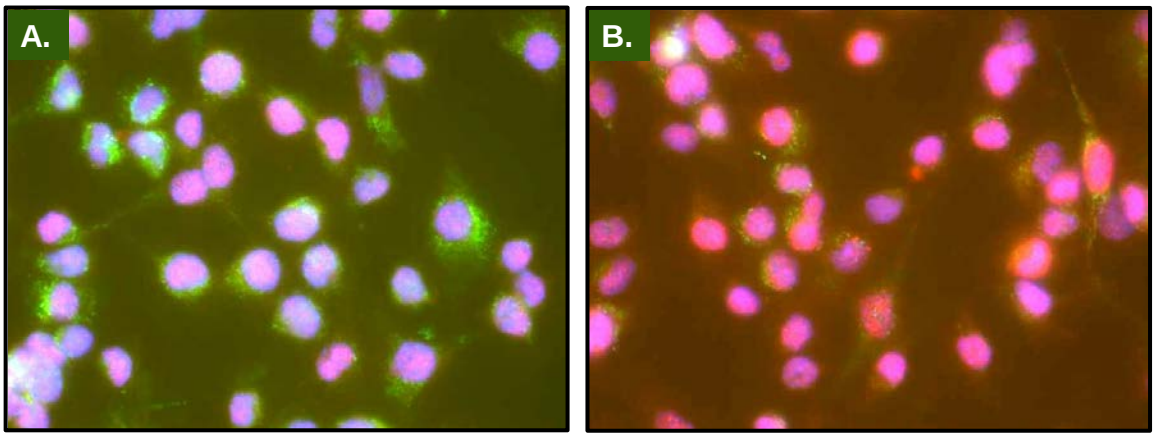

Figure 29. 3NT localization in HAPI nuclei. HAPI cells were immunostained for 3NT (green) and histone H3 (red) in either untreated (A) or treated with 50 ng $\times$ mL^{-1} LPS (B) for 12 h. DAPI (blue) was used to stain for DNA. Nitrotyrosine immunoreactivity was detected throughout the cytoplasm and appears to be within the nucleus. Histone H3 was also detected within the nucleus; however, confocal microscopy will be necessary to validate the co-localization of histone H3 and 3NT.

and histone H3 fluorescent antibody conjugates. Nitrotyrosine was expected to be present throughout the cell and histone H3 and 3NT were expected to colocalize with DNA inside the nucleus.

In the fluorescence microscope images seen in Figure 29, immunoreactivity from both nitrotyrosine and histone H3 was observed in the nucleus. This result remains inconclusive as to colocalization with histones, which will require high-resolution confocal microscopy. Also, future experiments should include staining for iNOS with the expectation that it will also localize to the nucleus, supporting the assertion that $ONOO^-$ can be generated within the compartment.

References cited

1. Abello N, Kerstjens HAM, Postma DS, Bischoff R. Protein tyrosine nitration: Selectivity, physicochemical and biological consequences, denitration, and proteomics methods for the identification of tyrosine-nitrated proteins. Journal of Proteome Research. 2009 07/06;8(7):3222-38.

2. Heilbronn LK, Ravussin E. Calorie restriction and aging: Review of the literature and implications for studies in humans. Am J Clin Nutr. 2003 September 1, 2003;78(3):361-9.

3. Beckman JS, Beckman TW, Chen J, Marshall PA, Freeman BA. Apparent hydroxyl radical production by peroxynitrite: Implications for endothelial injury from nitric oxide and superoxide. Proceedings of the National Academy of Sciences. 1990 February 01;87(4):1620-4.

4. Kirsch M, de Groot H. Formation of peroxynitrite from reaction of nitroxyl anion with molecular oxygen. J Biol Chem. 2002 April 19, 2002;277(16):13379-88.

5. Beckman JS. Oxidative damage and tyrosine nitration from peroxynitrite. Chem Res Toxicol. 1996 01/01;9(5):836-44.

6. Goldstein S, Merenyi G. The chemistry of peroxynitrite: Implications for biological activity. Globins and Other Nitric Oxide-Reactive Proteins, Pt a. 2008;436:49-61.

7. Hoek JB, Cahill A, Pastorino JG. Alcohol and mitochondria: A dysfunctional relationship. Gastroenterology. 2002 /6;122(7):2049-63.

8. Jaeschke H, Gores GJ, Cederbaum AI, Hinson JA, Pessayre D, Lemasters JJ. Mechanisms of hepatotoxicity. Toxicological Sciences. 2002 02/01;65(2):166-76.

9. Wheeler MD. Endotoxin and kupffer cell activation in alcoholic liver disease. Alcohol Research & Health. 2003 01/04;27(4):300-6.

10. Wheeler M, Nakagami M, Bradford B, Uesugi T, Mason R, Connor H, et al. Overexpression of manganese superoxide dismutase prevents alcohol-induced liver injury in the rat. Journal of Biological Chemistry. 2001 Sep 28;276(39):36664-72.

11. Das SK, Vasudevan DM. Alcohol-induced oxidative stress. Life Sci. 2007 /6/27/;81(3):177-87.

12. Albano E. Oxidative mechanisms in the pathogenesis of alcoholic liver disease. Molecular Aspects of Medicine. 2008 Feb-Apr;29(1-2):9-16.

13. Maher J. Exploring alcohol's effects on liver function. Alcohol Health & Research World. 1997;21(1):5-12.

14. Mantena SK, King AL, Andringa KK, Eccleston HB, Bailey SM. Mitochondrial dysfunction and oxidative stress in the pathogenesis of alcohol- and obesity-induced fatty liver diseases. Free Radical Biology and Medicine. 2008 Apr 1;44(7):1259-72.

15. Lieber C. Alcoholic fatty liver: Its pathogenesis and mechanism of progression to inflammation and fibrosis. Alcohol. 2004 AUG;34(1):9-19.

16. Thurman RG. Alcoholic liver injury involves activation of kupffer cells by endotoxin. American Journal of Physiology - Gastrointestinal and Liver Physiology. 1998 10/01;275(4):G605-11.

17. Kono H, Rusyn I, Yin M, Gäbele E, Yamashina S, Dikalova A, et al. NADPH oxidase-derived free radicals are key oxidants in alcohol-induced liver disease. J Clin Invest. 2000 01/01;106(7):867-72.

18. Joza N, Susin SA, Daugas E, Stanford WL, Cho SK, Li CYJ, et al. Essential role of the mitochondrial apoptosis-inducing factor in programmed cell death. Nature. 2001 03/29;410(6828):549-54.

19. Bhutia SK, Mallick SK, Stevens SM, Prokai L, Vishwanatha JK, Maiti TK. Induction of mitochondria-dependent apoptosis by abrus agglutinin derived peptides in human cervical cancer cell. Toxicology in Vitro. 2008 /3;22(2):344-51.

20. Chen Z, Jalabi W, Shpargel KB, Farabaugh KT, Dutta R, Yin X, et al. Lipopolysaccharide-induced microglial activation and neuroprotection against experimental brain injury is independent of hematogenous TLR4. The Journal of Neuroscience. 2012 August 22, 2012;32(34):11706-15.

21. MacMicking JD, Nathan C, Hom G, Chartrain N, Fletcher DS, Trumbauer M, et al. Altered responses to bacterial infection and endotoxic shock in mice lacking inducible nitric oxide synthase. Cell. 1995 /5/19/;81(4):641-50.

22. Xie Q, Nathan C. The high-output nitric oxide pathway: Role and regulation. J Leukoc Biol. 1994 11/01;56(5):576-82.

23. Mungrue IN, Husain M, Stewart DJ. The role of NOS in heart failure: Lessons from murine genetic models. Heart Fail Rev. 2002 Oct;7(4):407-22.

24. Neumann H, Hazen JL, Weinstein J, Mehl RA, Chin JW. Genetically encoding protein oxidative damage. J Am Chem Soc. 2008 03/01;130(12):4028-33.

25. Reynolds MR, Berry RW, Binder LI. Nitration in neurodegeneration: Deciphering the “Hows” “nYs”. Biochemistry (N Y). 2007 06/01; 2012/12;46(25):7325-36.

26. Giasson BI, Duda JE, Murray IVJ, Chen Q, Souza JM, Hurtig HI, et al. Oxidative damage linked to neurodegeneration by selective α-synuclein nitration in synucleinopathy lesions. Science. 2000 November 3, 2000;290(5493):985-9.

27. Cheepsunthorn P, Radov L, Menzies S, Reid J, Connor JR. Characterization of a novel brain-derived microglial cell line isolated from neonatal rat brain. Glia. 2001 Jul;35(1):53-62.

28. Aguzzi A, Barres BA, Bennett ML. Microglia: Scapegoat, saboteur, or something else? Science. 2013 January 11, 2013;339(6116):156-61.

29. Bell-Temin H, Barber DS, Zhang P, Liu B, Stevens SM,Jr. Proteomic analysis of rat microglia establishes a high-confidence reference data set of over 3000 proteins. Proteomics. 2012 Jan;12(2):246-50.

30. Seeley KW, Zhang P, Stevens Jr. SM, Liu B. Identification of LPS and ethanol-mediated protein nitration targets in microglia. J Neurotoxicology. 2013 (in preparation).

31. Schulz C, Perdiguero EG, Chorro L, Szabo-Rogers H, Cagnard N, Kierdorf K, et al. A lineage of myeloid cells independent of myb and hematopoietic stem cells. Science. 2012 April 6, 2012;336(6077):86-90.

32. Mildner A, Schlevogt B, Kierdorf K, Böttcher C, Erny D, Kummer MP, et al. Distinct and non-redundant roles of microglia and myeloid subsets in mouse models of alzheimer's disease. The Journal of Neuroscience. 2011 August 3, 2011;31(31):11159-71.

33. Ajami B, Bennett JL, Krieger C, McNagny KM, Rossi FMV. Infiltrating monocytes trigger EAE progression, but do not contribute to the resident microglia pool. Nat Neurosci. 2011 print;14(9):1142-9.

34. Ransohoff RM, Cardona AE. The myeloid cells of the central nervous system parenchyma. Nature. 2010 11/11;468(7321):253-62.

35. Austin SA, Floden AM, Murphy EJ, Combs CK. Alpha-synuclein expression modulates microglial activation phenotype. J Neurosci. 2006 Oct 11;26(41):10558-63.

36. Wilms H, Rosentiel P, Sievers J, Deuschl G, Zecca L, Lucius R. Activation of microglia by human neuromelanin is NF-kB dependent and involves p38 mitogen-activated protein kinase: Implications for parkinsons disease. The FASEB Journal. 2003 03/01;17(3):500-2.

37. Liu B. Modulation of microglial pro-inflammatory and neurotoxic activity for the treatment of parkinsons disease. The AAPS Journal. 2006 09/01;8(3):E606-21.

38. Block ML, Zecca L, Hong J. Microglia-mediated neurotoxicity: Uncovering the molecular mechanisms. Nat Rev Neurosci. 2007 print;8(1):57-69.

39. Marshall SA, McClain JA, Kelso ML, Hopkins DM, Pauly JR, Nixon K. Microglial activation is not equivalent to neuroinflammation in alcohol-induced neurodegeneration: The importance of microglia phenotype. Neurobiol Dis. 2013 /6;54(0):239-51.

40. Bell-Temin H, Zhang P, Chaput D, King MA, You M, Liu B, et al. Quantitative proteomic characterization of ethanol-responsive pathways in rat microglial cells. J Proteome Res. 2013 03/15; 2013/04.

41. Dutta G, Zhang P, Liu B. The lipopolysaccharide parkinson?s disease animal model: Mechanistic studies and drug discovery. Fundam Clin Pharmacol. 2008;22(5):453-64.

42. Svegliati-Baroni G, Saccomanno S, Van Goor H, Jansen P, Benedetti A, Moshage H. Involvement of reactive oxygen species and nitric oxide radicals in activation and proliferation of rat hepatic stellate cells. Liver. 2001 02/01;21(1):1-12.

43. Burguillos MA, Deierborg T, Kavanagh E, Persson A, Hajji N, Garcia-Quintanilla A, et al. Caspase signalling controls microglia activation and neurotoxicity. Nature. 2011 04/21;472(7343):319-24.

44. Saijo K, Collier J, Li A, Katzenellenbogen J, Glass C. An ADIOL-ERβ-CtBP transrepression pathway negatively regulates microglia-mediated inflammation. Cell. 2011 5/13;145(4):584-95.

45. Qin L, Block ML, Liu Y, Bienstock RJ, Pei Z, Zhang W, et al. Microglial NADPH oxidase is a novel target for femtomolar neuroprotection against oxidative stress. The FASEB Journal. 2005 April 01;19(6):550-7.

46. Qin L, Liu Y, Wang T, Wei S, Block ML, Wilson B, et al. NADPH oxidase mediates lipopolysaccharide-induced neurotoxicity and proinflammatory gene expression in activated microglia. J Biol Chem. 2004 01/09;279(2):1415-21.

47. Gao H, Jiang J, Wilson B, Zhang W, Hong J, Liu B. Microglial activation-mediated delayed and progressive degeneration of rat nigral dopaminergic neurons: Relevance to parkinson's disease. J Neurochem. 2002;81(6):1285-97.

48. Siuti N, Kelleher NL. Efficient readout of posttranslational codes on the 50-residue tail of histone H3 by high-resolution MS/MS. Anal Biochem. 2010 1/15;396(2):180-7.

49. Wisniewski JR, Zougman A, Nagaraj N, Mann M. Universal sample preparation method for proteome analysis. Nat Meth. 2009 print;6(5):359-62.

50. Ong S, Blagoev B, Kratchmarova I, Kristensen DB, Steen H, Pandey A, et al. Stable isotope labeling by amino acids in cell culture, SILAC, as a simple and accurate approach to expression proteomics. Molecular & Cellular Proteomics. 2002 May;1(5):376-86.

51. Keller A, Nesvizhskii AI, Kolker E, Aebersold R. Empirical statistical model to estimate the accuracy of peptide identifications made by MS/MS and database search. Anal Chem. 2002 10/01;74(20):5383-92.

52. Nesvizhskii AI, Keller A, Kolker E, Aebersold R. A statistical model for identifying proteins by tandem mass spectrometry. Anal Chem. 2003 09/01;75(17):4646-58.

53. Petre BA, Ulrich M, Stumbaum M, Bernevic B, Moise A, Doring G, et al. When is mass spectrometry combined with affinity approaches essential? A case study of tyrosine nitration in proteins. J Am Soc Mass Spectrom. 2012 Nov;23(11):1831-40.

54. Herce-Pagliai C, Kotecha S, Shuker DEG. Analytical methods for 3-nitrotyrosine as a marker of exposure to reactive nitrogen species: A review. Nitric Oxide. 1998 10;2(5):324-36.

55. Duncan MW. A review of approaches to the analysis of 3-nitrotyrosine. Amino Acids. 2003 12/01;25(3):351-61.

56. Block MR, Vignais PV. Substrate-site interactions in the membrane-bound adenine-nucleotide carrier as disclosed by ADP and ATP analogs. Biochim Biophys Acta. 1984 Nov 26;767(2):369-76.

57. Rich P, Moody AJ. Cytochrome c oxidase. In: GrÃ¤ber P, Milazzo G, Walz D, editors. BirkhÃ¤user Basel; 1996. p. 418-56.

58. Bosron WF, Li T. Genetic polymorphism of human liver alcohol and aldehyde dehydrogenases, and their relationship to alcohol metabolism and alcoholism. Hepatology. 1986 05/01;6(3):502-10.

59. Newton BW, Russell WK, Russell DH, Ramaiah SK, Jayaraman A. Liver proteome analysis in a rodent model of alcoholic steatosis. Journal of Proteome Research. 2009 04/03;8(4):1663-71.

60. Karamanakos PN, Pappas P, Boumba VA, Thomas C, Malamas M, Vougiouklakis T, et al. Pharmaceutical agents known to produce disulfiram-like reaction: Effects on hepatic ethanol metabolism and brain monoamines. International Journal of Toxicology (Taylor & Francis). 2007 09;26(5):423-32.

61. Kono Y, Fridovich I. Superoxide radical inhibits catalase. Journal of Biological Chemistry. 1982 May 25;257(10):5751-4.

62. Hayes JD, Pulford DJ. The glutathione S-transferase supergene family: Regulation of GST and the contribution of the isoenzymes to cancer chemoprotection and drug resistance. Crit Rev Biochem Mol Biol. 1995;30(6):445-600.

63. Takakusa H, Mohar I, Kavanagh TJ, Kelly EJ, Kaspera R, Nelson SD. Protein tyrosine nitration of mitochondrial carbamoyl phosphate synthetase 1 and its functional consequences. Biochem Biophys Res Commun. 2012 3/30;420(1):54-60.

64. Jitrapakdee S, St Maurice M, Rayment I, Cleland WW, Wallace JC, Attwood PV. Structure, mechanism and regulation of pyruvate carboxylase. Biochem J. 2008 Aug 1;413(3):369-87.

65. Greenfield RB, Cecava MJ, Donkin SS. Changes in mRNA expression for gluconeogenic enzymes in liver of dairy cattle during the transition to lactation. J Dairy Sci. 2000 Jun;83(6):1228-36.

66. Elfering SL, Haynes VL, Traaseth NJ, Ettl A, Giulivi C. Aspects, mechanism, and biological relevance of mitochondrial protein nitration sustained by mitochondrial nitric oxide synthase. American Journal of Physiology - Heart and Circulatory Physiology. 2004 January 01;286(1):H22-9.

67. Haynes V, Traaseth NJ, Elfering S, Fujisawa Y, Giulivi C. Nitration of specific tyrosines in FoF1 ATP synthase and activity loss in aging. American Journal of Physiology - Endocrinology And Metabolism. 2010 May 01;298(5):E978-87.

68. Thompson LV, Durand D, Fugere NA, Ferrington DA. Myosin and actin expression and oxidation in aging muscle. J Appl Physiol. 2006 12/01;101(6):1581-7.

69. Fujisawa Y, Kato K, Giulivi C. Nitration of tyrosine residues 368 and 345 in the beta-subunit elicits F0F1-ATPase activity loss. Biochem J. 2009 Oct 15;423:219-31.

70. Wang Y, Geer LY, Chappey C, Kans JA, Bryant SH. Cn3D: Sequence and structure views for entrez. Trends Biochem Sci. 2000 Jun;25(6):300-2.

71. Giulivi C. Functional implications of nitric oxide produced by mitochondria in mitochondrial metabolism. Biochem J. 1998 Jun 15, 1998;332(3):673-9.

72. Haqqani AS, Kelly JF, Birnboim HC. Selective nitration of histone tyrosine residues in vivo in mutatect tumors. J Biol Chem. 2002 02/01;277(5):3614-21.

73. Domon B, Aebersold R. Mass spectrometry and protein analysis. Science. 2006 /4/14;312(5771):212-7.

74. Fournier ML, Gilmore JM, Martin-Brown S, Washburn MP. Multidimensional separations-based shotgun proteomics. Chem Rev. 2007 08/01; 2013/04;107(8):3654-86.

75. Choi H, Fermin D, Nesvizhskii AI. Significance analysis of spectral count data in label-free shotgun proteomics. Molecular & Cellular Proteomics. Dec 2008;7(12):2373-85.

76. Annesley TM. Ion suppression in mass spectrometry. Clin Chem. 2003 Jul;49(7):1041-4.

77. Bjellqvist B, Hughes GJ, Pasquali C, Paquet N, Ravier F, Sanchez JC, et al. The focusing positions of polypeptides in immobilized pH gradients can be predicted from their amino acid sequences. Electrophoresis. 1993 Oct;14(10):1023-31.

78. Bjellqvist B, Basse B, Olsen E, Celis JE. Reference points for comparisons of two-dimensional maps of proteins from different human cell types defined in a pH scale where isoelectric points correlate with polypeptide compositions. Electrophoresis. 1994 Mar-Apr;15(3-4):529-39.

79. Dawson MA, Bannister AJ, Gottgens B, Foster SD, Bartke T, Green AR, et al. JAK2 phosphorylates histone H3Y41 and excludes HP1agr] from chromatin. Nature. 2009 10/08;461(7265):819-22.

Chapter 4: Novel mass spectrometric methods for PTN site detection and quantification

Introduction

Protein-tyrosine nitration site identification

A major obstacle to mass spectrometric PTN identification is the sensitivity required to identify specific nitration sites from a proteome-wide analysis, considering detection of a single representative unmodified peptide is often sufficient to establish reliable protein identification. Since 3NT occurs at abundances ~ five orders of magnitude lower than L-Tyr, integration of one of the enrichment techniques described in Chapter Three is justifiable. Nevertheless, if sensitivity can be enhanced sufficiently to overcome current MS detection limits, nitration site identification from complex biological samples may become possible, averting the pitfalls associated with chemical modification and immunological enrichment.

PTN site identification can facilitate more informed interpretations of the modification's contributions to the functional losses it is most often associated with. In Chapters Two and Three, the increased sensitivity potential of targeted MS/MS was demonstrated. This chapter describes the continuing process to further improve mass spectrometric methods for PTN investigation by exploiting physicochemical properties specific to protein-bound 3NT.

The nitrotyrosine immonium ion as a diagnostic marker

Nitrotyrosine's unique spectrophotometric and chromatographic properties can be advantageous when nitration is abundant (e.g. UV detection in-line with MS) or when the analyte of interest is known (e.g. targeted MS method). On the other hand, when PTN targets are not known or are at low levels, another characteristic of protein-bound 3NT can be exploited—its unique CID-derived immonium fragment ion.

Immonium ions are diagnostic fragments specific to each of the twenty common amino acid residues (Table 4) that can be produced by conventional CID, pulsed-Q collision-induced dissociation (PQD), higher energy collision induced dissociation (HCD), and source fragmentation. They are internal fragment ions formed by a double backbone cleavage characteristic of both y- and a-type ions resulting in the general structure $[H_2N{=}CH\text{-}R]^+$ (1, 2). However, most immonium ions appear with low frequency and those that do appear with stronger signal may not be consistently present (1). Since the immonium ion intensity for Tyr is listed among those considered strong (see Table 4) and 3NT is expected to produce immonium ions of similar intensity, the 3NT immonium ion was evaluated as a diagnostic tool for PTN identification and quantitation.

The 3NT immonium ion had previously been established as a diagnostic marker for nitroprotein identification from $ONOO^-$ reactions with purified protein (3). In this study, the presence of a 3NT immonium ion peak upon peptide fragmentation was used exclusively as confirmation for nitropeptide identifications (3). However, spectral quality for confirmations was less than

ideal, including low signal-to-noise ratios (S/N) and lacking annotations for multitudinous prominent peaks. Considering the analytes originated from *in vitro* reactions with purified protein, this study's results emphasize the challenging nature of PTN site identification.

Another experimental method exploited 3NT immonium ion detection as a trigger for precursor ion scanning on a triple-quadrupole time of flight (QTOF) mass spectrometer (4). The method acquired sequence information from precursor ions that produced 3NT immonium ions upon fragmentation (4). Angiotensin II and BSA standards were reacted with TNM to produce nitropeptides for 3NT immonium ion-based MS method development (4). Again, the resultant nitropeptide spectra generated by a 50-fold molar excess of TNM had low S/N and included many unidentified peaks. These results further demonstrate the difficulty of nitro-site identification from complex mixtures. Nevertheless, the results of these early investigations reinforce the potential applicability of the 3NT-specific immonium ion for PTN study.

Mass spectrometric method development for immonium ion analysis

A limitation to immonium ion detection in linear ion traps is the one-third rule governing MS/MS product ions (5, 6). The one-third rule refers to a low mass cut-off inherent to CID in a linear ion trap where product ion masses below 28% of the isolated precursor mass lose stability. The one-third rule narrows detection of the 3NT immonium ions using conventional CID to precursors below approximately m/z 650.

A potential solution to the one-third cut-off is the use of PQD activation. PQD induces fragmentation on a precursor at an elevated Q-value (high RF amplitude) by a short high resonance excitation pulse with a delay at high amplitude to allow for kinetic fragmentation (7). Then the RF amplitude is rapidly pulsed-down to lower Q, retaining the low mass fragment ions in the trap before scanning them to the detector (7). PQD, however, can require exhaustive collision energy (CE) optimizations before delivering quality spectra (7), and the unconventional resultant spectra can confound conventional search algorithms.

To overcome the deficiencies characteristic of CID and PQD, analysis using both activation types can furnish complementary data (e.g. sequence information from CID and immonium ion peaks from PQD of the same precursor). Mascot database searching can be useful for protein and nitration site identification from the large data sets acquired by these analyses. However, manual reconstruction of XICs containing 3NT immonium ions will likely be necessary to identify sequences from PQD-derived spectra and low-abundance targets co-eluting with peptides of isobaric mass. Fortunately, the modest number of nitropeptides expected within a given proteome supports the practicability of manual data mining for nitration sites.

Quantitative mass spectrometric methods using stable isotope coding

Many current quantitative proteomic methods use either metabolic (8) or chemical (9, 10) stable isotope label incorporation to code differential protein sets. These approaches facilitate quantitation either through comparison of relative MS intensities of peptide ion pairs (8) or through discrete low mass “tags”

resulting from CID of peptides containing isobaric labels (9, 10). High-resolution, accurate-mass (HR/AM) analyzers are generally considered essential for these applications; however, encouraging results produced by the application of novel strategies using linear ion trap (7, 11) and triple-quadrupole (3) mass analyzers warrant further consideration for comparably-equipped laboratories.

Stable isotope labeling by metabolic incorporation

Approaches using metabolic incorporation of stable isotopes such as SILAC (8) are valuable for eliminating downstream sampling errors by combining protein sets immediately following cell lysis (8, 11). Protein ratios are determined by MS signal intensities of differentially-labeled peptide peaks, and MS/MS spectra are employed for protein identifications (11). However, quantitation using MS peaks is complicated by varying levels of background noise and susceptibility to background signals is amplified for low-abundance or modified peptides such as nitropeptides (11). Linear quadrupole ion trap analysis can also amplify the background effects due to lower precursor mass accuracy. However, ion trap sensitivity can be enhanced by increasing the target ion number for CID or PQD activation.

Recently, a novel SILAC adaptation specific to the immonium ions of Leu, Ile, and Val generated by CID was successfully evaluated on an ion trap mass analyzer. Labeling was performed using media depleted for Leu, Ile, and Val and replacing the amino acids with one of two heavy isotope labeled sets. One set of amino acids contained a single ^{13}C label on each residue, while the alternate set contained a single ^{15}N label.

MS analysis yielded isobaric peptide precursor ions; however, CID spectra produced immonium ions pairs separated by 1 Da. The differential masses of immonium ion pairs were the result of the double-backbone cleavage specific to immonium ion production. The ^{15}N-containing peptides retained the +1 Da labels, while the ^{13}C labels were lost during CID (12). Additionally, sequence and quantitative data were both acquired using MS/MS spectra from a single analytical run. Since quantitation was based on MS/MS spectra, the magnitude of background noise was reduced as compared to MS precursor peak quantitation (12). Although this technique can be useful for relative quantitation of protein expression from Leu, Ile and/or Val containing peptides, it can be problematic as tryptic peptides can contain various combinations of coded residues. Moreover, quantitation can be complicated by the fact that Leu and Ile produce a strong immonium ion signal, while Val does not (1, 2).

Stable isotope labeling by chemical incorporation

Post-digestion chemical labeling methods (9, 10) can be both convenient and relatively inexpensive for bottom-up protein and posttranslational modification quantification. In these schemes, isobaric tags are applied to free amino termini on Lys residues, resulting in isobaric precursor ions that fragment to differentiated reporter ions (9, 10). Quantitation is based on ratios of reporter tag MS/MS signal intensities and has been demonstrated in multiplicities up to 8-plex. The major limitation to these approaches is variability among multiplex

Table 4. Immonium ion masses.

Residue	3-Letter Code	1-Letter Code	Immonium ion
Alanine	Ala	A	44
Arginine	Arg	R	129
Asparagine	Asn	N	87
Aspartic Acid	Asp	D	88
Cysteine	Cys	C	76
Glutamic Acid	Glu	E	102
Glutamine	Gln	Q	101
Glycine	Gly	G	30
Histidine	His	H	**110**
Isoleucine	Ile	I	**86**
Leucine	Leu	L	**86**
Lysine	Lys	K	101
Methionine	Met	M	104
Phenylalanine	Phe	F	**120**
Proline	Pro	P	**70**
Serine	Ser	S	60
Threonine	Thr	T	74
Tryptophan	Trp	W	**159**
Tyrosine	Tyr	Y	**136**
3-nitrotyrosine	*3NT*	*nY*	***181***
Valine	Val	V	72

Diagnostic immonium ions produced from internal fragmentation of each amino acid residue are listed. Immonium ion masses shown in **bold** indicate production of a strong signal (1, 2). Nitrotyrosine (in italics) was added since it is not one of the 20 naturally occurring amino acids. It is expected to produce an immonium ion signal commensurate to that of Tyr.

samples resulting in inaccurate quantitation and/or irreproducibility. The inconsistency typically results from excessive sample processing prior to the post-digestion labeling and combining of samples. Additionally, the mass range limitations for CID in an ion trap negate its utility for proteome-wide analysis using the low-mass reporter tags.

Multiplex tandem mass spectrometry with stable isotope labeling

To overcome the aforementioned limitations of protein quantitation in linear ion trap MS, a novel approach to metabolic labeling using MS/MS quantitation of non-isobaric precursors (multiplex MS/MS) has been described (11). In this approach, proteins were coded by supplementation with either normal or heavy [$^{15}N_4$] Arg and [$^{13}C_6$] Lys into Arg/Lys depleted media. Thus, MS peptide pairs resulting from trypsin digestion were expected to deviate by 2 or 3 Da (based on 2^+ precursor charge).

To cover the mass range containing multiplex parent ions, the MS/MS precursor selection window was extended to 10 m/z. Efficiencies for peptide and protein identifications from the extended isotope window were compared to data acquired using a conventional window of 2.5 m/z (11). As expected, the 10 m/z window was more sensitive than the 2.5 m/z window, since its range ensured inclusion of both precursor isotope clusters. However, specificity was diminished in the extended window, while background noise increased.

For automated quantitation of the complicated MS/MS spectra containing y and b ions with peptide pairs separated by 1 Da, it was necessary to develop a unique software program (MS2Ratio). MS2Ratio was designed to apply stringent rules for ratio calculations between $\leq 2^+$ y-type product ions from $\geq 2^+$ charged precursors (11). A second filter was integrated excluding y ions that overlapped with b and y ions with signal intensities $\leq$ 10% of the most abundant y ion pair (11). This multiplex MS/MS approach compared favorably to conventional stable-isotope-labeling using integrated XICs for quantification (11) and appears

to be versatile enough for use in other applications requiring the sensitivity of a linear ion trap or where HR/AM instrumentation is unavailable.

Nitrotyrosine-specific stable isotope labeling

Our isotope-labeling strategy was designed to capitalize on the advantages of the previously-described methods to develop a sensitive and quantifiable PTN-specific mass spectrometric method using a LTQ. The method would be adaptable to an Orbitrap for HR/AM analyses. Our plan was to exploit the unique 3NT immonium ion as a reporter for both PTN identification and as an agent for quantitation. To develop and test the method, a 3NT-specific chemical label was applied to free Tyr, two peptide standards and a protein standard using isotope-coded peroxynitrite. The long-term goal of this method was to apply PTN-specific stable isotope coding to a standard lysate representative of the experimental cell line for identification and quantitation of PTN resulting from oxidative/nitrative stress.

Mass spectrometric analysis of isotope-coded nitrotyrosine immonium ions

We have developed a method that incorporates both CID and PQD activation in a linear ion trap to obtain sequence data and immonium reporter ions throughout the mass range of a LTQ. Modified peptides can be identified by bioinformatic searches (e.g. Mascot) and/or *de novo* sequencing (13) of spectra found by manual screening of XICs reconstructed from ± 1 Da of the heavy-labeled immonium ion (182 m/z). Quantitation can be achieved using the ratios of the immonium ion peak pairs. The relative contributions to immonium ions from endogenously-generated peroxynitrite (181.06 amu) and synthetic heavy-

labeled peroxynitrite (m/z 182.06 amu) result in a ratio that is relevant to nitropeptide and, likewise, nitroprotein abundances. Also, because quantitation is based on MS/MS peaks, background interference is expected to be minimal.

Future plans include use of an Orbitrap analyzer for HR/AM precursor ion scans with CID/PQD activation in the linear ion trap. Also, application of HCD activation in an Orbitrap is in future plans to acquire HR/AM product ion spectra using shorter scan times than those required for high-resolution scans in a linear ion trap. On- or offline fractionation with UV detection at 3NT's unique absorbance λ of 356 nm can be employed to determine chromatographic fractions containing abundant 3NT. Finally, a steep reversed-phase gradient coupled to MS acquisition with source fragmentation on a LTQ can also be used as a nitropeptide screen. Signal for low abundance ions would be increased due to the steep gradient and sensitivity can be increased by implementation of a segmented MS method focusing on RTs where 3NT immonium ion signals were previously detected. MS^n target numbers can be increased during those segments. The methods described in this chapter are expected to facilitate more abundant and more confident PTN identifications as well as a means for site-specific nitration quantitation from complex protein sets.

Materials and Methods

Peroxynitrite synthesis

The following items were obtained to build a custom syringe pump-driven chemical synthesis system for authentic and stable isotope-labeled peroxynitrite. New Era Pump Systems (Farmingdale, NY, USA) supplied a NE-

1600 Six Syringe Pump capable of syringe size-dependent infusion rates from 0.452 µL× hr $^{-1}$ to 1451 ml/hr. Harvard Apparatus (Holliston, MA, USA) supplied the following: Monoject Plastic Syringes with Luer tips, Polypropylene Luer Connector Kit, 3.2 mm ID/4.8 mm OD Tygon R-3603 Tubing (For reagents and NaOH), and 2.4 mm ID/4.0 mm OD Tygon R-3603 Tubing (reaction tube).

Isotope-labeled and unlabeled peroxynitrite were synthesized from either "heavy" ^{15}N sodium nitrite (Icon isotopes, Summit, NJ, USA) or "light" ^{14}N sodium nitrite by reaction with acidified hydrogen peroxide (H_2O_2) using a modified version of a previously described method (14). Briefly, NO_2 or $^{15}NO_2$ and H_2O_2 were delivered to a "T"-junction at a static flow-rate using a six-syringe pump (New Era). Volumes of reagents and reaction times were controlled by pump speed, syringe size, tube lengths and tubing inside diameters (IDs).

Reactions were immediately quenched by downstream infusion of 1 M NaOH to a final concentration of 1 M (pH 13). Products were collected on ice prior to spectrophotometric concentration assay at the absorbance maximum for peroxynitrite of 302 nm (14-16) on a NanoDrop 1000 (Thermo Scientific, USA). The stocks were distributed into one mL aliquots and assayed for $ONOO^-$ concentration or immediately stored at $^-$ 80°C to minimize degradation. Assay results were followed by manipulations of reagent concentrations and the reaction tube length to optimize product yields as enumerated by Table 5. Syringe size (10 mL) was static and pump speed was maintained at the maximum flow-rate for 10 mL syringes of 415.9 mL × min^{-1}.

Stable isotope labeling using synthetic peroxynitrite

Free amino acid reactions

Products from the second synthesis (10 mM "light" and 8 mM "heavy") were used in reactions with 500 µM L-Tyr to test the nitration efficiency of dilutions from those starting concentrations. Reactions using dilutions to final concentrations of 200 µM, 400 µM and 800 µM were performed in triplicate by addition of concentrated light or heavy $ONOO^-$ to microcentrifuge tubes containing 500 µM L-Tyr (~ 9 µg in 0.1 mL) followed by immediate vortex at room temperature (RT). Reactions were incubated at RT for 1 h prior to quenching by addition of formic acid to 5%. Reactions were combined and desalted with Zip-Tip (EMD Millipore, Billerica, MA, USA) SPE columns, then suspended in 50:50 water: acetonitrile in 0.1% formic acid prior to direct infusion on a Finnigan LTQ. Peak intensities for 50:50 mixtures of the two nitrated species were analyzed to evaluate the ability of a Finnigan LTQ to resolve a +1 Da mass shift in zoom-scan mode as well as to empirically determine an ionization efficiency correction factor.

Peptide standard reactions

Angiotensin II (Asp-Arg-Val-Tyr-Ile-His-Pro-Phe) obtained from Bachem (Torrance, CA, USA) was diluted to 0.5 mg × mL^{-1} (~ 478 µM) in 500 µL phosphate-buffered saline (PBS) pH 7.4 and reacted with 800 µM synthetic $ONOO^-$ (Table 5, synthesis #4) to test its nitration efficiency. The pH was measured after $ONOO^-$ addition (in 1 M NaOH) with litmus paper which indicated a pH of ~10. A second reaction was performed with 440 µM $ONOO^-$, which

resulted in a final pH of ~8. Both reactions were incubated for 1 h at 37°C. Reactions were quenched by addition to 5% formic acid followed by desalt in centrifugal C_{18}/silica SPE columns (The Nest Group, Southborough, MA, USA). Peptides were eluted in 90:10 acetonitrile: water (0.1% formic acid) prior to concentration under vacuum at 50 °C until the volume was ~ 25 µL. Samples were resuspended in 50:50 water: acetonitrile in 0.1% formic acid prior to direct infusion into an Orbitrap to qualify nitrated product evolution.

Pentapeptide reactions

The pentapeptide GLYKG was selected for testing a 50:50 mixture of heavy and light (H&L) $ONOO^-$ due to its median nitration susceptibility demonstrated in Chapter Two. An 800 µM stock was prepared by measuring 683 µg into 1547 µL of PBS. A 500 µM stock was prepared by diluting 625 µL of 800 µM stock into 1 mL. The 500 µM stock was aliquotted for 100 µL reactions and reacted with 800 µM ONOO. Reactions were performed at RT, mixed on vortex immediately upon addition of ONOO and mixed again after 30 s, then incubated at 37 °C for 1 h.

Protein standard reactions

Separate reactions of 800 nM BSA with 800 µM, 400 µM, and 200 µM $ONOO^-$ were performed at RT for one hour. Reactions were trypsin digested by the in-solution method after alkylation in 6 M urea at RT in the dark. Equal volumes of the reactions were combined prior to desalt and speed-vac concentration. The combined samples were analyzed by HPLC-MS/MS on an

Orbitrap with HCD fragmentation to achieve high-resolution precursor masses and to exploit the extended mass range of the Orbitrap analyzer.

A second set of BSA reactions were performed in duplicate using equimolar amounts of H&L $ONOO^-$. Reaction mixtures were acid-quenched (5% formic acid) and combined in various ratios as outlined in Table 6. After trypsin digestion, a synthetic nitropeptide standard (Gly-Glu-$Tyr^{(nitro)}$-Leu-Gly) was spiked in as an IS prior to desalt. Reaction mixtures were analyzed by HPLC-MS/MS on a LTQ to evaluate nitropeptide identification and immonium ion quantitation.

Five µg of BSA plus 11.65 ng IS (assuming 100% recovery from C_{18} SPE) were loaded on column for HPLC-MS/MS analysis by the following procedure. The IS ($GEY^{(nitro)}LG$) was measured to 500 µM in 50 mM ABC, then diluted to 50 µM in 50 mM ABC. The IS was spiked-in using micropipette by adding 8 µL into 1 mL of protein suspension to a final concentration of 0.4 µM. Spiked BSA suspensions were desalted in centrifugal SPE columns and lyophilized. The samples were resuspended to 1 mg $\times$ mL^{-1} in 100 µL of 0.1% formic acid. The IS final concentration was 4 µM or 2.33 µg $\times$ mL^{-1}. Total mass on column was 5 µg BSA digest and 11.65 ng IS per 5 µL injection.

Liquid chromatography and mass spectrometric analyses

Direct infusions

Full-scans of light $ONOO^-$-treated angiotensin II were set to analyze from 400 – 1200 m/z. Tandem MS was done on both the 546.26 m/z and 1091.52 m/z peaks using CID, PQD and HCD on a LTQ Orbitrap XL (Thermo). CID and PQD energies were set to 35. HCD scans ranged stepwise from 35 to 80. H&L

$ONOO^-$-labeled angiotensin II mixtures were analyzed with five µscans in ultra-zoom mode in the range of 450 - 1200 m/z on a Finnigan LTQ.

Tandem-mass spectrometric analyses

Five microliter injections of the H&L $ONOO^-$ BSA digests were separated by reversed-phase HPLC on an LC Packings Ultimate system (Thermo Fisher Scientific, USA). Peptides were desalted on a capillary trap column (100 µm i.d.×2 cm C_{18}) packed with 5 µm silica spheres with 300 Å pores (ProteoPep II) prior to elution from a ProteoPep II 75 µm i.d.×10 cm C18 analytical column. The mobile phase flow-rate was 300 nL× min^{-1} and followed a linear gradient of 5% - 40% B over 90 minutes (mobile phase A was 0.1% formic acid in water and B was 0.1% formic acid in acetonitrile).

Two tandem MS methods were utilized to optimize for immonium ion detection. Tune parameters in the Finnigan LTQ for these analyses were as follows: Spray voltage: 2.5 kV, Capillary temperature: 200 °C, Capillary voltage: 40, Tube lens Voltage: 210, MS^n target: 4×10^4, Scan time: 2 microscans with a maximum inject time of 200 ms.

A “triple-play” (MS-MS/MS-MS/MS/MS) method was used for H&L nitro-BSA digests with MS acquisition in centroid mode, CID activation (MS^2) on the top three most abundant ions, and PQD activation (MS^3) on the top 3 product ions from the CID scan. Dynamic Exclusion was set for 90 s after two repeats and early expiration after 3 counts with a signal to noise (S/N) threshold of 3. Finnigan LTQ settings were as follows: spray voltage: 2.0 kV; capillary

temperature: 160 °C; capillary voltage: 46.0; tube lens (V): 160; MS^n target: $4x10^4$; 2 μscans; 200 ms. The scan range for full MS was set to 400-1200 m/z.

A second data-dependent top 4 CID/PQD method was used to acquire complementary spectral data from the same precursors. The method was set for data-dependent MS/MS on the top 4 ions using CID with a CE of 45, followed by top-4 MS/MS of the same precursors from the survey scan (MS) using PQD at CE of 45. This method was intended to acquire MS^2 spectra for the same precursors using both activation methods for comparison of immonium ion fragmentation efficiency.

The MS/MS spectra resulting from CID of tryptic peptides were isolated in a window of ± 2 Da. This extended range was implemented to account for non-isobaric parent ions coded by either +45 or +46 Da nitro-adducts. In the 4 Da isolation window, precursor ions containing heavy, light or a combination of H&L 3NT were activated simultaneously by CID or PQD. The resulting MS/MS spectrum contained differential 3NT immonium ion peaks separated by 1 Da would be indicative of the relative amount of H or L nitropeptide and, thus, nitroprotein content.

Results

Isotope-labeled Spike-in Nitroprotein Standard (SNiPS)

Overview

The methods described in this chapter are expected to facilitate identification and relative quantitation specific to PTN from complex protein mixtures. Identification will be assisted by database searches specifying Tyr-

nitration as a variable modification and screening of peptide spectra containing of H&L 3NT immonium reporter ions. Quantitation will be calculated from the ratios of 3NT immonium ion peak pair intensities. Immonium ion peak pairs will be the result of nitration imparted by either an isotope-labeled **S**pike-in **Ni**tro**P**rotein **S**tandard (SNiPS) or from endogenously-generated 3NT.

To initiate this process, stable isotope-labeled H&L $ONOO^-$ was synthesized using a syringe pump platform. Synthesis and reactivity was validated by reactions with free L-Tyr, angiotensin II, and the pentapeptide GEYLG. BSA was reacted with three concentrations of H&L $ONOO^-$ to test the feasibility of 3NT immonium ion screening for nitropeptides and quantitation using peak intensity ratios. The long-term goal for this project was to perform similar *in vitro* reactions with a microglia control lysate for use as a SNiPS to screen for endogenously-generated (light) PTN and for quantification of PTN under a variety of oxidative/nitrative stress conditions. Nitropeptides generated from a SNiPS are coded by a +46 Da mass increase resulting in 2^+ charged MS peptide pairs separated by 0.5 Da where both H&L isotopes are present.

Since nitropeptide pairs would differentiate by $\leq$ 1 Da, an isotope window of 4 m/z ($\pm$ 2 Da of monoisotopic m/z) was specified for MS/MS precursor mass selection, not the 10 m/z window described earlier for multiplex precursors with a Δm of +3 (11). Nitrotyrosine-containing y or b ion series were expected to exhibit doublet peaks with a Δm of +1 Da, which could be quantified by a method similar to the one described by Zhang (2006) using ratios of MS^2 fragment ions.

Preferably, our method will be quantifiable based exclusively on the ratio of peak intensities from the H&L 3NT immonium reporter ion pairs.

There are several advantages to using ratios of 3NT immonium ions for PTN quantitation. First, since the nitroproteome should be modest in size, manual screening for 3NT immonium ion pairs is practicable. Also, our focus is specific to a single isotope pair (181 & 182 m/z), negating the necessity for development of a complex search algorithm to pre-qualify peak pairs for quantitation. Finally, the low-mass immonium reporter ions are specific to 3NT in that they neither overlap with any of the other twenty immonium ions, nor are they isobaric with any of the twenty common amino acid residue masses.

Stable isotope-labeled peroxynitrite synthesis

Isotope-labeled $ONOO^-$ was a prerequisite to SNiPS development for immonium ion screening and quantitation described in the Introduction of this chapter. Using a scaled-down version of a previously-described method (14), 30 mL volumes of heavy or light isotope-labeled peroxynitrite were synthesized. A syringe pump system was used to combine $NaNO_2$ or $Na^{15}NO_2$ and acidified H_2O_2 to produce H or L $ONOO^-$ (Fig. 30). Due to $ONOO^-$ instability at low pH, concentrated NaOH was added post-reaction from a separate syringe. The product was collected on ice and either stored at – 80°C or assayed for concentration at 302 nm.

Because the syringe capacity used in this experiment was one-third the volume of the syringes used in the large-scale synthesis (14), optimization steps were necessary to maximize final product yields. Table 5 details the adjustments

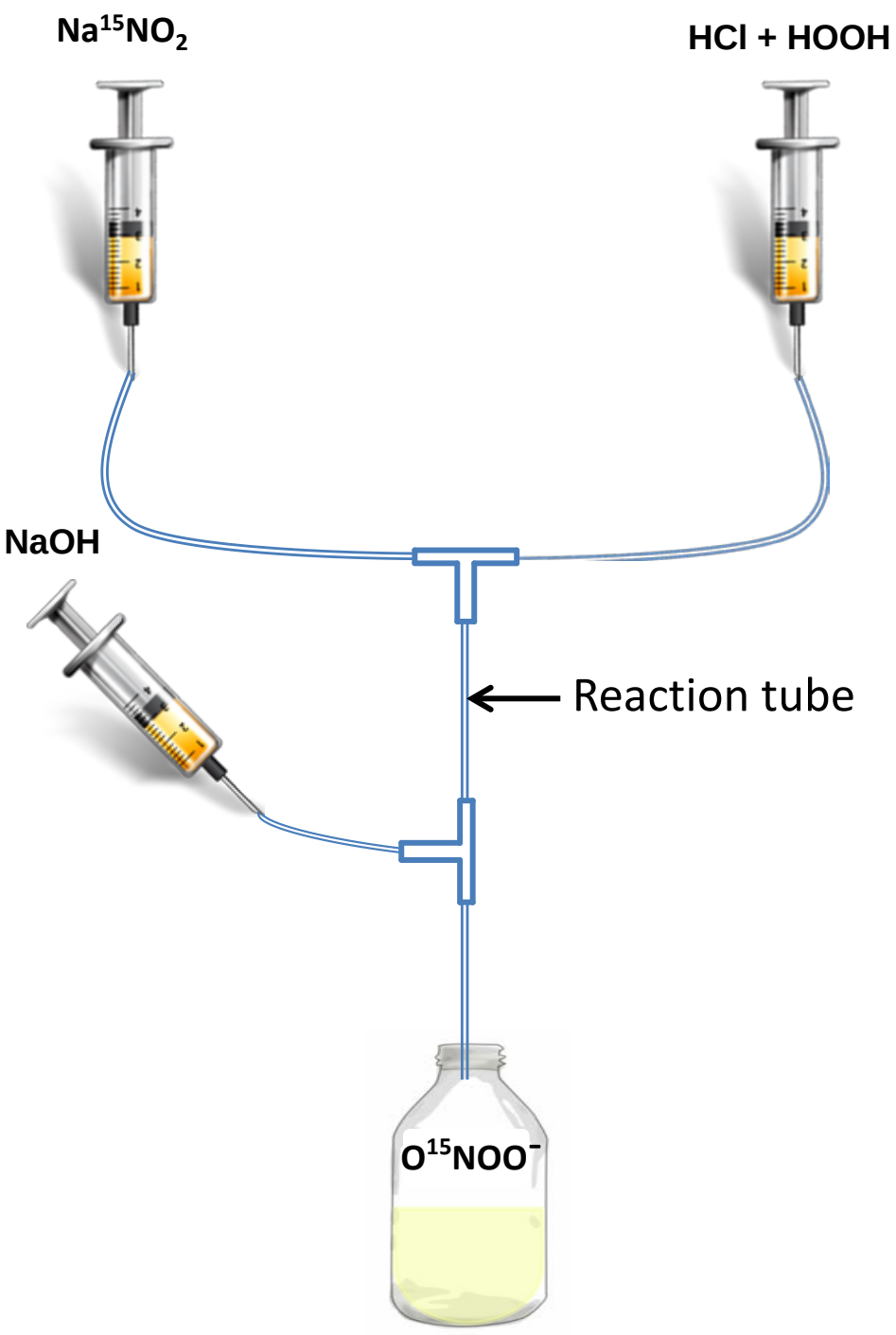

Figure 30. Peroxynitrite synthesis. A syringe pump method adapted from Robinson and Beckman (2005) was optimized using the general schema shown above with variations in tube lengths and reagent and storage buffer concentrations to synthesize both unlabeled and ^{15}N-labeled peroxynitrite.

Table 5. Peroxynitrite synthesis optimization.

Synthesis #	Peroxide Solution		Nitrite	Reaction Tube Length	Storage Buffer concentration	Peroxynitrite Yield (mM)	
	HCl (M)	H_2O_2 (M)	$NaNO_2$ (M)		NaOH (M)	Heavy	Light
1	0.700	0.600	0.600	4.0 cm	1.00	8	9
2	0.700	0.600	0.600	3.0 cm	1.00	8	10
3	0.350	0.300	0.300	3.0 cm	1.00	12	14
4	0.350	0.300	0.900	2.4 cm	1.00	14	16
5	0.725	0.900	0.900	2.4 cm	1.00	NA	18
6	0.350	1.200	1.200	2.0 cm	0.30	NA	16
7	**0.241**	**0.530**	**1.270**	**3.0 cm**	**0.30**	**24**	**22**

Seven separate synthesis attempts resulted in the $ONOO^-$ yields above. Reagent concentrations and reaction tube lengths were manipulated based on visual observation of the intensity of the yellow color of the product that is characteristic of 3NT, assay results, and MS analyses indicating the reactivity of the product.

made to reagent concentrations, tube lengths, and storage buffer concentrations for optimization of $ONOO^-$ yield (heavy $ONOO^-$ synthesis was discontinued temporarily to conserve isotope-labeled sodium nitrite). The syringe pump was programmed for the maximum flow rate for all reactions.

The limiting factor for reaction yield was likely to have been syringe size as the maximum flow rate for 10 mL syringes is 415.9 mL$\times$ h^{-1} compared to 862.8 mL $\times$ h^{-1} for 30 mL syringes and 2376 mL $\times$ h^{-1} for 140 mL syringes. Theoretically, the system described could produce $\geq$ 137 mM $ONOO^-$ using 140 mL syringes at full-speed—much closer to the 180 – 190 mM yields reported by Robinson & Beckman (2005) using 30 mL syringes. Nevertheless, the yield maxima for H&L $ONOO^-$ (24 mM and 22 mM for H&L $ONOO^-$, respectively) were

expected to be sufficient for our purposes. The relatively low yields resulting from early synthesis reactions (Table 5, syntheses 1-3) required larger volumes than the commercially available $ONOO^-$ from Cayman (40 - 80 mM) used in the experiments described in Chapter Two. The resulting reaction mixtures were read at pH above 8—possibly retarding efficient nitration at the standard $ONOO^-$ reaction concentrations of 200 µM, 400 µM and 800 µM.

Stock H&L $ONOO^-$ concentrates were reacted with free amino acid (L-Tyr), a peptide standard (Angiotensin II), a pentapeptide (Gly-Leu-Tyr-Lys-Gly), and a protein standard (BSA) to test H&L $ONOO^-$ reactivity and optimize mass spectrometric parameters prior to heavy $ONOO^-$ use for labeling a SNiPS quantitative multiplex MS/MS analytical calibrant. Reactions were performed by $ONOO^-$ addition to standards in PBS (pH 7.4) as described in Chapter Two and in Materials and Methods above. To our knowledge, this study represents the first example of stable isotope-labeled peroxynitrite synthesis and use for 3NT-specific isotope coding.

Free amino acid testing

Peroxynitrite (Table 5, synthesis 2) reactions with free L-Tyr were analyzed by MS/MS using both CID and PQD activation on a LTQ to determine CE optima and to test feasibility for use of the immonium ion isotopes for semi-quantitative analysis. Immonium ion signals were expected to be strong, since a low-complexity mixture comprising three analytes (L-Tyr and H&L 3NT) was being analyzed. Peptide-bound 3NT immonium ion signal intensities were expected to be significantly weaker than free amino acid as CID favors a single

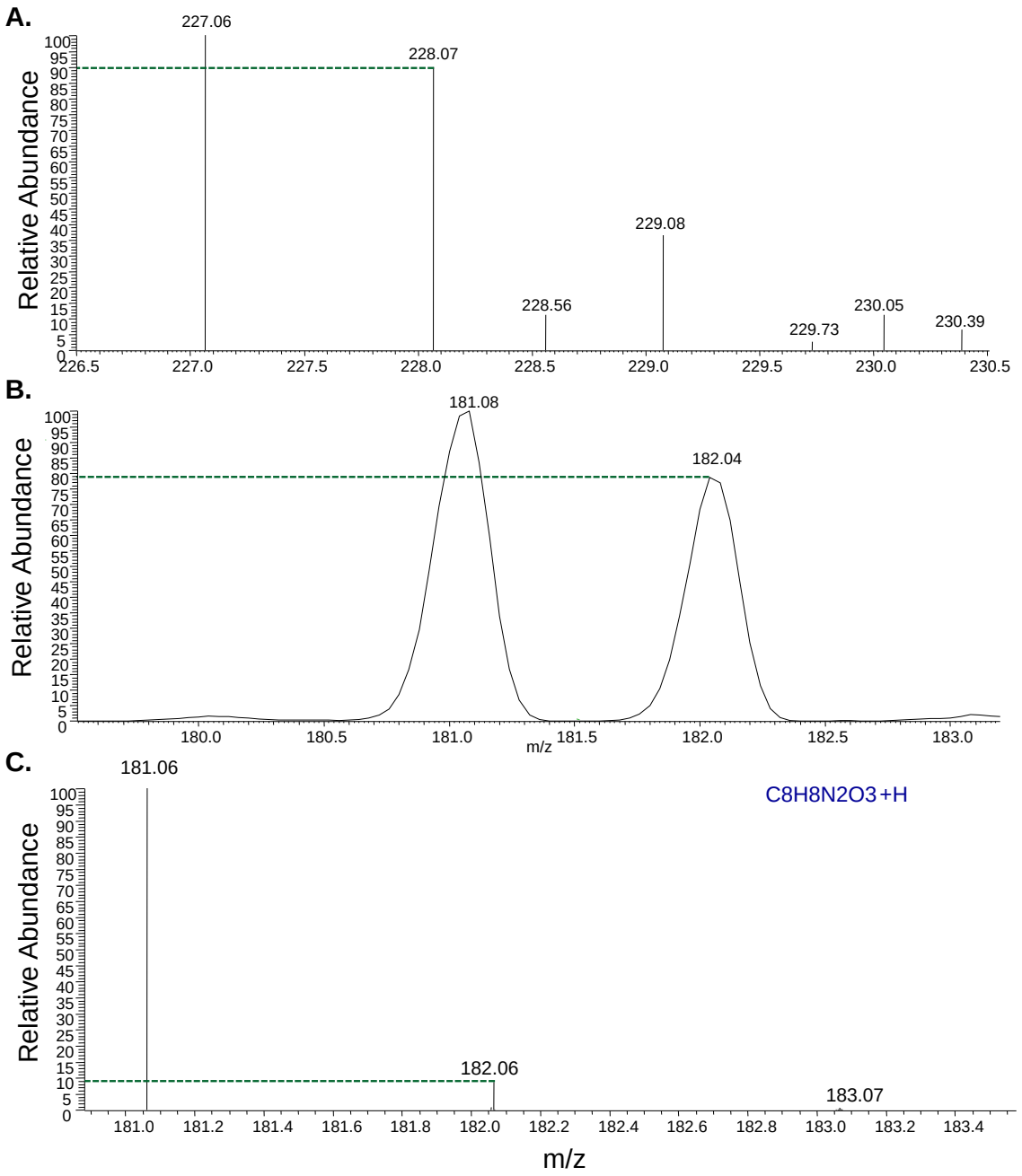

Figure 31. Isotope-labeled nitrotyrosine. A) A representative MS spectrum showing precursor ion peaks for both the unlabeled (227 Da) and heavy-labeled (228 Da) nitrotyrosine from a LTQ analysis in zoom-scan mode. B) Immonium ion peaks resulting from CID fragmentation of 227 Da (± 2 Da isolation window). C) Nitrotyrosine isotope cluster simulation showing the predicted intensity of the light immonium ion's 2nd isotopic peak at 182.06 to be ~9%. Green-dashed lines for A&B indicate the heavy 3NT peak intensities as follows: parent ion ~ 90%, immonium ion ~ 78% (average of 102 scans).

amide bond breakage. Nevertheless, 3NT immonium ion signals were expected to be detectable and quantifiable.

The heavy 3NT precursor ion peak (228 Da) intensity was expected to be ~ 3% greater than the light-labeled peak (227 Da). This calculation was based on two key factors. First, the theoretical contribution from the second isotope peak of light 3NT (XCalibur isotope simulation, Fig. 31C) was estimated to overstate the heavy 3NT peak by ~ 9%. Secondly, the stock purity of the $^{15}NO_2$ used for heavy $ONOO^-$ synthesis was 97%, which would result in a net 6% reduction of the 228 m/z signal from a 3% contribution to the monoisotopic peak of light 3NT and 3% reduction in the heavy 3NTpeak. Together, these factors would result in a net 3% increase on the heavy 3NT immonium ion isotope peak.

The experimental results showed the heavy labeled 3NT parent ion peak intensity to be closer to 90% of the light (Fig. 31A). This variance could be due to inefficient reaction of heavy $ONOO^-$ with L-Tyr due to the low stock concentration or overstated purity of the $Na^{15}NO_2$. Nevertheless, heavy 3NT labeling was considered successful based on the significant contribution to the 2^{nd} parent ion isotope peak of light 3NT at 228 Da (Fig. 31A) and the heavy immonium ion peak at 182 m/z (Fig. 31B). The ratio of L/H immonium ion intensities was ~ 1.25, correlating to the variance seen in the precursor intensities. Considering the isotope-labeling of free L-Tyr was successful and that the ratios in a multiplex experiment would be normalized, these results were encouraging for the continued development of the method.

Angiotensin II Peptide standard testing

Light synthetic peroxynitrite (Table 5, synthesis 5) was reacted with Angiotensin II (~ 500 µM) to validate its reactivity when diluted from a stock concentration of 18 mM and to determine the signal strengths of reporter ions from a short peptide. The 800 µM reaction mixture was measured to be pH 10, which may have stabilized the peroxynitrite anion, retarding its reactivity. A second reaction performed by addition of half the $ONOO^-$ volume (440 µM) was measured to be pH 8.

Both reactions were analyzed by direct infusion on an Orbitrap. Angiotensin II nitration peaks expected at 546.2 m/z and 1091.5 m/z were not detectable from analysis of the 800 µM reactions; however, nitro-Angiotensin II parent ion signals were detected from infusion of the 440 µM reactions. The nitropeptide precursor ion intensity was ~ 37%, relative to the unmodified peptide ion (Fig. 31). These results confirmed our prediction that the 18 mM synthetic $ONOO^-$ stock concentration would require dilution below 800 µM to be reactive, which was not a major concern since PTN had previously been detected from reaction with $ONOO^-$ concentrations above 200 µM. Another consideration was that the stock NaOH concentration could be lowered, reducing its impact on reaction mixture pH. Subsequent syntheses were collected in 0.3 M NaOH—a three-fold decrease from the original storage buffer concentration.

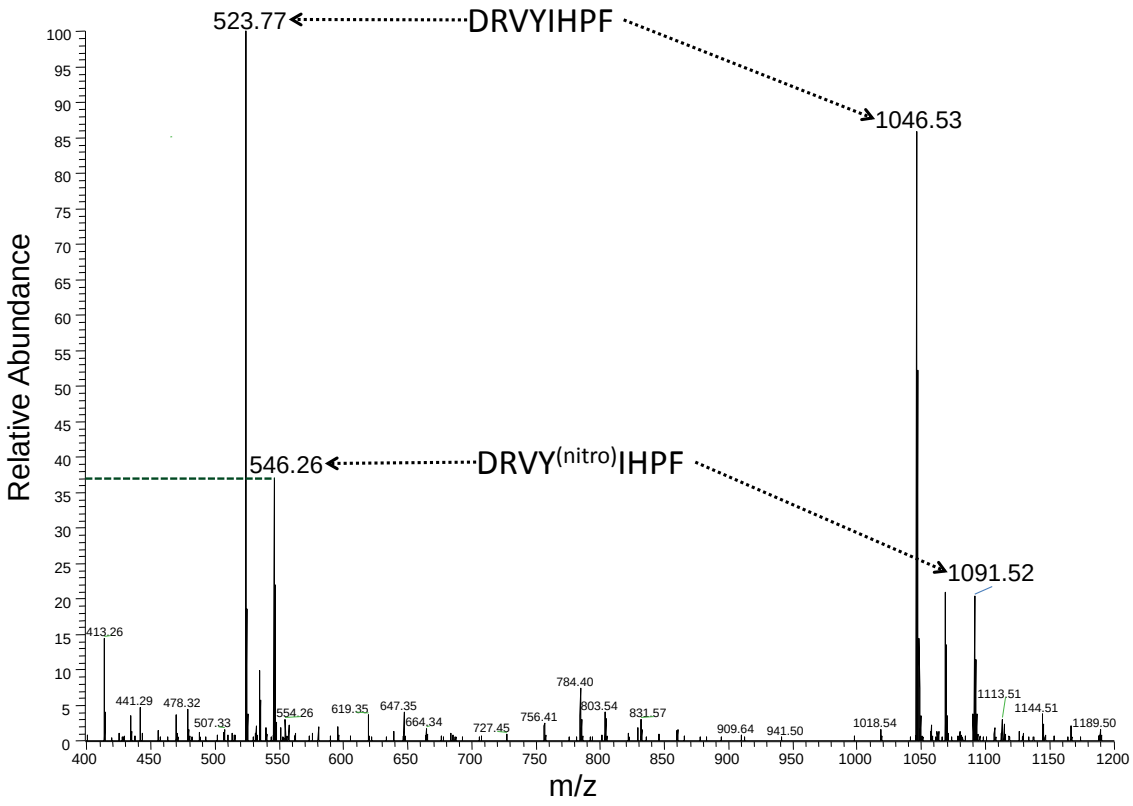

Figure 32. Synthetic peroxynitrite reactivity test using Angiotensin II. This mass spectrum represents nitration from reactions with 440 µM synthetic $ONOO^-$. The dashed green line indicates nitration peak intensity to be 37%. Due to pH increase from low concentration ONOO-, 800 µM reactions did not result in a detectable nitration peak.

Angiotensin II was also reacted with three concentrations (1 mM, 500 µM and 200 µM) of either H or L $ONOO^-$ (Table 5, synthesis 7) to quantify the relative contribution of each to the nitropeptide isotope cluster. Equal amounts of the reaction mixtures were combined prior to desalt to give H/L ratios of 1:1, 2:1, 4:1, 1:2, and 1:4. The mixtures were desalted, speed-vac concentrated, and resuspended in 50:50 acetonitrile: water in 0.1% formic acid and analyzed by five µscans in Ultra Zoom mode on a Finnigan LTQ.

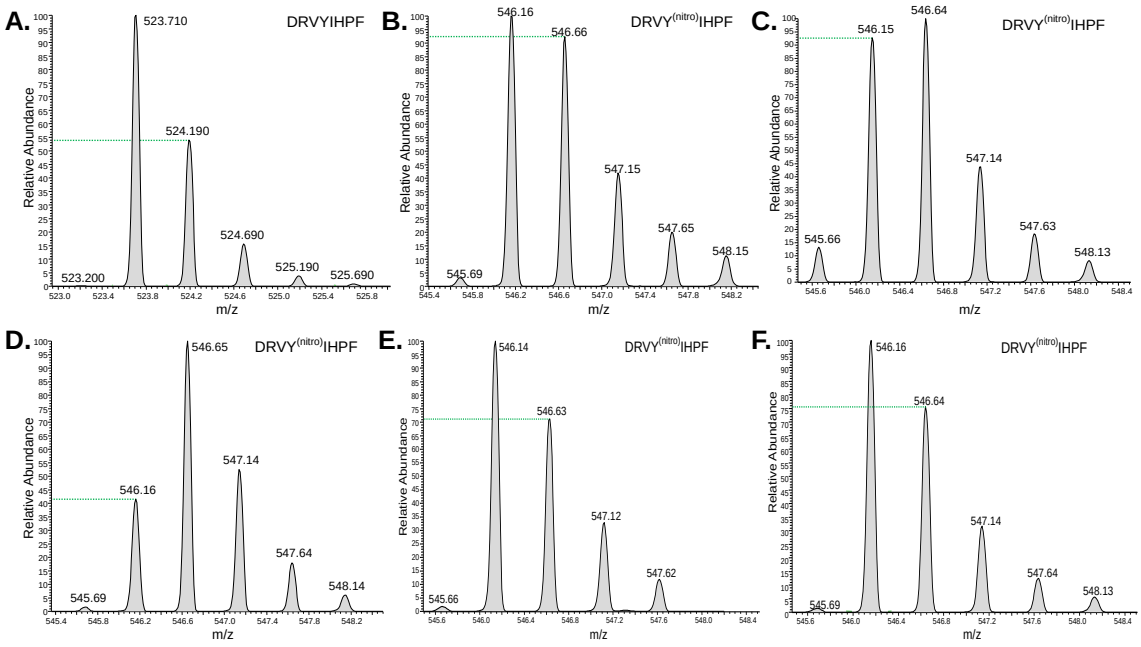

Figure 33. H/L nitro-Angiotensin II MS signal ratios. A-F) Mass spectra representing the average of ten scans from A) the unmodified peptide, B) H/L nitropeptide mixture ratios of 1:1, C) 2:1, D) 4:1, E) 1:2, F) 1:4. Dashed green lines indicate the relative abundances of (A) the 2nd isotopic peak of the unmodified peptide, (B) the 2nd peak of the nitropeptide with contributions from both H&L, (C&D) the monoisotopic peak of the light nitropeptide, (E&F) the 2nd peak of the H&L nitropeptide isotope cluster.

The monoisotopic peak for 2+ charged nitro-Angiotensin II was found at 546.2 m/z and the heavy isotope at 546.7 m/z. The average contribution from the second isotope from the light nitropeptide was estimated to be 55% based on the intensity of the second isotopic peak of the unmodified peptide (Fig. 33A) and XCalibur isotope cluster simulation (not shown). The ratios of mass spectrometric peak intensities were 0.93, 1.07, 0.74, and 0.77 for the reaction mixtures of 1:1, 2:1, 1:2 and 1:4, respectively (Fig. 33G). Ratios were not as expected considering the light nitropeptide second isotope contribution to the monoisotopic peak of the heavy nitropeptide (i.e. 546.7 m/z). However, the 4:1 mixture ratio (2.38) began to approach the expected ratio, indicating accurate

quantitation will require the heavy isotope to be present at greater than four-fold quantities. This should not present an issue for our proposed method as the heavy amount is controlled by spike-in addition.

A limitation to this method is in quantitation by peak intensity. Because a RP of 643,000 would be required to resolve the heavy monoisotopic peak from the second isotope peak of the light isotope, our calculations must take contributions from both into account. These contributions can be inaccurately measured using the one-dimensional metric of peak height. A more reliable measure of isotope contribution would be attained using AUCs as exemplified by the pentapeptide chromatograms in Chapter Two. Currently, however, XCalibur software does not accommodate spectral peak integration.

Pentapeptide standard testing

A pentapeptide (GLYKG) was reacted with 600 µM $ONOO^-$ (50:50 H&L) (Table 5, synthesis 4) to validate the reactivity of both H/L $ONOO^-$ and to validate the expected 3NT immonium reporter ion ratio. Reaction mixtures were analyzed by direct infusion on a LTQ XL. The isolation window for this experiment was opened to ± 6 Da to ensure capture of both parent masses. Although the wide isolation window would not be expected to perturb data from a single analyte, it could significantly increase noise from a complex mixture. Thus, our standard isolation width setting for SNiPS analyses will be ± 2 Da to attenuate background signals.

The H/L parent and immonium ion isotope ratios were ~ 1:1 as predicted (Fig. 33A&B). Although this experiment was conducted using a linear ion trap set

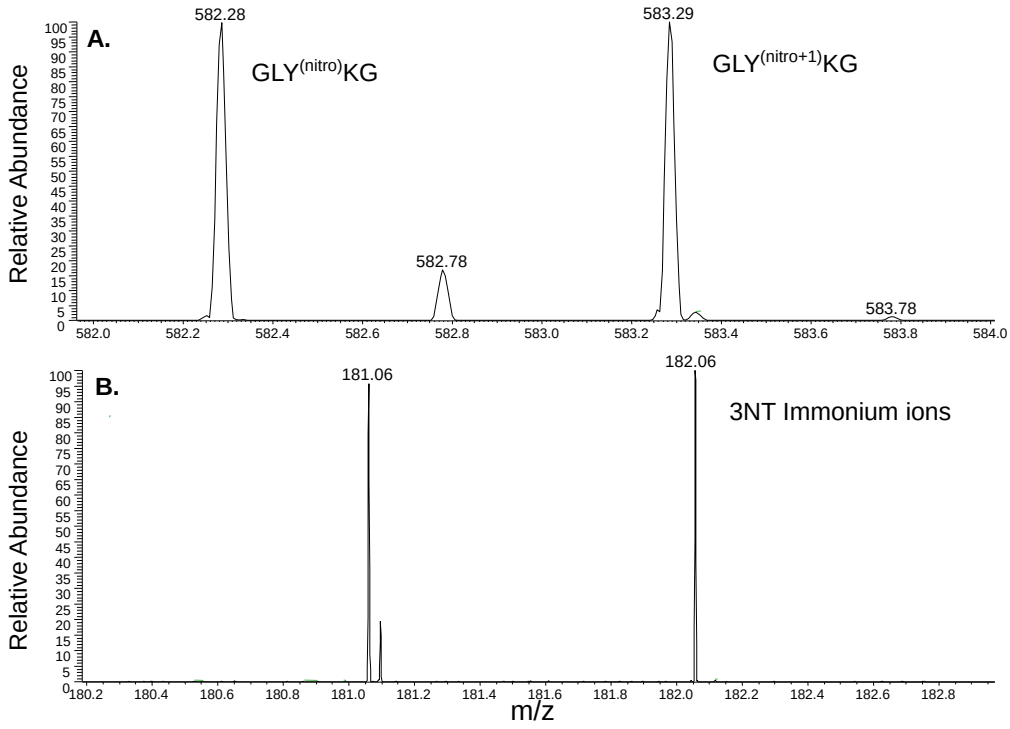

Figure 34. Pentapeptide nitrotyrosine isotope labeling. GLYKG peptide was reacted with equimolar concentrations of heavy and light synthetic peroxynitrite and analyzed via MS (A) to resolve H&L GLY(nitro)KG parent ions and MS/MS (B) to evaluate immonium ion peak intensities.

to unit resolution at full-width half-maximum (FWHM), a high-resolution analysis using an Orbitrap can easily resolve the isotope overlap between 3NT-derived immonium ion isotopes. Contributions to the ^{14}N-containing 2nd and 3rd isotopes can be separated by instrument resolving power (RP) $\geq$ 52,000. RP is determined by multiplying the mass resolution required between peaks by two. Mass resolution comes from application of the International Union of Pure and Applied Chemistry (IUPAC) definition—$R = \frac{M}{\Delta M}$. Since the second isotope peak from the ^{14}N-labeled 3NT equals 182.065 and the monoisotopic peak from ^{15}N-labeled 3NT equals 182.058, the RP required for 3NT immonium ion isotope is calculated by: 2 (182.065 / (182.065 − 182.058)) ≅ 52,000. The results of this

Table 6. Analytical sample combinations of H&L peroxynitrite reactions with BSA.

H/L 1:1 (μM $ONOO^-$)	H/L 2:1 (μM $ONOO^-$)	H/L 4:1 (μM $ONOO^-$)	H/L 1:2 (μM $ONOO^-$)	H/L 1:4 (μM $ONOO^-$)
800:800	800:400	800:200	400:800	200:800
400:400	400:200		200:400	
200:200				

To evaluate the reactivity and immonium reporter ion ratios of H&L nitropeptides generated from synthetic peroxynitrite on a protein standard, the above mixtures were made prior to HPLC-MS/MS analysis.

experiment bolstered the feasibility of synthetic $ONOO^-$ isotope-coding for SNiPS-assisted semi-quantitative nitration analysis of complex biological samples.

Protein standard testing

A protein standard (800 nM BSA) was reacted with 200 μM, 400 μM, and 800 μM H or L $ONOO^-$ to test $ONOO^-$ reactivity with a protein standard and to analyze the ratio of immonium ions detected from differential combinations of H&L reactions as specified by Table 6. The scheme for BSA treatment and analysis is identical to the intended approach for SNiPS production and application to cell culture lysates as outlined in Figure 35. BSA peptides were separated by reversed-phase chromatography using a linear gradient over 90 minutes to increase the probability of identification of the expected low-level nitropeptide ions. Note: the gradient used in a complex biological sample may require further optimization. Mass spectrometric analyses were performed using both a top-10 data-dependent method and a combined top-4 CID/PQD method. A custom tune method was incorporated to increase MS/MS precursor target by

33% to 4×10^4 and injection time was doubled to 200 ms to enhance PQD spectral quality as previously described (7).

Raw data files were searched against the full UniProt/SwissProt non-redundant database using Mascot with Tyr nitration specified as a variable modification to identify nitropeptides and PTN sites. Concurrently, manual reconstruction of peaks containing 3NT immonium ions was used to determine CID or PQD spectral prospects for identification of potential low abundance nitropeptides. Product ion masses from those spectra containing the expected ratios of H/L 3NT immonium ions were input directly into the Protein Prospector MS Fit program (http://prospector.ucsf.edu) and searched against the Swissprot.2012.12.3 database to mine for possible low-level nitropeptides not identified by Mascot searches.

Mascot searches identified a unique nitropeptide ($Y^{(nitro)}$ICDNQDTISSK) from a unique spectrum found in four of nine analytical replicates. Because the peptide was identified exclusively from CID spectra at an observed m/z of 744.2, immonium ion peaks were undetectable due to the one-third rule. MS Fit analyses were unsuccessful in identifying BSA nitropeptides from the peak lists of spectra containing the expected ratios of H/L 3NT immonium ions. Further experimentation will be necessary to determine the optimal $ONOO^-$ reaction concentration for SNiPS development.

This experiment was intended to evaluate quantitation among immonium ion intensities resulting from differential mixtures of protein reacted with three concentrations of H or L $ONOO^-$. The inability to detect BSA nitropeptides was

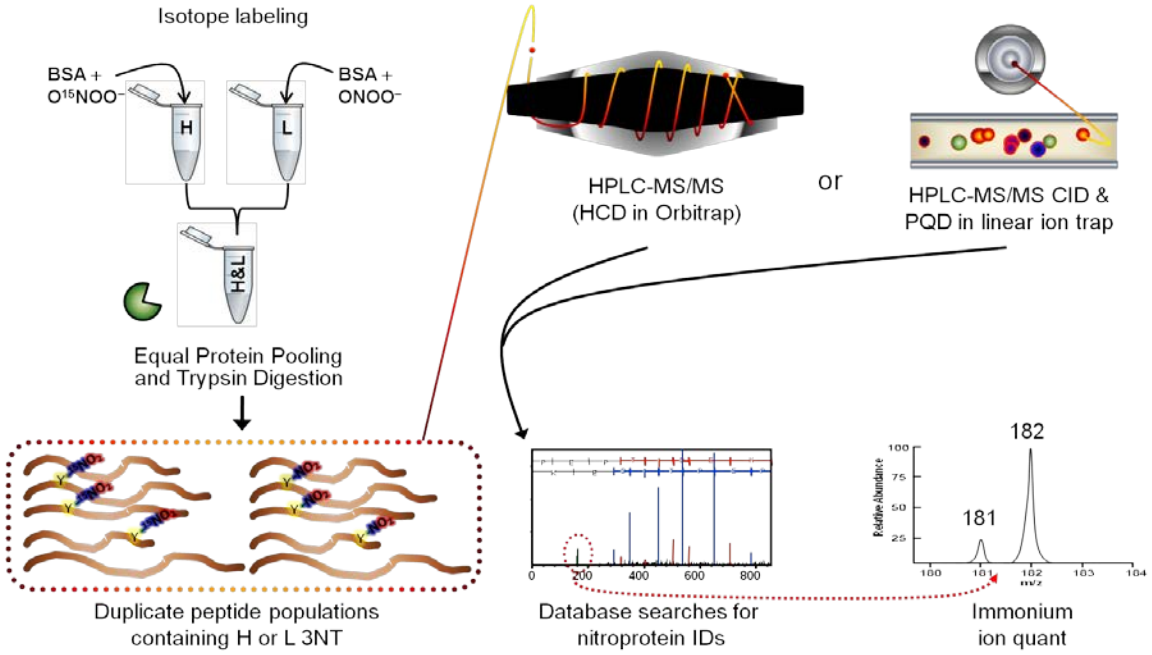

Figure 35. Schema for SNiPS production and application. A protein standard (BSA) was selected to test the qualitative and quantitative MS data for optimization of the SNiPS method. BSA was reacted with either H or L $ONOO^-$ at variant concentrations then pooled at known ratios prior to trypsin digestion. The digest was then analyzed by HPLC-MS/MS on a LTQ using both CID and PQD activation. Alternatively, HPLC-MS/MS analysis can be done on an Orbitrap using the HCD cell for HR/AM spectra. MS/MS spectra can be mined for H&L 3NT immonium ions for peptide/protein identification and PTN quantitation.

likely due to one or more of the following factors: insufficient $ONOO^-$ molar excess, inadequate sensitivity of the MS method, or inadequate instrument sensitivity. A targeted method had been intentionally omitted because endogenous nitration sites would remain largely unknown. Thus, the use of the heavy 3NT immonium ion as a screening device to detect low-level PTN from a standard data-dependent MS/MS analysis was evaluated. Assuming cell lysate reaction with bolus $ONOO^-$ would result in site-identifications from a SNiPS, a targeted method can be built to enhance nitropeptide detection from experimental protein sets as described in the following section.

Table 7. Observed nitropeptides from reactions with isotope-labeled peroxynitrite.

Observed m/z	Charge	Nitropeptide Sequence	Modifications
806.87	2+	(-)DAFLGSFLYEySR(-)	Nitro (+45)
762.26	2+	(-)ETyGDMADccEK(-)	Nitro (+45), Carbamidomethyl (+57), Carbamidomethyl (+57)
967.46	2+	(-)HPYFYAPELLyYANK(-)	Nitro (+45)
645.31	3+	(-)HPYFYAPELLyYANK(-)	Nitro (+45)
762.89	2+	(-)LGEyGFQNALIVR(-)	Nitro (+45)
590.61	3+	(-)MPcTEDyLSLILNR(-)	Carbamidomethyl (+57), Nitro (+45)
885.41	2+	(-)MPcTEDyLSLILNR(-)	Carbamidomethyl (+57), Nitro (+45)
893.41	2+	(-)mPcTEDyLSLILNR(-)	Oxidation (+16), Carbamidomethyl (+57), Nitro (+45)
495.61	3+	(-)RHPEyAVSVLLR(-)	Nitro (+45)
697.35	3+	(-)RHPYFYAPELLyYANK(-)	Nitro (+45)
642.64	3+	(-)RPcFSALTPDETyVPK(-)	Carbamidomethyl (+57), Nitro (+45)
963.46	2+	(-)RPcFSALTPDETyVPK(-)	Carbamidomethyl (+57), Nitro (+45)
744.82	2+	(-)ylcDNQDTISSK(-)	Nitro (+45), Carbamidomethyl (+57)
896.85	2+	(-)yNGVFQEccQAEDK(-)	Nitro (+45), Carbamidomethyl (+57), Carbamidomethyl (+57)
1266.55	2+	(-)yNGVFQEccQAEDKGAcLLPK(-)	Nitro (+45), Carbamidomethyl (+57), Carbamidomethyl (+57), Carbamidomethyl (+57)
844.70	3+	(-)yNGVFQEccQAEDKGAcLLPK(-)	Nitro (+45), Carbamidomethyl (+57), Carbamidomethyl (+57), Carbamidomethyl (+57)

Nitropeptides identified from analysis of peroxynitrite-treated BSA. Experimental data from this table was considered when building the targeted MS/MS method to improve sensitivity for BSA nitropeptides. Predictions in Table 8 were used to determine complementary precursor ion targets.

SNiPS-based targeted MS method development

Although SNiPS master mix production is intended for use as a spike-in screening and quantitation tool specific to PTN from cell culture, an ancillary application can be identification of putative nitration sites. A SNiPS lysate can be analyzed by shotgun HPLC-MS/MS, followed by database searching with Tyr nitration as a constant modification. From this, a list of protein targets and representative nitropeptides can be compiled. An MS/MS targeted method can be developed from the list to increase sensitivity for likely nitration sites as discussed in Chapter Three.

Additionally, targeted MS method development for a SNiPS can be augmented by computational methods. *In silico* digestion can be employed to identify all potential PTN sites from a given protein of interest (e.g. a nitration target identified from shotgun MS analysis of the SNiPS). Programs such as the

Table 8. Nitropeptide target list from empirical data and *in silico* digest predictions.

Predicted 2+	Tri-nitro	Di-nitro	Mono-nitro	Previously Observed			Average	Nitropeptide Sequence
399.40							797.80	(K)NY(Nitro)QEAK(D)
509.54	487.04						1018.08	(K)Y(Nitro)LY(Nitro)EIAR(R)
665.25				495.61			1329.51	(R)HPEY(Nitro)AVSVLLR(L)
745.28				744.82			1489.57	(K)Y(Nitro)IC(Carbamidomethyl)DNQDTISSK(L)
762.81				762.26			1524.61	(R)ETY(Nitro)GDMADC(Carbamidomethyl)C(Carbamidomethyl)EK(Q)
763.36				762.89			1525.71	(K)LGEY(Nitro)GFQNALIVR(Y)
774.83							1548.65	(K)EY(Nitro)EATLEEC(Carbamidomethyl)C(Carbamidomethyl)AK(D)
800.84							1600.67	(K)DDPHAC(Carbamidomethyl)Y(Nitro)STVFDK(L)
829.87			807.37	806.87			1658.73	(K)DAFLGSFLY(Nitro)EY(Nitro)SR(R)
886.02				590.61	885.41	893.41	1771.03	(R)MPC(Carbamidomethyl)TEDY(Nitro)LSLILNR(L)
897.45				896.85	1266.55	844.70	1793.90	(K)Y(Nitro)NGVFQEC(Carbamidomethyl)C(Carbamidomethyl)QAEDK(G)
964.08				642.64	963.46		1927.16	(R)RPC(Carbamidomethyl)FSALTPDETY(Nitro)VPK(A)
1025.20							2049.39	(K)WVTFISLLLLFSSAY(Nitro)SR(G)
1035.58	1013.08	990.58	968.08	967.46	645.31	697.35	2070.15	(R)HPY(Nitro)FY(Nitro)APELLY(Nitro)Y(Nitro)ANK(Y)
1269.95							2538.90	(K)GLVLIAFSQY(Nitro)LQQC(Carbamidomethyl)PFDEHVK(L)

Using the MS-Digest tool from Protein Prospector (http://prospector.ucsf.edu/prospector/mshome.htm), peptides with fixed modifications including Cys-alkylation, Met-oxidation, and Tyr-nitration were considered in calculating precursor m/z targets for increased sensitivity for the detection of nitropeptides modified with either H or L $ONOO^-$.

Protein Prospector (prospector.ucsf.edu) MS-Digest tool allow you to enter FASTA sequences or protein accession numbers to calculate proteolytic digestion products. User input includes database selection, taxonomy, proteolytic enzyme (e.g. trypsin), constant modifications (e.g. carbamidomethylation to Cys), variable modifications (e.g. oxidation of Met), and the type of instrument to be used for analysis. For PTN applications Tyr-nitration should be specified as a variable modification to acquire parent masses relevant to all possible modification states or as a constant modification for outputs limited to precursors with all Tyr residues in the nitro- modified state.

To demonstrate target identification for method development using complementary data from HPLC-MS/MS analysis of a SNiPS and an *in silico* digestion, Tables 7 and 8 were created using BSA as the target protein. Table 7 represents nitropeptides that were detected from $ONOO^-$ reacted BSA using a

Top-5 data-dependent method on an Orbitrap. Table 8 represents the consolidation of target masses from Table 7 and those calculated by *in silico* digestion. The targeted MS method can be built using Table 8 data, resulting in increased sensitivity for nitropeptides detected by data-dependent methods as well as those that were not previously observed.

References cited

1. Falick AM, Hines WM, Medzihradszky KF, Baldwin MA, Gibson BW. Low-mass ions produced from peptides by high-energy collision-induced dissociation in tandem mass spectrometry. J Am Soc Mass Spectrom. 1993 11;4(11):882-93.

2. Papayannopoulos IA. The interpretation of collision-induced dissociation tandem mass spectra of peptides. Mass Spectrom Rev. 1995 01/01;14(1):49-73.

3. Crow J, Ye Y, Strong M, Kirk M, Barnes S, Beckman J. Superoxide dismutase catalyzes nitration of tyrosines by peroxynitrite in the rod and head domains of neurofilament-L. J Neurochem. 1997 NOV;69(5):1945-53.

4. Petersson A, Steen H, Kalume D, Caidahl K, Roepstorff P. Investigation of tyrosine nitration in proteins by mass spectrometry. J Mass Spectrom. 2001 06/01;36(6):616-25.

5. Griffin TJ, Xie H, Bandhakavi S, Popko J, Mohan A, Carlis JV, et al. iTRAQ reagent-based quantitative proteomic analysis on a linear ion trap mass spectrometer. J Proteome Res. 2007 11/01; 2013/04;6(11):4200-9.

6. Want EJ, Cravatt BF, Siuzdak G. The expanding role of mass spectrometry in metabolite profiling and characterization. ChemBioChem. 2005 11/04;6(11):1941-51.

7. Guo T, Gan CS, Zhang H, Zhu Y, Kon OL, Sze SK. Hybridization of pulsed-Q dissociation and collision-activated dissociation in linear ion trap mass spectrometer for iTRAQ quantitation. J Proteome Res. 2008 11/07; 2013/03;7(11):4831-40.

8. Ong S, Blagoev B, Kratchmarova I, Kristensen DB, Steen H, Pandey A, et al. Stable isotope labeling by amino acids in cell culture, SILAC, as a simple and accurate approach to expression proteomics. Molecular & Cellular Proteomics. 2002 May;1(5):376-86.

9. Ross PL, Huang YN, Marchese JN, Williamson B, Parker K, Hattan S, et al. Multiplexed protein quantitation in saccharomyces cerevisiae using amine-reactive isobaric tagging reagents. Mol Cell Proteomics. 2004 Dec;3(12):1154-69.

10. Thompson A, Schafer J, Kuhn K, Kienle S, Schwarz J, Schmidt G, et al. Tandem mass tags: A novel quantification strategy for comparative analysis of complex protein mixtures by MS/MS. Anal Chem. 2003 04/01; 2013/04;75(8):1895-904.

11. Zhang G, Neubert TA. Automated comparative proteomics based on multiplex tandem mass spectrometry and stable isotope labeling. Molecular & Cellular Proteomics. February 2006 February 2006;5(2):401-11.

12. Colzani M, Schutz F, Potts A, Waridel P, Quadroni M. Relative protein quantification by isobaric SILAC with immonium ion splitting (ISIS). Molecular & Cellular Proteomics. May 2008 May 2008;7(5):927-37.

13. Ma B, Zhang K, Hendrie C, Liang C, Li M, Doherty-Kirby A, et al. PEAKS: Powerful software for peptide de novo sequencing by tandem mass spectrometry. Rapid Commun Mass Spectrom. 2003 10/30;17(20):2337-42.

14. Robinson KM, Beckman JS. Synthesis of peroxynitrite from nitrite and hydrogen peroxide. In: Lester Packer aEC, editor. Methods in Enzymology. Academic Press; 2005. p. 207-14.

15. Kirsch M, de Groot H. Formation of peroxynitrite from reaction of nitroxyl anion with molecular oxygen. J Biol Chem. 2002 April 19, 2002;277(16):13379-88.

16. Ghesquière B, Colaert N, Helsens K, Dejager L, Vanhaute C, Verleysen K, et al. In vitro and in vivo protein-bound tyrosine nitration characterized by diagonal chromatography. Molecular & Cellular Proteomics. 2009 December 01;8(12):2642-52.

Chapter 5: Conclusions and Future Directions

Conclusions

The preceding chapters described methods exploiting the physicochemical attributes specific to protein-bound Tyr nitration that were developed and tested with the goal of elucidating the pathophysiological basis for PTN-related damage induced by oxidative/nitrative stress. To that end, a proteomics-based workflow was developed to address PTN from both global and local perspectives. Global nitration profiling emphasizes proteome-wide oxidative/nitrative stress effects, while identification of specific PTN targets and sites elucidates the metabolic pathways and molecular mechanisms affected by PTN.

Results of the described methods have successfully demonstrated increased mass spectrometric sensitivity for the identification of putative nitroproteins. Progress has also been made linking nitration and energy metabolism through identification of site-specific nitration to ATPase-β. Optimized molecular methods combined with targeted mass spectrometry were shown to enhance analytical sensitivity for ATPase-β Tyr^{345}.

Other putative PTN targets identified using the methods described herein had previously been affirmed to be nitration targets supporting our assertion that the mitochondrion is a nitration center. The plenitude of protein targets involved

in energy metabolism and ROS disposition also indicates PTN's potentially exacerbating effect on cellular injury. PTN to core histones has even further-reaching potential as it may modulate normal transcription of a variety of genes and may be involved in tumorigenesis (1).

Nitration targets such as myosin isoforms have been implicated in age-related muscle atrophy and tissue damage due to dysfunctional energy metabolism. PTN reported in skeletal muscle myosin isoforms have been shown to result in diminished interaction with actin (2), possibly contributing to age-related muscle strength attenuation. Nitrotyrosine IP experiments in this study identified abundant non-muscle myosin heavy chain IIa (myosin 9) as a novel putative PTN target. Myosin 9 functions in mitochondrial DNA maintenance (3). Thus, myosin-9 nitration could promote mtDNA damage resulting in attenuated energy metabolism or apoptosis.

Also, a recurring trend of increased histone nitration was observed in activated microglia. Histone nitration at sites normally occupied by other PTMs (e.g. acetylation, methylation, or phosphorylation) could alter chromatin remodeling and gene expression. Identification of histone nitration sites and the associated genes can elucidate possible PTN-mediated regulation of gene expression.

Histones are essential for maintaining cell fitness through chromatin assembly and access to genes for transcription (4-7). Normal gene expression is regulated by what is known as the histone code (4, 6-8). The histone code refers to the specific patterns of histone posttranslational modifications regulating

normal transcriptional states (4, 6-8). Many of these modifications are transmitted epigenetically (4, 6-8), which implies alterations to posttranslational states caused by stress may also be perpetuated.

Histone levels are also regulated through proteasomal degradation (4). Unbound histone accumulation within the nucleus is toxic as excess histones can non-specifically bind DNA due their inherent high-basicity, which can result in dysfunctional transcription (4). Posttranslational modifications such as polyubiquitination on specific sites of excess histones are molecular markers for proteolysis (4). Mutations or alternative modifications to those sites can result in histone accumulation and cell injury (4). For example, histone H3 is regulated by polyubiquitination at Tyr^{99} under normal conditions. Site-directed mutagenesis to Tyr^{99} has also been shown to result in genome instability (4).

The putative nitration site on Histone H3 Tyr^{41} identified in this study (Fig. 28) is a phosphorylation site that is essential for cell viability (4, 9, 10). However, hyper-phosphorylation to histone H3 Tyr^{41} by mutation-activated Janus kinase 2 (JAK2) has been associated with leukemia (11). JAK2 mediated phosphorylation to histone H3 Tyr^{41} inhibits the normal binding of heterochromatin protein 1α (HP1α) to the site, resulting in increased *Imo2* expression and the leukemic phenotype (11). Hyper-nitration to H3 Tyr^{41} could possibly mimic JAK2-mediated hyper-phosphorylation in an oxidative/nitrative stress-induced alternate pathway to leukemia. It could also compete with normal phosphorylation related to viability.

Our working hypothesis is that PTN modification to the regulatory sites on both chromatin-bound and unbound histones alters normal transcription and may be transmitted epigenetically due to the stability of the nitro- modification. Future directions include experiments designed to identify PTN sites on histones and the genes affected by alternative Tyr modification. Results of these experiments are expected to provide insight into gene regulation under oxidative/nitrative stress conditions. Additionally, a complementary experiment is planned to determine Tyr^{41} site occupancy changes under nitrative stress conditions. MRM analyses will be performed to assay both nitration and phosphorylation Tyr^{41} site occupancy.

Moreover, putative PTN targets discovered during this project represent strong prospects for further development of our immonium ion quantitative method using a Spike-in NitroProtein Standard (SNiPS). Preliminary data are encouraging for quantification of greater than four-fold nitration variation. Sensitivity, however, is not limited to a four-fold variation between treatment and control since SNiPS addition is at the discretion of the investigator. Quantitation will be determined by the ratio of SNiPS to endogenous nitration and is quantified among protein sets by the ratio of ratios. SNiPS can also establish preliminary targeted MS methods as well as SRM/MRM methods specific to a biological model system. These methods can be optimized by data inputs from analytical trials.

In conclusion, viable methods have been developed and tested that are specific for the nitrative stress-induced posttranslational modification, protein-

tyrosine nitration. Future development will continue the trend of novel approaches specific for the identification and quantitation of PTN targets and sites toward a more comprehensive understanding of the complex and diverse PTN roles in cellular processes.

Future Directions

Application of a mass spectrometric workflow for nitration site identification

The results described in Chapter Three were encouraging for future method development as the proteomics-based workflow discussed in Chapters One and Two can be applied to histone nitration—a posttranslational modification with potential to extend the scope of the current histone code (8). *In vitro* $ONOO^-$ reactions can be performed with histone extracts at physiological pH to induce nitration in protein native conformations.

HPLC-MS/MS analysis of the reaction products and *in silico* analysis can assist in the identification of putative nitration targets for sensitive targeted MS method development. Additional data-dependent scans will be possible with targeted scans limited to high-probability targets—facilitating more in-depth examination of the histone nitroproteome.

Histone H3 peptide synthesis for nitration site validation

To validate histone H3 Tyr^{41} nitration, $KPHRY^{(nitro)}RPGTVALR$ and the unmodified and nitro-modified permutations of YRPGTVALR can be synthesized and analyzed by HPLC-MS/MS. Assuming validation of RTs and spectral characteristics, an MRM method can be developed for quantitative analyses.

Additionally, the phosphorylated states of the peptide can be synthesized for MRM development specific to a well-characterized phosphorylation site that is potentially modulated by nitration.

Nitrotyrosine immunoprecipitation of histone fractions

Since a robust histone isolation method has been established, further isolation of the nitroproteome can be acquired from those fractions. Western blotting can be used to validate 3NT enrichment and nitration variation among differential treatment sets. Parallel Coomassie detection can expedite accurate localization of cognate PTN-containing bands from the western blot, followed by application of the MS workflow described in Chapters One and Two as well as the histone nitroprotein targeted HPLC-MS/MS analysis described in Chapter Four.

Histone purification using reversed-phase liquid chromatography

Acid extracted histones can be purified by a shallow reversed-phase HPLC method (12) to isolate histone H3, for example. This method could be used to increase analytical sample while averting potential gel extraction pitfalls. Also, a chromatographic separation will allow for UV-Vis spectroscopy to identify fractions showing peaks at 356 nm—the unique 3NT absorbance wavelength at acidic pH. Solution fractions can be digested and analyzed by targeted MS.

An alternate approach can be HPLC separation of the nuclear protein fraction acquired prior to histone acid extraction. Because histone nitration remains undetected after acid extraction (e.g. by Western analysis), there is suspicion that chemical alteration may be occurring to the nitro- moiety.

Elimination of the acid extraction step will eradicate that particular variable. Western analysis of the nuclear fraction can also be performed to validate PTN retention.

Colocalization analysis of inducible nitric oxide synthase, nitrotyrosine, and histones

Confocal microscopy is expected to improve resolution sufficiently over IF analysis to validate 3NT and histone colocalization. In addition to LPS treatment, a cell-permeable iNOS-specific inhibitor such as *N*-(3-(Aminomethyl)benzyl) acetamidine (1400W) (13) can be applied to HAPI cultures to remove the iNOS background for localization experiment controls and to evaluate global changes to the nitroproteome in the absence of iNOS generated NO. This approach can also be used to determine if iNOS localizes to the nucleus.

Chromatin immunoprecipitation-sequencing to identify genes associated with histone nitration

To identify the genes associated with PTN induced by LPS-mediated microglial activation, a modified approach to chromatin immunoprecipitation with parallel DNA sequencing (ChIP-seq) can be performed. Typical ChIP-seq experiments target specific proteins for immunoprecipitation with cross-linked DNA fragments. An alternate approach would be to immunoprecipitate only 3NT-containing proteins using either nitrotyrosine affinity sorbent (Cayman) or anti-3NT bound to magnetic beads. Upon liberation of DNA fragments from the associated nitroproteins, the DNA can be isolated and sequenced as is

customary. DNA sequence results can be correlated to gene expression data to determine the functional impact of histone nitration.

Spike-in nitroprotein standard-based workflow application to microglia

LPS has been shown to induce the classical activation phenotype in microglia (14, 15), which results in iNOS upregulation as well as increased ROS—conditions that favor increased PTN. Our plan is to create a stable isotope-labeled microglial cell master lysate. The heavy nitroprotein containing lysate can be used as a SNiPS to analyze nitration induced by direct (LPS-stimulated) activation or by indirect activation resulting from neuronal secreted factor signaling after ethanol exposure.

HAPI cell lysate labeling can be performed by reaction with bolus heavy $ONOO^-$ to induce nitration of available residues representing prospective nitration targets/sites. HPLC-MS/MS analysis of the standard with database searching can be used to identify putative nitration sites for targeted method development as well as a 3NT immonium ion quantitation optimization resource (Fig. 36A). A SNiPS lysate can also be analyzed by SDS-PAGE with parallel Western blotting and in-gel digestion with HPLC-MS/MS analysis as described in Chapter Three. Nitrotyrosine or protein- specific immunoprecipitation may be necessary to accumulate enough material for site identification from gel extracts.

Offline chromatography of SNiPS tryptic digests can pinpoint specific chromatographic fractions that are likely to contain 3NT by UV detection of its unique acidic absorbance λ of 356 nm. Fractions showing strong absorbance at 356 nm can be analyzed by data-dependent MS/MS to identify nitropeptide MS

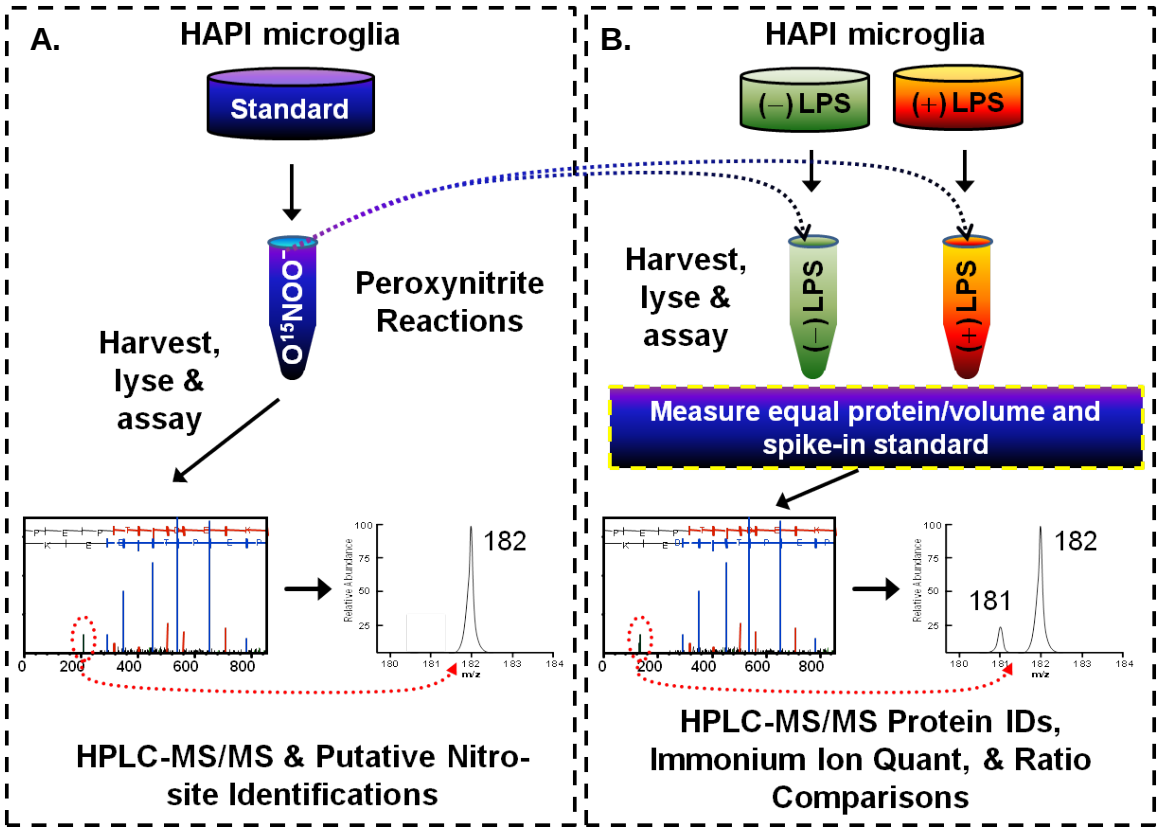

Figure 36. Application of SNiPS to activated microglia. A) Nitration reactions are performed on a standard HAPI culture for putative PTN target identification. Prospective nitration sites are identified through Mascot database searches and Scaffold validation as well as manual reconstruction of XICs containing heavy 3NT immonium ions. LOD is determined for the identified nitropeptides to set the SNiPS spike-in amount. B) SNiPS from (A) is applied to equal amounts of each protein set. Protein sets are analyzed separately by targeted and data-dependent MS/MS. Nitropeptide sequences are identified and Log_2 ratios are calculated for individual protein sets using the 3NT immonium ion pair relative intensities. The H/L Log_2 ratio of ratios is then calculated to determine relative nitration changes between treatment groups (Fig. 37).

targets. However, shotgun LC-MS analysis of SNiPS may be sufficient for PTN target/site identifications. The shotgun approach will eliminate protein or peptide losses associated with gel extraction and 2D LC. Nitropeptide identifications from SNiPS can be validated by manual spectral analyses and peptide synthesis for sites of particular interest.

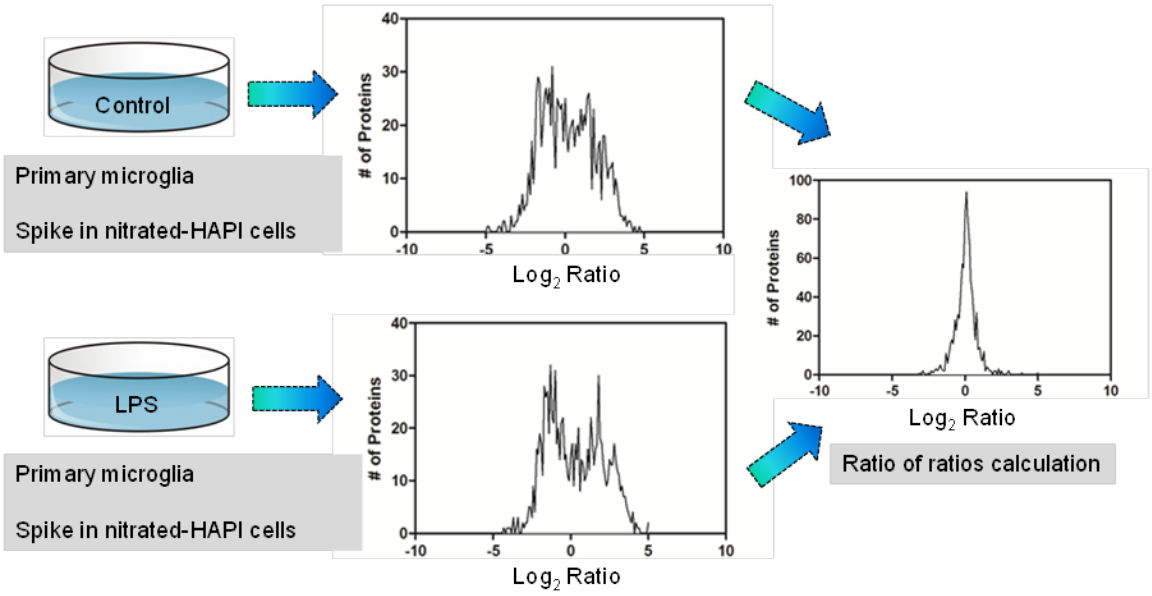

Figure 37. SNiPS generated 3NT immonium ion pair quantitation. In this scheme, both the control and LPS treatment groups inoculated with equal SNiPS content are analyzed separately. A Log_2 ratio of 3NT immonium ion pair intensities is determined individually for each protein set. A Log_2 ratio of ratios is then calculated between the two protein sets to determine change in nitration.

SNiPS application for quantitative nitration analysis

Upon successful characterization of the microglial SNiPS, it can be applied as a SILAC control to a variety of microglial treatments. For example, HAPI cells can be grown to near confluence and treated with 50 ng $\times$ mL^{-1} LPS or standard DMEM for 24 h. After lysis and protein assay, SNiPS can be introduced in equal amounts to each protein group. Trypsin digestion will provide duplicate peptide sets that can be analyzed by a combination of data-dependent and nitropeptide-targeted MS/MS acquisitions. Database searches and manual mining for spectra containing heavy 3NT immonium ions can be conducted to identify nitration sites and quantify PTN from classical microglia activation based on ratios of 3NT immonium ion pair intensities (Fig. 36B).

The Log_2 ratios of immonium ion pairs can be calculated for all validated nitropeptide spectra (Fig. 37) and normalized for the contribution of any previously-identified endogenously-generated 3NT. The Log_2 ratio of ratios between protein groups and the SNiPS can then be calculated for improved correlation and to determine variation between experimental protein sets (Fig. 37). This process can be performed for entire proteomes as well to determine variant expression profiles between microglia expressing differential activation stages (e.g. resting stage versus classical activation) (15). Successful SNiPS development is a novel approach that is expected to become a powerful tool for the elucidation of the contribution of PTN to the cellular injury associated with oxidative/nitrative stress.

Nitration and phosphorylation analyses using a triple quadrupole mass spectrometer

Another MS method that can exploit the generation of 3NT immonium ions to identify PTN is precursor ion scanning (PIS) in a triple quadrupole MS. Precursor ions enter Q1 from the source and are scanned, transmitting narrow mass ranges into the collision cell (Q2) where they are fragmented by CID. Q3 would be set to transmit product ions of 181 or 182 m/z. A mass spectrum would then be generated for all parent ion m/z that produced an immonium ion (Fig. 38A).

A subsequent SRM (selected reaction monitoring) analysis can be developed using the precursor ion masses identified from PIS spectra with product ion selection of 181 and 182 m/z. This method will provide sequence

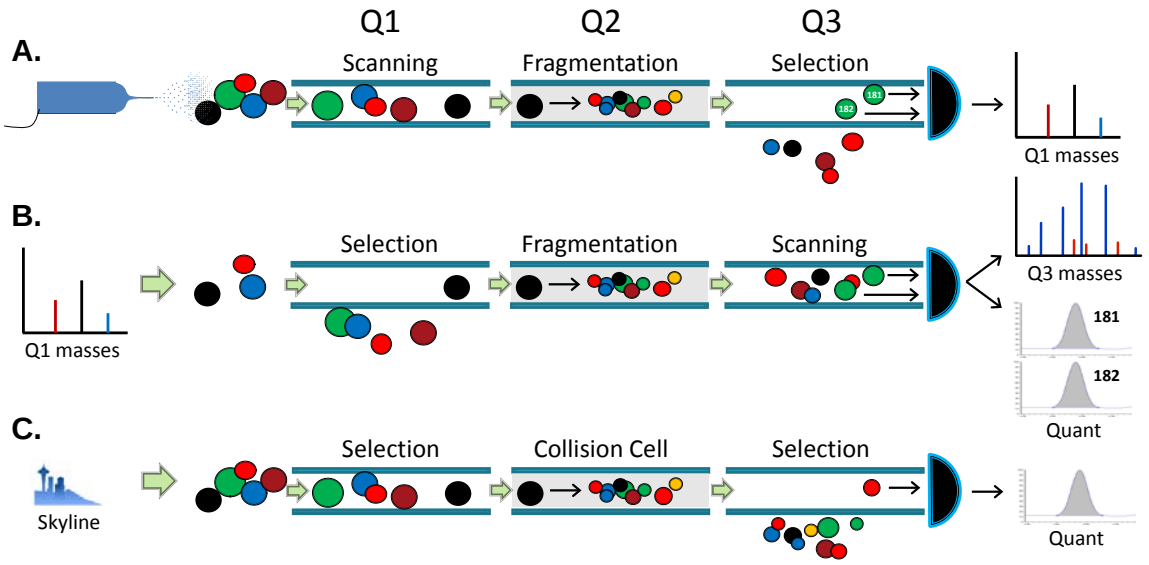

Figure 38. Triple quadrupole scans for PTN characterization. A) A precursor ion scan (PIS) scans the entire instrument mass range in Q1. The collision cell (Q2) fragments the Q1 masses individually and Q3 selects for H&L 3NT immonium ion masses. Spectra result exclusively for m/z scanned in Q1 that produced 3NT immonium ions upon CID. B) Precursor ions identified from (A) that resulted in 3NT immonium ion products from PIS are selected in Q1, fragmented by CID in Q2 and scanned in Q3 to produce MS_2 spectra for sequence identification and immonium ion quantitation. C) PTN target sequences identified from (B) can be input into Pinpoint or Skyline programs to calculate all permutations of Tyr nitration to create a comprehensive SRM or MRM method as described in Chapters One and Two. Quantitation is based on the AUCs of the SRM/MRM peaks.

information for nitropeptide identification as well as the potential for quantitation of AUCs for each SRM containing either the heavy or light 3NT isotope (Fig. 38B).

To augment SRM scanning, Pinpoint (Thermo) or Skyline (16) programs can be employed to calculate SRM or MRM transitions for specific target proteins. Table S2 demonstrates a Skyline output from input of FASTA sequences of the four histone isoforms from both mouse and rat. Nitration was specified as a variable modification, trypsin was specified as the proteolytic

enzyme and MRM transitions were limited to three. The MRM method can be input into the TSQ method builder, resulting in quantifiable nitropeptide-specific MRM peaks (Fig. 38C) similar to those described for the pentapeptides in Chapter Two.

A major advantage to TSQ analysis is the range of CE available in the collision cell. A TSQ collision cell uses argon as the collision gas, which facilitates energy-dependent fragmentation similar to HCD in an Orbitrap—allowing for optimization of 3NT immonium ion signal by CE optimization. SRM and MRM specificity is extremely reliable, since peak detection is dependent upon precursor mass transitioning to specific product ion masses. Sensitivity and specificity can be further enhanced by modification of the method based on experimental RTs. The analytes of interest can be isolated in truncated time windows (segments)—resulting in more data points across quantifiable peaks.

Histone phosphorylation MRM assays can be set up in a similar manner to the PTN method. To determine the impact of nitration on a known phosphorylation site (e.g. histone H3 Tyr^{41}) precursor mass entries will reflect YRPGTVALR with both +45 Da for nitration and +80 Da for phosphorylation. Site occupancy for both modifications will be calculated by dividing the signal for the each modification by the sum of the modified and unmodified peptide signals.

Expected outcomes and significance

Together, these experiments are expected to improve the characterization of PTN from complex biological matrices. The identification and quantitation of

PTN targets and sites are expected to provide insight into its impact on protein function, metabolic pathways, transcription, and intracellular signaling.

References cited

1. Haqqani AS, Kelly JF, Birnboim HC. Selective nitration of histone tyrosine residues in vivo in mutatect tumors. J Biol Chem. 2002 02/01;277(5):3614-21.

2. Thompson LV, Durand D, Fugere NA, Ferrington DA. Myosin and actin expression and oxidation in aging muscle. J Appl Physiol. 2006 12/01;101(6):1581-7.

3. Reyes A, He J, Mao CC, Bailey LJ, Di Re M, Sembongi H, et al. Actin and myosin contribute to mammalian mitochondrial DNA maintenance. Nucleic Acids Res. 2011 07/01;39(12):5098-108.

4. Singh RK, Kabbaj MM, Paik J, Gunjan A. Histone levels are regulated by phosphorylation and ubiquitylation-dependent proteolysis. Nat Cell Biol. 2009 print;11(8):925-33.

5. Cosgrove MS, Wolberger C. How does the histone code work? Biochemistry & Cell Biology. 2005 08;83(4):468-76.

6. Garcia BA, Siuti N, Thomas CE, Mizzen CA, Kelleher NL. Characterization of neurohistone variants and post-translational modifications by electron capture dissociation mass spectrometry. International Journal of Mass Spectrometry. 2007 /1/1/;259(1-3):184-96.

7. Strahl BD, Allis CD. The language of covalent histone modifications. Nature. 2000 Jan 6;403(6765):41-5.

8. Jenuwein T, Allis CD. Translating the histone code. Science. 2001 08/10;293(5532):1074-80.

9. Dai J, Hyland EM, Yuan DS, Huang H, Bader JS, Boeke JD. Probing nucleosome function: A highly versatile library of synthetic histone H3 and H4 mutants. Cell. 2008 Sep 19;134(6):1066-78.

10. Nakanishi S, Sanderson BW, Delventhal KM, Bradford WD, Staehling-Hampton K, Shilatifard A. A comprehensive library of histone mutants identifies nucleosomal residues required for H3K4 methylation. Nat Struct Mol Biol. 2008 Aug;15(8):881-8.

11. Dawson MA, Bannister AJ, Gottgens B, Foster SD, Bartke T, Green AR, et al. JAK2 phosphorylates histone H3Y41 and excludes HP1agr] from chromatin. Nature. 2009 10/08;461(7265):819-22.

12. Allis CD, Dormann HL, Hake SB, Shechter D. Extraction, purification and analysis of histones. Nature Protocols. 2007 06; 2013/4;2:1445-57.

13. Garvey EP, Oplinger JA, Furfine ES, Kiff RJ, Laszlo F, Whittle BJR, et al. 1400W is a slow, tight binding, and highly selective inhibitor of inducible nitric-oxide synthase in vitro and in vivo. Journal of Biological Chemistry February 21;272(8):4959-63.

14. Bell-Temin H, Zhang P, Chaput D, King MA, You M, Liu B, et al. Quantitative proteomic characterization of ethanol-responsive pathways in rat microglial cells. J Proteome Res. 2013 03/15; 2013/04.

15. Marshall SA, McClain JA, Kelso ML, Hopkins DM, Pauly JR, Nixon K. Microglial activation is not equivalent to neuroinflammation in alcohol-induced neurodegeneration: The importance of microglia phenotype. Neurobiol Dis. 2013 /6;54(0):239-51.

16. MacLean B, Tomazela DM, Shulman N, Chambers M, Finney GL, Frewen B, et al. Skyline: An open source document editor for creating and analyzing targeted proteomics experiments. Bioinformatics. 2010 Apr 1;26(7):966-8.

Appendix A: Journal of Proteomics #749

JOURNAL OF PROTEOMICS 75 (2012) 1691–1700

Available online at www.sciencedirect.com

SciVerse ScienceDirect

www.elsevier.com/locate/jprot

Investigation of local primary structure effects on peroxynitrite-mediated tyrosine nitration using targeted mass spectrometry

Kent W. Seeley, Stanley M. Stevens Jr. *

Department of Cell Biology, Microbiology, and Molecular Biology, University of South Florida, Tampa, FL, USA

ARTICLE INFO

Article history:
Received 18 September 2011
Accepted 21 November 2011
Available online 2 December 2011

Keywords:
Nitration
Nitrosative stress
Oxidative stress
Tandem mass spectrometry
PTM
MRM

ABSTRACT

Protein-tyrosine nitration (PTN) is a posttranslational modification resulting from cellular nitrosative stress that has been implicated in a wide variety of disease states. Determination of factors that influence selectivity of PTN remains a major challenge due to several issues including low biological levels of PTN, proximity of target sites on a single analyte, and analytical limitations for site-specific quantification of the nitration modification. We report a systematic approach that addresses relevant contributing factors to PTN with particular focus on determining the effect of changing proximal amino acid side chain structure on tyrosine nitration yield. A trend was observed in which nitration yield tends to be greater when the tyrosine residue is surrounded by basic and/or uncharged polar residues compared to nitration levels observed when hydrophobic and acidic residues are proximal to the tyrosine residue. Moreover, an electric dipole effect was observed where a higher degree of charge asymmetry surrounding the tyrosine residue correlates with an increased tyrosine nitration yield in certain cases. The reported data are expected to facilitate site-specific prediction and validation of PTN, especially in cases of potential target residues that share a similar solvent exposure environment and contain elements of known higher-order structure.

1. Introduction

Posttranslational modification (PTM) to proteins induced by oxidative and nitrosative stress can contribute to the pathophysiological events associated with the progression of certain diseases [1–8]. Protein-tyrosine nitration is a PTM characterized by covalent addition of a nitro- group ($-NO_2$) to the three-position carbon on the phenolic ring of a tyrosine residue. Although nitration occurs under normal physiological conditions, it can be exacerbated during oxidative stress. Nitro- group addition to tyrosine shifts the pK_a of its hydroxyl group from 10.1 to ~7.2—altering its charge state and reactivity at physiological pH [9]. Nitration also confers a bulk addition of 35 $Å^3$ to the residue. These physicochemical changes in tyrosine may distort conformation locally or in a remote part of a protein and can potentially alter enzymatic activity or protein-protein interaction [1]. Nitrotyrosine also occurs at a low steady state meaning that fewer than approximately 1 in 10^5 tyrosine residues are modified endogenously [5]. Peroxynitrite, a major contributor to protein tyrosine nitration, has a half-life of less than one second [10,11] and nitroproteins can be degraded at accelerated rates with half-lives of hours versus days for unmodified [12].

Since nitration can alter major biological processes including tyrosine kinase signaling pathways [1], identification of nitra-

* *Corresponding author at:* Department of Cell Biology, Microbiology, and Molecular Biology, University of South Florida, 4202 East Fowler Avenue, BSF 218 Tampa, FL 33620, USA. Tel.: +1 813 974 8146; fax: +1 813 974 1614.
E-mail address: smstevens@usf.edu (S.M. Stevens).

1874-3919/$ – see front matter © 2011 Elsevier B.V. All rights reserved.
doi:10.1016/j.jprot.2011.11.025

tion sites within a particular nitroproteome can help predict functional outcomes in the cell due to oxidative/nitrosative stress. While PTM site prediction programs and servers (e.g., http://www.biocuckoo.org) use algorithms developed from empirical data, such data remain relatively sparse compared to other common protein modifications. Also, earlier annotations reported in the scientific literature without stringent validation may require further scrutiny [13]. Although high molecular weight proteins would logically be more susceptible to nitration due to the generally higher tyrosine abundance, experimental data show that nitration preference does not always correlate with the number of tyrosine residues available. For example, β-casein (~2% tyrosine content), has been shown to be more susceptible to nitration than phospholipase A2 (~8% tyrosine content) [4]. Also human serum albumin (HSA) was observed to have preferential nitration on only two of its 18 available sites [14]. Other studies have indicated that tyrosines residing in α-helices or β-turn structures are preferentially nitrated [3,15]. Although compelling, these predictors do not account for incidents where nitration occurs on only one of two or more neighboring tyrosine residues that meet all or most of the same structural criteria. Our study attempts to elucidate the factors influencing nitration preference in these cases, especially those where local environment appears to be the determinant of selective nitration.

Here we report a fundamental analytical investigation of local primary structure effects on peroxynitrite-mediated tyrosine nitration. Although putative susceptibility motifs have been published [3,12,15], none explain the phenomenon of preferential nitration based on adjacent residue structure since most nitration mapping experiments are performed under native conditions where higher-order protein structure would presumably be a major influence on nitration selectivity. Nitration yield is expected to be similar with regard to proximal residues that share similar local structure and solvent accessibility; however, our data from a peroxynitrite-treated protein standard, nitrotyrosine bovine serum albumin (nBSA), as well as data from others showed multiple cases of preferential chemical modification in which only certain tyrosine residues were nitrated within a relatively short amino acid sequence of the protein. These data led to our hypothesis that local primary structure plays a role in determining site-selective modification by peroxynitrite. To test this hypothesis, we synthesized sixteen pentapeptides with a single tyrosine flanked by representative hydrophobic, uncharged polar, acidic and basic residues (Leu, Ser, Glu, and Lys, respectively) in all possible perturbations with glycine termini. These short peptides were designed to negate any higher-order structural effects. The pentapeptides were reacted with peroxynitrite under standard conditions to induce nitration and a triple-quadrupole mass spectrometric (MS) method was developed to select for each pentapeptide's modified and unmodified parent to product ion transitions, allowing us to determine the relative nitration efficiencies of each peptide. To the best of our knowledge, this study is the first of its kind to systematically evaluate the effect of amino acid sequence surrounding tyrosine on its susceptibility to nitration. This study also highlights the utility of an MRM-based approach to accurately assess nitration selectivity for multiple proximal tyrosine residues contained within the same peptide analyte.

2. Materials and methods

All reagents were purchased from Sigma-Aldrich (St. Louis, MO, USA) unless otherwise specified.

2.1. *Peroxynitrite-treated BSA tryptic digestion*

Peroxynitrite-treated BSA (Cayman Chemical, Ann Arbor, MI, USA) was digested with trypsin by first suspending 8 μg in 100 μL of 6 M urea (Acros Organics, NJ, USA), 25 mM ammonium bicarbonate (ABC). Dithiothreitol (DTT) in 25 mM ABC was added to a final concentration of 10 mM and incubated for 1 h at 25 °C to reduce disulfide bonds. Cysteines were alkylated by reaction with 40 mM iodoacetamide in 25 mM ABC in the dark at 25 °C for 1 h. Alkylation was stopped by addition of DTT to 40 mM. The urea buffer was diluted to less than 1 M, followed by addition of TPCK-treated trypsin (Applied Biosystems, Foster City, CA, USA) at a ratio of 1:50 trypsin: protein. Digestion was carried out overnight at 37 °C and stopped by addition of 5% formic acid (FA). Digests were desalted by C_{18} solid-phase extraction in 1 mL columns (Supelco, Bellefonte, PA, USA) followed by concentration by centrifugation at 45 °C under vacuum. Dry peptides were resuspended by sonication for 10 min in 0.1% FA prior to HPLC-MS/MS analyses. Digests were done in triplicate with one analytical replicate for each.

2.2. *BSA nitration site identification by LC-MS/MS*

Five microliter injections of the BSA digests were separated by HPLC on an Eksigent NanoLC 2D Ultra system (Dublin, CA, USA). A capillary trap column (ProteoPep II™ 100 μm i.d.×2 cm C_{18}) was used to desalt prior to loading on the analytical column (ProteoPep II™ 75 μm i.d.×10 cm C_{18}) both manufactured by New Objective (Woburn, MA, USA). The mobile phase flow-rate was 250 nL/min and followed a linear gradient of 0 min 2% B, 0–60 min 2%–40% B; 60–65 min 40%–80% B; 65–70 min 80% B; 70.1–85 min 2% B (mobile phase A=0.1% FA in water and B=0.1% FA in acetonitrile).

Tryptic peptides were analyzed by data-dependent electrospray ionization (ESI)-MS/MS on a hybrid linear ion trap–Fourier transform Orbitrap mass spectrometer (LTQ Orbitrap XL, Thermo Scientific, USA) equipped with XCalibur (version 2.0.7) data acquisition software. Full-scan mass resolving power was set to 60,000 (at m/z 400) followed by data-dependent MS/MS of the top five most intense ions in the LTQ linear ion trap with one MS/MS scan repeat and dynamic exclusion set for 180 s. Database searches of raw MS/MS data were performed on Mascot (Matrix Science, London, UK; version 2.2) with the IPI bovine database (version 3.47) specifying trypsin as the digestion enzyme. An additional search of a subset database from initial identifications was performed using X! Tandem (The GPM, thegpm.org; version 2007.01.01.1). Parent ion mass tolerance was set to 5.0 ppm and fragment ion tolerance was set to 0.50 Da. Carbamidomethylation of cysteine was specified as a fixed modification while oxidation of methionine, n-terminal acetylation, and tyrosine nitration were all specified as variable modifications. Scaffold (version Scaffold_3_00_08, Proteome Software Inc., Portland, OR) was used to validate MS/MS based peptide and protein

Appendix A continued

identifications. Peptides were accepted if the probability was >95.0% as specified by the Peptide Prophet algorithm [16] and protein identifications were accepted at probabilities >99.9% as specified by the Protein Prophet algorithm [17]. Manual analyses of putative 3-nitrotyrosine (3NT)-containing peptides were performed prior to selection of prototype peptide synthesis [13].

2.3. Tyrosine reactions with peroxynitrite

Tyrosine (Tyr, 500 μM) was reacted in triplicate with 5 μM, 10 μM, 20 μM, and 50 μM $ONOO^-$ in PBS (pH 7.4 at 25 °C). Reactions were quenched after 1 h with 5% FA prior to the addition of 500 nM "heavy" Tyr ($^{13}C_6$-Tyr) which served as the internal standard (IS). Nitrotyrosine (Cayman Chemical, Ann Arbor, MI, USA) was serially diluted to 50 μM, 100 μM, 250 μM, 500 μM, and 750 μM for use as an external calibrant for the nitrotyrosine generation assay. The IS was also added to 3NT dilutions and unreacted Tyr controls. Tyrosine and nitrotyrosine were separated at a flow-rate of 250 μL/min (Surveyor, Thermo Scientific, USA) through a 150×2.1 mm i.d. C_{18} (5 μm particle) analytical column (Higgins Analytical, Mountain View, CA, USA) with the following gradient: 0–2 min 100% A, 2–15 min 20% B, 15–20 min 20-40% ACN in 0.1% FA; and 20–30 min 0.1% FA in water. Mobile phase A composition included 0.1% FA in water and mobile phase B composition was 0.1% FA in acetonitrile (Honeywell International, Inc). A Biotek XS plate reader was used to determine the initial absorption maximum for 3NT (427 nm at pH 7.4 and 356 nm at pH 3) by full-spectrum scan. This wavelength and the literature absorbance maximum of 280 nm for Tyr [18] were specified in all LC methods (amino acid and pentapeptide assays [2.4]), which employed photodiode array (PDA) detection (Surveyor, Thermo).

2.4. Pentapeptide peroxynitrite reactions

Sixteen peptides with the sequence Gly-Xaa-Tyr-Xaa-Gly (where Xaa=Glu, Leu, Lys, and Ser) were synthesized by Fmoc solid phase chemistry using 5-chloro-1-[bis(dimethylamino)methylene]-1H-benzotriazolium 3-oxide (HCTU) as an activating agent. All pentapeptide syntheses were done at the 25 μmole synthesis scale using Protein Technologies Symphony Peptide Synthesizer at the University of South Florida Peptide Synthesis and Mass Spectrometry Facility. For each coupling step, 5 equivalents of Fmoc-amino acid and 7.5 equivalents of HCTU were dissolved in 0.4 M N-methylmorphorine in dimethylformamide (DMF). Fmoc deprotection was done using 20% piperidine/2% 1,8-diazobicyclo[5.4.0] undec-7- ene (DBU). After synthesis, the resin was washed with N-methylpyrrolidone (NMP) followed by dichloromethane (DCM) and cleaved using a cocktail mixture (94% TFA, 2.5% water, 2.5% ethanedithiol, 1% triisopropyl silane), precipitated in cold ether, analyzed by reversed phase high performance liquid chromatography and characterized by matrix-assisted laser desorption ionization time of flight mass spectrometry (MALDI-TOF-MS).

The residues flanking the tyrosine in the pentapeptides were chosen based on the selective nitration that was observed on the peptide DAFLGSFLYEYSR from BSA nitration mapping experiments with the addition of a basic residue for comprehensiveness. Pentapeptides (500 μM) were reacted with three concentrations (500 μM, 350 μM and 200 μM) of peroxynitrite and assayed semi-quantitatively by MRM. A time course analysis was also performed on the least nitration susceptible (GEYLG) and most susceptible (GKYKG) species where each was reacted with 200 μM $ONOO^-$ and quenched after 1 min and one hour. All reactions mentioned above were done at room temperature in PBS (pH 7.4) in quintuplicate with two replicate LC-MS/MS injections for each. The LC gradient used for the pentapeptides was the following with mobile phase A=0.1% FA in water and B =0.1% FA in acetonitrile (ACN): 0–3 min=98% A: 2% B, 3–15 min 2–20% B, 15–20 min 20–40% B, and 20–30 min 2% B.

2.5. MRM method development

The top three MRM transitions from each analyte's precursor mass-to-charge ratio (m/z) were determined via syringe-pump infusion in the tune mode of the triple quadrupole mass spectrometer (TSQ Quantum Ultra, Thermo). Ion transmission optics for both precursor and product ions and product collision energies were optimized in this mode as well. The precursors and transitions monitored for each analyte are listed in Table S1. UV/Vis absorbance was also used to support the identification of nitrated peptides given the unique absorbance (356 nm) of nitrotyrosine under acidic conditions. MRM transitions and collision energies for the unmodified pentapeptide library were determined by direct infusion as described above. However, because nitropentapeptides were not synthesized, Pinpoint software (version 1.0, Thermo Scientific, USA) was used to predict MRM settings for the

Table 1 – Comparison of nitration yield for pentapeptide positional isomers. A general trend of increased nitration was observed for positional isomers with a lower Krokhin Hydrophobicity Index value [22]. Data provided represents 500 μM pentapeptide reactions with 500 μM peroxynitrite. Hydrophobicity indices were calculated using the online calculator available at http://hs2.proteome.ca/SSRCalc/SSRCalcX.html and confirmed through rpHPLC retention time differences observed experimentally.

Pentapeptide	Avg. % Nitration	Hydrophobicity Index	rpHPLC retention time (min)
GKYLG*	5.85±1.16%	10.51	9.85±0.02
GLYKG*	4.35±0.48%	8.05	9.62±0.02
GSYKG	5.06±0.64%	3.04	2.55±0.01
GKYSG	4.24±0.73%	3.52	2.58±0.01
GLYSG*	4.99±0.59%	8.75	10.94±0.01
GSYLG*	2.47±0.29%	10.33	11.30±0.02
GLYEG*	4.53±0.34%	9.69	11.23±0.02
GEYLG*	1.17±0.13%	10.52	11.32±0.04
GEYKG*	3.16±0.47%	2.3	2.91±0.03
GKYEG*	1.87±0.24%	3.18	2.94±0.04
GEYSG	2.46±0.26%	2.1	4.47±0.15
GSYEG	2.26±0.21%	2.58	4.69±0.08

* Positional isomers that show statistically significant difference ($p<0.05$, t-test) in nitration yield.

modified species (Table S1). Pinpoint parameters were set to calculate transitions for both 1⁺ and 2⁺ gas-phase precursor charge states.

2.6. *Statistical testing*

All statistical tests were performed using GraphPad Software's (La Jolla, CA, USA) Prism and InStat 3 (Table 1 only) programs.

3. Results and discussion

3.1. *Nitration mapping of peroxynitrite-treated BSA*

Fig. 1A shows the sequence coverage and identified nitration sites for the peroxynitrite-reacted BSA standard. We identified 7 tyrosine nitration sites from 18 total tyrosine residues (out of 21 tyrosine residues available in BSA) on tryptic peptides from LC-MS/MS analysis (Fig. 1; Fig. S1 A-F). Interestingly, four MS/MS spectra representing the tryptic peptide, DAFLGSFLYEYSR, indicated nitration specificity for Tyr 357 as shown in Fig. 1B, while no spectra associated with Tyr 355 modification were identified (16 MS/MS spectra were identified for DAFLGSFLYEYSR with no modification). Scaffold PTM analysis using the Ascore algorithm [19] of the nBSA standard calculated Tyr 357 nitration probability at 100% (highest Ascore at 35.71) in contrast to Tyr 355 at 0% (no Ascore reported). This preferred nitration site (Tyr 357) has been identified previously in tetranitromethane-treated BSA using PSD on a MALDI-TOF instrument [20]. The same nitration site in BSA was also recently reported in human serum albumin (HSA) at Tyr 358 [21], where the unmodified peptide was recovered in the enrichment process without identifying the alternate site at Tyr 356. The identification of preferential nitration at this tyrosine residue in both human and bovine serum albumin from our study as well as others highlights the consistency of nitration selectivity in this region of the protein and thus provided impetus to further investigate the structural features that would influence this phenomenon.

3.2. *Nitration quantitation of tyrosine amino acid by MRM*

To determine the effect of $ONOO^-$ on 3NT generation, a multiple reaction monitoring (MRM) MS method was first developed to quantify the ratio of 3NT to unmodified Tyr at the amino acid level in order to validate the method prior to nitration quantitation at the peptide level. Area under the curve (AUC) values from extracted ion chromatograms (XICs) were normalized to the internal standard and used to quantify each analyte from the

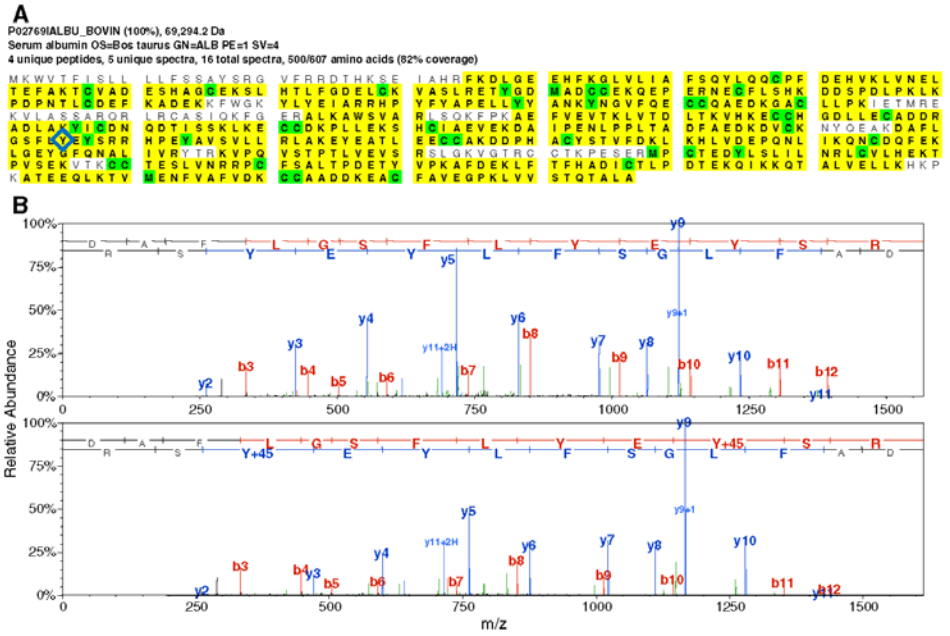

Fig. 1 – Nitration site selectivity. a) Nitrotyrosine sites identified from peroxynitrite treated BSA standard. Shaded squares indicate any modification specified in the database search (e.g. carbamidomethyl-C, oxidation-M, nitro-Y). A nitration preference for BSA Tyr 357 over Tyr 355 (diamond) was evident in the nitro-Y BSA standard (Cayman Chemical). b) MS/MS spectra for the unmodified BSA tryptic peptide DAFLGSFLYEYSR (Top) and DAFLGSFLYEY$^{[nitro]}$SR (Bottom).

reactions. The equation derived from the standard curve of 3NT dilutions was used to calculate the amount of 3NT generated from $ONOO^-$ reactions (Fig. 2A).

Nitrotyrosine formation at the amino acid level was found to be linear with respect to peroxynitrite concentration (Fig. 2B). Additionally, the unique absorbance of 3NT at acidic pH (~356 nm) was used to facilitate detection which could prove useful as a chromatographic screening method to help target fractions containing abundant nitropeptides. A quantitative assay based on the MRM method developed for Tyr can be adapted to those peptides, providing a useful assay for nitration mapping under various physiological conditions.

3.3. *Peptide prototype prospecting*

Manual analyses of MS/MS spectra derived from 3NT-containing peptides facilitated the identification of prototype prospects for MRM method development. The criteria used for prototype peptide selection were as follows: both modified and unmodified permutations of the prospect were identified, missed cleavage parent ions were absent, and residues prone to oxidative modification (Cys and Met) were also absent.

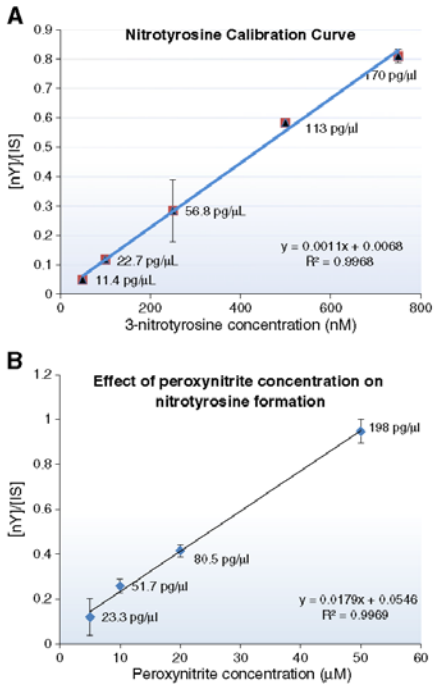

Fig. 2 – MRM quantitation of 3NT generated from L-tyrosine reactions with peroxynitrite. A) External calibration curve. B) 3NT products from 500 µM L-tyrosine reactions with various concentrations of $ONOO^-$.

Three synthetic stable isotope-labeled AQUA™ peptides (Thermo Scientific, USA) with the sequences DAFLGSFLYEYSR[13C,15N], DAFLGSFLYEY[3-nitro]SR[13C,15N], and DAFLGSFLY[3-nitro]EYSR[13C,15N] were analyzed by HPLC-MS/MS as previously mentioned for BSA digests to validate spectra observed from nitro-BSA analysis using the LTQ Orbitrap XL (Fig. S2). We developed an MRM method for these peptides in the same manner described for the free amino acid. MRM analyses were performed on the synthetic peptide, DAFLGSFLYEYSR, reacted with 200 µM $ONOO^-$. Our data showed near baseline resolution between DAFLGSFLYEY[3-nitro]SR and DAFLGSFLY[3-nitro]EYSR (Fig. 3A), demonstrating the usefulness of the LC-MRM method for applications in which site-specific quantitation of proximal target residues is necessary. The MRM transitions used to distinguish between the two peptides comprised one specific to each species (DAFLGSFLYEY[3-nitro]SR: 807→599; DAFLGSFLY[3-nitro]EYSR: 807→1188) and one common to both (807→762) as shown in Fig. 3A. However, peptide-specific transitions may not be useful quantitatively as the abundance of the y or b-ion series transitions could vary based on the location of the nitro group. Thus, a quantitative assay was developed using selected reaction monitoring (SRM) that scanned for the common transition (807→762) while referencing each analyte's RT. Five reactions of DAFLFSFLYEYSR with 200 µM $ONOO^-$ showed a statistically significant ($p<0.01$, t-test) higher yield of nitration at Tyr 11 (Fig. 3B). The doubly-nitrated version of the peptide, DAFLGSFLYEYSR, could not be synthesized for MRM characterization due to low solubility (as determined by the Krokhin retention index value of 44.86) ([22]). Furthermore, we did not observe this permutation in the nBSA standard. These data do not preclude the existence of the double-nitrated species, rather it may be indicative of its high hydrophobicity that would affect consistent LC-MS analysis.

Our reactions with the synthetic peptide DAFLGSFLYEYSR showed similar nitration selectivity at Tyr 11 as observed for BSA in its native protein conformation although nitration was detected at Tyr 9 at the peptide level. Given the magnitude of selectivity difference upon comparison of the protein and peptide nitration results, it is apparent that higher-order structural effects of BSA play a much larger role in peroxynitrite-mediated nitration selectivity in this region of BSA structure; however, it can be concluded that primary structure does have some contribution. We hypothesized that the peptide DAFLGSFLYEYSR may adopt a similar secondary structure in solution as observed for HSA and/or that local primary structure proximal to the tyrosine residues could affect tyrosine nitration yield. It was unclear from circular dichroism spectroscopy (CD) analysis (Alliance Protein Laboratories, Thousand Oaks, CA, USA) as to the peptide's solution structure (Fig. S3) and therefore, our efforts focused on elucidating the effect of local primary structure on tyrosine nitration.

3.4. *Primary structure effect on nitration efficiency*

In order to test the effect of proximal amino acid sequence on tyrosine nitration yield, sixteen tyrosine-containing pentapeptides with different amino acids (Lys, Glu, Leu, Ser) surrounding the tyrosine residue were synthesized and reacted with peroxynitrite. Nitration yield of each peptide was analyzed using MRM methods developed from infusion of the

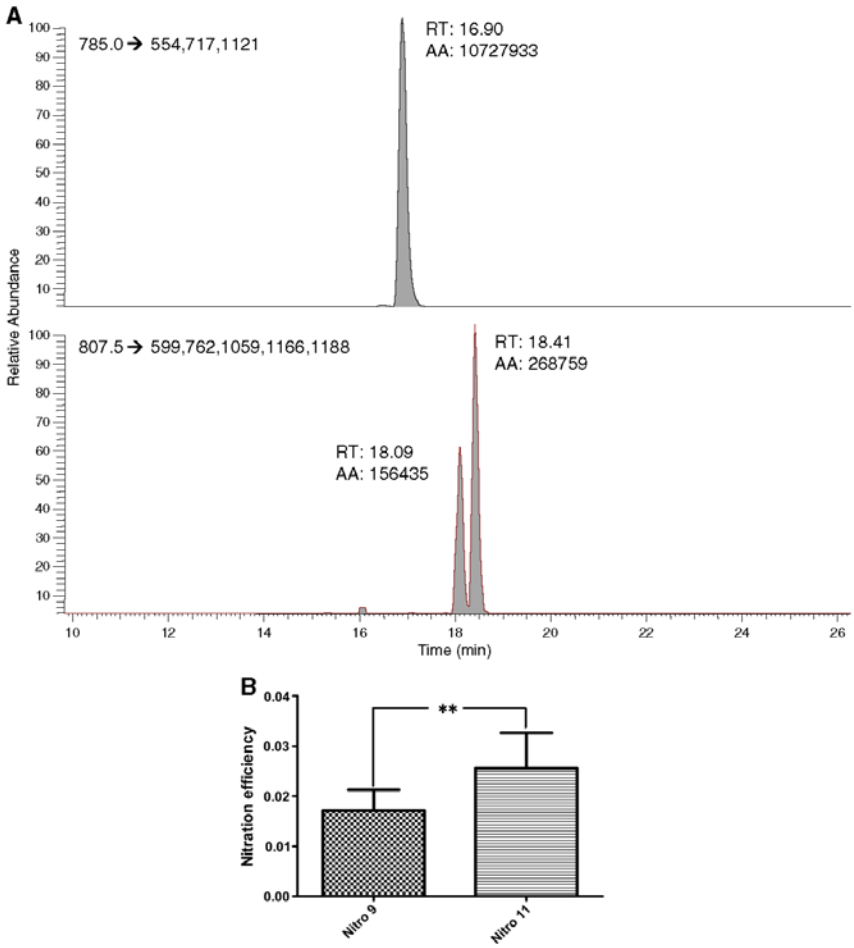

Fig. 3 – MRM chromatogram of DAFLGSFLYEYSR reactions with peroxynitrite. A) The upper trace is the unmodified peptide peak. The lower trace shows near baseline resolution for peaks representing nitro-Y 9 (RT 18.09) and nitro-Y 11 (RT 18.41). B) Reactions with 200 μM $ONOO^-$ show statistically significant nitration preference for Tyr 11 (n=10, **t-test, P<0.01).

native peptides as well as Pinpoint software predictions for the nitropeptides. Percent nitration was calculated as the ratio of nitrated pentapeptide to total (modified+unmodified) based on the AUC of MRM peaks acquired by the triple quadrupole mass spectrometer. The AUCs for all peaks representing nitropeptides and unmodified cognate peptides, including the 2^+ charge precursor→product peaks for Lys-containing species, were considered in calculating the ratio. Semi-quantitative analysis was performed to determine nitration efficiency for each of the pentapeptides (Fig. 4 and Fig. S4). A one-way analysis of variance (ANOVA) followed by a Tukey-Kramer multiple comparison test showed significant variance in nitration efficiencies among the majority of pentapeptides with the highest q of 61.80 ($p<0.001$) for GEYLG vs. GKYKG. The reactions showed nitration efficiency to be highest where tyrosine was flanked by basic residues and/or uncharged polar residues which implies that a positive charge or polar amino acid side chain may increase nitration yield while hydrophobic residues surrounding the tyrosine may be an inhibitory factor.

Positional isomers of the pentapeptides (e.g., GSYLG and GLYSG) showed an interesting trend in terms of nitration yield. As demonstrated in Table 1, change in the order of the

amino acid residues surrounding tyrosine in the pentapeptide sequence resulted in alteration of overall hydrophobicity of the peptide as represented by the Krokhin Hydrophobicity Index value [22] (using the online calculator at http://hs2.proteome.ca/SSRCalc/SSRCalcX.html). Relative accuracy of the hydrophobicity values was confirmed by experimentally determined retention times obtained from reversed phase HPLC separation of the positional isomers (Table 1). We observed a general trend in which nitration yield decreased upon increased hydrophobicity of the peptide isomer. The only outliers based on this trend are the peptides GKYLG and GLYKG where we posit that charge asymmetry surrounding the tyrosine could modulate nitration yield in this case. In other words, the additive effect of the positive charge of the N-terminal amino group and lysine residue of GKYLG could be a driving force for the increased nitration observed for this peptide compared to GLYKG in which the positive charge of lysine is possibly negated by the C-terminal carboxyl group. In the case of GLYEG and GEYLG, there was a significant difference in nitration yield (3.9 fold increase in GLYEG) between the two isomers. This result could be explained by the higher hydrophobic index value in addition to the decreased charge asymmetry for GEYLG. It is difficult to determine from this limited set of peptides if negative charge is truly an inhibitory factor of nitration; however, based on the data obtained for all of the pentapeptides (Fig. S4), there is a general trend that suggests nitration yield decreases when net charge of the peptide (at the reaction pH of 7.4) is negative.

In addition to overall charge and hydrophobicity surrounding tyrosine, side chain flexibility could enhance the ability of certain amino acids to interact with other proximal residues more readily and mitigate the effect of the side chain influence on nitration efficiency at a nearby tyrosine residue. Moreover, adjacent side chain groups that exhibit a bulkier structure could also prevent peroxynitrite-mediated nitration of tyrosine through steric hindrance. Other factors that could influence nitration yield are pH as well as modulation of pK_a values of proximal ionizable functional groups based on local microenvironment. Specifically, peroxynitrite stability is pH-dependent where decreased availability would occur upon decrease in local pH given its acid lability [1,10]. Based on the results from our study, local microenvironment that could significantly decrease the pK_a values of Lys, Arg or His functional groups or increase the pK_a value of the His functional group at physiological pH may have a negative or positive effect, respectively, on nitration yield at a nearby tyrosine residue.

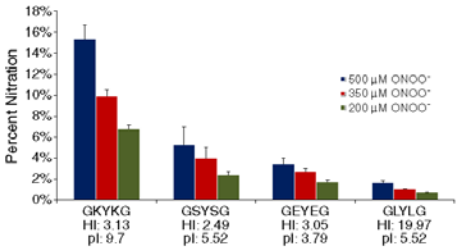

Fig. 4 – Hydrophobicity and net charge influences on nitration efficiencies of representative pentapeptides. Percent nitration for pentapeptides (500 μM) is shown for three peroxynitrite concentrations reacted for 1 h. Hydrophobicity indices were calculated using the online calculator available at http://hs2.proteome.ca/SSRCalc/SSRCalcX.html. Error bars represent standard deviation for 5 replicate reactions (2 injections each).

It is important to note that tyrosine nitration yield can be misrepresented by MS analyses if the ionization/detection efficiencies of the precursor ions vary between the unmodified and nitrated cognate peptide and if the change in ionization/detection efficiency between the unmodified and nitrated peptide is significantly different based on surrounding amino acid sequence. We have found for the AQUA-grade BSA peptide and nitropeptides, that the nitrated peptide shows a lower AUC value than the unmodified cognate peptide when loaded on column at the same amount (where [AUC nitrated peptide] / [AUC unmodified peptide] = 0.59 ± 0.07). Therefore, nitration yields may actually be higher if this ratio value is considered as a general ionization/detection efficiency correction factor. Our study assumes that ionization/detection efficiencies for the nitropeptide would be altered but this factor would remain relatively constant across all sixteen pentapeptides. AQUA-grade synthetic peptides representing modified and unmodified forms with all relevant permutations would need to be synthesized and characterized by LC-MRM in order for variances to be accurately normalized. It is also possible that nitration selectivity may change based on the molar ratio of peptide target to peroxynitrite; however, based on the ratio range that was used in this study, nitration response was generally linear with respect to peroxynitrite concentration as shown in Fig. 5 for the selected pentapeptides GKYKG and GEYLG.

Time course peroxynitrite reactions with GKYKG (highest nitration susceptibility) and GEYLG (lowest nitration susceptibility) showed statistically significant increases in nitration of GKYKG ($p<0.01$) after one hour as compared to one minute as shown in Fig. 6. This result was unexpected considering peroxynitrite's half-life of <1 s at physiological pH [1,7]. Nitration to GEYLG was unaltered after 1 min as expected. The results from the time course analysis suggest that positive charge surrounding tyrosine may increase nitration yield through electrostatic attraction of peroxynitrite and perhaps enhanced stabilization of the $^{\bullet}NO_2$ radical or other intermediates along the reaction coordinate of peroxynitrite-mediated 3NT formation [23]. The lower tyrosine nitration yield observed for GEYLG is contrary to postulated consensus motifs that suggest nitration is induced where acidic and/or hydrophobic residues are adjacent to tyrosine [14,15]; however, these reports are based on nitration that occurs at the protein level which would not exclusively take into consideration local primary structure.

3.5. *Implications in prediction/validation and biological consequences of PTN*

Based on the results from this study, we conclude that proximal positive charge and polarity could increase tyrosine nitration yield while hydrophobicity is an inhibitory factor. In order to facilitate prediction and/or validation of PTN, it is obvious that higher-order structural effects need to be considered. The nitration map of BSA generated in this study (Fig. 1)

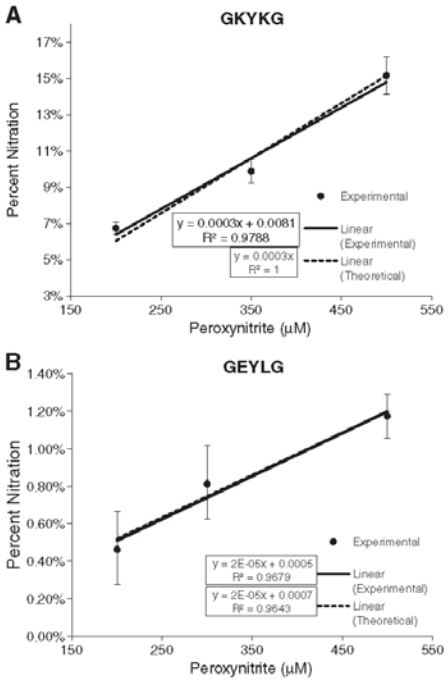

Fig. 5 – Peroxynitrite concentration response curves for GKYKG and GEYLG. A linear response with respect to peroxynitrite concentration was observed for the pentapeptides representing the highest and lowest percent nitration when reacted for 1 hr at 25 °C. Theoretical values were calculated using 500 μM values ($ONOO^-$) for each as a reference point. Error bars represent standard deviation for 5 replicates (2 injections each). This result was a general observation for most pentapeptides, suggesting minimal selectivity differences due to changes in molar ratio of peroxynitrite: pentapeptide.

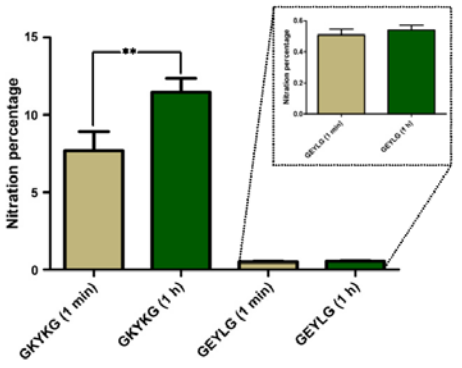

Fig. 6 – Time course response to $ONOO^-$. Pentapeptides representing the highest (A) and lowest (B) percent nitration under reaction conditions were employed. Theoretical values were calculated using 200 μM values for each as a reference point. Error bars represent the standard deviation for five reactions (2 injections each, ** $p < 0.01$).

resulted in two nitrotyrosine sites that are flanked by basic and/or polar residues while three are flanked by acidic residues. If it is assumed that BSA shares a similar three-dimensional structure with HSA and that the monomeric form was the predominant structure in the nitration reaction, then the high resolution pdb structures of HSA (available at www.pdb.org) can be used as models to extend our findings to the native BSA protein structure and how this structure would influence nitration susceptibility. In the initial peptide sequence (DAFLGSFLYEYSR) used as a model to pursue local primary structure effects, Tyr 357 is flanked by glutamate and serine residues. This region of the albumin structure is an α-helix until the helix is broken at Pro 362 at which point a loop structure is formed. His 361 is close in distance to Tyr 357 which can be expected given this histidine is n+4 residues away from the tyrosine in the α-helix. Interestingly, Tyr 364, another target of nitration determined experimentally, is part of the loop structure that occurs after the proline-induced break of the α-helix and is also close in distance to His 361. Another nitration target in BSA, Tyr 475, is adjacent to a hydrophobic (Leu) and acidic (Asp) residue. In this particular case, the adjacent aspartate would be involved in an interaction with an arginine residue closer to the N-terminus of the BSA protein (Lys in the HSA structure). Moreover, Arg 459 in BSA (Lys 460 in HSA) seems to be proximal to Tyr 475 allowing for a positively charged environment to potentially promote nitration at this tyrosine residue. These interactions are mapped for better visualization in Fig. S5.

In terms of validation or prediction of PTN in native protein structures based on the results of our study, solvent accessibility should be the obvious key factor to consider in relation to nitration susceptibility. Additionally, if a tyrosine residue is predicted to be in an α-helix, then nitration may occur more readily if the amino acid located n±4 residues from the tyrosine is basic or polar. In situations where the high-resolution structure of the protein is available, the hydrophobicity and charge distribution can be mapped based on a certain defined distance from solvent-accessible tyrosine residues and used as a predictive measure of nitration susceptibility. Although there are several other structural features that could influence nitration selectivity at the protein level, these guidelines provide some context for future work that would aim to assess the applicability of the results generated from this study on PTN selectivity at the native protein level in which proteins with known high-resolution structures are investigated.

The presence of a proximal basic residue as a structural feature that promotes tyrosine nitration is supported by data reported in a proteomics-based investigation of endogenously

nitrated proteins from mouse brain in which basic residues proximal to nitrotyrosine were found in a majority of the identified nitropeptides [24]. Those data as well as the data reported here suggest a potentially higher impact, in terms of competitive modification between nitration and phosphorylation, on tyrosine kinase signaling pathways in which the tyrosine phosphorylation consensus sequences contain basic residues. Also, it is tempting to speculate that nitrosative stress may have a lower impact on pathways regulated by tyrosine O-sulfation, a modification that is generally found on secreted and membrane-bound proteins, given that acidic residues adjacent to O-sulfotyrosine have been identified as a predictor of this particular tyrosine modification [25,26]. Although accurate predictions regarding the biological impact of PTN cannot be made from the limited peptide library analyzed, this study does mark the first attempt to address the role of primary structure on tyrosine nitration and provides additional framework for the development of nitration site prediction and validation tools for global-scale analysis of PTN.

4. Conclusions

Peroxynitrite-mediated tyrosine nitration yield is influenced by the amino acid residues proximal to the tyrosine residue that is nitrated. Results from model peptide reactions with peroxynitrite performed in this study indicate a statistically significant increase in nitration yield when tyrosine is flanked by basic residues. Tyrosine nitration yield was also greater when an uncharged polar residue was adjacent, while the presence of a hydrophobic residue hindered nitration susceptibility. The role of negative charge and electric dipole effect on nitration yield remain unclear and require further investigation. Additionally, the molar ratio of nitration target/peroxynitrite did not significantly affect nitration selectivity—at least in the ratio range used in this study. Future work will aim to analyze a more comprehensive peptide library that would include extended linear peptide sequences to determine the effect of changing amino acid side chain structure farther away from the tyrosine nitration target as well as mapping peroxynitrite-mediated nitration sites of proteins with known three-dimensional structures under native conditions to determine if findings from this study are applicable in this regard. Additionally, computational modeling is expected to augment experimental data in an effort to improve mechanistic understanding of tyrosine nitration and to enhance current prediction and validation protocols for PTN characterization.

Supplementary materials related to this article can be found online at doi:10.1016/j.jprot.2011.11.025.

Acknowledgements

We thank the Florida Center of Excellence for Drug Discovery and Innovation (USF-CDDI) Proteomics Core Facility for use of the TSQ Quantum Ultra and LTQ Orbitrap XL. We also thank Dr. Mohanraja Kumar, USF Dept of Chemistry, for peptide synthesis and Dr. Tsutomu Arakawa, Alliance Protein Laboratories, Thousand Oaks, CA, for CD analysis.

REFERENCES

[1] Abello N, Kerstjens HAM, Postma DS, Bischoff R. Protein tyrosine nitration: Selectivity, physicochemical and biological consequences, denitration, and proteomics methods for the identification of tyrosine-nitrated proteins. J Proteome Res 2009;8:3222–38.
[2] Batthyany C, Souza JM, Duran R, Cassina A, Cervenansky C, Radi R. Time course and site(s) of cytochrome c tyrosine nitration by peroxynitrite. Biochemistry 2005;44:8038–46.
[3] Ischiropoulos H. Biological selectivity and functional aspects of protein tyrosine nitration. Biochem Biophys Res Commun 2003;305:776–83.
[4] Ischiropoulos H. Biological tyrosine nitration: A pathophysiological function of nitric oxide and reactive oxygen species. Arch Biochem Biophys 1998;356:1–11.
[5] Souza JM, Peluffo G, Radi R. Protein tyrosine nitration–functional alteration or just a biomarker? Free Radic Biol Med 2008;45:357–66.
[6] Halliwell B, Zhao K, Whiteman M. Nitric oxide and peroxynitrite. The ugly, the uglier and the not so good: a personal view of recent controversies. Free Radic Res 1999;31:651–69.
[7] Beckman JS, Koppenol WH. Nitric oxide, superoxide, and peroxynitrite: the good, the bad, and ugly. Am J Physiol 1996;271:C1424–37.
[8] Ischiropoulos H, Beckman JS. Oxidative stress and nitration in neurodegeneration: cause, effect, or association? J Clin Invest 2003;111:163–9.
[9] Sokolovsky M, Riordan JF, Vallee BL. Conversion of 3-nitrotyrosine to 3-aminotyrosine in peptides and proteins. Biochem Biophys Res Commun 1967;27:20–5.
[10] Goldstein S, Merenyi G. The chemistry of peroxynitrite: implications for biological activity. Methods Enzymol 2008;436:49–61.
[11] Beckman JS. Oxidative damage and tyrosine nitration from peroxynitrite. Chem Res Toxicol 1996;9:836–44.
[12] Elfering SL, Haynes VL, Traaseth NJ, Ettl A, Giulivi C. Aspects, mechanism, and biological relevance of mitochondrial protein nitration sustained by mitochondrial nitric oxide synthase. Am J Physiol Heart Circ Physiol 2004;286:H22–9.
[13] Stevens SM, Prokai-Tatrai K, Prokai L. Factors that contribute to the misidentification of tyrosine nitration by shotgun proteomics. Mol Cell Proteomics 2008;7:2442–51.
[14] Jiao K, Mandapati S, Skipper PL, Tannenbaum SR, Wishnok JS. Site-selective nitration of tyrosine in human serum albumin by peroxynitrite. Anal Biochem 2001;293:43–52.
[15] Souza J. JM, Daikhin E, Yudkoff M, Raman CS, Ischiropoulos H. Factors determining the selectivity of protein tyrosine nitration. Arch Biochem Biophys 1999;371:169–78.
[16] Keller A, Nesvizhskii AI, Kolker E, Aebersold R. Empirical statistical model to estimate the accuracy of peptide identifications made by MS/MS and database search. Anal Chem 2002;74:5383–92.
[17] Nesvizhskii AI, Keller A, Kolker E, Aebersold R. A statistical model for identifying proteins by tandem mass spectrometry. Anal Chem 2003;75:4646–58.
[18] Holiday ER. Spectrophotometry of proteins: Absorption spectra of tyrosine, tryptophan and their mixtures. II. estimation of tyrosine and tryptophan in proteins. Biochem J 1936;10:1795–800.
[19] Beausoleil SA, Villen J, Gerber SA, Rush J, Gygi SP. A probability-based approach for high-throughput protein phosphorylation analysis and site localization. Nat Biotechnol 2006;24:1285–92.
[20] Ghesquière B, Colaert N, Helsens K, Dejager L, Vanhaute C, Verleysen K, et al. In Vitro and in Vivo Protein-bound Tyrosine Nitration Characterized by Diagonal Chromatography. Mol Cell Proteomics 2009;8:2642–52.

Appendix A continued

[21] Prokai-Tatrai K, Guo J, Prokai L. Selective chemoprecipitation and subsequent release of tagged species for the analysis of nitropeptides by liquid chromatography-tandem mass spectrometry. Mol Cell Proteomics 2011;10.
[22] Krokhin OV, Craig R, Spicer V, Ens W, Standing KG, Beavis RC, et al. An improved model for prediction of retention times of tryptic peptides in ion pair reversed-phase HPLC. Mol Cell Proteomics 2004;3:908–19.
[23] Gunaydin H, Houk KN. Mechanisms of Peroxynitrite-Mediated Nitration of Tyrosine. Chem Res Toxicol 2009;22:894–8.
[24] Sacksteder CA, Qian W, Knyushko TV, Wang H, Chin MH, Lacan G, et al. Endogenously nitrated proteins in mouse brain: links to neurodegenerative disease. Biochemistry 2006;45:8009–22.
[25] Monigatti F, Gasteiger E, Bairoch A, Jung E. The sulfinator: Predicting tyrosine sulfation sites in protein sequences. Bioinformatics 2002;18:769–70.
[26] Rosenquist GL, Nicholas HB. Analysis of sequence requirements for protein tyrosine sulfation. Protein Sci 1993;2:215–22.

Appendix B: Journal of Proteomics #749 Supplemental Figures

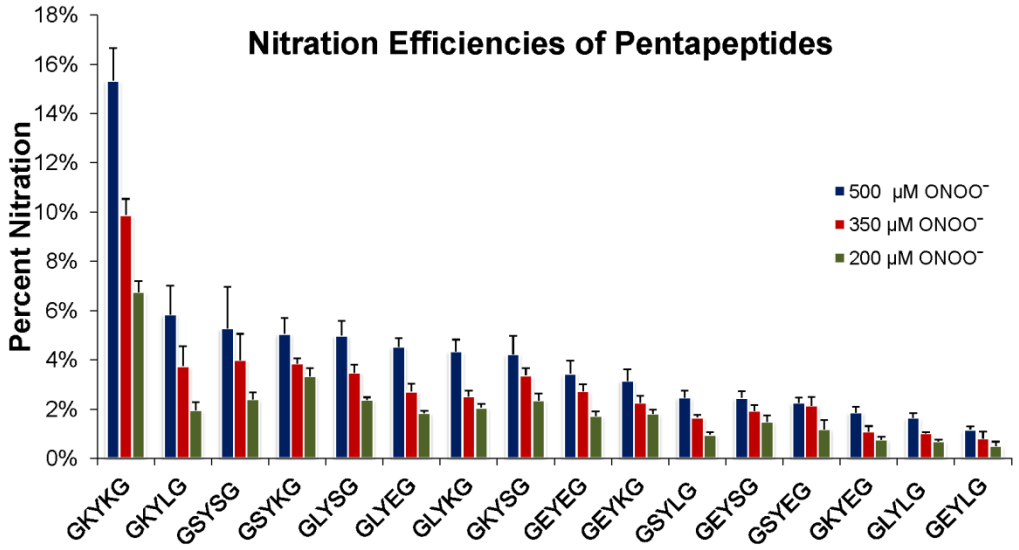

Fig. S1

Appendix B continued

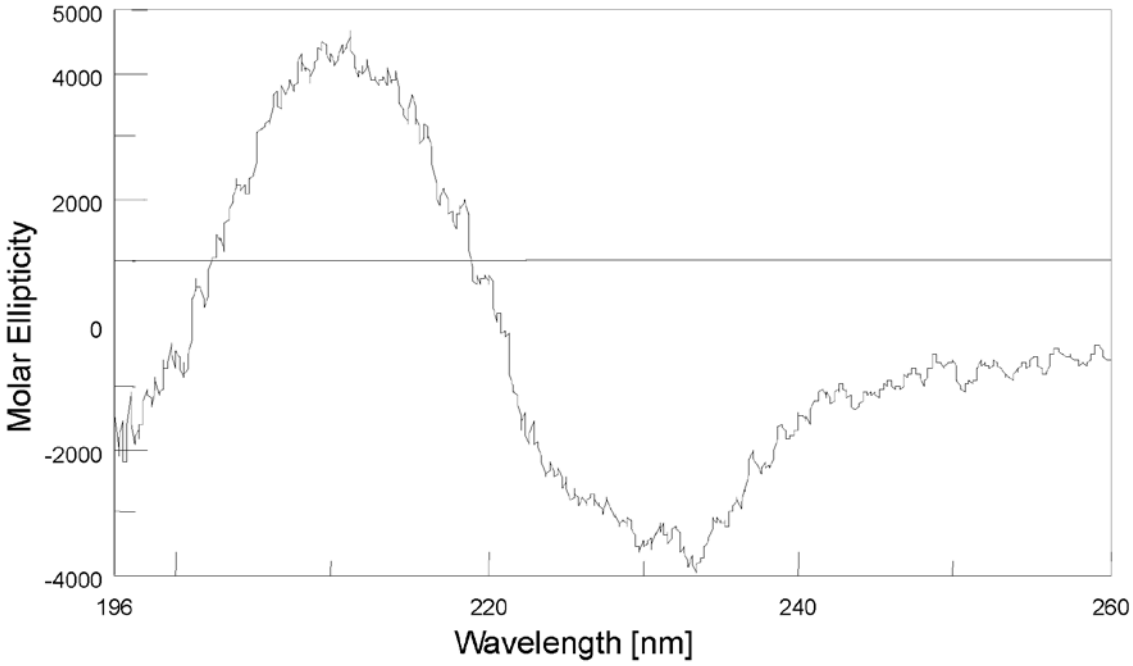

Fig. S2

Appendix B continued

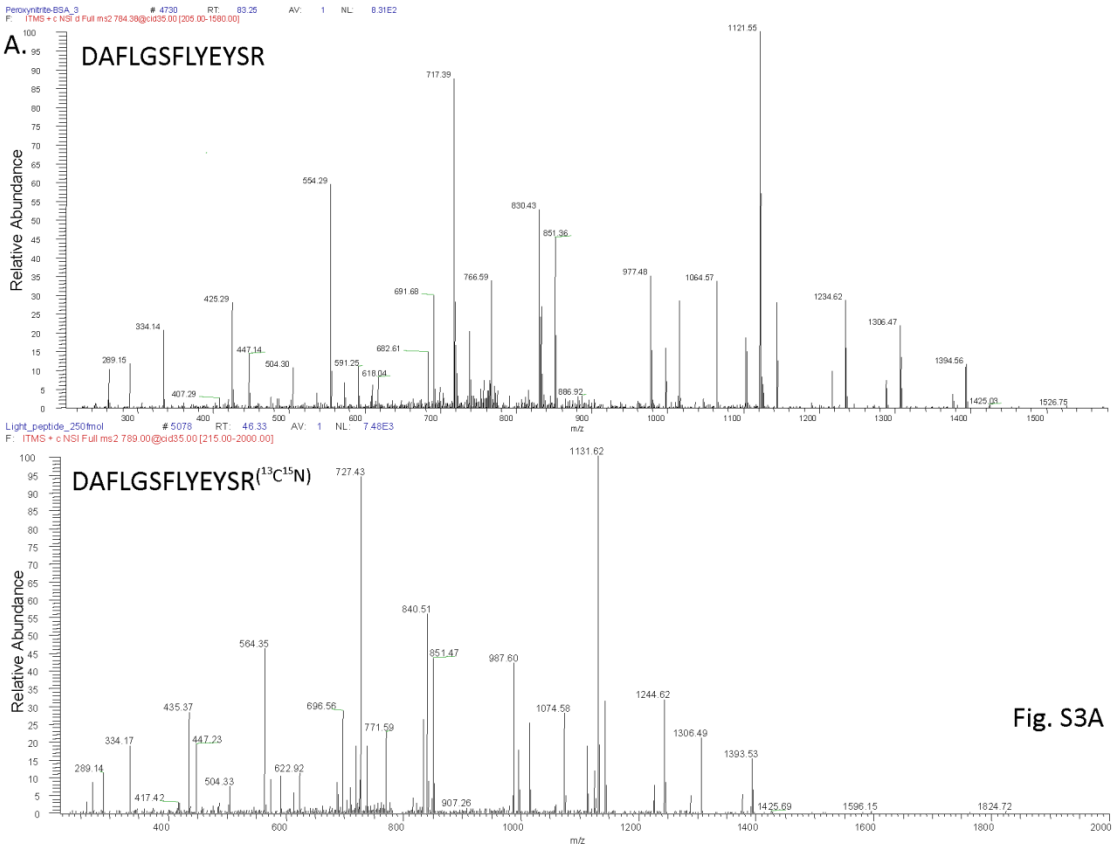

Fig. S3A

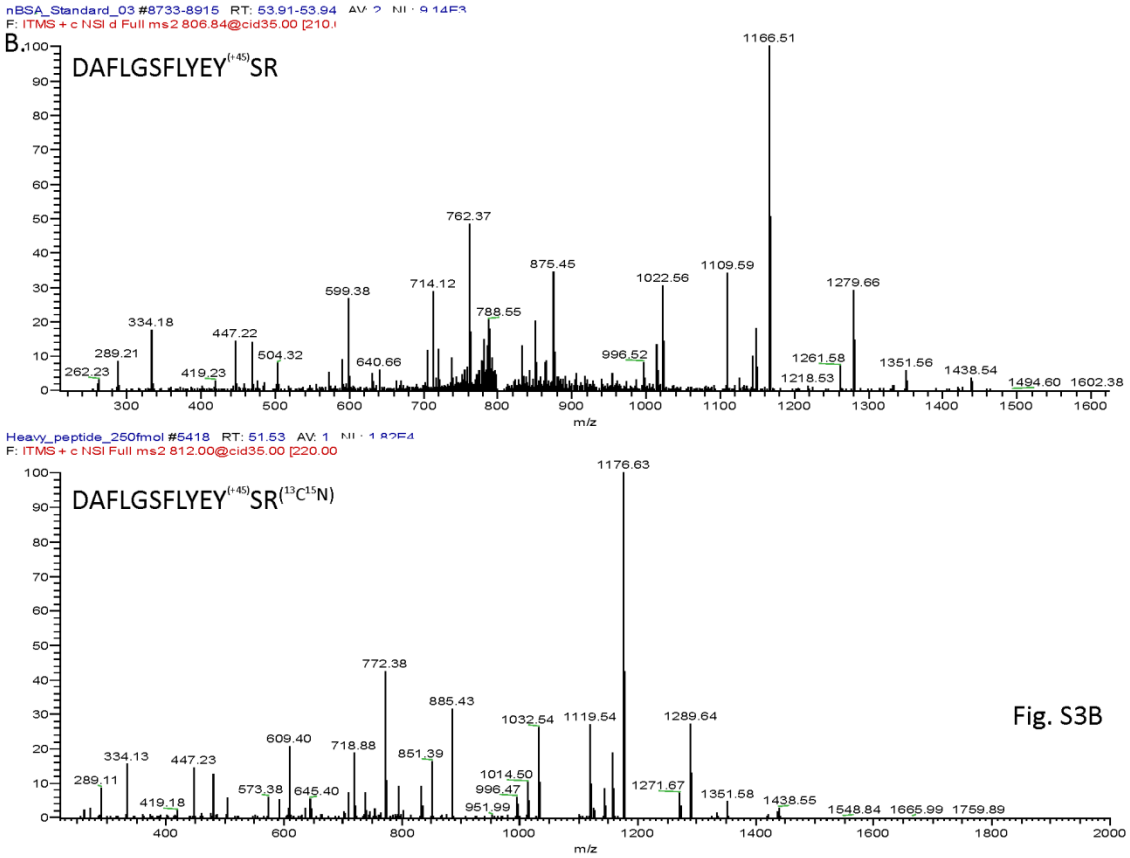
nBSA_Standard_03 #8733-8915 RT: 53.91-53.94
F: ITMS + c NSI d Full ms2 806.84@cid35.00
B.
DAFLGSFLYEY(+45)SR
1166.51
762.37
875.45
1109.59
714.12
1022.56
599.38
1279.66
788.55
334.18
447.22
289.21
504.32
640.66
996.52
1261.58
262.23
419.23
1218.53
1351.56
1438.54
1494.60
1602.38
m/z
Heavy_peptide_250fmol #5418 RT: 51.53
F: ITMS + c NSI Full ms2 812.00@cid35.00
DAFLGSFLYEY(+45)SR(13C15N)
1176.63
772.38
885.43
1032.54
1119.54
1289.64
609.40
718.88
851.39
334.13
447.23
1014.50
996.47
1271.67
289.11
573.38
645.40
951.99
1351.58
1438.55
419.18
1548.84
1665.99
1759.89
m/z

Fig. S3B

Appendix B continued

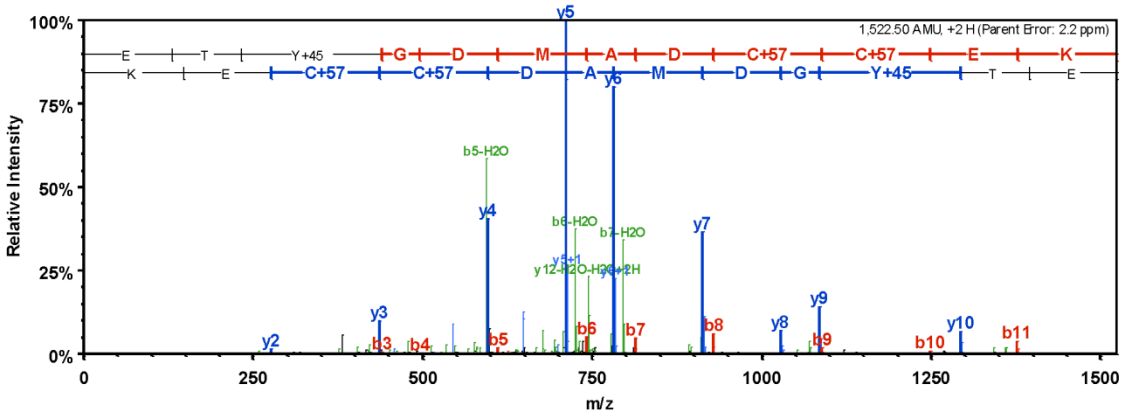

Fig. S4A

Appendix B continued

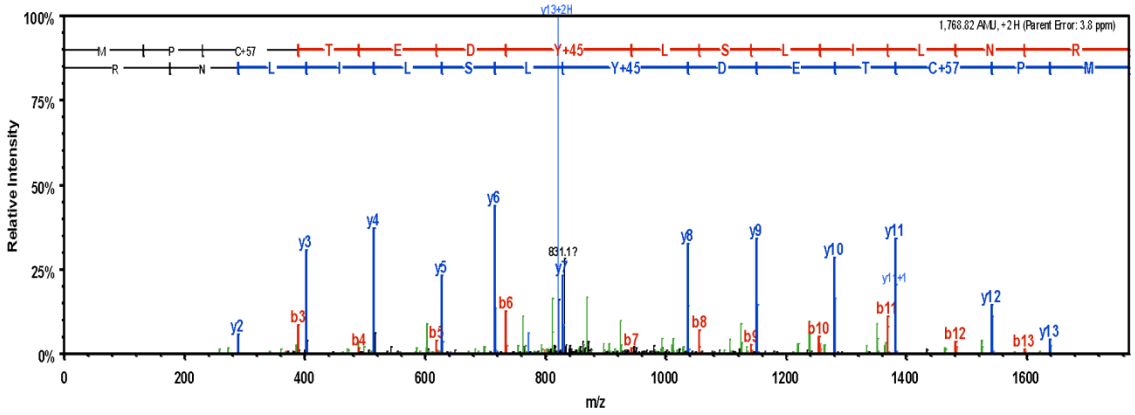

Fig. S4B

Appendix B continued

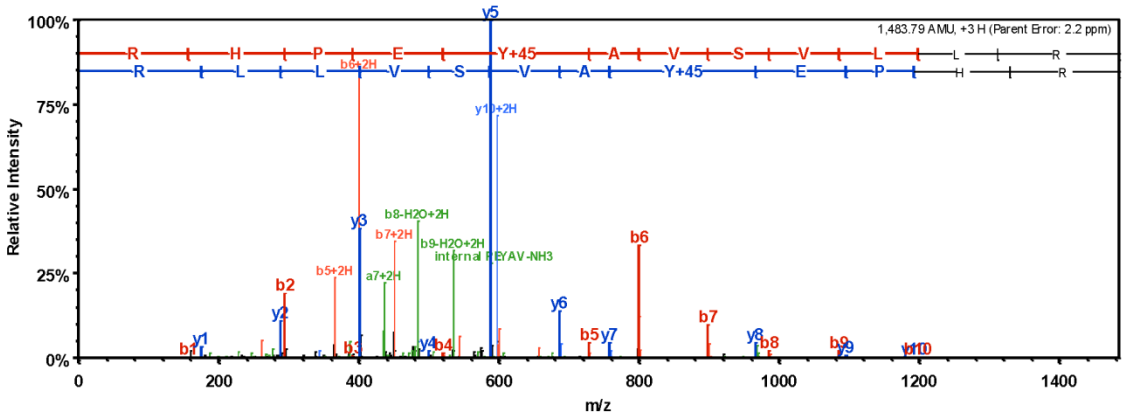

Fig. S4C

Appendix B continued

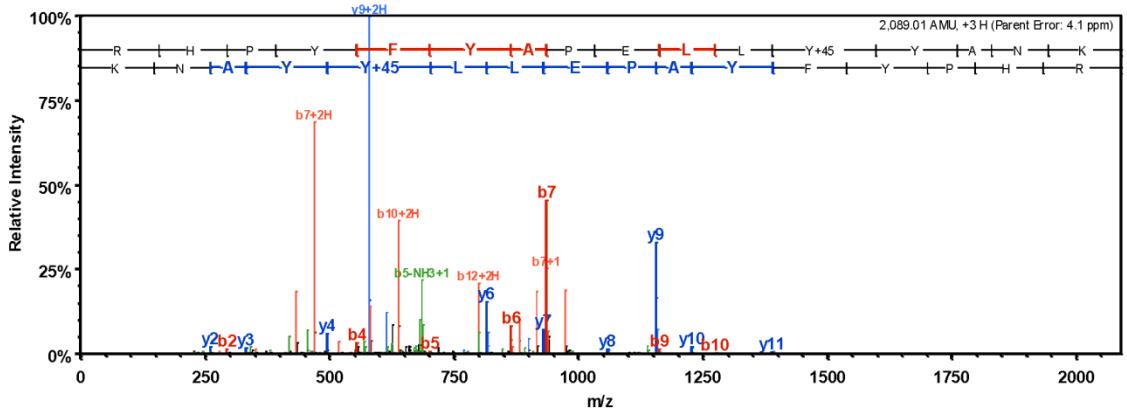

Fig. S4D

Appendix B continued

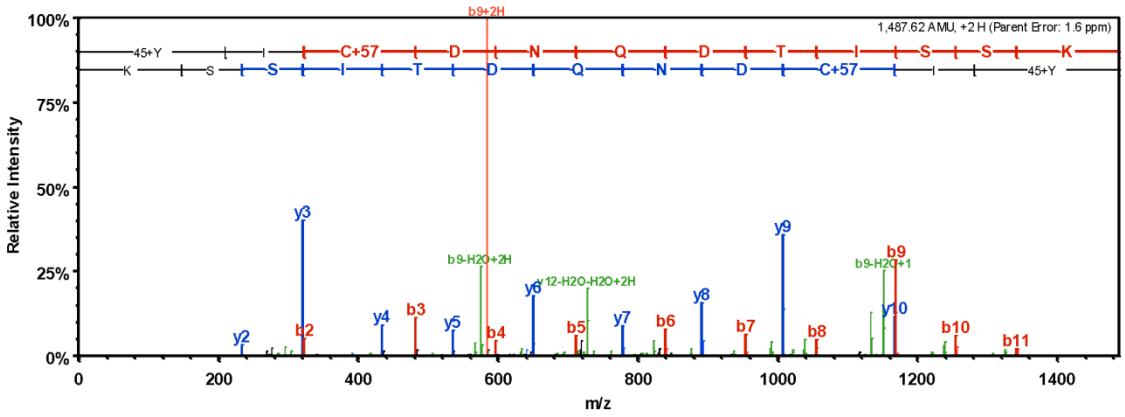

Fig. S4E

Appendix B continued

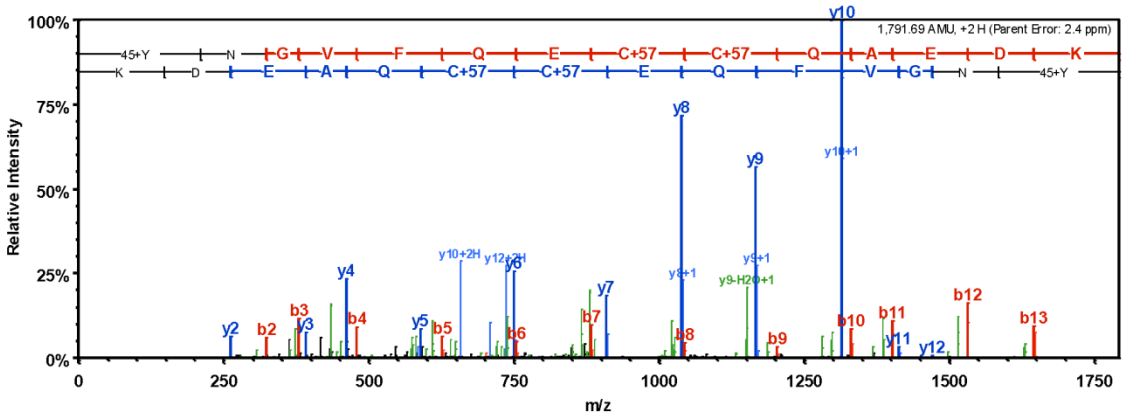

Fig. S4F

Appendix C: Supplemental Figure Legends

Supplemental Figure 1. Nitration efficiencies of pentapeptides. Percent nitration for pentapeptides (500 μM) is shown for three peroxynitrite concentrations reacted for 1 h. A general trend was observed where nitration efficiency is influenced by both hydrophobicity and net peptide charge. Error bars represent standard deviation for 5 replicate reactions (2 injections each).

Supplemental Figure 2. Circular dichroism spectrum of 0.1 mg/mL synthetic DAFLGSFLYEYSR. This spectrum proved to be inconclusive with regard to the secondary structure of the peptide in the reaction buffer.

Supplemental Figure 3. Validation of spectra from nitrotyrosine BSA standard with synthetic AQUA™ peptides. AQUA™ peptides were analyzed via HPLC-MS/MS in LTQ Orbitrap XL to validate sequence and nitration site-specificity. A) Comparison of spectra from unmodified DAFLGSFLYEYSR (top) and AQUA peptide analogue (bottom). B) Comparison of DAFLGSFLYEY $^{[3\text{-nitro}]}$ SR (top) with AQUA peptide analogue (bottom).

Supplemental Figure 4. Alternate nitropeptides identified from peroxynitrite-treated BSA standard. These spectra (A-F) represent additional nitration sites identified from the Cayman nitrotyrosine BSA standard. These peptides meet all identification criteria outlined in 2.2 of the manuscript.

Appendix D: Table S1 Journal of Proteomics #749

Supplemental Table 1. MRM method parameters.

Analyte	Parent Ion m/z	Charge State	Transition 1	Transition 2	Transition 3	Spray Voltage (V)	Capillary Temperature (°C)	Sheath Gas (Arb)	Aux Gas (Arb)
L-tyrosine	182	1	91	123	136	4200	270	30	10
^{13}C L-tyrosine	191	1	98	130	144	4200	270	30	10
3-nitrotyrosine	227	1	117	181		4200	270	30	10
DAFLGSFLYEYSR	785	2	554	717	1121	4200	270	30	10
DAFLGSFLYEY*SR	807	2	599	762	1166	4200	270	30	10
DAFLGSFLY*EYSR	807	2	599	762	1188	4200	270	30	10
GEY[Nitro]KG	599	1	204	412	542	4200	270	30	10
GKY[Nitro]EG	599	1	205	413	542	4200	270	30	10
GKY[Nitro]KG	598	1	204	412	541	4200	270	30	10
GKY[Nitro]LG	583	1	189	397	526	4200	270	30	10
GKY[Nitro]SG	557	1	163	371	500	4200	270	30	10
GLY[Nitro]KG	583	1	204	412	526	4200	270	30	10
GSY[Nitro]KG	557	1	204	412	500	4200	270	30	10
GSYSG	236	2	163			4200	270	30	10
GSYSG	236	2	326			4200	270	30	10
GSYSG	236	2	413			4200	270	30	10
GSYSG	470	1	163			4200	270	30	10
GSYSG	470	1	326			4200	270	30	10
GSYSG	470	1	413			4200	270	30	10
GSY[Nitration]SG	258	2	163			4200	270	30	10
GSY[Nitration]SG	258	2	371			4200	270	30	10
GSY[Nitration]SG	258	2	458			4200	270	30	10
GSY[Nitration]SG	515	1	163			4200	270	30	10
GSY[Nitration]SG	515	1	371			4200	270	30	10
GSY[Nitration]SG	515	1	458			4200	270	30	10
GSYLG	249	2	189			4200	270	30	10
GSYLG	249	2	352			4200	270	30	10
GSYLG	249	2	439			4200	270	30	10
GSYLG	496	1	189			4200	270	30	10
GSYLG	496	1	352			4200	270	30	10

Appendix D continued

GSY[Nitration]LG	271	2	189			4200	270	30	10
GSY[Nitration]LG	271	2	397			4200	270	30	10
GSY[Nitration]LG	271	2	484			4200	270	30	10
GSY[Nitration]LG	541	1	189			4200	270	30	10
GSY[Nitration]LG	541	1	397			4200	270	30	10
GSY[Nitration]LG	541	1	484			4200	270	30	10
GSYEG	257	2	205			4200	270	30	10
GSYEG	257	2	368			4200	270	30	10
GSYEG	257	2	455			4200	270	30	10
GSYEG	512	1	205			4200	270	30	10
GSYEG	512	1	368			4200	270	30	10
GSYEG	512	1	455			4200	270	30	10
GSY[Nitration]EG	279	2	205			4200	270	30	10
GSY[Nitration]EG	279	2	413			4200	270	30	10
GSY[Nitration]EG	279	2	500			4200	270	30	10
GSY[Nitration]EG	557	1	205			4200	270	30	10
GSY[Nitration]EG	557	1	413			4200	270	30	10
GSY[Nitration]EG	557	1	500			4200	270	30	10
GLYLG	262	2	189			4200	270	30	10
GLYLG	262	2	352			4200	270	30	10
GLYLG	262	2	465			4200	270	30	10
GLYLG	522	1	189			4200	270	30	10
GLYLG	522	1	352			4200	270	30	10
GLYLG	522	1	465			4200	270	30	10
GLY[Nitration]LG	284	2	189			4200	270	30	10
GLY[Nitration]LG	284	2	397			4200	270	30	10
GLY[Nitration]LG	284	2	510			4200	270	30	10
GLY[Nitration]LG	567	1	189			4200	270	30	10
GLY[Nitration]LG	567	1	397			4200	270	30	10
GLY[Nitration]LG	567	1	510			4200	270	30	10
GLYSG	249	2	163			4200	270	30	10
GLYSG	249	2	326			4200	270	30	10
GLYSG	249	2	439			4200	270	30	10
GLYSG	496	1	163			4200	270	30	10
GLYSG	496	1	326			4200	270	30	10
GLYSG	496	1	439			4200	270	30	10

Appendix D continued

GLY[Nitration]SG	271	2	163			4200	270	30	10
GLY[Nitration]SG	271	2	371			4200	270	30	10
GLY[Nitration]SG	271	2	484			4200	270	30	10
GLY[Nitration]SG	541	1	163			4200	270	30	10
GLY[Nitration]SG	541	1	371			4200	270	30	10
GLY[Nitration]SG	541	1	484			4200	270	30	10
GLYEG	270	2	205			4200	270	30	10
GLYEG	270	2	368			4200	270	30	10
GLYEG	270	2	481			4200	270	30	10
GLYEG	538	1	205			4200	270	30	10
GLYEG	538	1	368			4200	270	30	10
GLYEG	538	1	481			4200	270	30	10
GLY[Nitration]EG	292	2	205			4200	270	30	10
GLY[Nitration]EG	292	2	413			4200	270	30	10
GLY[Nitration]EG	292	2	526			4200	270	30	10
GLY[Nitration]EG	583	1	205			4200	270	30	10
GLY[Nitration]EG	583	1	413			4200	270	30	10
GLY[Nitration]EG	583	1	526			4200	270	30	10
GEYEG	278	2	205			4200	270	30	10
GEYEG	278	2	368			4200	270	30	10
GEYEG	278	2	497			4200	270	30	10
GEYEG	554	1	205			4200	270	30	10
GEYEG	554	1	368			4200	270	30	10
GEYEG	554	1	497			4200	270	30	10
GEY[Nitration]EG	300	2	205			4200	270	30	10
GEY[Nitration]EG	300	2	413			4200	270	30	10
GEY[Nitration]EG	300	2	542			4200	270	30	10
GEY[Nitration]EG	599	1	205			4200	270	30	10
GEY[Nitration]EG	599	1	413			4200	270	30	10
GEY[Nitration]EG	599	1	542			4200	270	30	10
GEYSG	257	2	163			4200	270	30	10
GEYSG	257	2	326			4200	270	30	10
GEYSG	257	2	455			4200	270	30	10
GEYSG	512	1	163			4200	270	30	10
GEYSG	512	1	326			4200	270	30	10
GEYSG	512	1	455			4200	270	30	10

Appendix D continued

GEY[Nitration]SG	279	2	163			4200	270	30	10
GEY[Nitration]SG	279	2	371			4200	270	30	10
GEY[Nitration]SG	279	2	500			4200	270	30	10
GEY[Nitration]SG	557	1	163			4200	270	30	10
GEY[Nitration]SG	557	1	371			4200	270	30	10
GEY[Nitration]SG	557	1	500			4200	270	30	10
GEYLG	270	2	189			4200	270	30	10
GEYLG	270	2	352			4200	270	30	10
GEYLG	270	2	481			4200	270	30	10
GEYLG	538	1	189			4200	270	30	10
GEYLG	538	1	352			4200	270	30	10
GEYLG	538	1	481			4200	270	30	10
GEY[Nitration]LG	292	2	189			4200	270	30	10
GEY[Nitration]LG	292	2	397			4200	270	30	10
GEY[Nitration]LG	292	2	526			4200	270	30	10
GEY[Nitration]LG	583	1	189			4200	270	30	10
GEY[Nitration]LG	583	1	397			4200	270	30	10
GEY[Nitration]LG	583	1	526			4200	270	30	10

Isobaric precursor masses were differentiated by 0.002 Da (not shown in table).

Appendix E: Permissions

Appendix E continued

ELSEVIER LICENSE
TERMS AND CONDITIONS

Jun 03, 2013

This is a License Agreement between Kent W Seeley ("You") and Elsevier ("Elsevier") provided by Copyright Clearance Center ("CCC"). The license consists of your order details, the terms and conditions provided by Elsevier, and the payment terms and conditions.

All payments must be made in full to CCC. For payment instructions, please see information listed at the bottom of this form.

Supplier	Elsevier Limited The Boulevard,Langford Lane Kidlington,Oxford,OX5 1GB,UK
Registered Company Number	1982084
Customer name	Kent W Seeley
Customer address	6450 4th Palm Point SAINT PETERSBURG, FL 33706
License number	3161660543052
License date	Jun 03, 2013
Licensed content publisher	Elsevier
Licensed content publication	Journal of Proteomics
Licensed content title	Investigation of local primary structure effects on peroxynitrite-mediated tyrosine nitration using targeted mass spectrometry
Licensed content author	Kent W. Seeley,Stanley M. Stevens
Licensed content date	16 March 2012
Licensed content volume number	75
Licensed content issue number	6
Number of pages	10
Start Page	1691
End Page	1700
Type of Use	reuse in a thesis/dissertation
Portion	full article
Format	electronic
Are you the author of this Elsevier article?	Yes
Will you be translating?	No
Order reference number	

Appendix E continued

Title of your thesis/dissertation	Improved Methods for the Detection and Characterization of Protein-Tyrosine Nitration
Expected completion date	Jun 2013
Estimated size (number of pages)	214
Elsevier VAT number	GB 494 6272 12
Permissions price	0.00 USD
VAT/Local Sales Tax	0.0 USD / 0.0 GBP
Total	0.00 USD
Terms and Conditions	

INTRODUCTION

1. The publisher for this copyrighted material is Elsevier. By clicking "accept" in connection with completing this licensing transaction, you agree that the following terms and conditions apply to this transaction (along with the Billing and Payment terms and conditions established by Copyright Clearance Center, Inc. ("CCC"), at the time that you opened your Rightslink account and that are available at any time at http://myaccount.copyright.com).

GENERAL TERMS

2. Elsevier hereby grants you permission to reproduce the aforementioned material subject to the terms and conditions indicated.

3. Acknowledgement: If any part of the material to be used (for example, figures) has appeared in our publication with credit or acknowledgement to another source, permission must also be sought from that source. If such permission is not obtained then that material may not be included in your publication/copies. Suitable acknowledgement to the source must be made, either as a footnote or in a reference list at the end of your publication, as follows:

"Reprinted from Publication title, Vol /edition number, Author(s), Title of article / title of chapter, Pages No., Copyright (Year), with permission from Elsevier [OR APPLICABLE SOCIETY COPYRIGHT OWNER]." Also Lancet special credit - "Reprinted from The Lancet, Vol. number, Author(s), Title of article, Pages No., Copyright (Year), with permission from Elsevier."

4. Reproduction of this material is confined to the purpose and/or media for which permission is hereby given.

5. Altering/Modifying Material: Not Permitted. However figures and illustrations may be altered/adapted minimally to serve your work. Any other abbreviations, additions, deletions and/or any other alterations shall be made only with prior written authorization of Elsevier Ltd. (Please contact Elsevier at permissions@elsevier.com)

6. If the permission fee for the requested use of our material is waived in this instance, please be advised that your future requests for Elsevier materials may attract a fee.

7. Reservation of Rights: Publisher reserves all rights not specifically granted in the combination of (i) the license details provided by you and accepted in the course of this licensing transaction, (ii) these terms and conditions and (iii) CCC's Billing and Payment terms and conditions.

8. License Contingent Upon Payment: While you may exercise the rights licensed immediately upon issuance of the license at the end of the licensing process for the transaction, provided that you have disclosed complete and accurate details of your proposed use, no license is finally effective unless and until full payment is received from you (either by publisher or by CCC) as provided in CCC's Billing and Payment terms and conditions. If full payment is not received on a timely basis, then any license preliminarily granted shall be deemed automatically revoked and shall be void as if never granted. Further, in the event that you breach any of these terms and conditions or any of CCC's Billing and Payment terms and conditions, the license is automatically revoked and shall be void as if never granted. Use of materials as described in a revoked license, as well as any use of the materials beyond the scope of an unrevoked license, may constitute copyright infringement and publisher reserves the right to take any and all action to protect its copyright in the materials.

9. Warranties: Publisher makes no representations or warranties with respect to the licensed material.

10. Indemnity: You hereby indemnify and agree to hold harmless publisher and CCC, and their respective officers, directors, employees and agents, from and against any and all claims arising out of your use of the licensed material other than as specifically authorized pursuant to this license.

11. No Transfer of License: This license is personal to you and may not be sublicensed, assigned, or transferred by you to any other person without publisher's written permission.

12. No Amendment Except in Writing: This license may not be amended except in a writing signed by both parties (or, in the case of publisher, by CCC on publisher's behalf).

13. Objection to Contrary Terms: Publisher hereby objects to any terms contained in any purchase order, acknowledgment, check endorsement or other writing prepared by you, which terms are inconsistent with these terms and conditions or CCC's Billing and Payment terms and conditions. These terms and conditions, together with CCC's Billing and Payment terms and conditions (which are incorporated herein), comprise the entire agreement between you and publisher (and CCC) concerning this licensing transaction. In the event of any conflict between your obligations established by these terms and conditions and those established by CCC's Billing and Payment terms and conditions, these terms and conditions shall control.

14. Revocation: Elsevier or Copyright Clearance Center may deny the permissions described in this License at their sole discretion, for any reason or no reason, with a full refund payable to you. Notice of such denial will be made using the contact information provided by you. Failure to receive such notice will not alter or invalidate the denial. In no event will Elsevier or Copyright Clearance Center be responsible or liable for any costs, expenses or damage incurred by you as a result of a denial of your permission request, other than a refund of the amount(s) paid by you to Elsevier and/or Copyright Clearance Center for denied permissions.

LIMITED LICENSE

Appendix E continued

The following terms and conditions apply only to specific license types:

15. **Translation**: This permission is granted for non-exclusive world **English** rights only unless your license was granted for translation rights. If you licensed translation rights you may only translate this content into the languages you requested. A professional translator must perform all translations and reproduce the content word for word preserving the integrity of the article. If this license is to re-use 1 or 2 figures then permission is granted for non-exclusive world rights in all languages.

16. **Website**: The following terms and conditions apply to electronic reserve and author websites:
Electronic reserve: If licensed material is to be posted to website, the web site is to be password-protected and made available only to bona fide students registered on a relevant course if:
This license was made in connection with a course,
This permission is granted for 1 year only. You may obtain a license for future website posting,
All content posted to the web site must maintain the copyright information line on the bottom of each image,
A hyper-text must be included to the Homepage of the journal from which you are licensing at http://www.sciencedirect.com/science/journal/xxxxx or the Elsevier homepage for books at http://www.elsevier.com , and
Central Storage: This license does not include permission for a scanned version of the material to be stored in a central repository such as that provided by Heron/XanEdu.

17. **Author website** for journals with the following additional clauses:

All content posted to the web site must maintain the copyright information line on the bottom of each image, and the permission granted is limited to the personal version of your paper. You are not allowed to download and post the published electronic version of your article (whether PDF or HTML, proof or final version), nor may you scan the printed edition to create an electronic version.
A hyper-text must be included to the Homepage of the journal from which you are licensing at http://www.sciencedirect.com/science/journal/xxxxx . As part of our normal production process, you will receive an e-mail notice when your article appears on Elsevier's online service ScienceDirect (www.sciencedirect.com). That e-mail will include the article's Digital Object Identifier (DOI). This number provides the electronic link to the published article and should be included in the posting of your personal version. We ask that you wait until you receive this e-mail and have the DOI to do any posting.

Central Storage: This license does not include permission for a scanned version of the material to be stored in a central repository such as that provided by Heron/XanEdu.

18. **Author website** for books with the following additional clauses:
Authors are permitted to place a brief summary of their work online only.
A hyper-text must be included to the Elsevier homepage at http://www.elsevier.com . All content posted to the web site must maintain the copyright information line on the bottom of each image.
You are not allowed to download and post the published electronic version of your chapter, nor may you scan the printed edition to create an electronic version.

Central Storage: This license does not include permission for a scanned version of the material to be stored in a central repository such as that provided by Heron/XanEdu.

19. **Website** (regular and for author): A hyper-text must be included to the Homepage of the journal from which you are licensing at http://www.sciencedirect.com/science/journal/xxxxx. or for books to the Elsevier homepage at http://www.elsevier.com

20. **Thesis/Dissertation**: If your license is for use in a thesis/dissertation your thesis may be submitted to your institution in either print or electronic form. Should your thesis be published commercially, please reapply for permission. These requirements include permission for the Library and Archives of Canada to supply single copies, on demand, of the complete thesis and include permission for UMI to supply single copies, on demand, of the complete thesis. Should your thesis be published commercially, please reapply for permission.

21. **Other Conditions**:

v1.6

If you would like to pay for this license now, please remit this license along with your payment made payable to "COPYRIGHT CLEARANCE CENTER" otherwise you will be invoiced within 48 hours of the license date. Payment should be in the form of a check or money order referencing your account number and this invoice number RLNK501035252. Once you receive your invoice for this order, you may pay your invoice by credit card. Please follow instructions provided at that time.

Make Payment To:
Copyright Clearance Center
Dept 001
P.O. Box 843006
Boston, MA 02284-3006

For suggestions or comments regarding this order, contact RightsLink Customer Support: customercare@copyright.com or +1-877-622-5543 (toll free in the US) or +1-978-646-2777.

Gratis licenses (referencing $0 in the Total field) are free. Please retain this printable license for your reference. No payment is required.

Appendix F: Table S2 Predicted MRM transitions for mouse and rat histone nitropeptides

Peptide Sequence	Modified Sequence	Precursor Charge	Precursor m/z	Product m/z	Product Charge	Fragment Ion
ALAAAGYDVEK	ALAAAGYDVEK	2	554.29	781.37	1	y7
ALAAAGYDVEK	ALAAAGYDVEK	2	554.29	710.34	1	y6
ALAAAGYDVEK	ALAAAGYDVEK	2	554.29	653.31	1	y5
ALAAAGYDVEK	ALAAAGYDVEK	2	554.29	618.32	1	b7
ALAAAGYDVEK	ALAAAGYDVEK	2	554.29	733.35	1	b8
ALAAAGYDVEK	ALAAAGYDVEK	2	554.29	832.42	1	b9
ALAAAGYDVEK	ALAAAGY[+45]DVEK	2	576.78	826.36	1	y7
ALAAAGYDVEK	ALAAAGY[+45]DVEK	2	576.78	755.32	1	y6
ALAAAGYDVEK	ALAAAGY[+45]DVEK	2	576.78	698.30	1	y5
ALAAAGYDVEK	ALAAAGY[+45]DVEK	2	576.78	663.31	1	b7
ALAAAGYDVEK	ALAAAGY[+45]DVEK	2	576.78	778.34	1	b8
ALAAAGYDVEK	ALAAAGY[+45]DVEK	2	576.78	877.41	1	b9
YSDMIVAAIQAEK	YSDMIVAAIQAEK	2	719.87	942.56	1	y9
YSDMIVAAIQAEK	YSDMIVAAIQAEK	2	719.87	829.48	1	y8
YSDMIVAAIQAEK	YSDMIVAAIQAEK	2	719.87	730.41	1	y7
YSDMIVAAIQAEK	YSDMIVAAIQAEK	2	719.87	780.36	1	b7
YSDMIVAAIQAEK	YSDMIVAAIQAEK	2	719.87	851.40	1	b8
YSDMIVAAIQAEK	YSDMIVAAIQAEK	2	719.87	964.48	1	b9
YSDMIVAAIQAEK	Y[+45]SDMIVAAIQAEK	2	742.36	1073.60	1	y10
YSDMIVAAIQAEK	Y[+45]SDMIVAAIQAEK	2	742.36	942.56	1	y9
YSDMIVAAIQAEK	Y[+45]SDMIVAAIQAEK	2	742.36	829.48	1	y8
YSDMIVAAIQAEK	Y[+45]SDMIVAAIQAEK	2	742.36	754.31	1	b6
YSDMIVAAIQAEK	Y[+45]SDMIVAAIQAEK	2	742.36	825.34	1	b7
YSDMIVAAIQAEK	Y[+45]SDMIVAAIQAEK	2	742.36	896.38	1	b8
GNYSER	GNYSER	2	363.16	668.30	1	y5
GNYSER	GNYSER	2	363.16	554.26	1	y4
GNYSER	GNYSER	2	363.16	391.19	1	y3
GNYSER	GNYSER	2	363.16	422.17	1	b4
GNYSER	GNYSER	2	363.16	551.21	1	b5
GNYSER	GNY[+45]SER	2	385.66	713.28	1	y5
GNYSER	GNY[+45]SER	2	385.66	599.24	1	y4
GNYSER	GNY[+45]SER	2	385.66	391.19	1	y3

Appendix F continued

GNYSER	GNY[+45]SER	2	385.66	467.15	1	b4
GNYSER	GNY[+45]SER	2	385.66	596.19	1	b5
GNYAER	GNYAER	2	355.17	652.30	1	y5
GNYAER	GNYAER	2	355.17	538.26	1	y4
GNYAER	GNYAER	2	355.17	375.20	1	y3
GNYAER	GNYAER	2	355.17	406.17	1	b4
GNYAER	GNYAER	2	355.17	535.21	1	b5
GNYAER	GNY[+45]AER	2	377.66	697.29	1	y5
GNYAER	GNY[+45]AER	2	377.66	583.25	1	y4
GNYAER	GNY[+45]AER	2	377.66	380.12	1	b3
GNYAER	GNY[+45]AER	2	377.66	451.16	1	b4
GNYAER	GNY[+45]AER	2	377.66	580.20	1	b5
EESYSIYIYK	EESYSIYIYK	2	647.81	949.50	1	y7
EESYSIYIYK	EESYSIYIYK	2	647.81	786.44	1	y6
EESYSIYIYK	EESYSIYIYK	2	647.81	699.41	1	y5
EESYSIYIYK	EESYSIYIYK	2	647.81	709.30	1	b6
EESYSIYIYK	EESYSIYIYK	2	647.81	872.37	1	b7
EESYSIYIYK	EESYSIYIYK	2	647.81	985.45	1	b8
EESYSIYIYK	EESY[+45]SIYIYK	2	670.31	994.49	1	y7
EESYSIYIYK	EESY[+45]SIYIYK	2	670.31	786.44	1	y6
EESYSIYIYK	EESY[+45]SIYIYK	2	670.31	699.41	1	y5
EESYSIYIYK	EESY[+45]SIYIYK	2	670.31	754.29	1	b6
EESYSIYIYK	EESY[+45]SIYIYK	2	670.31	917.35	1	b7
EESYSIYIYK	EESY[+45]SIYIYK	2	670.31	1030.44	1	b8
EESYSIYIYK	EESYSIY[+45]IYK	2	670.31	994.49	1	y7
EESYSIYIYK	EESYSIY[+45]IYK	2	670.31	831.42	1	y6
EESYSIYIYK	EESYSIY[+45]IYK	2	670.31	744.39	1	y5
EESYSIYIYK	EESYSIY[+45]IYK	2	670.31	709.30	1	b6
EESYSIYIYK	EESYSIY[+45]IYK	2	670.31	917.35	1	b7
EESYSIYIYK	EESYSIY[+45]IYK	2	670.31	1030.44	1	b8
EESYSIYIYK	EESYSIYIY[+45]K	2	670.31	994.49	1	y7
EESYSIYIYK	EESYSIYIY[+45]K	2	670.31	831.42	1	y6
EESYSIYIYK	EESYSIYIY[+45]K	2	670.31	744.39	1	y5
EESYSIYIYK	EESYSIYIY[+45]K	2	670.31	709.30	1	b6
EESYSIYIYK	EESYSIYIY[+45]K	2	670.31	872.37	1	b7
EESYSIYIYK	EESYSIYIY[+45]K	2	670.31	985.45	1	b8
EESYSIYIYK	EESY[+45]SIY[+45]IYK	2	692.80	1039.47	1	y7
EESYSIYIYK	EESY[+45]SIY[+45]IYK	2	692.80	831.42	1	y6
EESYSIYIYK	EESY[+45]SIY[+45]IYK	2	692.80	744.39	1	y5
EESYSIYIYK	EESY[+45]SIY[+45]IYK	2	692.80	754.29	1	b6

Appendix F continued

EESYSIYIYK	EESY[+45]SIY[+45]IYK	2	692.80	962.34	1	b7
EESYSIYIYK	EESY[+45]SIY[+45]IYK	2	692.80	1075.42	1	b8
EESYSIYIYK	EESY[+45]SIYIY[+45]K	2	692.80	1039.47	1	y7
EESYSIYIYK	EESY[+45]SIYIY[+45]K	2	692.80	831.42	1	y6
EESYSIYIYK	EESY[+45]SIYIY[+45]K	2	692.80	744.39	1	y5
EESYSIYIYK	EESY[+45]SIYIY[+45]K	2	692.80	754.29	1	b6
EESYSIYIYK	EESY[+45]SIYIY[+45]K	2	692.80	917.35	1	b7
EESYSIYIYK	EESY[+45]SIYIY[+45]K	2	692.80	1030.44	1	b8
EESYSIYIYK	EESYSIY[+45]IY[+45]K	2	692.80	1039.47	1	y7
EESYSIYIYK	EESYSIY[+45]IY[+45]K	2	692.80	876.41	1	y6
EESYSIYIYK	EESYSIY[+45]IY[+45]K	2	692.80	789.38	1	y5
EESYSIYIYK	EESYSIY[+45]IY[+45]K	2	692.80	709.30	1	b6
EESYSIYIYK	EESYSIY[+45]IY[+45]K	2	692.80	917.35	1	b7
EESYSIYIYK	EESYSIY[+45]IY[+45]K	2	692.80	1030.44	1	b8
EESYSIYIYK	EESY[+45]SIY[+45]IY[+45]K	2	715.29	1084.46	1	y7
EESYSIYIYK	EESY[+45]SIY[+45]IY[+45]K	2	715.29	876.41	1	y6
EESYSIYIYK	EESY[+45]SIY[+45]IY[+45]K	2	715.29	789.38	1	y5
EESYSIYIYK	EESY[+45]SIY[+45]IY[+45]K	2	715.29	754.29	1	b6
EESYSIYIYK	EESY[+45]SIY[+45]IY[+45]K	2	715.29	962.34	1	b7
EESYSIYIYK	EESY[+45]SIY[+45]IY[+45]K	2	715.29	1075.42	1	b8
ESYSIYIYK	ESYSIYIYK	2	583.29	786.44	1	y6
ESYSIYIYK	ESYSIYIYK	2	583.29	699.41	1	y5
ESYSIYIYK	ESYSIYIYK	2	583.29	586.32	1	y4
ESYSIYIYK	ESYSIYIYK	2	583.29	743.32	1	b6
ESYSIYIYK	ESYSIYIYK	2	583.29	856.41	1	b7
ESYSIYIYK	ESYSIYIYK	2	583.29	1019.47	1	b8
ESYSIYIYK	ESY[+45]SIYIYK	2	605.78	994.49	1	y7
ESYSIYIYK	ESY[+45]SIYIYK	2	605.78	786.44	1	y6
ESYSIYIYK	ESY[+45]SIYIYK	2	605.78	699.41	1	y5
ESYSIYIYK	ESY[+45]SIYIYK	2	605.78	625.25	1	b5
ESYSIYIYK	ESY[+45]SIYIYK	2	605.78	788.31	1	b6
ESYSIYIYK	ESY[+45]SIYIYK	2	605.78	901.39	1	b7
ESYSIYIYK	ESYSIY[+45]IYK	2	605.78	831.42	1	y6
ESYSIYIYK	ESYSIY[+45]IYK	2	605.78	744.39	1	y5
ESYSIYIYK	ESYSIY[+45]IYK	2	605.78	631.31	1	y4
ESYSIYIYK	ESYSIY[+45]IYK	2	605.78	788.31	1	b6
ESYSIYIYK	ESYSIY[+45]IYK	2	605.78	901.39	1	b7
ESYSIYIYK	ESYSIY[+45]IYK	2	605.78	1064.46	1	b8
ESYSIYIYK	ESYSIYIY[+45]K	2	605.78	831.42	1	y6
ESYSIYIYK	ESYSIYIY[+45]K	2	605.78	744.39	1	y5

Appendix F continued

ESYSIYIYK	ESYSIYIY[+45]K	2	605.78	631.31	1	y4
ESYSIYIYK	ESYSIYIY[+45]K	2	605.78	743.32	1	b6
ESYSIYIYK	ESYSIYIY[+45]K	2	605.78	856.41	1	b7
ESYSIYIYK	ESYSIYIY[+45]K	2	605.78	1064.46	1	b8
ESYSIYIYK	ESY[+45]SIY[+45]IYK	2	628.28	831.42	1	y6
ESYSIYIYK	ESY[+45]SIY[+45]IYK	2	628.28	744.39	1	y5
ESYSIYIYK	ESY[+45]SIY[+45]IYK	2	628.28	631.31	1	y4
ESYSIYIYK	ESY[+45]SIY[+45]IYK	2	628.28	833.29	1	b6
ESYSIYIYK	ESY[+45]SIY[+45]IYK	2	628.28	946.38	1	b7
ESYSIYIYK	ESY[+45]SIY[+45]IYK	2	628.28	1109.44	1	b8
ESYSIYIYK	ESY[+45]SIYIY[+45]K	2	628.28	831.42	1	y6
ESYSIYIYK	ESY[+45]SIYIY[+45]K	2	628.28	744.39	1	y5
ESYSIYIYK	ESY[+45]SIYIY[+45]K	2	628.28	631.31	1	y4
ESYSIYIYK	ESY[+45]SIYIY[+45]K	2	628.28	788.31	1	b6
ESYSIYIYK	ESY[+45]SIYIY[+45]K	2	628.28	901.39	1	b7
ESYSIYIYK	ESY[+45]SIYIY[+45]K	2	628.28	1109.44	1	b8
ESYSIYIYK	ESYSIY[+45]IY[+45]K	2	628.28	876.41	1	y6
ESYSIYIYK	ESYSIY[+45]IY[+45]K	2	628.28	789.38	1	y5
ESYSIYIYK	ESYSIY[+45]IY[+45]K	2	628.28	676.29	1	y4
ESYSIYIYK	ESYSIY[+45]IY[+45]K	2	628.28	788.31	1	b6
ESYSIYIYK	ESYSIY[+45]IY[+45]K	2	628.28	901.39	1	b7
ESYSIYIYK	ESYSIY[+45]IY[+45]K	2	628.28	1109.44	1	b8
ESYSIYIYK	ESY[+45]SIY[+45]IY[+45]K	2	650.77	876.41	1	y6
ESYSIYIYK	ESY[+45]SIY[+45]IY[+45]K	2	650.77	789.38	1	y5
ESYSIYIYK	ESY[+45]SIY[+45]IY[+45]K	2	650.77	676.29	1	y4
ESYSIYIYK	ESY[+45]SIY[+45]IY[+45]K	2	650.77	833.29	1	b6
ESYSIYIYK	ESY[+45]SIY[+45]IY[+45]K	2	650.77	946.38	1	b7
ESYSIYIYK	ESY[+45]SIY[+45]IY[+45]K	2	650.77	1154.43	1	b8
LAHYNK	LAHYNK	2	373.20	632.32	1	y5
LAHYNK	LAHYNK	2	373.20	561.28	1	y4
LAHYNK	LAHYNK	2	373.20	424.22	1	y3
LAHYNK	LAHYNK	2	373.20	485.25	1	b4
LAHYNK	LAHYNK	2	373.20	599.29	1	b5
LAHYNK	LAHY[+45]NK	2	395.70	677.30	1	y5
LAHYNK	LAHY[+45]NK	2	395.70	606.26	1	y4
LAHYNK	LAHY[+45]NK	2	395.70	469.20	1	y3
LAHYNK	LAHY[+45]NK	2	395.70	530.24	1	b4
LAHYNK	LAHY[+45]NK	2	395.70	644.28	1	b5
YTSSK	YTSSK	2	293.15	422.22	1	y4
YTSSK	YTSSK	2	293.15	321.18	1	y3

Appendix F continued

YTSSK	YTSSK	2	293.15	352.15	1	b3
YTSSK	YTSSK	2	293.15	439.18	1	b4
YTSSK	Y[+45]TSSK	2	315.64	422.22	1	y4
YTSSK	Y[+45]TSSK	2	315.64	321.18	1	y3
YTSSK	Y[+45]TSSK	2	315.64	397.14	1	b3
YTSSK	Y[+45]TSSK	2	315.64	484.17	1	b4
ISGLIYEETR	ISGLIYEETR	2	590.81	923.48	1	y7
ISGLIYEETR	ISGLIYEETR	2	590.81	810.40	1	y6
ISGLIYEETR	ISGLIYEETR	2	590.81	697.32	1	y5
ISGLIYEETR	ISGLIYEETR	2	590.81	647.38	1	b6
ISGLIYEETR	ISGLIYEETR	2	590.81	776.42	1	b7
ISGLIYEETR	ISGLIYEETR	2	590.81	905.46	1	b8
ISGLIYEETR	ISGLIY[+45]EETR	2	613.31	968.47	1	y7
ISGLIYEETR	ISGLIY[+45]EETR	2	613.31	855.38	1	y6
ISGLIYEETR	ISGLIY[+45]EETR	2	613.31	742.30	1	y5
ISGLIYEETR	ISGLIY[+45]EETR	2	613.31	692.36	1	b6
ISGLIYEETR	ISGLIY[+45]EETR	2	613.31	821.40	1	b7
ISGLIYEETR	ISGLIY[+45]EETR	2	613.31	950.45	1	b8
DAVTYTEHAK	DAVTYTEHAK	2	567.77	849.41	1	y7
DAVTYTEHAK	DAVTYTEHAK	2	567.77	748.36	1	y6
DAVTYTEHAK	DAVTYTEHAK	2	567.77	585.30	1	y5
DAVTYTEHAK	DAVTYTEHAK	2	567.77	651.30	1	b6
DAVTYTEHAK	DAVTYTEHAK	2	567.77	780.34	1	b7
DAVTYTEHAK	DAVTYTEHAK	2	567.77	917.40	1	b8
DAVTYTEHAK	DAVTY[+45]TEHAK	2	590.27	993.46	1	y8
DAVTYTEHAK	DAVTY[+45]TEHAK	2	590.27	894.40	1	y7
DAVTYTEHAK	DAVTY[+45]TEHAK	2	590.27	793.35	1	y6
DAVTYTEHAK	DAVTY[+45]TEHAK	2	590.27	595.24	1	b5
DAVTYTEHAK	DAVTY[+45]TEHAK	2	590.27	696.28	1	b6
DAVTYTEHAK	DAVTY[+45]TEHAK	2	590.27	825.33	1	b7
TVTAMDVVYALK	TVTAMDVVYALK	2	655.85	938.50	1	y8
TVTAMDVVYALK	TVTAMDVVYALK	2	655.85	807.46	1	y7
TVTAMDVVYALK	TVTAMDVVYALK	2	655.85	692.43	1	y6
TVTAMDVVYALK	TVTAMDVVYALK	2	655.85	718.34	1	b7
TVTAMDVVYALK	TVTAMDVVYALK	2	655.85	817.41	1	b8
TVTAMDVVYALK	TVTAMDVVYALK	2	655.85	980.48	1	b9
TVTAMDVVYALK	TVTAMDVVY[+45]ALK	2	678.35	983.49	1	y8
TVTAMDVVYALK	TVTAMDVVY[+45]ALK	2	678.35	852.45	1	y7
TVTAMDVVYALK	TVTAMDVVY[+45]ALK	2	678.35	737.42	1	y6
TVTAMDVVYALK	TVTAMDVVY[+45]ALK	2	678.35	718.34	1	b7

Appendix F continued

TVTAMDVVYALK	TVTAMDVVY[+45]ALK	2	678.35	817.41	1	b8
TVTAMDVVYALK	TVTAMDVVY[+45]ALK	2	678.35	1025.46	1	b9
TLYGFGG	TLYGFGG	2	357.68	613.30	1	y6
TLYGFGG	TLYGFGG	2	357.68	500.21	1	y5
TLYGFGG	TLYGFGG	2	357.68	378.20	1	b3
TLYGFGG	TLYGFGG	2	357.68	435.22	1	b4
TLYGFGG	TLYGFGG	2	357.68	582.29	1	b5
TLYGFGG	TLY[+45]GFGG	2	380.17	658.28	1	y6
TLYGFGG	TLY[+45]GFGG	2	380.17	545.20	1	y5
TLYGFGG	TLY[+45]GFGG	2	380.17	423.19	1	b3
TLYGFGG	TLY[+45]GFGG	2	380.17	480.21	1	b4
TLYGFGG	TLY[+45]GFGG	2	380.17	627.28	1	b5

Data acquired using Skyline Targeted Proteomics Environment (v1.1) (18). These data can be entered into method software on a TSQ Ultra for pilot quantitative measurements. The actual RTs and spectral intensities can be entered into the skyline platform to optimize the method before uploading back to TSQ.